The Impact of Microbial Biofilms on the Performance of Materials Relevant to the Nuclear Fuel Cycle

Kim Alexandra Patel, BSc (Hons)

A thesis submitted to the University of Huddersfield in partial fulfilment of the requirements for the degree of Doctor of Philosophy

Department of Biological and Geographical Sciences

March 2021

This studentship was supported by the EPSRC Materials Doctoral Training Programme

Copyright statement

i. The author of this thesis (including any appendices and/ or schedules to this thesis) owns any copyright in it (the “Copyright”) and s/he has given The University of Huddersfield the right to use such Copyright for any administrative, promotional, educational and/or teaching purposes.

ii. Copies of this thesis, either in full or in extracts, may be made only in accordance with the regulations of the University Library. Details of these regulations may be obtained from the Librarian. This page must form part of any such copies made.

iii. The ownership of any patents, designs, trademarks and any and all other intellectual property rights except for the Copyright (the “Intellectual Property Rights”) and any reproductions of copyright works, for example graphs and tables (“Reproductions”), which may be described in this thesis, may not be owned by the author and may be owned by third parties. Such Intellectual Property Rights and Reproductions cannot and must not be made available for use without permission of the owner(s) of the relevant Intellectual Property Rights and/or Reproductions.

I would like to dedicate this thesis to my grandad Robert Brewer (1935 - 2017) and my granny Kamlaben Patel (1939 - 2019) who both sadly passed away during my time as a PhD student.

Acknowledgements

Firstly, I'd like to express sincere gratitude and thanks to my supervisor Professor Paul Humphreys for his continued support and guidance not only through my PhD but during earlier days as his placement student too. I'd also like to say thank you to my second supervisor Dr Paul Bills. I would like to sincerely thank Dr Simon Rout for helping me on countless occasions when I'm sure he would have preferred to be doing something else. I don't know where I would be without his support. Many thanks to my colleagues Dr Richard Wormald and Carolanne Allen for always being there for me whether it was to have a moan when times were bad or just have a laugh when we were having a good day. From our microbiology lab I must also give thanks to Kirsty Davies for her support throughout my PhD. Lastly from University I would like to say a big thankyou to my friends and members of "Girl Street" – Hollie, Sophie, Megan, Naomi, Courtney, Zoe & Carla – for always being there to supply great conversation, coffee and cake (in excess).

At home I of course have to say a massive thank you to my family who I love very much; my parents Jane & Dinesh who were always there to support me, my sisters Katie, Sarah & my twin Abi, my brother Nick, my nephews Ellis, Ewan and Sebastian and my grandma Dorothy. Thank you to my friends back home who, despite always saying they had no idea what I was doing, always appreciated how hard I found my PhD and were there to offer support when needed. Finally, I must thank my amazing fiancé, James, who has been with me since day one of my postgraduate, comforted me through the darkest days and always told me he believed in me even when I didn't believe in myself (most of the time). You're all the best.

Abstract

The proposed strategy for long-term storage of nuclear waste within the UK involves emplacement within geological disposal facilities (GDF). Highly alkaline and anoxic conditions expected to develop will result in the chemical degradation of cellulosic content present within intermediate level waste facilities (ILW-GDF). The major constituents of cellulose degradation products (CDP) will be isosaccharinic acid (ISA), the α and β forms of which can form soluble complexes with a range of radionuclides subsequently altering the sorption capacity of materials engineered to contain radioactive contaminants.

Migrating radionuclides that are able to transport out of the GDF to the far-field environment through complexation processes may be controlled by sorption processes and pore water chemistry that surrounds the host rock at a pH that is milder than the near-field. Biofilm communities that are able to survive under the alkaline and anaerobic conditions could aid in the retention of radiological species by utilising ISA as a carbon source.

By using flow-cell systems which in corporate sand as a substrate for sorption, the behaviour of natural analogues and radionuclides was studied to understand how they would behave if they were present within the far-field. Ni(II), Eu(II) and Th(IV) were found to adsorb to sand under the relevant conditions, however the presence of ISA as a complexing agent only influenced Ni(II) migration through the system. Microbes capable of biofilm formation on the sand surface were capable of the degradation of CDPs through fermentation processes which resulted in Ni(II) movement being hindered via removal of the complexed ISA. Contrastingly, the transport of soluble U(VI) was not restricted through adsorption to sand. Microbial reduction induced by the introduction of biofilm-forming microbes lead to a decrease in measured U(VI) within effluent samples due to its reduction to insoluble U(IV).

Microscopy and molecular techniques investigated for the analysis of biofilms on complex surfaces allowed the elemental, extra polymeric substance (EPS), and community composition of microbial biofilms grown within sand columns to be studied.

Contents Page

List of Figures

List of Tables

List of Equations

List of Abbreviations

CDP – Cellulose degradation products

CLSM – Confocal laser scanning microscopy

ConA – Concanavalin A

CTAB – Cetyltrimethylammonium bromide

DNA – Deoxyribonucleic acid

EDX – Energy dispersive x-ray analyzer

EPS – Extracellular polymeric substances

FITc – Fluorescein isothiocyanate

GC – Gas chromatography

GDF – Geological disposal facility

HLW – High level waste

HPAEC-PAD – High-performance anion-exchange chromatography with pulsed amperometric detection

IC – Ion chromatography

ICP-MS – Inductively coupled plasma mass spectrometry

ILW – Intermediate level waste

ILW-GDF – Intermediate level waste geological disposal facility

ISA – Isosaccharinic acid

LLW – Low level waste

NDA – Nuclear Decommissioning Authority

NRVB – Nirex reference vault backfill

PBS – Phosphate buffered saline

PCR – Polymerase chain reaction

rRNA – Ribosomal RNA

SEM – Scanning electron microscopy

SRB – Sulphate reducing bacteria

TEA – Terminal electron acceptor

UK – United Kingdom

UPW – Ultrapure water

VFA – Volatile fatty acids

XRD – X-ray diffraction

Chapter 1.0 Geological Disposal and the Generation of Isosaccharinic Acids

1.1 Overview

Currently one of the proposed concepts for radioactive waste disposal within the United Kingdom (UK) involves an underground storage solution known as a geological disposal facility (GDF). Details regarding the nuclear waste industry within the UK as well as the GDF concept and construction are discussed in this chapter. While there are three main waste categories only high and intermediate level wastes fall within the specification for disposal via a GDF, with cellulose containing wastes present within the intermediate sector only. The highly alkaline, anaerobic conditions set to prevail within a GDF will subsequently lead to cellulose within the waste to undergo alkaline chemical hydrolysis, producing cellulose degradation products (CDP), the main components of which are isosaccharinic acids (ISA). The ability of ISA to form complexes with various radionuclides makes this degradation product of particular interest when researching the long-term operation of a GDF and the mobility of the radionuclides within it.

1.2 Nuclear Waste Legacy

There are a number of processes within the UK that result in the generation of radioactive waste, the primary contributor being the ‘nuclear fuel cycle’, a complex sequence of activities within the industrial sector that lead to the fabrication of nuclear fuel needed for the generation of electricity. Additionally operations within defence, research and medical fields also produce significant quantities of waste (N.D.A, 2015b). Generally, radioactive waste can be split into three main categories: low, intermediate and high level wastes (as well as a small portion of very low level waste). These groups are then assigned to either higher activity wastes (HAW) or lower activity wastes (LAW), as shown in Figure 1.1 (N.D.A, 2019b)

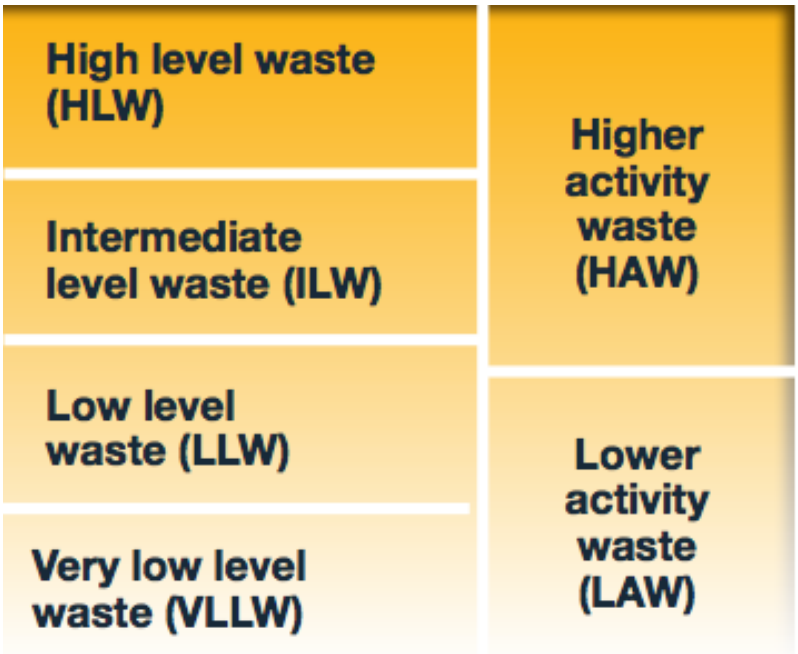

Figure 1. 1. UK assignment of radioactive waste groups into higher activity waste (HAW) and lower activity wastes (LAW). Figure is taken from the 2019 N.D.A report "Integrated Waste Management: Radioactive Waste Strategy" (N.D.A, 2019b).

1.2.1 Low level waste

Low level waste (LLW) is characterised as having the lowest radioactivity levels where material does not exceed 4 gigabecquerels (GBq) per tonne of alpha activity or 12 GBq per tonne of beta/gamma activity. Soil, rubble and steel items such as reinforcement and framework of dismantled nuclear reactors are the main components as well as scrap metal, plastics and paper (N.D.A, 2019a). Due to low radioactive emissions LLW is not destined for disposal within a GDF but is instead compacted into steel containers and immobilised in cement before emplacement in vaults lined with concrete (N.D.A, 2017) (N.D.A, 2019a). While LLW contains cellulose this material will not undergo alkaline chemical hydrolysis but will be subjected to microbial-based degradation (Beadle, Humphreys, Pettit, & Small, 2000).

1.2.2 Intermediate level waste

Intermediate level waste (ILW) predominantly consists of concrete, steel, graphite, cement and sand and as of 2019 makes up around 500,000 m^3 of total packaged

waste, 1,200 tonnes of which is cellulosic material including paper, wood and cloth (N.D.A, 2019a). Steel fuel cladding and reactor modules, graphite content from moderator blocks from the dismantling of Advanced Gas-cooled reactors (AGR) and Magnox power stations, concrete generated from the demolition of nuclear power stations as well as flocculants, non-exchange resins and sludge produced from liquid effluent treatment all contribute to the existence of other organic and inorganic material within the ILW repository (N.D.A, 2019a). Radioactive content here surpasses LLW threshold but does not give off significant heat during disposal which is why cooling isn't taken into consideration when designing storage/ disposal facilities (N.D.A, 2010b).

1.2.3 High level waste

Spent nuclear fuel that is reprocessed gives rise to the high-level waste (HLW) stored at Sellafield nuclear power station. As a result of radioactive decay HLW will produce heat during its emplacement within a GDF and therefore must be conditioned differently to LLW/ILW prior to disposal (N.D.A, 2010c). HLW is produced as a concentrated nitric acid solution before it's conditioning to a solid glass block to immobilise the waste through a process called vitrification. Despite HLW containing the highest levels of radioactivity the reported volume is a very small portion, which is in contrast to LLW/VLLW reporting the largest volume but lowest radioactivity levels (Figure 1.2). There are no cellulosic materials within the HLW inventory (N.D.A, 2019a).

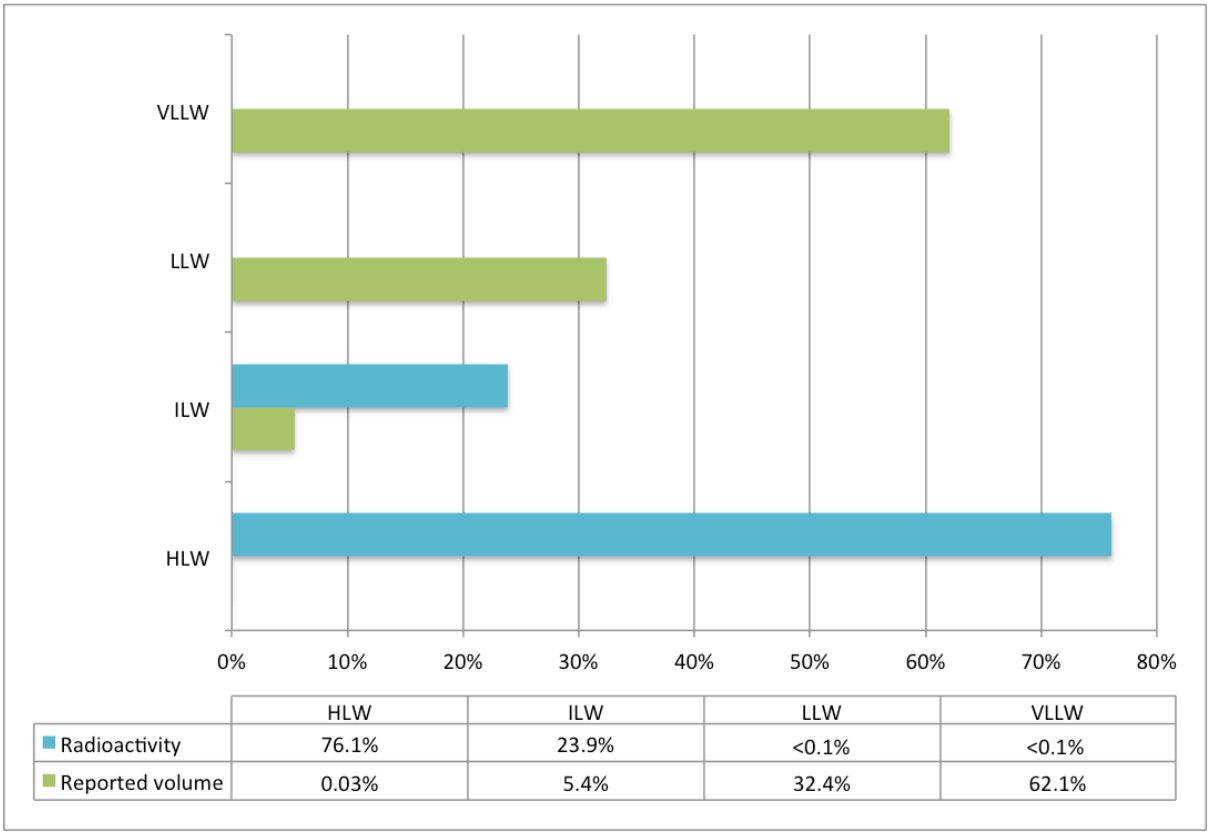

	HLW	ILW	LLW	VLLW
Radioactivity	76.1%	23.9%	<0.1%	<0.1%
Reported volume	0.03%	5.4%	32.4%	62.1%

Figure 1. 2. Relationship between reported volume of waste and its associated radioactivity at 1.4.2200. Figure adapted from the 2019 N.D.A report "2019 UK Radioactive Waste Inventory (N.D.A, 2019a).

1.3 Geological Waste Disposal

1.3.1 Geological disposal facility (GDF)

Currently within the UK the government's long-term management plan for ILW and HLW involves emplacement of these higher activity wastes within a GDF (N.D.A, 2010a). The principle of a GDF is to ensure that radioactive waste is isolated deep underground, between 200-1000m in a suitable host rock formation (Figure 1.3), to prevent the release of harmful radioactivity into the environment (N.D.A, 2016c). At the time of writing an appropriate UK host site and geological setting has not yet been identified. A GDF will be composed of a surface level facility where waste will be received and an underground facility assumed to be constructed directly beneath it allowing for the conveyance of ILW/HLW through underground drifts and shafts (Figure 1.3) (N.D.A, 2016c).

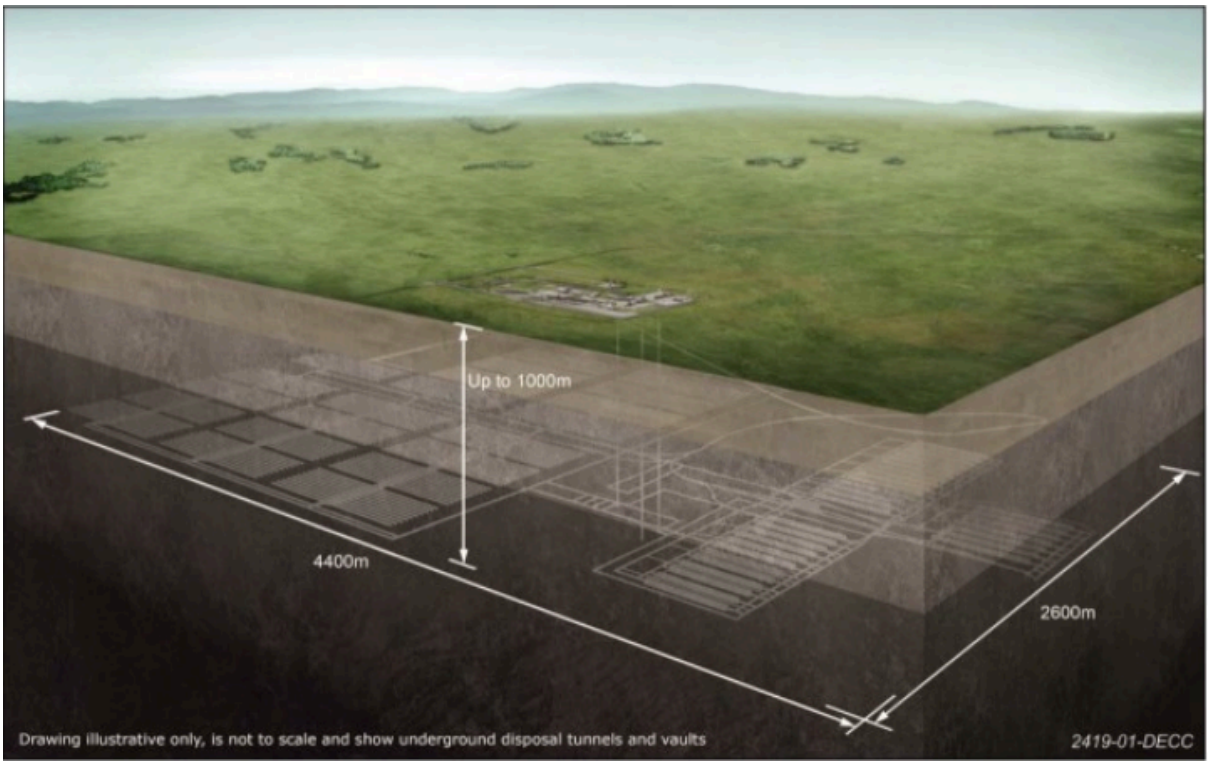

Figure 1. 3. Artist impression of a geological disposal facility. Figure taken from N.D.A "2019 Radioactive Waste Inventory report" illustrating the UK's GDF concept (N.D.A, 2019a).

1.3.2 Multi-barrier system

Waste enclosed in the disposal facilities will be confined below the surface using a multi-barrier approach (Figure 1.4) employing a range of both natural and engineered barriers to contain radioactive elements affiliated with the waste and prevent them from reaching the biosphere. The first barrier is the waste form itself, which in the instance of ILW involves compacting waste into steel drums and encapsulating it using cement grout to supply a stable matrix with a high sorption capacity to immobilise the radionuclides (Figure 1.5) (N.D.A, 2010a) (N.D.A, 2010c). The steel packages allow for safe transportation and handling of ILW, as well as being a physical barrier between the waste and any potential groundwater that has penetrated the facility (N.D.A, 2010c). Steel containers housing ILW will also be vented to accommodate for any gas release due to pressurisation (N.D.A, 2016d). Next, any material that encompasses waste packages within the disposal facility is known as the buffer or backfill, a chemical barrier providing environmental conditioning between the groundwater and steel containers. Depending on the

geological setting and rock formation of the host environment different mediums may be considered as a buffer/ backfill, for example Nirex Reference Vault Backfill (NRVB), a cement-based component, was developed for use in high strength rock. NRVB is a highly porous material and is known to have a large sorption capacity as well the ability to create an alkaline environment once hydrated which will further limit the migration of certain radionuclides (N.D.A, 2010c).

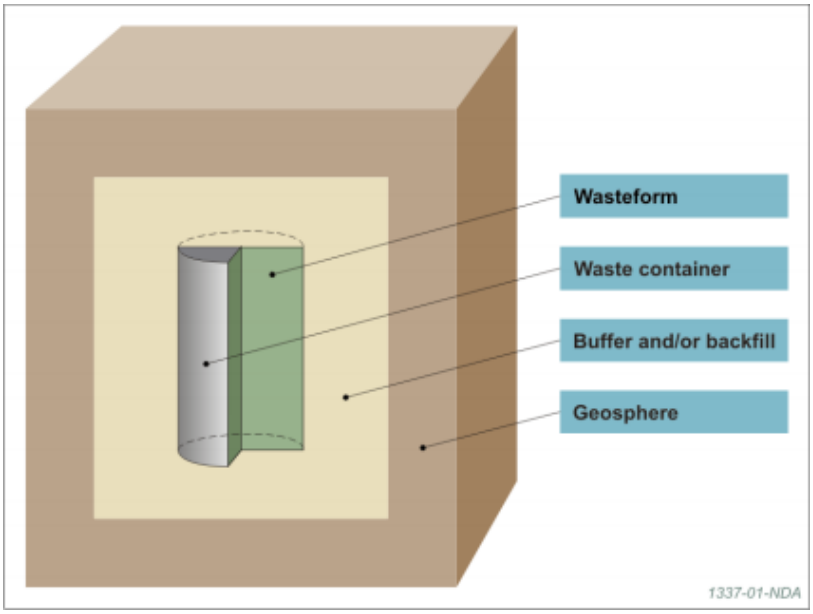

Figure 1. 4. Schematic diagram of the multi-barrier system approach. Figure taken from the 2010 "Near-field evolution status report" (N.D.A, 2010c).

The final physical barrier will be provided by the host rock in which construction of the GDF will take place. The host rock or geosphere imparts a significant level of defence against mobilisation of radioactive elements by securing their isolation deep below the surface. As well as providing physical protection in the form of stable underground surroundings, the geology aids in retention of long-lived radionuclides by conditioning the chemistry of the water when reacting with the surrounding rock (N.D.A, 2016e) (N.D.A, 2016a). Selection of the natural geological barrier will depend on its ability to withstand these varying conditions. Radioactive Waste Management (RWM) have so far selected the following as potential host rocks: Evaporite rock (eg. halite), lower strength sedimentary rock (eg. clay) and higher strength rock (eg. granite) (N.D.A, 2016d).

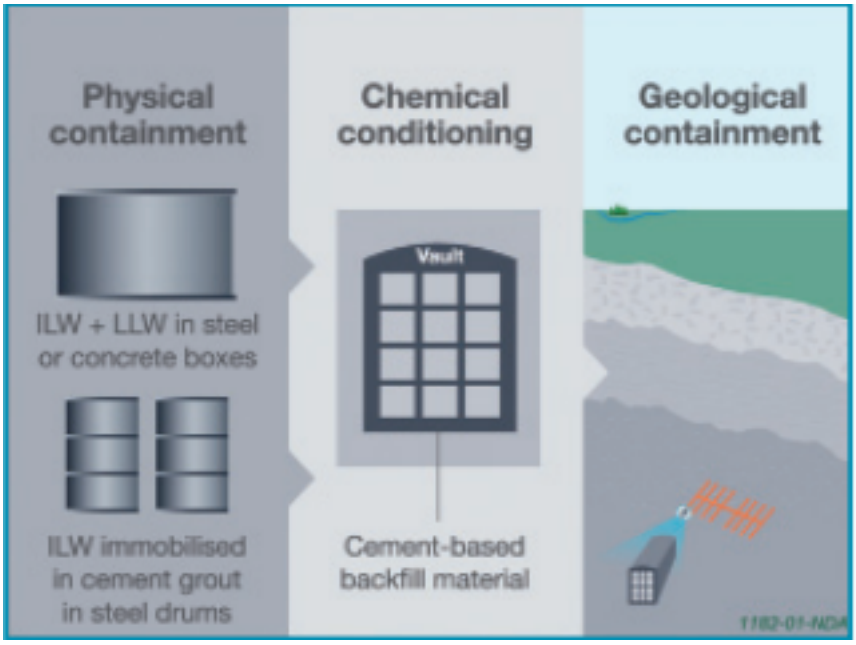

Figure 1. 5. Design concept of an ILW disposal facility in higher strength rock. Figure taken from the 2010 N.D.A report "An introduction to the generic Disposal System Safety Case" (N.D.A, 2010a).

1.3.3 Near-field conditions of an ILW-GDF

Post-closure, a number of processes could impact the chemistry of a GDF from the waste form to the geology and the surrounding geosphere, leading to alterations in the repository's evolution. During saturation of groundwater the NRVB encapsulated ILW disposal facility will become hydrated, producing hydroxyl ions (OH^-). A constant flow of pore water continuously buffers and dominates the chemistry, resulting in an alkaline pH of ~12.5. Over time this dissolution of portlandite (Equation 1.1) and the subsequent cement hydration products ie. calcium-silica-hydrates (CSH) will buffer surrounding waters to yield a pH of ~ 10 to 12.5 (Figure 1.6) (N.D.A, 2010c).

$$Ca(OH)_{2\,(s)} + H_2O_{(l)} = Ca_{(aq)} + 2OH^-_{(aq)}$$

Equation 1. 1. Hydration of portlandite present within ordinary portland cement (OPC).

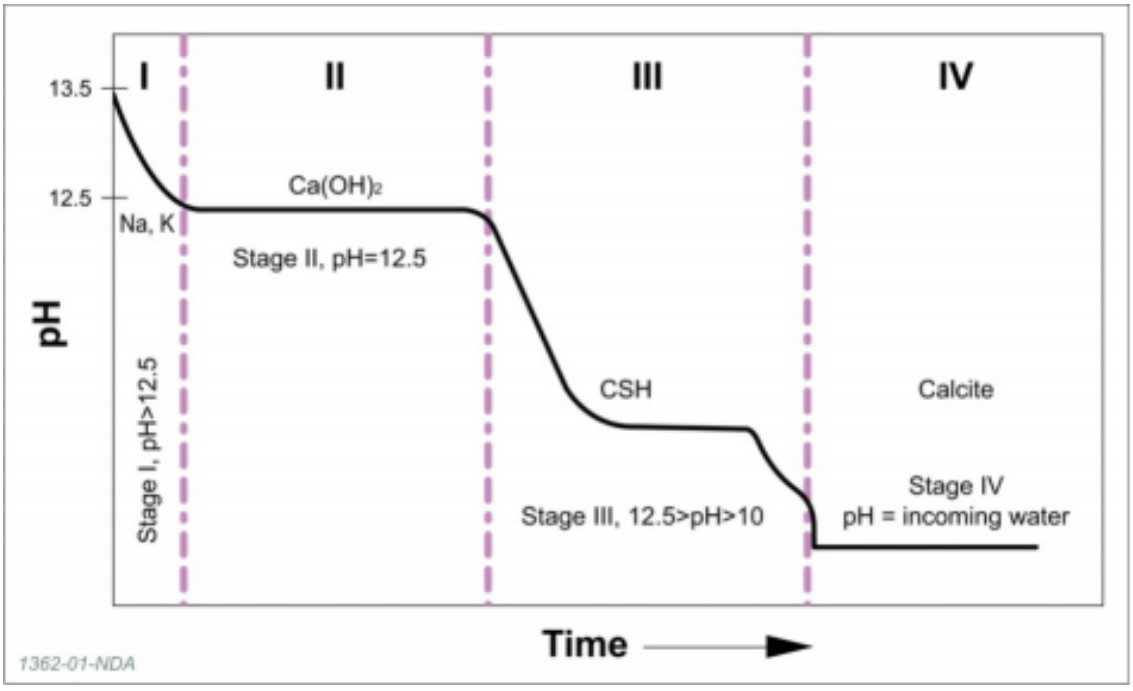

Figure 1. 6. Evolution of pH (at room temperature) as a result of cement dissolution.
Figure taken from N.D.A report "Near-field evolution status report (N.D.A, 2010c).

Consequently, alkaline conditions that prevail play an important role in preventing the migration of radioactive elements through the waste packages. By limiting radionuclide solubility to the water chemistry the sorption of these elements onto cement material can be enhanced as they become less soluble under high pH environments (N.D.A, 2010c). Post-closure, the generation of gases within a GDF can lead to a number of processes that could impact the near field evolution. As anoxic conditions are established, hydrogen gas is produced in bulk through corrosion of metal present in the waste form as well as from the steel containers and also in components of the GDF structure itself. In addition, microbial degradation of organic matter will contribute to the generation of carbon dioxide and methane, albeit in lesser quantities. Nevertheless, the repercussions of gas production would depend on the potential for it to move through near field and into the surrounding geosphere (N.D.A, 2016b). Moreover, the long-term adaptation of the geosphere is influenced by surface conditions, natural evolution and also any affects that construction of the disposal facilities may have on the host rock (Mazurek, 2017). These expectations for the evolution of an ILW-GDF in a cement-backfilled multi-barrier system are illustrated in Figure 1.7.

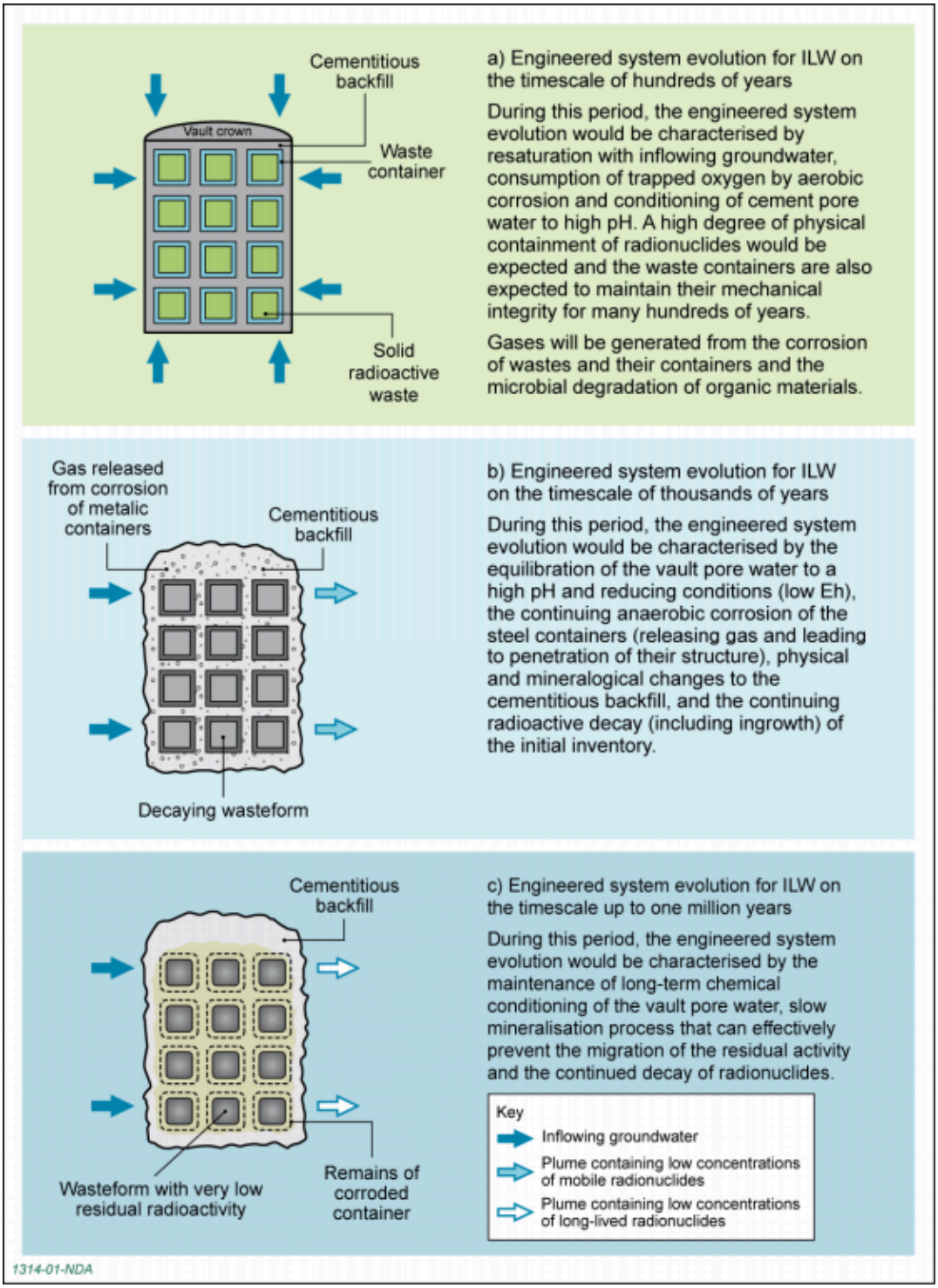

Figure 1. 7. The evolution of an ILW-GDF post-closure based on an engineered barrier system using cementitious backfill. Figure taken from the 2010 N.D.A "Near-field evolution status report" (N.D.A, 2010c)

1.4 Alkaline Cellulose Degradation under ILW-GDF Conditions

1.4.1 Cellulosic materials

The ILW repository will house a number of materials such as paper, wood and cloth, resulting in a rich cellulosic content (N.D.A, 2019a). While wood and paper is composed of a number of polymers including cellulose, hemicellulose and lignin, cotton is less complex and is made up primarily of cellulose polymers (Bugg, Ahmad, Hardiman, & Rahmanpour, 2011). Cellulose is a linear polysaccharide with a structure that comprises β-1-4 glycosidic linkages that join repeated units of D-anhydroglucose ring pairs, known as cellobiose (Figure 1.8). The molecular chain can twist, with each consecutive unit rotating through the molecular axis 180°C. Hydrogen bonds join chains of cellulose together by attaching neighbouring hydroxymethyl (-CH_2OH) and hydroxyl (-OH) groups to form microfibrils (Ansell & Mwaikambo, 2009). Hemicellulose molecules present in paper in wood are branched polymers of various sugars including glucose, hexose and pentose monosaccharides. Their structures are more complex and are more readily hydrolysed than cellulose therefore more susceptible to chemical degradation (Machmudah, Wahyudiono, Kanda, & Goto, 2017).

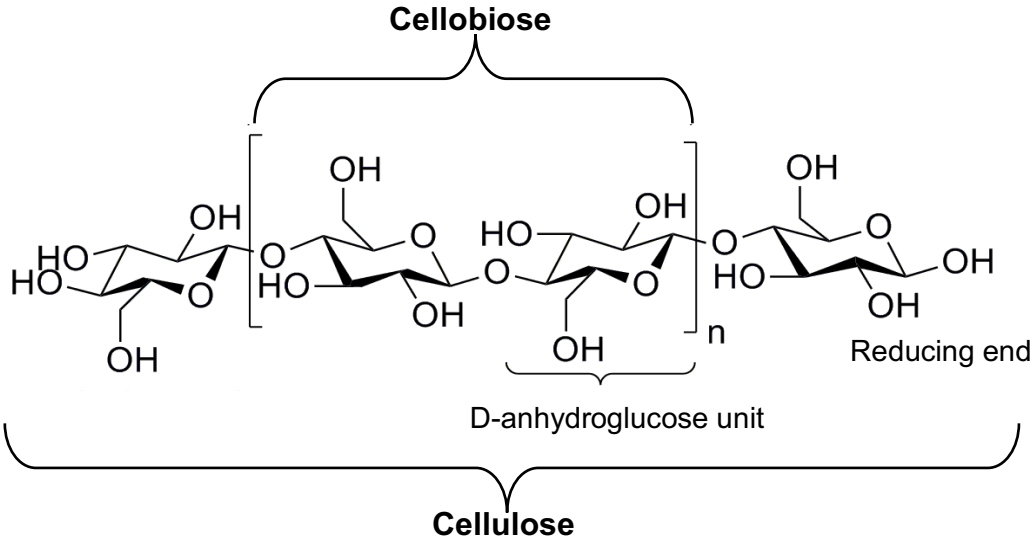

Figure 1. 8. Structures of cellulose and cellobiose. Figure adapted from (Olsson & Westman, 2013)

1.4.2 Alkaline, anaerobic degradation of cellulose

Post-closure anaerobic, alkaline and chemically reducing conditions are set to prevail within an ILW-GDF as a result of ground water saturation and the subsequent dissolution of cement backfill. At a steady pH of ~10 to 12.5 by means of constant resaturation the cellulose present in the waste will begin to undergo chemical alkaline hydrolysis (Knill & Kennedy, 2003) (Humphreys, Laws, et al., 2010). This process of degradation occurs via the 'peeling' mechanism that takes place at the reducing end group of the cellulose molecule (Figure 1.9). One terminal D-glucose unit is stripped or "peeled" resulting in the generation of isosaccharinic acids (ISA), collectively known as cellulose degradation products (CDP), the two main components being 3-deoxy-2-C-(hydroxymethyl)-erythro-pentonic acid (α-ISA) and 3-deoxy-2-C-(hyroxymethyl-threo-pentonic acid (β-ISA) (Figure 1.10). In addition to ISAs, other small chain fatty acids are also produced but in low abundance (Humphreys, Laws, et al., 2010). The peeling reaction will continue, moving along the cellulose chain revealing new reducing end groups, and if unchecked would result in the complete degradation of cellulose material. However, this is not the case and stabilisation is attained via the "stopping" mechanism. This is contrast to hemicelluloses which cannot undergo the stopping reaction due to being alkali soluble (Knill & Kennedy, 2003).

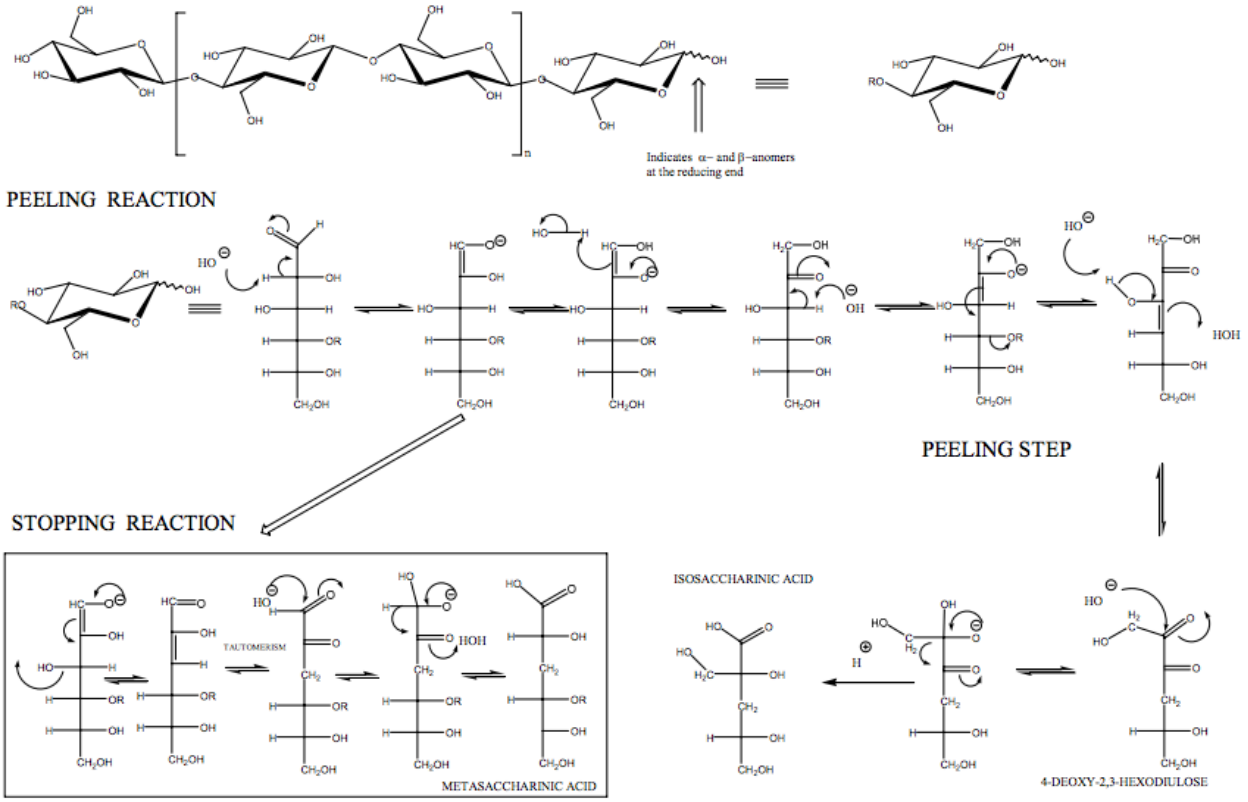

Figure 1. 9. Alkaline chemical hydrolysis of cellulose. Figure taken from (Humphreys, Laws, & Dawson, 2010)

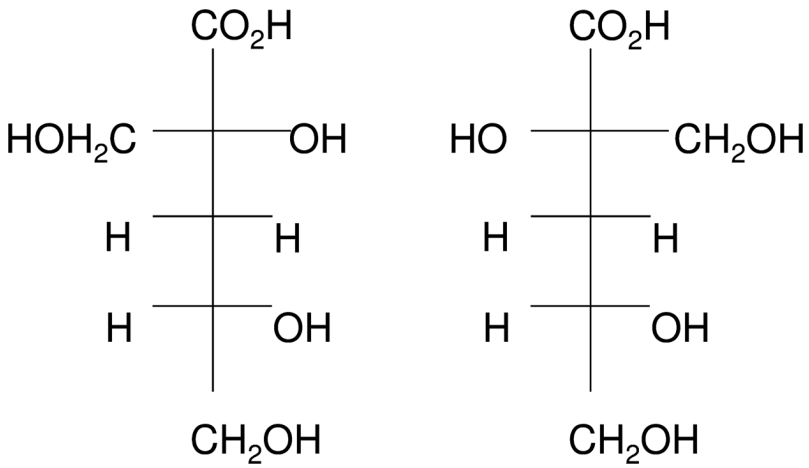

Figure 1. 10. Alpha (L) and beta (R) diastereomers of isosaccharinic acid. Figure taken from (Rout, Charles, Garratt, et al., 2015)

1.4.3 Complexation of ISA to radionuclides

The generation of α and β forms of ISA could pose a considerable threat to the long-term performance of a GDF by potentially enhancing the mobility of radionuclides. Tri- and tetravalent metals including Th(V) and Eu(III) would be the most affected by the presence of CDP's due to the high complexation affinity ISA has to these elements (Loon & Glaus, 1998). Numerous studies have demonstrated that under hyperalkaline conditions certain radionuclides can become soluble complexes with ISA including Ni(II) (Warwick, Evans, Hall, & Vines, 2003), Eu(III) (Karlien Vercammen, Glaus, & Loon, 2001), U(IV) (Warwick, Evans, Hall, & Vines, 2004) and Th(IV) (Karlien Vercammen et al., 2001). Investigations into nickel-ISA complexation revealed that products of their reaction differed depending on pH, with $Ni_2ISA(OH)_4$ forming at pH >10.0, $Ni_2ISA(OH)_3$ at pH 7.0-10.0 and NiISA forming at pH <7.0 (Warwick et al., 2003). A study by Vercammen *et al* demonstrated that in the absence of calcium (Ca) 1:1 Th:ISA complexes were dominant under at pH 10.7 – 13.3, and that in the same pH range in the presence of calcium Th:ISA:Ca complexes dominated 1:2:1, consistent with a previous study demonstrating that under hyperalkaline conditions one Th ion associates with two ISA molecules. (K. Vercammen, Glaus, & Loon, 1999) (K. Vercammen, Glaus, & Van Loon, 2001) In the same experiment 1:1 Eu:ISA was found to be the dominant forming complex in both calcium and calcium free systems in the same pH range 10.7 – 13.3 indicating europium sorption was not influenced by calcium (K. Vercammen et al., 2001).

ISA present within ILW repositories could impact the high sorption capacity radionuclides have for cementitious backfill material and subsequently influence the release of radioactive elements from an ILW waste form out into the geosphere. Dario *et al* reported that at concentrations higher than 10^{-4} mol dm^{-3} ISA the sorption of Eu onto cement decreases at pH 12.5 (Dario, Molera, & Allard, 2006). A study by Wieland *et al* revealed that at pH 13.3 Th(IV)-ISA complexes in solution reduce the uptake of Th(IV) onto hardened cement paste (HCP) when $[ISA]_{aq} > 10^{-4}$M (Wieland, Tits, Dobler, & Spieler, 2002). ISA degrading microorganisms could potentially reduce the mobility of radionuclides by liberating them from organic complexants.

1.5 Summary of Chapter

As of 2019 the UK reported a total packaged volume of 4,470,000 m^3 of radioactive waste, 11.2% of which was intermediate-level wastes (ILW) (499,000 m^3) (N.D.A, 2019a). Cellulosic content makes up 1,200 tonnes of the intermediate-level inventory which, when degraded under the anoxic and hyperalkaline conditions expected within an ILW-GDF, yields a high volume of cellulose degradation products. CDPs known as α- and β- isosaccharinic acid may form soluble complexes with a variety of radioelements, affecting their ability to undergo adsorption to cement backfill material leading to an increase threat of enhanced radionuclide migration, potentially out of the chemically disturbed zone of a GDF.

Chapter 2.0 Microbial Processes Relevant to ILW-GDF

2.1 Overview

ISA generated through cellulose degradation could present itself as a vital carbon source for microorganisms capable of survival under anoxic and alkaline conditions. During the construction phase microbes introduced from the biosphere or subsurface could potentially colonise an ILW-GDF and subsequently metabolise ISA during processes such as fermentation. An influx of groundwater during re-saturation will disperse a number of TEAs through the geosphere that will be utilised mostly within the far-field, however high levels of sulphate within UK water may bring about sulphate-reducing conditions surrounding the GDF. Biofilms have been well described for their ability to colonise a multitude of surfaces in a variety of environments and could potentially enhance microbial survival under harsh conditions. This chapter will discuss microbial presence within the near- and far-field of an ILW-GDF and the processes expected to take place. This chapter will also address the potential for microbial-metal interactions to occur and what affect they will have under the relevant conditions.

2.2 Microbial Presence and Survival under ILW-GDF Conditions

2.2.1 Survival at high pH

Highly alkaline (pH 10.0 to 12.5), anaerobic and chemically reducing conditions are expected to dominate the near-field environment of an ILW-GDF (N.D.A, 2010c). *In vivo* investigations into the survival of microorganisms at high pH have been extensive, including in ikaite columns in the fjords of Greenland (Glaring et al., 2015), environments affected by serpentinization in Portugal (Tiago, Chung, & Veríssimo, 2004) and soda lakes worldwide (Grant & Sorokin, 2011), as well as *in vitro* isolation of these microbes in laboratory conducted studies (Kanekar, Nilegaonkar, Sarnaik, & Kelkar, 2002). Known collectively as alkaliphiles these microorganisms are named so because of their ability to thrive in environments of extreme pH (9.0 and above) but are unable to grow sufficiently in neutral pH conditions (Horikoshi, 1999). Alkaliphilic bacteria are capable of tolerating external environmental stresses by

regulating their pH homeostasis through electrogenic transport of Na^+/H^+ antiporters, whereas microorganisms growing in circumneutral environments maintain a cytoplasmic pH of 7.4 to 7.8 (Padan, Bibi, Ito, & Krulwich, 2005). *Bacillus pseudofirmus* OF4, one of the most extreme alkaliphiles, is able to quickly shift from environments of pH 8.5 to 10.5 without causing any disruption to the cytoplasmic gradient. This process is made possible by the addition of a solute, α-aminoisobutyric acid (AIB), to cotransport Na^+ into the cytoplasm, enhancing pH homeostasis and reducing cytoplasmic pH back to around 8.2 (Krulwich, Federbush, & Guffanti, 1985).

2.2.2 Microbial presence in both near-field and far-field

As discussed in section 2.2.1 Survival at high pH there is potential for certain microbial species to survive under the conditions of an ILW-GDF (McKinley & Grogan, 1991) and while some bacteria may become dormant there is also the capacity for others ie. sulphate reducing bacteria (SRB) to thrive and transform the chemistry within the GDF, albeit their performance may be limited by factors such as pH and redox (N.D.A, 2010c). Construction and operation of a GDF's engineered barriers will inevitably bring about the introduction of microorganisms, as well as sources of nutrients, into this extreme environment (near-field) from the biosphere through the subsurface (Humphreys, West, & Metcalfe, 2010). However, there will already be a range of species present within the geology, or "far-field", surviving within cracks and upon surfaces of the host rock as alkalinity becomes less extreme here due to being further away from cementitious backfill material (N.D.A, 2016e).

2.2.2.1 Natural analogue sites

Various naturally occurring alkaline sites are distributed throughout the world and are known for exhibiting conditions analogous to that of an ILW-GDF. Soda lakes have been well investigated for the diverse array of microorganisms that thrive within their hyperalkaline (>pH 10.0) waters and are characterised by the large concentrations of dissolved carbonates present as well as varying levels of NaCl, resulting in some lakes having high saline levels (up to 35% w/v) (Antony et al., 2013) (Grant & Sorokin, 2011). Lonar Lake, a crater formed within basalt rock and situated in the Buldhana district of India, is the home of a rich geomicrobiological environment.

Taxonomic analysis from both sediment and pore water samples demonstrate that 30% of relative abundance was dominated by the Proteobacteria phylum, followed by Actinobacteria at 24% and Firmicutes making up 11%, with the *Gammaproteobacteria* and *Actinobacteria* groups of bacteria being predominately present within sediment and pore water samples, respectively (Paul et al., 2016). Analysis of sediment extracted from shorelines of the alkaline (pH 9.7 $\pm$ 0.3) and strictly anaerobic Mono Lake in California, USA indicated the presence of several SRB in the Deltaproteobacteria class of Proteobacteria including *Desulfobacteraceae* and *Desulfobubaceae* (Rojas et al., 2018). This data corroborates earlier findings by Stam *et al* who described sulphate reduction occurring at the lakes bottom waters due to the presence of high sulphide concentration (Stam, Mason, Pallud, & Van Cappellen, 2010). Proteobacteria, Bacteroidetes and Firmicutes were identified as the three most abundant Phyla reported across all sediment samples (74% combined) (Rojas et al., 2018). A range of microbial processes have been identified under the extreme conditions seen in soda lakes, including methanogenesis (Surakasi, Wani, Shouche, & Ranade, 2007), sulphate reduction (Foti et al., 2007) and the oxidation of methane under anaerobic conditions (Joye, Connell, Miller, Oremland, & Jellison, 1999).

Serpentinization is a geologic process that oxidizes minerals present within mafic-ultramafic rock complexes known as Ophiolite (Fones et al., 2019). This generates methane (CH_4) and other reduced carbon containing compounds through the consumption of hydrogen (H_2), which are then utilized as substrates for microbial metabolism. Ophiolites that have undergone sepentinization will also influence the pH of surrounding waters causing them to become highly alkaline (Seewald, Zolotov, & McCollom, 2006). Natural analogue sites for microbial diversity in this environment have been investigated including in the Troodos ophiolite in Cyprus (Rizoulis, Milodowski, Morris, & Lloyd, 2016), the Samail ophiolite in Oman and the Leka ophiolite in Norway (Daae et al., 2013). Samples taken from the hyperalkaline and Ca-rich waters of the Allas Springs (Troodos mountains, Cyprus) indicated that Proteobacteria dominated at Phylum level and isolation studies in the laboratory revealed facultative anaerobic species belonging to the *Paenibacillus* genus to be present in 82/84 of isolates (Rizoulis et al., 2016).

2.2.2.2 Anthropogenic analogue sites

In contrast to natural occurring sites hyper-alkaline environments can also be established as a result of anthropogenic contamination from industrial works such as bauxite processing, manufacturing of limestone and steelwork slags (Mayes et al., 2011) (Burke et al., 2012). Contaminants from these processes may contain heavy metals including chromium, copper and zinc that are considered toxic to the microbial population surviving in these environments (Turpeinen, Kairesalo, & Häggblom, 2004) (Hiroki, 1992), leading to a potential decrease in diversity and population size. However over time the local consortia will acclimatize and evolve in response to the extreme geochemical conditions, allowing for a shift in microbial diversity (Hemme et al., 2010), an example of which is demonstrated in the evolution of acid-tolerant microorganisms in acid mine drainage (Hallberg, 2010).

An anthropogenic alkaline site in Harpur Hill, Buxton, UK has been investigated as an analogue for some ILW-GDF conditions. Previously a lime kiln waste facility the materials deposited on site include lime, coal ash and calcined limestone (Milodowski et al., 2015). Highly alkaline (> pH 12.0) leachates dominated by calcium hydroxide are produced as a result of groundwater and rain filtering through the waste form and flowing downstream, surfacing at the brook bottom valley (Milodowski et al., 2015). Leaches react with bicarbonate water and carbon dioxide in the atmosphere leading to soft limestone deposits of calcium carbonate developing at the valley bottom (Figure 2.1), an area that rarely becomes diluted with fresh water therefore preserving an alkaline pH (Burke et al., 2012) (Milodowski et al., 2015).

Figure 2. 1. Buxton lime kiln site exhibiting calcination of limestone on the grounds surface.
Figure taken from (Milodowski et al., 2015)

Studies have shown that beneath the surface of tufa deposits the sediment harbours an active microbial community including unidentified species of Bacteroidetes, Comamonadaceae and Firmicutes (Burke et al., 2012). Experiments carried out by Rout *et al* indicated the presence of ISA in alkaline leachates from the Harpur Hill site, as well as revealing that the microbial consortia detected in extracted sediment cores were able to degrade all forms of the ISA present (Rout, Charles, Doulgeris, et al., 2015) (Rout, Charles, Garratt, et al., 2015). The degradation of ISA utilizing Buxton sediment has been demonstrated over a range of alkali pH under iron reducing, sulphate reducing and methanogenic conditions, in addition to using acetate and lactate as electron donors (Bassil, Bryan, & Lloyd, 2015) (Rizoulis, Steele, Morris, & Lloyd, 2012). Illumina MiSeq analysis of extracted soil samples reveals a diverse community of microbes present at this hyperalkaline site where Proteobacteria is the dominating phylum, followed by Firmicutes and Bacteroidetes (Kyeremeh, Charles, Rout, Laws, & Humphreys, 2016).

2.3 Biofilm Formation

Biofilms are an accumulation of microbial cells, usually at an interface or surface, embedded in a matrix known as extracellular polymeric substances (EPS) which function entirely differently to planktonic cells (Wingender, Neu, & Flemming, 1999). EPS contains a spectrum of biopolymers including extracellular DNA (eDNA), lipids, polysaccharides and proteins, which give the biofilm structure and stability in addition to providing cohesion properties to allow the biofilm to attach to a multitude of surfaces (Flemming, Neu, & Wozniak, 2007). For the majority of biofilms the EPS matrix will accommodate >90% of the total mass, with the microorganisms only accounting for the remaining <10% (Flemming & Wingender, 2010). Microbial consortia of mixed species are easily established within biofilms due to close cell-cell proximity, which is enhanced by cell immobilisation qualities of the extracellular matrix. Furthermore, dissolved nutrients within the water phase of EPS can be digested by retained enzymes and subsequently used as an energy source for microbial cells (Flemming & Wingender, 2010). The EPS component of biofilms can act as a protective barrier from external factors including pH shifts, osmotic shock and radiation from the sun (Davey & O'Toole, 2001). Increased antibiotic resistance can occur as a result of biofilms providing protection by delaying antibiotic penetration, housing slow-growing bacteria and providing adapted microenvironments (Stewart, 2002). A recent study by Charles *et al* (2017) demonstrated the ability of an alkaliphilic microconsortia to adapt its microenvironment in response to external pH stresses to aid in the survival of these microorganisms at high pH. Results of micro pH profiling performed on surviving flocculates revealed that a shift in pH was occurring through the centre of the microbial flocs due to the presence of a hydrophobic core (Charles, Rout, Patel, et al., 2017).

Biofilm formation is a process dependant on several factors including surface material and composition, species of bacteria and gene products and is initiated by the adhesion of bacterial cells (Dunne, 2002). The first stage of this process involves surface conditioning that enables primary adhesion to occur. A conditioning film composed of water molecules, proteins and ions that exist in the surrounding medium can affect the hydrophobicity of the surface and subsequently the

interactions to it (Boland, Latour, & Stutzenberger, 2000). An example is shown by Herrmann *et al* who demonstrated that when Fibronectin and other plasma proteins were coated onto polymethylmethacrylate the attachment of coagulase-negative staphylocci to the surface was enhanced (Herrmann et al., 1988). Surface chemistry assumes that organic matter present within solution will congregate within the vicinity of an interface or surface in a similar manner that microorganisms will gather towards an area rich in nutrients (Costerton, Lewandowski, Caldwell, Korber, & Lappin-Scott, 1995). The primary phase of bacterial adhesion involves “docking” of a planktonic microbe to a nearby (<1 nm) conditioned surface through both repulsive and attractive forces including van der Waals forces and hydrophobic and electrostatic interactions (An, Dickinson, & J, 2000). Microbial cells will either propel over surfaces through the fluid, interact through a chance encounter, or be driven through motility and chemotaxis towards the surface (Dunne, 2002). During the primary stage adsorption of microorganisms is reversible and permanent adhesion is dependent on composition of the conditioning film (Boland et al., 2000). Irreversible adsorption occurs during the “locking” or secondary phase whereby fibrillae or fimbriae adhesion structures of the cell bind to specific receptors on the surface material (Dunne, 2002). In aquatic systems the pilus of mannose-sensitive hemagglutinin was shown to be integral as the essential adhesion for formation of biofilms by locking on to abiotic surfaces (Watnick, Fullner, & Kolter, 1999). During this secondary stage aggregates of planktonic cells begin to form upon the surface, with the attachment of one species leading to the potential adhesion of another (W. et al., 1998). Irreversible attachment initiates the maturation phase of a biofilm in which surface-bound cells begin to divide and generate components of EPS leading to an increase in biofilm mass and complexity, a progression that can be limited by lack of available nutrients, as well as environmental factors such as osmolarity and internal pH (Carpentier & Cerf, 1993) (Dunne, 2002). During the later stages of maturation cells situated directly upon the surface become dormant or die due to nutrient deficiency while the external layer of biofilm produces planktonic cells that break loose and are free to occupy other nearby surfaces, as well as shedding bulk biofilm material voluntarily producing small aggregates or flocs (Figure 2.2) (Dunne, 2002) (Donlan, 2002). Population density within a biofilm is controlled through quorum sensing, or cell-cell communications, by releasing signalling molecules known as autoinducers to regulate gene expression (Li & Tian, 2012).

While biofilms can be considered slow developing due to having limited space for cells grow, they have an advantage over planktonic cultures in that they can harbour diverse microbial communities in range of environments on both abiotic and biotic surface (Stewart & Franklin, 2008) (Kostakioti, Hadjifrangiskou, & Hultgren, 2013).

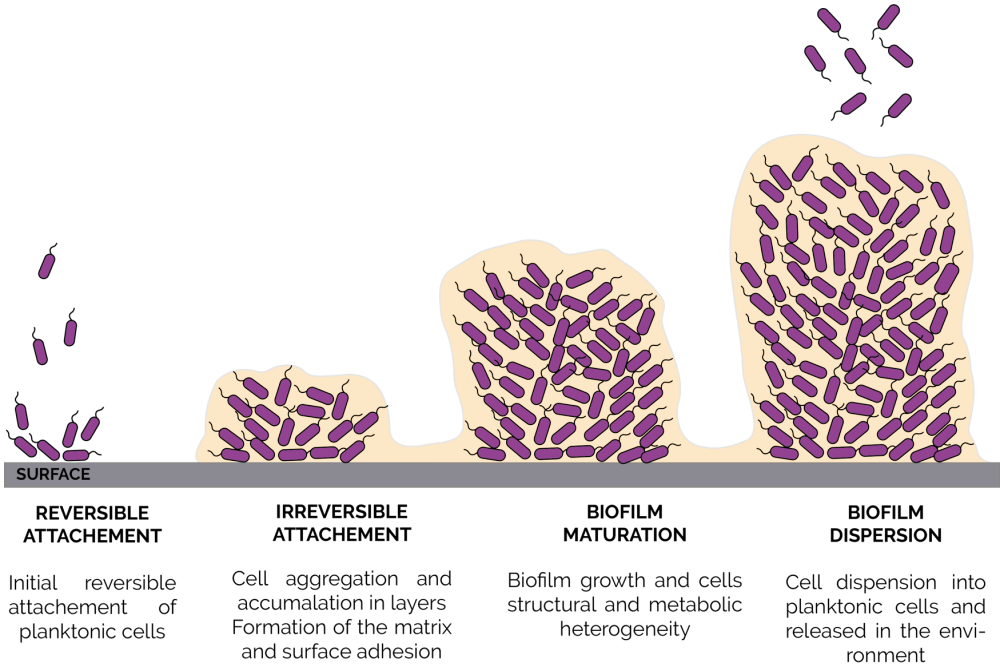

Figure 2. 2. The formation of a microbial biofilm. 1) Planktonic cells attach to conditioned surface 2) Cells accumulate and EPS forms 3) Maturation of biofilm 4) Cells begin to disperse and escape the biofilm.

2.3.1 Impact of biofilms on subsurface transport under ILW-GDF conditions

Microbial biofilm formation is a process sometimes used as a survival technique for microorganisms living under environmentally harsh conditions through the enhanced resistance to external stresses such as pH, low temperature and UV radiation (Yin, Wang, Liu, & He, 2019). The presence of biofilm communities in these diverse and extreme environments has been demonstrated, including in alkaline hot springs of the Copahue geothermal area in Argentina (Urbieta, González-Toril, Bazán Á, Giaveno, & Donati, 2015) and of the Lower Geyser Basin in Yellowstone National Park, USA (Schubotz et al., 2015) in addition to colonisation of surfaces in aquatic

systems operating at temperatures as low as 4°C (Kelley, Turng, Williams, & Baer, 1997). A recent study by Charles *et al* presented evidence of successful biofilm formation under highly alkaline, anaerobic and calcium saturated conditions, analogous of those set to dominate an ILW-GDF. At pH 11.0 aggregates of loose biofilm material known as flocs were able to attach and successfully colonise to form biofilms on the NRVB surface used in a GDF's cementitious backfill. Level of surface adhesion decreased at pH 12.0, with only the flocs and associated EPS material sparsely attached to the NRVB at pH 13.0 (Charles, Rout, Laws, et al., 2017). If microbes are able to freely transport and colonise surfaces in this harsh environment there is potential for biofilms communities and their processes to directly and indirectly affect the long-term performance of a GDF (Humphreys, West, et al., 2010).

The production of biomass in porous media can result in bioclogging within cracks and pore throats, a process that affects permeability and porosity of the media (Abdel Aal, Atekwana, & Atekwana, 2010). Generally, biofilm aggregation and the formation of micro-colonies have a greater impact on hydraulic conductivity than bulk EPS production as a result of completely clogging small pores within the host rock, rather than filamentous biofilms dividing large pore holes into smaller sections (Abdel Aal et al., 2010) (Hand, Lloyd, Vaughan, Wilkins, & Boult, 2008) (Coombs et al., 2010). In crystalline host rock microbial biofilms can hinder the movement of contaminants through reduction of groundwater flow as a result of mineral precipitation. In addition, biofilms are able to minimise permeability of the media by behaving as a filter to catch colloids and mineral particles (Coombs et al., 2010). However, microbes can also alter sorption properties of the host rock if biofilms embed themselves between the rock surface and the surrounding fluid, with Anderson *et al* showing a reduced level of adsorption of thorium, cobalt and neptunium upon subsurface granite coated in microbial biofilm (Anderson, Jakobsson, & Pedersen, 2007). A reduction in ISA sorption to cement backfill material has been observed in alkaline systems (<pH 13.0) due to the presence of a microbial biofilm restricting interaction of ISA to the NRVB surface, therefore potentially enhancing migration of the ISA through a GDF to the near field (Charles, Rout, Laws, et al., 2017). Biofilms established on NRVB can also induce the formation of crystals through microbial carbonate precipitation, which physically

modifies the surface porosity of the cement material and subsequently the ability for radionuclides to successfully sorb to it (De Muynck, Debrouwer, De Belie, & Verstraete, 2008). Rout *et al* demonstrated that microbial biofilms were able to readily form on radioactive graphite under alkaline conditions but did not give rise to a release of gaseous ^{14}C from these samples into the near field (Rout et al., 2018). As discussed in section 1.4.3 certain radionuclides are able to complex with ISA making them mobile under ILW-GDF conditions. However, if microorganisms surviving in these harsh environments are able to degrade the complexing agent this could potentially preserve the long-term storage of radioactive elements within geological disposal facilities.

2.4 Microbial Processes Relevant to ILW-GDF

ISA and other associated CDPs generated via alkaline hydrolysis of cellulose could support the metabolism of microorganisms within an ILW-GDF by providing a vital carbon source. Potential terminal electron acceptors (TEA) will be limited due to subsurface thermodynamics (Bethke, Sanford, Kirk, Jin, & Flynn, 2011) so it's expected that the most likely TEA's will already be present within the vicinity of a GDF or its near field. The majority of natural ground waters within the UK house an abundance of sulphate (Shand, Edmunds, Lawrence, Smedley, & Burke, 2007) suggesting this would be the most probable TEA utilized by microorganisms here, subsequently giving rise to sulphate reducing conditions within the repository. In addition, CDP's and other organics will yield a number of electron donors which in turn will generate other TEAs through microbial metabolism including Fe(III) and nitrate (Bassil et al., 2015). The generation of acetate and other volatile fatty acids (VFA) during fermentation will provide essential electron donors required for subsequent anaerobic respiration, in addition to iron and uranium operating as TEA for the microbial reduction of metals.

2.4.1 Bacterial fermentation

Fermentation processes take place anaerobically by relying on energy synthesised during oxidative phosphorylation in systems where no other high energy TEA is available. Nucleic acids, protein, lipids and polysaccharides undergo hydrolysis to generate sugars (tetroses, pentoses and hexoses), organic acids and amino acids, which are further degraded during the fermentation process yielding a number of alcohols and VFA, together with hydrogen and carbon dioxide gases (Figure 2.3). These are collectively known as fermentation end products, a potential fuel for downstream microbial processes such as sulphate reduction to occur (Müller, 2008).

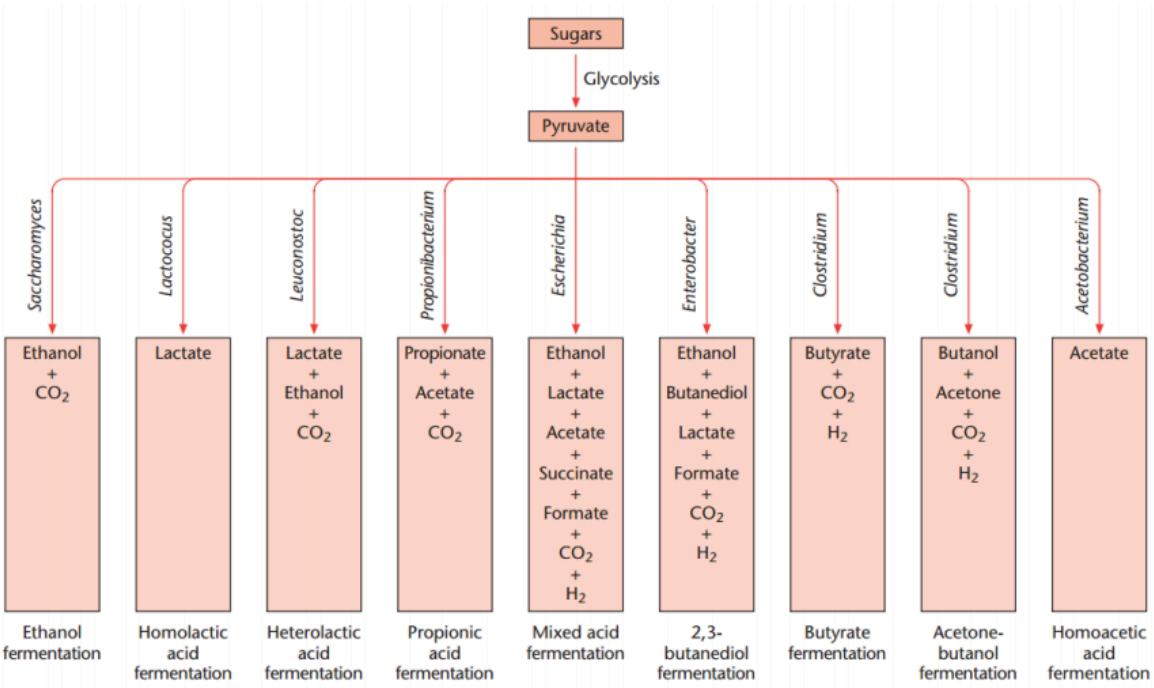

Figure 2. 3. The numerous fermentation end products generated from the breakdown of sugars by different bacteria. Figure taken from (Müller, 2008)

2.4.2 Sulphate reduction

The assimilatory and dissimilatory pathways are two mechanisms utilized for the reduction of sulphate. During assimilatory reduction, only the minimum amount of sulphate is reduced in order to accommodate nutritional needs of the cell. The dissimilatory pathway is used by SRB, an obligate anaerobe, during anaerobic respiration by employing sulphate as TEA in addition to using a variety of electron donors such as hydrogen and organic acids (Peck, 1961) (Muyzer & Stams, 2008). SRB are well known for their ability to thrive in a range of extreme conditions including hypersaline Mono Lake (California, USA) where sulphate reduction was measured in the range of 7.6×10^{4} - 3.2×10^{-6} hr^{-1} (Kulp et al., 2006) and in the alkaline hot springs of Yellowstone National Park (Wyoming, USA) where the highest measurable rates of reduction were 483 ± 300 nmol cm^{-3} day^{-1} (Roychoudhury, 2010). Their survival under these diverse conditions is supported by the capacity of SRBs to also utilize nitrate, iron and manganese as TEAs in sulphate-limited environments (Marietou, 2016). Dissimilatory sulphate reduction produces sulphide (a corrosive agent) (Figure 2.4) as an end product, heavily influencing the corrosion of metals through microbially induced corrosion (MIC) (Bertran et al., 2018). MIC is an important factor to consider when assessing the long-term safety of an ILW-GDF and its steel components, as some SRB can utilize metallic iron as an energy source and then consume the hydrogen produced during the corrosion process, subsequently accelerating corrosion rates (Rajala et al., 2015). SRB biofilms can enhance corrosion of metal surfaces by accumulating hydrogen sulphide within the EPS matrix forming localised areas of corrosion known as corrosion pits (Heggendorn et al., 2018).

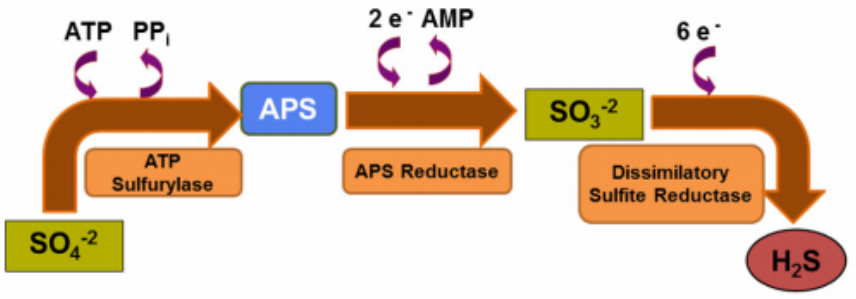

Figure 2. 4. Dissimilatory sulphate reduction pathway. Figure taken from (Carbonero et al., 2012)

2.4.3 Methanogenesis

Methanogenesis is a process carried out by members of archaea (exclusively) by utilizing fermentation products generated during anaerobic degradation. Methanogens can be categorised by order, of which there are 5: Methanomicrobiales, Methanobacteriales, Methanococcales, Methanopyrales and Methanosarcinales (Luo et al., 2009) Different pathways exist for the metabolism of methanogens, each using various electron donors, these include the acetotrophic pathway which uses acetate and the CO_2 reduction pathway which utilises H2 or formate (Ho et al., 2016) (Pan et al., 2016). Surakasi *et al* successfully isolated methanogens extracted from a soda lake operating at pH 10, with Worakit *et al* isolating four alkaliphilic methanogens from low-salt sediments (Surakasi et al., 2007) (Worakit et al., 1986). Recently, Wormald *et al* was

2.4.4 Microbial degradation of ISA

The ability of microorganisms to degrade ISA under aerobic and anaerobic conditions has been investigated extensively. Studies by Strand *et al* looked into the utilization of α-ISA, a Kraft paper by-product, as a substrate for microbial growth under aerobic conditions. A number of environmental isolates, including samples taken from the influent and effluent of a pulp mill pond, indicated the degradation of α-ISA by *Ancylobacter aquaticus* at pH 7.2 - 9.5 (Strand, Dykes, & Chiang, 1984). Investigations by Rout *et al* explored how under sulphate reducing, methanogenic and iron reducing conditions bacteria present in anaerobic circumneutral canal sediments were able to successfully degrade α and β forms of ISA, with the dominating TEA being sulphate (Rout et al., 2014). In a similar study, Rout *et al* explored the degradation of ISA under methanogenic conditions up to pH 10.0 by a non-alkaliphilic consortium found in neutral pH sediments. Methane generation was detected at pH 7.5, 9.5 and 10.0 as well as the degradation of both α- and β-ISA over a 7-day period. Members of Clostridia drove the majority of ISA fermentation that occurred and hydrogenotrophic methanogenesis dominated the methanogenic pathways, illustrating the neutral community's ability to shift diversity under extreme conditions (Rout, Charles, Doulgeris, et al., 2015). Studies using bacteria found in alkaline Harpur Hill sediment revealed that calcium ISA was degraded under

anaerobic and alkaline (~pH 10.0) cultures, as well as coupling this process to the reduction of iron(III) and nitrate (individually), although no degradation was observed in cultures operating under sulphate reducing conditions (Bassil et al., 2015). Rout *et al* investigated and established for the first time the *in-situ* generation of both ISA diastereomers within hyperalkaline anthropogenic sites up to pH 10.0. Furthermore, the microbial community surviving in this environment was capable of fermenting the ISA present, indicating that the population may have developed over time to utilize ISA as an electron donor for growth (Rout, Charles, Garratt, et al., 2015). A study by Charles *et al* confirmed previous reports that bacteria existing within these hyperalkaline conditions were capable of producing ISA and other associated CDPs. Cellulose cotton was incubated *in-situ* with alkaline leachate and then transferred to laboratory microcosms operating at at pH 11.0. After two weeks fibres were visibly coated with EPS material representative of biofilm formation and it was reported that partial degradation of the cotton had taken place, indicating alkaline hydrolysis of cellulose by a microbial biofilm under conditions analogous to a GDF (Charles et al., 2015b).

2.4.4 Bacteria-metal interactions

2.4.4.1 Heavy metal and radionuclide toxicity

The toxicity of heavy metals to bacteria has been broadly investigated in communities present within sediment (Oliveira & Pampulha, 2006), bacteria in mixed liquid cultures (Saeki, Kunito, Oyaizu, & Matsumoto, 2002) and species in pure isolates (Madhaiyan, Poonguzhali, & Sa, 2007). Over time soils can become contaminated with heavy metals including nickel (Ni), lead (Pb), arsenic (As) and chromium (Cr) through leaching of wastewater, sewage sludge, applied fertilizer and other anthropogenic sources (Wuana & Okieimen, 2011). Uptake of heavy metals into the bacterial cell occurs via ion channels and can have detrimental effects on physical and chemical properties of the cell (Monballiu et al., 2015). Ni causes oxidative stress and cell membrane disruption in bacteria, Pb causes destruction of proteins and nucleic acids (Fashola, Ngole-Jeme, & Babalola, 2016) and Cr inhibits bacterial growth and the uptake of oxygen (Cervantes et al., 2001). Heavy metal toxicity to microorganisms is dependent on environmental factors including pH, presence of humic acids and temperature which can have knock on effects on the

bioavailability of metals towards the microbes. Occasionally however, bacterial growth can be enhanced by the presence of metal until such a concentration is reached that growth becomes inhibited (Banaszak, Rittmann, & Reed, 1999). Microbial detoxification involves a number of processes that microorganisms undertake in order to survive in the presence of these metals including metal-organic complexation, surface sorption and heavy metal reduction (Igiri et al., 2018). In environments of elevated nickel concentrations certain microorganisms respond by manufacturing nickel efflux pumps to release high levels of the toxic metal from inside the cell. *Escherichia coli* and *Cupriavidus metallidurans,* an extremophile, are both known microbial species known to exhibit features characteristic of nickel-resistance (Macomber & Hausinger, 2011). Metal toxicity can also be minimized in the presence of chelating agents, with Puls *et al* reporting that inhibitory effects of cadmium are reduced following the metal sorption to clay minerals Montmorillonite and Kaolinite (Puls & Bohn, 1988).

Chemical toxicity is similar when regarding radioactive metals, in particular actinides thorium (Th) and uranium (U), but with the added radiotoxic impact of ionization (Shtangeeva, 2004). Actinides can penetrate the groundwater through leaching of nuclear waste contaminants, entering environments that are highly alkaline, strongly reducing and anoxic and in large quantities these actinides, like Pb, become toxic due to offering no biological benefit to microorganisms (Banaszak et al., 1999). Microbial DNA material can be significantly damaged and/or altered by ionizing radiations in addition to radioactive gamma rays potentially supressing reproductive capabilities of the bacteria (Shukla, Saraf, & Parmar, 2017). However, an investigation by Ruggiero *et al* revealed that chemical toxicity, rather than radiological toxicity, is the dominating mechanism (Ruggiero et al., 2005).

2.4.4.2 Microbial metal reduction

Dissimilatory metal reduction is a process that occurs as a result of microorganisms utilizing heavy metals and certain radioactive elements as TEAs in the absence of oxygen. By coupling this process with the oxidation of alcohols or organic acids some microbes are able to conserve energy to sustain their survival in harsh environments (Lovley, 1993).

Iron(III)-reducing microorganisms are known to be responsible for oxidizing organic material present within subsurface environments where Fe(III) is potentially a dominant TEA for anaerobic respiration. A number of Fe(III) reducers have been identified in the environment, including *Shewanella*, *Desulfromonas and Pelobacter* species, all of which employ different electron donors in the process of reduction including hydrogen, lactate, formate or acetate (Lloyd, 2003). Due to the presence of iron within an ILW both in a GDF's structural components and within the wasteform itself it's crucial to investigate the behaviour of iron in these environments (Williamson et al., 2014). A study by Williamson *et al* looked into the microbially mediated reduction of Fe(III) under high pH conditions analogous to an ILW-GDF using anthropogenic Harpur Hill sediment. In anoxic microcosms with added lactate they observed an increase in extractable Fe(II) concentration in comparison to anoxic only systems where minimal reduction occurred, a reaction that was further enhanced by the incorporation of anoxic electron shuttle riboflavin. Results here indicate that under conditions of a GDF where the presence of organic acids is expected Fe(III) reducers could employ ISA as an electron donor for microbial growth, in addition to utilizing electron shuttles to transfer electrons at a quicker rate (Williamson et al., 2013).

The presence of uranium-reducing microorganisms is vital for the control of uranium mobility and geochemistry in subsurface environments that have been contaminated by radioactivity. Whilst Uranium (VI) exists in a thermodynamically stable state under highly alkaline, anoxic and moderately reducing conditions, it's U(IV) that will dominate in these environments (Xavier Gaona, Kulik, Mace, & Wieland, 2012). U(VI) is reasonably soluble in comparison to the relatively insoluble U(IV), but is able to readily bind to minerals (ie. Ferrihydrite) through sorption processes, leading to investigations into U(VI) biogeochemistry and its manipulation under conditions set to prevail with in an ILW-GDF. In a study by Williamson *et al* the reduction of U(VI) to U(IV) using anthropogenic Harpur Hill sediment was reported at pH 10.0 – 10.5 for the first time. In microcosms with added electron donor only 45.5 $\pm$ 2.8% of U(VI) remained in solution after 1hr. In microcosms incubated with Fe(III) as ferrihydrite in addition to an electron donor 95.1 $\pm$ 0.2% of uranium demonstrated sorption to the sediment after 1hr, indicative of bioreduction to U(IV). Bacteroidetes and Firmicutes were the dominating phyla at the end of these experiments (Williamson et al., 2014).

Uranium reduction by SRB has been investigated in a number of studies. Lovley and Phillips reported the ability of *Desulfovibrio Sulfuricans* to reduce uranium, with cytochrome c_3 being a key element to this process (Lovley & Phillips, 1994). Tebo and Obraztsova revealed that uranium can act as an electron acceptor for the growth of *Desulfotomaculum reducens* sp nov MI-1, a spore-forming SRB (Tebo & Obraztsova, 1998). Ganesh *et al* demonstrated that U(VI) in complexation with an aromatic ligand could successfully be reduced to U(IV) by *D. Sulfuricans* (Ganesh, Robinson, Reed, & Sayler, 1997).

2.5 Summary of Chapter

A number of processes are expected to take place under the chemically reducing, alkaline and anaerobic conditions of an ILW-GDF. Microorganisms are expected to colonise both the near- and far-field environments, with biofilm formation potentially enhancing their survival under the harsh environmental stresses. ISA degradation has been reported under conditions that range from neutral to hyperalkaline pH values (~pH 7.0 – 11.0), indicating this process is likely to occur throughout the geosphere that surrounds a GDF. There is potential for biofilms to drive the removal of complexant ISA, in addition to modifying the surface chemistry of the host environment to further protect the long-term performance of an ILW-GDF. Additionally, microbial populations present could hinder radionuclide transport through metal-microbe interactions.

Chapter 3.0 Methods for the Characterisation and Investigation of Microbiology within Model and Natural Systems

3.1 Overview

Various scientific techniques available today successfully allow for the analysis of both model and natural microbially diverse systems. The isolation, cultivation and characterisation of microbes from environments analogous to potential geological disposal sites can generate information about the processes expected to occur that could affect the long-term performance of the waste facilities. ILW-GDF conditions can be simulated in controlled laboratory settings in order to replicate these environments. By means of modern molecular approaches and utilising the 16S rRNA gene, complete microbial communities and their individual functions can be analysed and characterised at species level, giving an even deeper depth of understanding here. Furthermore, visualisation of biofilms and their components through advanced microscopic techniques can provide an insight into their surface attachment and growth under GDF conditions. Also, the use of column experiments to simulate far-field conditions and the materials present within that environment allow the transport of radioactive contaminants to be investigated. This chapter will discuss the current methods employed for the analysis and characterisation of microorganisms within natural and model systems.

3.2 Culturing Techniques

The direct culturing of microbes from environmental samples is an important initial technique in the study of environmental microbiology. Using either solid or liquid media, an array of microorganisms can be isolated depending on the culture conditions set in place such as pH, O_2 level, temperature, carbon source and nutrients (Rappé & Giovannoni, 2003). The installation of microcosms to simulate specific environmental conditions within the laboratory is an effective method widely used for the isolation and characterisation of both pure and mixed cultures. These types of systems can either be developed using a waste/feed method whereby the necessary nutrients are supplied on a scheduled or continuous basis in order to enrich the existing microbes, or in a sealed reactor where the chemistry gradually develops over time in order to isolate certain types of microorganisms. By establishing microcosms, particular in a batch series, the production and consumption of substances can be easily analysed within the laboratory, yielding

vital information in regards to the processes that take place under certain conditions, in addition to the microbial community that may be present in that environment. Numerous studies within the literature describe the set-up of long-term batch microcosm experiments. Wormald *et al* used batch microcosms to detect and measure the generation of methane from sediment samples collected from lime kiln waste sites (Wormald, Rout, Mayes, Gomes, & Humphreys, 2020). A batch-fed microcosm established by Rout *et al* was set-up to monitor ISA fermentation processes coupled with the generation of methane under ILW repository conditions (Rout, Charles, Garratt, et al., 2015). Batch microcosms were prepared to study the activity of microorganisms under different pH conditions (Smith, Rizoulis, West, & Lloyd, 2016) and to ascertain rates of sulphate reduction, mineral formation and cell growth within acid mine drainage locations (Meier, Piva, & Fortin, 2012). Enrichment cultures do not always necessarily represent the specific processes that may occur in-situ as direct culturing may bring about selection bias under strict conditions. The isolation of microorganisms from environmental samples is possible using growth media containing essential nutrients, streak plate techniques and serial dilution methods. However culturing and isolating particular organisms within a microbial community remains an extremely difficult task, with some proving to be unculturable (Rappé & Giovannoni, 2003). Direct culturing alone can only provide a limited amount of information about the organisms of interest so by coupling this with microscopy and DNA sequencing techniques a more detailed analysis of environmental systems can be produced.

3.3 Nucleic Acid Techniques

Genetic information concerning the microbial communities within environmental samples or laboratory enrichment cultures can be retrieved through extraction of nucleic acids and their subsequent sequencing. The sequencing of DNA allows the genes present to be identified, however RNA is required to determine which of these genes are actively switched on within the community. Griffiths *et al* developed a rapid direct method for the coextraction of DNA and RNA from environmental samples which can produce high quality results in short timeframes (Griffiths, Whiteley, O'Donnell, & Bailey, 2000). For an even quicker protocol, scientific companies sell various commercial DNA extraction kits for specific samples, such as

DNeasy UltraClean Microbial Kit for the isolation of pure organisms or DNeasy PowerSoil Kit for soil and sediment samples (both Qiagen, Germany) (Lear et al., 2017). However, presence of minerals, humic acids, clay material or issues due to low biomass can lead to problems during the extraction of nucleic acids from samples (Hurt et al., 2014).

3.3.1 Amplicon sequencing

Polymerase chain reaction (PCR) is a beneficial technique to use in situations mentioned above where the sample of interest contains very little biomass and therefore only amplifies specific regions of the genomic DNA (gDNA). PCR employs a heat-stable DNA polymerase, in this case “Taq polymerase”, an enzyme isolated from *Thermus aquaticus* bacteria (Verma, Sharma, Sharma, & Shrikot, 2014). Complimentary oligonucleotide primers are added to the PCR reaction and bind to DNA strands at the 3’ end to amplify the region of interest using Taq. A series of cycles heat and cool the PCR reaction exponentially which amplifies DNA in the presence of deoxynucleoside triphosphates (dNTPs), the substrate of DNA polymerase (Stillman, 2013). Taq polymerase is able to withstand the extreme temperatures due to its thermophilic nature. As a highly conserved sequence the 16S rRNA gene is a popular target for PCR amplification within microbial community studies of diverse environmental samples and its sequence is commonly used to draw comparisons between different species. Following amplification, gel electrophoresis techniques are used to separate PCR products based on their GC content over a chemical gradient. PCR-generated chimeras may occur when DNA polymerases stop prematurely and the incomplete elongated strands of DNA anneal resulting in a mixed template of two sequences (Omelina, Ivankin, Letiagina, & Pindyurin, 2019). In addition, it is also possible that some of the DNA cannot be amplified due to primer bias, leading to whole microbial communities being misrepresented (Acinas, Sarma-Rupavtarm, Klepac-Ceraj, & Polz, 2005).

3.3.2 Next generation techniques

The generation of millions of 16S rRNA gene copies allows a more in-depth evaluation of bacterial systems by means of various high-throughput procedures. Metagenomic and metatranscriptomic sequencing techniques have become possible

by the development of powerful sequencing platforms such as Illumina HiSeq, generating data regarding the present (metagenome) and active (metatranscriptome) genes from both mixed and pure environmental samples. Metatranscriptomic analysis more accurately reflects the microbial community as it sequences cDNA from rRNA therefore providing information regarding only actively metabolising microbes, whereas metagenomics (using rDNA) also describes dormant or inactive species (Milanese et al., 2019). A study by Moeseneder *et al* compared RNA and DNA libraries from the same marine community and discovered individual phylotypes could be characterised based on the rRNA genes (Moeseneder, Arrieta, & Herndl, 2005).

3.3.3 Microbial 16S community analysis

Next generation sequencing techniques allow entire microbial communities to be analysed within the laboratory by utilizing the 16S rRNA gene to produce data sets comprising millions of individual species. Speciality software packages enables the user to analyse sequences, in addition to categorizing them according to their taxonomic ranking and allow comparisons of communities from multiple samples. EzBioCloud by ChunLab (South Korea), for example, generates operational taxonomic units (OTUs) to classify closed related sequences and other diversity statistics which can further describe the microbial population within a community (Yoon et al., 2017). Alpha diversity statistics produce rarefaction curves to demonstrate the level of sequencing performed within a sample where a plateaued curve indicates complete saturation therefore sufficient sequencing achieved. This method accounts for libraries of varying sizes to aid in comparison (Willis, 2019). Rank abundance curves indicate species richness within the microbial population and are useful tools for studying changes in a community over periods of time (Avolio et al., 2019). Quantitative analysis of the diversity and abundance of species within microbial communities can be measured using Shannon diversity indices (Keylock, 2005). Next generation sequencing techniques involve using a reference to align sequences, such as the Silva reference alignment (Quast et al., 2013) then using platforms such as the BLAST algorithm (M. Johnson et al., 2008) to compare sequences to previously identified species within the database. UCHIME is

subsequently utilized to analyse any chimeric sequences (Edgar, Haas, Clemente, Quince, & Knight, 2011).

3.4 Microscopy Techniques

In-depth and direct visualisation of microbial systems is made possible through an array of modern microscopy techniques. The approach of scanning electron microscopy (SEM) is widely utilized within the literature and allows the framework of microbial biofilms to be viewed in addition to the arrangement of individual cells due to high magnification and resolution (El Abed, Saad, Latrache, & Hamadi, 2012). SEM was employed for the visualisation of *Staphylococcus aureus* biofilm within skin lesions in the presence of LL-37, an antimicrobial peptide (Sonesson et al., 2017). Baum *et al* studied the structural components involved in biofilm assembly using SEM, presenting useful details on the identification of microbial biofilms *in vivo* (Baum et al., 2009). Bacterial specimens are prepared for SEM analysis by fixation and drying of samples, following by application of a conductive coating to enable visualisation under high vacuum (Priester et al., 2007). The application of SEM coupled with energy dispersive X-ray analysis (EDX) provides an even deeper understanding by generating both quantitative and qualitative elemental information about the sample of interest (Scimeca, Bischetti, Lamsira, Bonfiglio, & Bonanno, 2018). Özen *et al* utilized SEM-EDX to assess the distribution of heavy metals within soil samples up to 15 m below the surface, with Abdullah *et al* analysing microbially induced corrosion (MIC) products of carbon steel by SRB (Abdullah, Yahaya, Noor, & Rasol, 2014).

By combining microscopy with fluorescent staining techniques, the individual cells and structural components of microbial biofilms can be visualised. Fluorophores SYTO 9 and propidium iodide (PI) are widely applied within microbiology for the detection of live and dead cells, respectively. Live cells emit fluorescence green in colour binding to DNA/RNA, with permeation of dead cells by PI releasing a red fluorescence (Deng, Wang, Chen, & Long, 2020). The EPS components of biofilms and flocs can be individually stained and observed simultaneously, with Charles *et al* revealing microbial flocs surviving at alkaline pH were composed of proteins, lipids, carbohydrates, eDNA and cells (Charles, Rout, Patel, et al., 2017). The use of

individual fluorescent stains coupled with confocal laser scanning microscopy (CLSM) enables high quality, high resolution analysis of microbial biofilms and their architecture. In addition, the locality and distribution of certain EPS components could provide novel insights into adhesion and attachment of biofilms under different environmental conditions.

3.5 Modelling Techniques

Column experiments are commonly used within microbiology to study the transport of contaminants in specific environmental settings on a controlled, laboratory scale. Some studies may focus on the mobility of substances in groundwater alone however others may set-up columns packed with materials such as sediment, clay or cement (Banzhaf & Hebig, 2016). The surfaces of certain materials might play a part in the transport of both organic and inorganic substances as their movement becomes governed by sorption processes that occur at the aqueous-surface interface. In addition, chemistry of the surrounding groundwater, porosity of media and presence of minerals can also influence and potentially hinder mobility. Davis *et al* utilized polyvinyl chloride pipe (PVC) columns to investigate the conductivity of porous media in the presence of microbial biofilms (Davis et al., 2006), with Hutzler *et al* employing sandy loam soil columns to observe the breakthrough and exhaustion of organic chemicals through the sediment (Hutzler, Crittenden, Gierke, & Johnson, 1986). Column experiments are an effective technique to use within the laboratory as it allows control of a wide variety of parameters including flow rate, geological media, substrate and porosity (Banzhaf & Hebig, 2016). The use of these experiments within environmental microbiology are incredibly valuable as they allow hydrogeochemical environments to be simulated on a laboratory scale, enabling the processes and sorption events that may occur to be revealed and analysed.

3.6 Summary of Chapter

The techniques and methodology outlined within this chapter demonstrate how environmental microbiology can be investigated within the laboratory. Microcosms and reactors can be utilized for isolation of a pure organism or development of a particular bacterial population. Microscopic techniques provide qualitative and

quantitative analysis regarding biofilm material and their composition. Next generation sequencing methods allow microbial communities to be described, providing vital insights into their metabolic pathways. Finally, the set-up and operation of column experiments allow behaviours of contaminants within environment under certain conditions to be explored with ease and efficiency within the laboratory.

Chapter 4.0 Aims & Objectives

The performance of natural and engineered barriers encompassing ILW must be assessed to determine how radionuclides may behave under the relevant GDF conditions. The high alkalinity expected to purge the wasteform will give rise to the generation of CDPs, in particular ISA, which are capable of forming soluble complexes with a range of radionuclides. Enhanced migration of radioactive contaminants could lead to their release from the waste form out into the geosphere and subsequently the biosphere. Previous research has focussed on ISA-radionuclide interactions within the hyperalkaline near-field or at circumneutral pH further out into the geosphere, however the highly alkaline conditions of a GDF are expected to prevail post-closure, which indicates that pH of the environment surrounding a GDF will likely remain mildly alkaline. This research will focus on processes that take place within the subsurface that sits between an ILW-GDF and the outer geosphere, known as the far-field.

Biofilms can form on a multitude of surfaces in a range of environmental settings and stresses depending on their microbial populations and can reportedly adapt to survive under harsh conditions. Alkaliphiles and anaerobic microorganisms capable of ISA degradation could play a vital role in the removal of the organic complexants, subsequently restricting the mobility of radionuclides within the far-field. Previous investigations into these processes have focussed on microcosms experiments exclusively, which do not necessarily represent the host environment and flow conditions that are expected.

Work presented within this thesis aims to investigate the behaviours of different elements and radio-elements in the presence of sand as a host-rock substrate by developing flow-cell systems which simulate conditions analogous to that of an ILW-GDF far-field. The sand columns will then be subjected to CDPs and biofilm-forming microorganisms to study the formation of possible ISA complexes, their potential degradation and the long-term fate of radioactive elements within ILW. The use of flow-cell systems here will provide a more accurate representation of how these complexes may behave as they migrate through the host rock. Furthermore, by utilising a range of microscopy and molecular techniques, the composition of both microbial biofilms and their populations will be investigated in other to further understand the processes that may occur within these subsurface environments.

Chapter 5.0 Experimental Methodologies

5.1 General Reagents

Unless stated otherwise all reagents used within experimental methodology described in this thesis were purchased from: Sigma-Aldrich Company Ltd (Dorset, United Kingdom), Fisher Scientific UK (Loughborough, United Kingdom) or Lab M Ltd (Bury, United Kingdom).

5.1.1 Minimal media

Minimal media was prepared by adding reagents in Table 5.1 to a 250 mL Schott bottle containing 250 mL of deionised water. Once fully mixed the solution was purged in a a stream of N_2 gas for approximately 30 minutes before autoclaving under a N_2 headspace at 121° for 20 minutes. Afterwards the cooled media was amended to contain Ni/ Eu/ Th/ U solutions to 1 ppm of the metal salt or contain cellulose degradation products (CDP) or both, and then adjusted to the desired pH of 9.5 using 4M sodium hydroxide or 2M hydrochloric acid as required.

Reagent	Chemical formula	Concentration g/L
Sodium bicarbonate	$NaHCO_3$	2.52
Ammonium chloride	NH_4Cl	0.26
Sodium dihydrogen phosphate	NaH_2PO_4	0.52
Potassium chloride	KCl	0.10
10 mL trace element solution	*See Table 5.2*	*See Table 5.2*

Table 5. 1. Composition of minimal media per 1 litre

Reagent	Chemical formula	Concentration g/ 250mL
Magnesium sulphate heptahydrate	$MgSO_4.7H_2O$	0.7500
Manganese(II) sulphate tetrahydrate	$MnSO_4.4H_2O$	0.1500
Sodium chloride	NaCl	0.2500
Iron(II) sulphate heptahydrate	$FeSO_4.7H_2O$	0.0250
Cobalt chloride hexahydrate	$CoCl_2.6H_2O$	0.0460
Calcium chloride dehydrate	$CaCl_2.2H_2O$	0.0250
Zinc sulphate pentahydrate	$ZnSO_4.5H_2O$	0.0450
Copper sulphate pentahydrate	$CuSO4.5H_2O$	0.0025
Disodium molybdate dihydrate	$Na_2.MoO_4.2H_2O$	0.0025

Table 5. 2. Composition of minimal media trace elements solution per 250 mL

5.1.2 Mineral media

Mineral media was prepared by adding reagents, except disodium sulphide in Table 5.3 to a 1 L Schott bottle containing 1 L of deionised water. Once fully mixed the solution was N_2 purged for approximately 30 minutes before being autoclaved under nitrogen headspace at 121°C for 20 minutes. Afterwards, the cooled media was purged again with N_2 followed by the addition of disodium sulphide to chemically reduce the media, a process illustrated by the redox indicator (Resazurin) becoming clear. Media was adjusted to the desired pH of 11.0 using 4M sodium of hydroxide or 2M hydrochloric acid as required.

Reagent	Chemical Formula	Mass (g/L)
Potassium dihydrogen phosphate	KH_2PO4	0.270
Disodium hydrogen phosphate dodecahydrate	$Na_2HPO_4.12H_2O$	1.120
Ammonium chloride	NH_4Cl	0.530
Calcium chloride dihydrate	$CaCl_2.2H_2O$	0.075
Magnesium chloride hexahydrate	$MgCl_2.6H_2O$	0.100
Iron(II) chloride tetrahydrate	$FeCl_2.4H_2O$	0.020
Resazurin (oxygen indicator)		0.001
Disodium sulphide nonahydrate	$Na_2S.9H_2O$	0.100
10 mL trace element solution	*See Table 5.4*	*See Table 5.4*

Table 5. 3. Composition of mineral media per 1 litre

Reagent	Chemical Formula	Mass (g/L)
Manganese chloride tetrahydrate	$MnCl_2.4H_2O$	0.050
Boric acid	H_3BO_3	0.005
Zinc chloride	$ZnCl_2$	0.005
Copper chloride	$CuCl_2$	0.003
Disodium molybdate dihydrate	$Na_2MoO_4.2H_2O$	0.001
Cobalt chloride hexahydrate	$CoCl_2.6H_2O$	0.100
Nickel chloride hexahydrate	$NiCl_2.6H_2O$	0.010
Disodium selenite	Na_2SeO_3	0.005
Disodium tungstate	$Na_2WO_4.2H_2O$	0.002

Table 5. 4. Composition of mineral media trace elements solution per 1 litre

5.1.3 Production of cellulose degradation products (CDP)

200g of standard laboratory tissue (Pristine paper hygiene, London, UK) was selected as the cellulose source for degradation and CDP was subsequently synthesised as previously described by Rout *et al* (2014). a pressure vessel, 0.1 M NaOH and 10 g/L $Ca(OH)_2$ was added to 1.8 L UPW and N_2 purged for 30 minutes before the addition of laboratory tissue. The vessel was sealed and the headspace flushed with N_2 for 30 minutes before being incubated for 30 days at 80°C. After incubation, the subsequent fluid was filtered under anaerobic conditions through a 0.22 µM Steritop filter (Merck Millipore, UK) and into a 1 L Schott bottle that had previously been autoclaved at 121°C for 15 minutes. Bottles were sealed and stored in autoclaved Schott bottles under ambient conditions.

5.2 Sample Preparation

5.2.1 Liquid preparation

Unless stated otherwise, liquid samples from flow-through experiments were collected and transferred to 15 mL centrifuge tubes. 1 mL aliquots were taken and centrifuged at 10,000 rpm for 5 minutes to remove any particles or bacteria before being stored in sterile 1.5 mL Eppendorf tubes. Both 1.5 mL and 15 mL tubes were stored at -80°C until required for further analysis.

5.2.2 Sand preparation

Post completion of column experiments biofilm sand material was removed under anaerobic conditions and transferred to sterile 50 mL tubes which were stored at -80°C until further analysis.

5.3 Analytical Methodologies

5.3.1 High performance anion exchange chromatography with pulsed amperometric detection (HPAEC-PAD)

5.3.1.1 Detection of ISA

HPAEC-PAD employing a Dionex 5000 ion chromatograph with autosampler was used for the detection and quantification of alpha and beta forms isosaccharinic acids (ISA). A 10μL injection was passed through a CarboPac PA20 (150 mm x 3) guard column before being separated by a Dionex CarboPac PA20 column (250 mm length, 3 mm internal diameter, 6 μm particle size with a 10 Å pore size). An isocratic mobile phase of 50mM NaOH with a flow rate of 0.5 mL/min was used in this system and a regeneration of the column using 200mM NaOH for 15 minutes was performed after every 3 samples. D-Isosaccharinic acid-1,4-lactone (Santa Cruz Biotechnology, Texas, USA) generated a standard curve for the quantification of both alpha and beta forms of ISA and prior to analysis all samples were modified with 25 ppm D-ribonic-acid as an internal standard. Integration and analysis of chromatograms was performed using the Chromeleon 7.0 software package.

5.3.2 Ion chromatography (IC)

5.3.2.1 Detection of ISA

Detection and quantification of isosaccharinic acid (both α and β forms) was also carried out using the Metrohm 930 Compact IC Flex Deg fitted with an IC Amperometric Detector and 889 IC Sample Centre (Metrohm, Switzerland). A 20μL injection was pumped through the a CarboPac PA20 (150 mm x 3) guard column before being separating by a Dionex CarboPac PA20 column (250 mm length, 3 mm internal diameter, 6 μm particle size with a 10 Å pore size). A 50 mM NaOH mobile phase with a 0.3 mL/min flow rate was employed. Standards were prepared as previously described and chromatographic analysis was performed by using the MagIC Net Ion Chromatography software.

5.3.2.2 Cation analysis

A Metrohm Eco IC fitted with a Professional IC Conductivity Detector (Metrohm, Switzerland) was utilized for cation detection and quantification within liquid CDP samples. 20 μL of sample was injected through a Metrosep C 4 – Guard/4.0 (5 x 4.0 mm) guard column then immediately into a Metrosep C4 – 250/4.0 cation column (4.0 x 250 mm). Signals generated were analysed by reprocessing peak areas against a chromatograph of known cation concentrations (Multi Cation Standard for IC, Merck, Germany) using MagIC Net Ion Chromatography software.

5.3.3 Gas chromatography (GC)

5.3.3.1 Detection and quantification of volatile fatty acids

The composition and concentration of volatile fatty acids (VFA) was carried out using a HP GC6890 gas chromatograph system with autosampler (Hewlett Packard). Prior to a 1 μL manual injection samples were acidified by the addition of concentrated phosphoric acid (10% v/v). Using helium as a carrier gas, liquid samples were passed through a HPFFAP column (30 m x 0535 m x 1.00 μm, Agilent Technologies, UK). A blend of hydrogen/ compressed air gas was used to detect VFA's using a flame ionisation detector under the following conditions: initial temperature 95°C for 2 minutes, followed by an increase in temperature to 140°C at a ramp rate of 10°C min^{-1} with no hold, followed by a second increase in temperature to 200°C at a ramp rate of 40°C min^{-1} with a hold of 10 minutes, and finally falling to a post-run temperature of 50°C. Measurements from a 1 μL injection of a 10 mM standard mix of VFA's (Sigma Aldrich, USA) were used to identify and quantify samples against. Chromatographs were produced and processed using the Chemstation software package (Agilent Technologies, UK).

5.3.3.2 Headspace gas composition

An Agilent GC6850 system fitted with a HP-PLOT/Q column with particle traps (35 m x 0.32 mm x 30 μm, Agilent Technologies, UK) was used to measure the composition of reactor headspace gas. Using a lockable syringe 100 μL of headspace gas was removed and injected into the column. With nitrogen employed as the carrier gas, a thermal conductivity detector within the system was used to

identify different gas species with the operating conditions as follows: initial temperature 60°C for 2 minutes, followed by an increase in temperature to 120°C at a ramp rate of 30°C min^{-1} with a detector temperature of 250°C. Standards of gas species with known compositions together with the ideal gas law were used for the quantification of samples using the following equation:

$$PV = nRT$$

Equation 5. 1. Ideal gas law. Where P = pressure (bar), V = volume (L), n = Moles of gas (mol), R = universal gas constant (8.314 L bar K-1 mol-1), T = temperature of gas (K)

5.3.4 Inductively coupled plasma mass spectrometry (ICP-MS)

5.3.4.1 Trace-level elemental analysis

Determination of dissolved metals present in sand column effluent was performed on an Agilent 7700e ICP-MS with an ASX-500 series autosampler. Liquid is introduced into the system via a peristaltic pump before entering a spray chamber where the sample becomes nebulized, resulting an aerosol. Injection of the aerosol into a 6000-8000 K argon-plasma removes any solution from the liquid sample as well as atomizing and ionizing the sample. Only a fraction of the ions generated migrate to a high vacuum area (<0,001 Pa) where positive ions are aimed into a mass spectrometer and ions are separated according to their mass by four metal rods known as a quadrupole. Ion pulses are generated from signals and then measured using a detector known as an electro-multiplier to assign the correct mass number for the pulses. Effluent samples were diluted in sterile UPW and internal standards (Scandium for Ni/ Eu and Rhenium for Th/ U) were added to a final concentration of 100 ppb. Standards of a suitable concentration range were prepared from elemental stock solutions that were made up by dissolving the appropriate metal salt in sterile

UPW. In addition, a blank solution was set up containing UPW that was run alongside the other standards as a control.

5.4 Microscopy

5.4.1 Sample preparation

Unless stated otherwise, biological samples were initially fixed in 4% paraformaldehyde in phosphate buffered saline (PBS) overnight at 4°C, washed twice in PBS, and then covered in a storage buffer solution (Table 5.5) at -80°C until further analysis.

Ingredient	mL per Litre
Ultrapure water (UPW)	350
1M TRIS-HCl (pH 7.5)	25
96% (v/v) ethanol	625

Table 5. 5. Composition of storage buffer solution per 1 litre

5.4.2 Fluorescence microscopy

Live dead staining of flocculates and sand biofilm material was performed using the LIVE/DEAD™ *Bac*Light™ Bacterial Viability Kit (Invitrogen, USA) and visualised on an Olympus BX41 laboratory microscope (Olympus, USA). Flocculates were firstly collected via centrifugation and washed with phosphate buffered saline (PBS) and then stained in-situ with a mixture of SYTO 9 nucleic acid stain (3.34 mM in DMSO) and propidium iodide (20 mM in DMSO). Samples were incubated in the dark for 15 minutes at room temperature before 5 μL of suspension was trapped between a glass slide and square coverslip for observation under the microscope at both 40x and 100x objectives. Excitation and emissions of staining components are listed in Table 5.6. Samples not subjected to stains were also visualised as controls to observe any auto fluorescence.

Component	Excitation (nm)	Emission (nm)
SYTO 9	485	498
Propidium iodide	535	617

Table 5. 6. Excitation and emission values of fluorescent microscopy staining components

5.4.3 Confocal laser scanning microscopy (CLSM)

A Zeiss LSM880 inverted confocal microscope was utilised for imaging of biological samples and the analysis was performed using Zen 2.1 software (Zeiss Microscopy). Microscopy was carried out either at in the Zeiss suite of 3M Buckley Innovation Centre in Huddersfield or at the Bioimaging facility at the University of Leeds.

5.4.3.1 5-colour biofilm EPS staining

Staining and visualisation of extra cellular polymeric substances (EPS) in samples containing bioaggregates was carried out using methods previously described (Chen, Lee, Tay, & Show, 2007). FITc was used for the visualisation proteins, calcofluor white was used to visualise β-1,4 and β-1,3 polysaccharides and Nile red for visualising lipids and hydrophobic sites. Concanavalin A was used to visualise α-mannopyranosyl and α-glucopyranosyl sugars and syto 63 was used for the visualisation of total cells and extracellular DNA. Samples not exposed to stains were also analysed as a negative control and to indicate any auto-fluorescence. Timing and concentrations of stains are shown in Table 5.7, as well as absorption and emission values.

Chemical stain	Concentration	Time (minutes)	Excitation (nm)	Emission (nm)
Calcofluor white	30 mg L-1	30	400	410-480
Concanavalin A (Con A)	25 mg L-1	30	543	550-600
Fluorescein isothiocyanate (FITc)	100 mg L-1	60	488	500-550
Nile red	0.6 mg L-1	15(?)	514	625-700
SYTO 63	2μM	30	633	650-700

Table 5. 7. 5 colour CLSM staining properties

5.4.4 Scanning electron microscopy (SEM) with energy-dispersive X-ray spectroscopy (EDX)

Scanning electron microscopy was performed using a Quanta FEG 250 microscope (FEI, USA) fitted with an Oxford instruments X-Max detector for EDX analysis. Prior

to analysis samples were dehydrated by applying 25, 50, 75 and 100% ethanol dilutions for 2 minutes each step. A thin layer of gold/palladium plasma (15-20nm) was sputter coated (CA7625 Polaron, Quorum Technologies Ltd, UK) on to samples mounted on carbon tape and aluminium stubs (Agar Scientific, UK) to increase conductivity. Oxford instruments INCA software was utilised for EDX elemental analysis.

5.4.5 Optical microscopy

Images of the inner lining of lead pipe sections and samples set in resin were taken using a Keyence VHX-6000 series digital microscope fitted with a VHX-J250 lens. The software package (Keyence) was utilized for visualisation and processing of images.

5.5 Environmental Sample Analysis

5.5.1 pH determination

The pH value of liquid effluent samples, microcosm fluid and liquid media were determined using a portable handheld pH meter (Mettler Toledo, UK) and long reach combination pH probe. Calibration of the probe was performed before each application using pH 4.0, 7.0 and 10.0 buffers.

5.5.2 X-ray diffraction

A D2 PHASER X-ray diffractometer (Bruker) fitted with a LYNXEYE™ detector was employed to perform X-ray powder diffraction (XRD). Samples were crushed to a fine powder using a pestle and mortar after the sand material had been dried for 24 hours at 80°C. Once transferred to a powder specimen holder the sample was scanned for 4 minutes and diffraction patterns were monitored on the DIFFRAC Suite Measurement Centre V4 software before generating graphs through Microsoft Excel.

5.6 Molecular Biology

5.6.1 Extraction of nucleic acids

5.6.1.1 DNA extraction method for liquid samples

The Griffiths method (Griffiths et al., 2000) was adapted for the extraction of genomic DNA from an environmental microcosm (floc reactor). DNAse free reagents were prepared by incubating them with 0.1% diethylpyrocarbonate (DEPC) for 2 hours at 37°C before autoclaving at 121°C for 20 minutes to deactivate the DEPC. A pellet of biological material was collected by centrifugation of 25 mL microcosm liquid for 30 minutes at 4800 rpm. 25 mL pH 7.0 phosphate buffer was then used to re-suspend the pellet as described by Hurt et al (reference) and after a second centrifugation the supernatant was discarded and the pellet finally re-suspended in 5 mL pH 7.0 UPW. Once the pellet was fully mixed and re-suspended 0.5 mL of suspension was added to a 0.1 mm glass bead tube (Fisher Scientific, UK) along with 0.5 mL of phenol chloroform isoamyl alcohol (25:24:1) (Sigma-Aldrich, USA) and 0.5 mL cetyl-trimethylammonium bromide (CTAB) (Fisher Scientific, UK). To prepare CTAB, 0.7 M sodium chloride and 240 mM phosphate buffer were mixed with 10% (w/v) cetyl-trimethylammonium bromide and the resulting mixture was then diluted 50:50 in 240 mM phosphate buffer (pH 8.0). A BeadBlasterTM 24 was then used to homogenise glass bead tubes for 5 cycles of 30 seconds at 5.0 m/s before being centrifuged for 5 minutes at 13,000 RPM. Approximately 450 μL of supernatant was transferred to a sterile 1.5 mL Eppendorf tube in addition to an equal volume of chloroform/ isoamyl alcohol (24:1) (Sigma Aldrich, USA), which was mixed by pipetting to form an emulsion and centrifuged again at 13,000 RPM for 5 minutes. A maximum of 450 μL supernatant was transferred to a sterile 1.5 mL Eppendorf tube along with two volumes of 30% w/v polyethylene glycol-6000 (PEG) (Fisher Scientific, UK) in 1.6M sodium chloride then the tube was mixed and stored at 4°C overnight. After the incubation period tubes were centrifuged for 20 minutes at 13,000 RPM and the resulting supernatant was discarded. The pellet was re-suspended in 200 μL ice-cold absolute ethanol (molecular grade) and washed by centrifuging at 13,000 RPM for 5 minutes. Again, the supernatant was completely removed and the pellet left to air dry

for 10-15 minutes to allow any remaining ethanol to evaporate before re-suspending the pellet in DNAse free UPW.

5.6.1.2 DNA extraction method for biofilm sand samples

Extraction of genomic DNA from biofilm sand samples was also carried out using a modified version of the Griffiths protocol mentioned previously. 0.5 g sand material was removed from columns using a sterile spatula and placed directly into 0.1 mm glass bead tubes, followed by the addition of 0.5 mL of CTAB and 0.5 mL phenol chloroform isoamyl alcohol in the same manner as above. The above protocol resumes here.

5.6.1.3 DNA extraction method for lead pipe material

Genomic DNA from lead pipe material was extracted using the Griffiths method but with a few alterations and attempting two different methods.

Method 1. Direct extraction of material from the inner lining of lead pipe

Material on the surface of the lead pipe inner lining was gently scraped with a sterile spatula into sterile 50 mL tubes along with the stagnant water contained within the pipes. These tubes were centrifuged for 30 minutes at 4800 RPM after which 5 mL supernatant was kept, the remaining supernatant discarded, and the pellet was re-suspended in the 5 mL to make a suspension. 1mL aliquots were centrifuged in 1.5mL Eppendorf tubes for 2 minutes at max speed, after which the supernatant was poured off and the pellet re-suspended in 500 μL 10 mM acetic acid. Pipetting and vortexing mixed the suspension for 5 minutes before 0.5 mL was transferred to a 0.1 mm glass bead tube and continuing with Griffiths method here.

Method 2. Freezing of the lead pipes and then removal of the ice core

Lead pipes were immediately frozen (-20°C) upon arrival to the laboratory and once fully frozen the ice cores were easily removed and stored at -80°C until further analysis. Ice cores were placed into sterile 50 mL tubes and left to defrost before being centrifuged for 30 minutes at 4800 RPM. All but 5 mL of the supernatant was discarded and the pellet re-suspended in the 5 mL to make a suspension. 1mL aliquots were centrifuged in 1.5mL Eppendorf tubes for 2 minutes at max speed,

after which the supernatant was poured off and the pellet re-suspended in 500 μL 10 mM acetic acid. Pipette and vortex techniques were used to mix the suspension for 5 minutes before 0.5 mL was transferred to a 0.1 mm glass bead tube. The Griffiths method protocol then started at this point.

5.6.1.4 Quantification of nucleic acids

The Qubit™ dsDNA HS Assay Kit along with a Qubit™ 4 Fluorometer (Invitrogen, UK) was utilised for the fluorometric quantification of nucleic acids, per the manufacturers instructions. Alternatively, a Jenway Genova Nano Spectrophotometer (Bibby Scientific, UK) was used for spectrophotometric quantification by exposing 1 μL of sample to UV light at a wavelength of 260nm. The extinction coefficient for DNA was used to determine purity ratios.

5.6.1.5 Visualisation of DNA products

Genomic DNA was visualised on 1% agarose gels by employing the gel electrophoresis method. Gels were prepared by mixing 1g molecular grade agarose (Bioline, UK) in 100 mL tris-acetate-EDTA buffer (TAE buffer) to yield a 1% agarose solution. This solution was microwaved for 30-60 seconds until the powder had fully dissolved, after which 1 μL SYBR® safe gel stain was added and the beaker swirled to mix. The hot solution was poured into a gel mould with a well comb fitted and was left to fully set at room temperature for around 20-30 minutes. Set gels were removed from the mould and immersed into an electrophoresis tank containing TAE buffer. Using a pipette 1μL of 5X loading dye (Bioline, UK) was mixed with 5 μL of genomic DNA and then inserted into each well along with 5 μL of 1 kB Hyperladder (Bioline, UK). Electrophoresis of the gels was run for 60 minutes at 100 V and then visualised using the BioDoc-it® 210 Imaging system (UVP LLC, US) under UV light.

5.6.2 Polymerase chain reaction (PCR)

5.6.2.1 Hot start PCR for 16s rRNA gene amplification for microbial community analysis

PCR products for analysis via Illumina MiSeq platform were generated by a hot-start approach, a method used to lower the chance of non-specific amplification of

products and the formation of primer dimers, using a thermocycler. PCR reactions were composed of 25 μL MyTaq™ 2X HS red mix (Bioline, UK), template genomic DNA (10-100 ng), 2 μL of a forward and reverse primer mix (each 20 μM) - sequences of which can be found in Table 5.8 - and DNase free water to top up final volume to 50 μL. The MyTaq™ 2X HS red mix contained reaction buffer, magnesium, dNTPs and Taq polymerase. Reactions were run under the following conditions: an initial denaturation for 1 minute at 95°C then 30 cycles of: denaturation for 15 seconds at 95°C, annealing for 30 seconds at 60°C and extension for 15 seconds at 72°C. Lastly, there was a final extension for 2 minutes at 72°C. PCR products were run on 1% agarose gels for 60 minutes at 100 V before being visualised under UV light in a BioDoc-it® 210 Imaging machine. Genomic DNA was replaced with DNAse free water in negative PCR controls and *Escherichia coli* cultured in the laboratory was utilised as a positive control. All reaction tubes were kept at -20°C until further application or sent for analysis.

Primer	Sequence 5' → 3'	16S region	Reference
314f	TCGTCGGCAGCGTCAGATGTGTATAAGAGACAG CCTACGGGNGGCWGCAG	V4	(Takahashi, Tomita, Nishioka, Hisada, & Nishijima, 2014)
805r	GTCTCGTGGGCTCGGAGATGTGTATAAGAGACA G GACTACHVGGGTATCTAATCC	V4	

Table 5. 8. 16S rRNA gene primer information used for PCR amplification and community analysis

5.6.1.2 Primer synthesis

Primers were prepared in the laboratory to a final stock concentration of 100 pmol/μL as per the synthesis report instructions and using synthesised primers purchased from MWG Operons (Eurofins Genomics, Germany).

5.6.3 Microbial community analysis via Illumina MiSeq platform

Sequencing of both Genomic DNA and PCR products was performed through a commercial service provided by ChunLab (South Korea) using the MiSeq nano

platform (Illumina, USA). Once genomic DNA and PCR amplicons had been generated the next step involved barcoding these amplicons through means of an index PCR technique. Next, the amplicons were purified and quantified then run at 250 bp paired ends via the MiSeq nano platform. Chimeric sequences were identified and then removed using the UCHIME algorithm (Edgar et al., 2011) as well as utilising PandaSeq to merge paired ends (Masella, Bartram, Truszkowski, Brown, & Neufeld, 2012). Phylogeny sequences were assigned by employing the EzTaxon database (Chun et al., 2007) OTU clustering at a 95% confidence interval was implemented through use of CD-HIT-EST programs (Huang, Niu, Gao, Fu, & Li, 2010). Finally, rarefaction curves, rank abundance curves and alpha diversity statistics were generated using the EzBioCloud online bioinformatics suite (Chunlab, South Korea).

5.7 Column Investigations

The main focus of this research involved utilising biofilm sand columns to create a system whereby the conditions within a GDF repository could be replicated on a small laboratory scale. In these systems conditions simulated that of the far field environment of a geological disposal facility where pore water pH isn't as highly alkaline as near field and the surrounding host rock is also geologically different due to its placement around the subsurface. For experiments described here sand was used as a substrate for radionuclide sorption.

5.7.1 Single pass sand column biofilm system

Sterile 300 mm DWK Life Sciences Kimble™ Kontes™ FlexColumn™ Economy columns were filled with approximately 185 g of acid washed Ottawa sand (Fisher Scientific, UK) to fill the column and the sand was then saturated with minimal media (pH 9.5). The system, described in Figure 5.1 was constructed using neoprene tubing (Masterflex, Cole-Parmer, UK) with an internal diameter of 0.31 mm to attach the influent media bottle to a peristaltic pump (Watson-Marlow, UK) leading to the inlet valve of the column, and also to connect the outlet of the column to a CF-2 fraction collector (Spectrum Chemical, USA). A 3-port lid (GL45, Schott UK) fitted to the media bottle also allowed the attachment of N_2 filled gasbag in order to keep the

system anaerobic. For experiments involving Ni & Eu the peristaltic pump passed the influent media mix clockwise at a rate of 0.22 mL min^{-1}, allowing the full volume of the media to pass through the tubing and column in ~18 hours. At the outlet valve effluent dropped into glass test tubes fitted into the fraction collector which shifted one place every 30 minutes, collecting approximately 6 mL per sample. Due to unforeseen circumstances involving laboratory equipment another peristaltic pump (Watson-Marlow, UK) had to be utilized for Th & U experiments. As a result, the flow-rate changed to 0.47 mL min^{-1}, generating 8 mL per sample every 17 minutes.

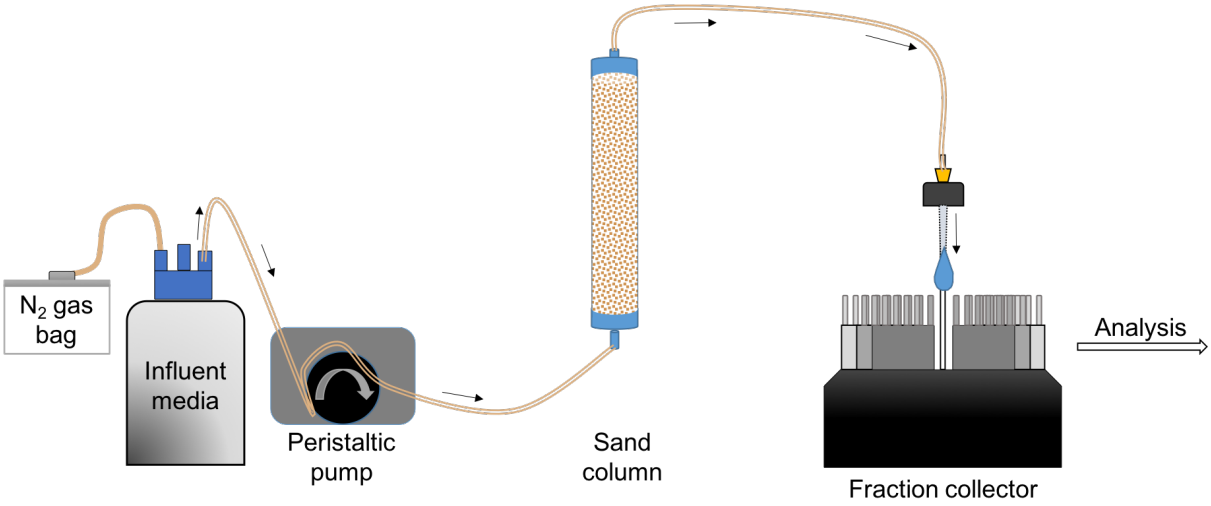

Figure 5. 1. Schematic diagram of a single-pass sand column flow-through system.

5.7.2 Preparation of sand

Sand material for column investigations was prepared by adding 1% hydrochloric acid solution to Ottawa sand, letting it stand for two hours and then washing with sterile UPW and decanting. This process was repeated twice to displace any cations before leaving to dry in an oven overnight at 80°C.

5.7.3 Established microbes

Inoculum used within sand columns investigations were taken from a previously established anaerobic bioreactor operating at pH 11.0 and run on a 2 weekly 10% waste feed cycle for approximately 2 years. 50 mL of enrichment fluid was removed and spun down then all but 25 mL of supernatant was discarded and the pellet

resuspended in the retained liquid. Initially the subculture microcosm was set-up on a recirculation system to pump the reactor fluid through a flow-cell unit, allowing for the formation of a steady state microbial biofilm.

5.7.4 Preparation of chemical stocks

Stocks were prepared by dissolving 1000mg/ L of Nickel (II) chloride/ Europium (II) chloride/ Thorium (IV) chloride/ Uranyl (VI) chloride in sterile UPW to yield a 1000ppm concentration of the compound. These were diluted further to give a 10ppm stock which was then added to influent media for a final concentration of 1ppm. Metal concentrations were then calculated based on their molecular weights. Th/ U stocks were measured using a weighing scales fitted with a glass chamber placed within a fume hood. Th & U chemicals were kept in locked in a safe within a fume hood cupboard only accessible by myself and my supervisor for health and safety reasons.

5.7.5 Trace determination of U(VI) using UV-VIS spectroscopy

The concentration of U(VI) in effluent solutions was determined using methods previously described by Das *et al* (Das, Kedari, & Tripathi, 2010). Briefly, for each sample to be analysed the following were added to a 15 mL centrifuge tube (in this order):, 1.0 mL complexing solution (Table 5.9), 1.0 mL sample, 1.0 mL buffer solution, 0.5 mL Br-PADAP solution (0.05%), 4.0 mL 80% ethanol and 2.5 mL double distilled ethanol to a final volume of 10.0 mL Solutions were allowed to stabilise for 30 minutes before measuring optical density (OD) at 578 nm against a water blank. Concentration of U(VI) within effluent samples were then calculated against a calibration curve.

Reagent	Composition
Complexing solution	0.25 g sodium fluoride, 1.25 g cyclohexane diamine tetra acetic acid and 3.25 g sulphosalicylic acid were added to 40 mL redistilled water, pH was adjusted to 7.8 and final volume made up to 100 mL
Buffer solution	To 80 mL redistilled water 14 mL triethanolamine was added and pH adjusted to 7.8 using concentrated perchloric acid. The pH was re-adjusted to 7.8 after letting stand overnight and the resulting solution made up to 100mL
0.05% Br-PADAP solution	0.025 g Br-PADAP added to 50 mL double distilled ethanol

Table 5. 9. Methodology for the preparation of reagents used in section 5.7.5.

5.8 Microcosm Investigations

5.8.1 Batch sorption experiment

K_d experiments were prepared in sterile 100 mL conical flasks. Volumes were kept constant using 30 mL minimal media spiked with Ni to yield varying concentrations which was added to 1 g of acid washed sand (each run in duplicate). Rubber bungs were used to seal flasks in addition to Parafilm to prevent pH drift that may occur due to exchange of gases. Conical flasks were placed into a shaking incubator at room temperature and set at 130 rpm for 24 hours, after which the supernatant was filtered off. ICP-MS measured initial and final Ni concentrations in solution and the following Equation 5.2 was used to generate K_d values:

$$\left(\frac{(I - F)}{F}\right) x \left(\frac{V}{m}\right)$$

Equation 5. 2. Where I = Initial concentration (mg/ L), F = Final concentration (mg/ L), V = Volume in litres, m = Mass in kilograms.

5.8.2 Complexation experiment

All reactions were prepared in sterile 6 mL rubber butyl glass stoppered bottles with aluminium seal caps. Microcosm experiments were set up in order to investigate the degradation of the $NiISA_2$ complex in both pure and mixed bacterial culture. To 0.08g ISA-1,4-lactone 0.057g Ni(II) chloride was added and dissolved in 10 mL minimal media. Next, 3 mL of this mix was added to 27 mL minimal media for a 1:10 dilution. For pure culture studies a suspension of the alkaliphilic *Exiguobacterium sp. HUD* strain was prepared in minimal media to an absorbance of 0.300 at a wavelength of 620 nm. This suspension was diluted 2-fold by preparing serial dilutions and then 1:10 by injecting 0.5 mL into 4.5 mL of the Ni-ISA media mix, giving a final volume of 5 mL Ni-ISA. For mixed culture studies an inoculum extracted from a pH 11.0 enrichment was utilized by spinning down 10mL of fluid, retaining 5 mL of supernatant and discarding the remainder then resuspending pellet in the 5 mL of liquid. As with the pure culture studies, 0.5 mL of the suspension was added to 4.5 mL of the ISA mix. Control microcosms were set up using the same experimental conditions, with minimal media only in place of bacterial suspensions. The pH of all reactions was adjusted using a hand-held meter and 200 μL samples were immediately extracted for day 0 measurements. Glass bottles were individually flushed with N_2 for 6 seconds to ensure anoxic conditions before being sealed and crimped. Test and control reaction vessels were prepared in duplicate and incubated at 30°C. Samples (200 μL) were taken every 2 days up to a period of 2 weeks, day 14 inclusive, and used to measure pH and ISA concentration through HPAEC-PAD analysis. Headspace gas measurements were taken prior to extraction of liquid samples.

5.9 Lead Pipe Investigations

Lead pipes provided for a separate project were utilized to develop the techniques required during later parts of this study in the characterisation and analysis of complex surfaces.

5.9.1 Surface analysis

Using sterile ratchet-assisted manual pipe cutters lead pipes samples were cut into 1.5 cm sections which were then split into thirds (Figure 5.2) to expose the inner lining for microscopy analysis.

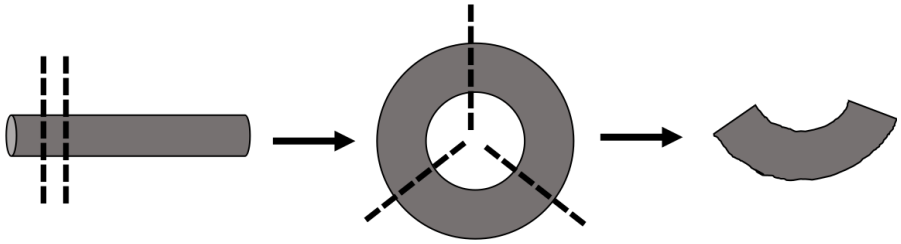

Figure 5. 2. Schematic diagram to demonstrate how lead pipe samples were cut for analysis.

5.9.2 Cross-sectional analysis

An EpoFix™ kit (Struers, Denmark) was utilized for the slow-curing transparent epoxy mounting of lead pipes. 1.5 cm sections of pipe were positioned into individual Fixiform cups and then covered with the EpoFix blend consisting of 25g of resin plus 3g hardener (per sample) which had been mixed for exactly 2 minutes. Cups were placed into a vacuum desiccator which was sealed and the inside air evacuated until pressure of 100 mbar (0.1 bar) was reached. The vacuum tap was immediately closed and pressure within the chamber brought back up to atmospheric pressure (~ 1000 mbar) using an air admittance valve. This process was repeated a further two times, after which samples were covered with disposable cups (to prevent resin becoming sticky) and left for 12 hours to harden.

Embedded samples were manually ground and polished to reveal the layers of the lead pipe surface. Resins were gently ground with 240 Sic Paper for 2 minutes, rotating samples 90°C every 30 seconds and using detergent to prevent the paper from tearing. This process was repeated with P600 and P1200 papers, each for 5 minutes. The specimens were polished using a selvyt cloth sprayed with a 1 μM diamond suspension and then inspected under stereomicroscope to ensure the lead

pipe layers were visible. Samples were rinsed with tap water, wiped with methanol and then left to air dry before analysis under SEM.

5.10 Data processing

All data was processed in Microsoft Excel unless stated otherwise.

Chapter 6.0 Investigation into the Techniques Required for the Analysis and Characterisation of Microbial Biofilms on Complex Surfaces

6.1 Rationale

The current chapter explores the relevant techniques necessary for the investigation and characterisation of microbial biofilms on surfaces, methods which are then utilized for studies later in this project. Readily available lead pipe samples exhibiting signs of microbial colonisation presented an opportunity to perform these practices. By employing optical microscopy, scanning electron microscopy (SEM), confocal laser scanning microscopy (CLSM) and DNA extraction protocols this allowed for visualisation of not only the structure of microbial biofilms but also the morphology of individual cells in addition to the components involved in the bacterial aggregation and surface attachment.

In relevance to the main body of this thesis, lead also plays a role in the nuclear waste inventory. Vast containers made of lead (amongst other materials) are utilized for radiation shielding known as “lead shielding” during transport and storage of wastes. The subsequent disposal of these containers then brings into question the behaviour of radioactive contaminated lead in the GDF surroundings (NNL, 2016). Data presented within this chapter of work could potentially be relevant to the fate of lead in the presence of phosphates within subsurface environments, although these would need to be oxic conditions.

6.2 Results & Discussion

6.2.1 Surface Analysis

6.2.1.2 Keyence Optical Microscopy

Preliminary analysis of the inner lining of lead pipes via optical microscope revealed a rough lead surface beneath patchy layers of organic deposits indicative of biological material (with a combined thickness of ~20–150 μM). Within the data set the pipes displayed varying degrees of biofilm coverage, ranging from very sparse areas to full coverage of the inner diameter (Figure 6.1)

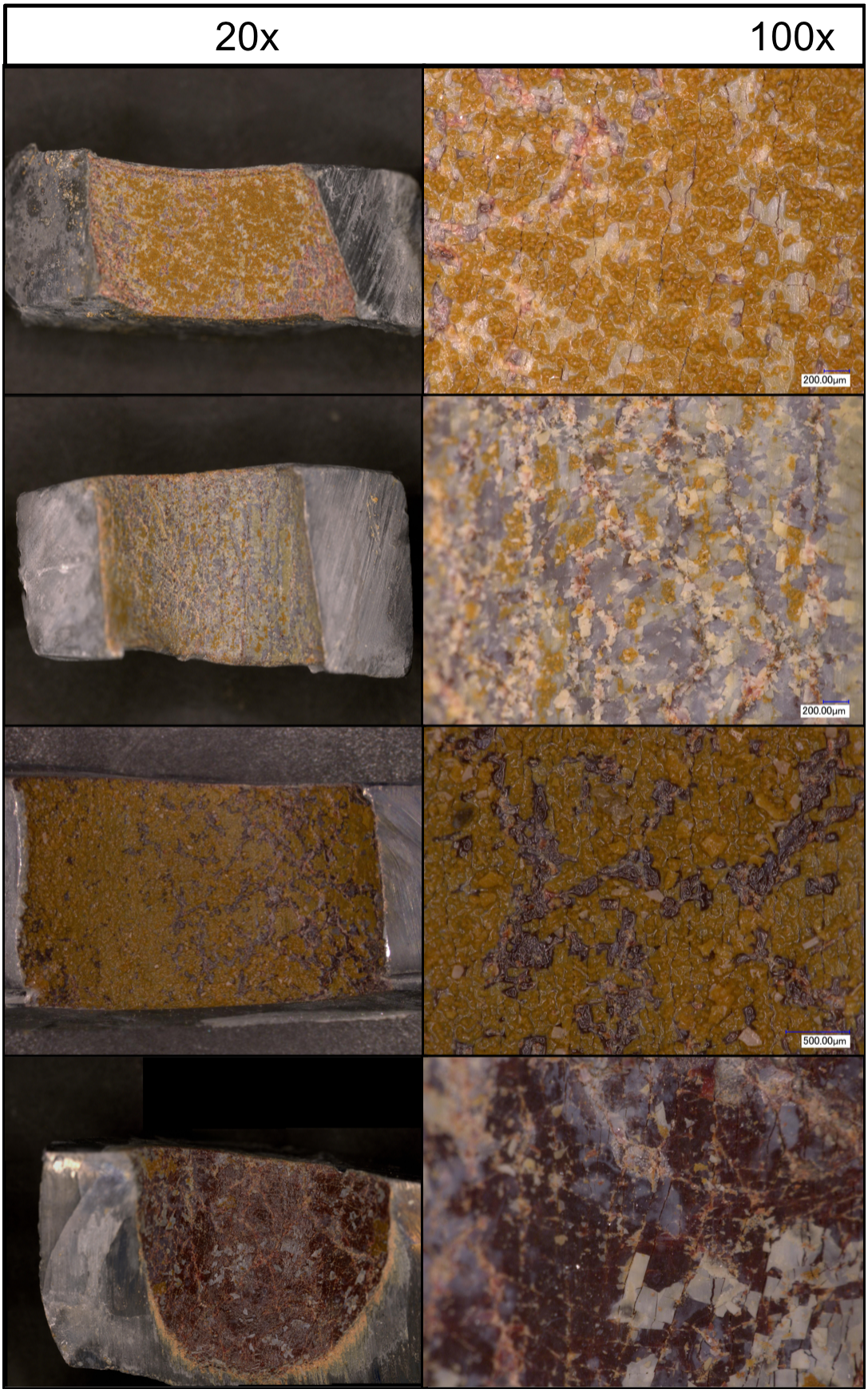

Figure 6. 1. Optical microscopy of the inner lining of lead pipes. Grey colour indicates lead material with potential mineralisation and suspected yellow biofilm material on top.

Prior to 1970 lead was the preferred material for pipes supplying houses with drinking water within the UK. In order to reduce the level of lead leaching in domestic water a process known as “phosphate dosing” was introduced whereby phosphate, most commonly in the form of orthophosphate, was added to water systems to decrease the solubility of lead compounds and the subsequent release or detachment of lead from the pipe (Jarvis, Quy, Macadam, Edwards, & Smith, 2018). The formation of these lead phosphate compounds can result in mineral aggregation at the surface of pipe, which is potentially what is being observed in these samples. However, the inner lining appeared to be both red/brown and grey in colour throughout the samples, potentially indicating a lead oxide layer, patches of white lead phosphate mineralisation above and then organic material layered on top (Figure 6.2).

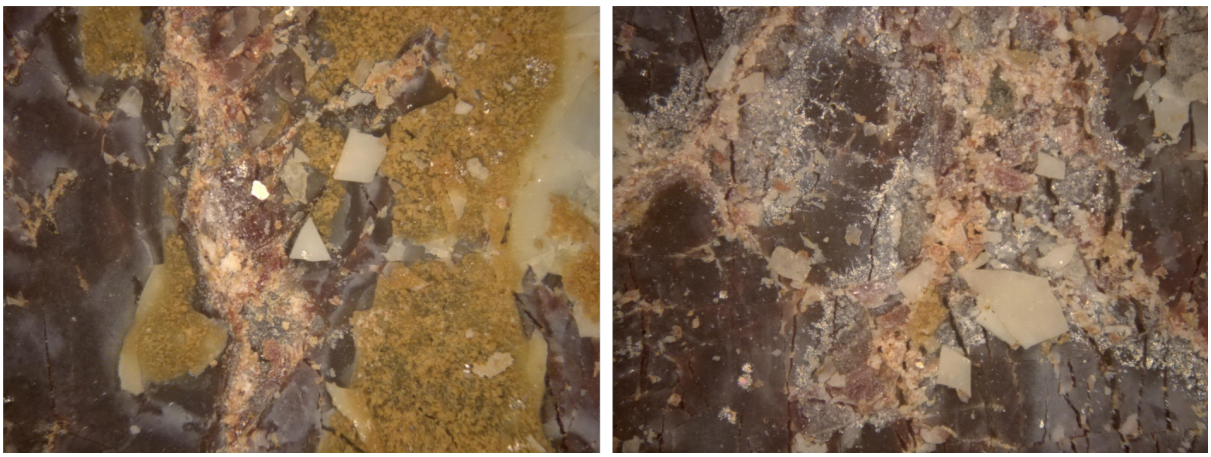

Figure 6. 2. Keyence optical microscopy (x250 magnification) displaying varied levels of mineralisation and bacterial colonisation.

Biofilms are known to form in a variety of environments and on a multitude of surfaces therefore it’s possible colonisation could occur as a result of these mineral aggregates rather than at the expense of them. The rougher texture of the pipe as a result of mineralisation could promote microbial colonisation by enhancing surface area in addition to providing protection from shear forces that could cause sloughing of the biofilm (Fish, Osborn, & Boxall, 2016). Optical microscopy allows physical properties of a material to be observed and analysed up to 2500x, however, in order to investigate specific elemental characteristics, other forms of microscopy were employed.

6.2.1.2 Scanning Electron Microscopy & Energy Dispersive X-ray Analyzer

Visualisation via through scanning electron microscopy (SEM) highlighted the contrasting surface layers of the lead pipe. Under a backscattered electron detector (BSED) of an SEM different material appear brighter or darker depending on their elemental composition, with heavier elements presenting brighter due to a higher volume of electrons released from the sample. Figure 6.3 depicts the lead surface as bright light grey areas, a contrast to the darker patches of what appears to be organic matter. Furthermore, the lead surface is uniform in texture in comparison to the irregularity of the clusters of unknown material, the shape and distribution of which is indicative of microbial biofilm described previously (Figure 6.4).

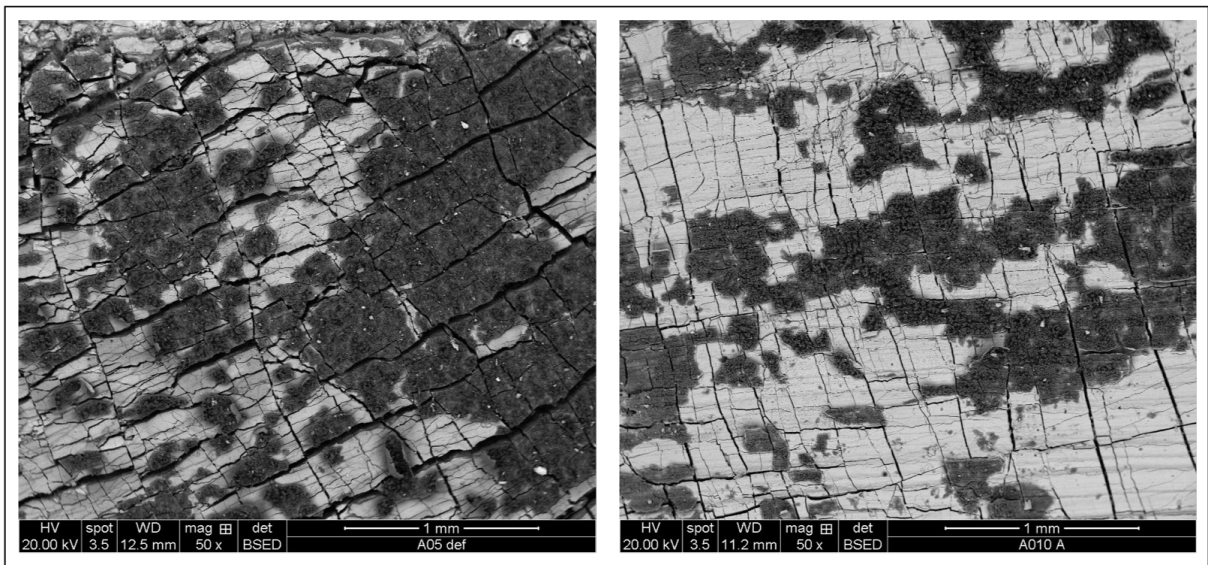

Figure 6. 3. SEM images depicting bright lead material with darker areas of potential microbial colonisation (x50 magnification).

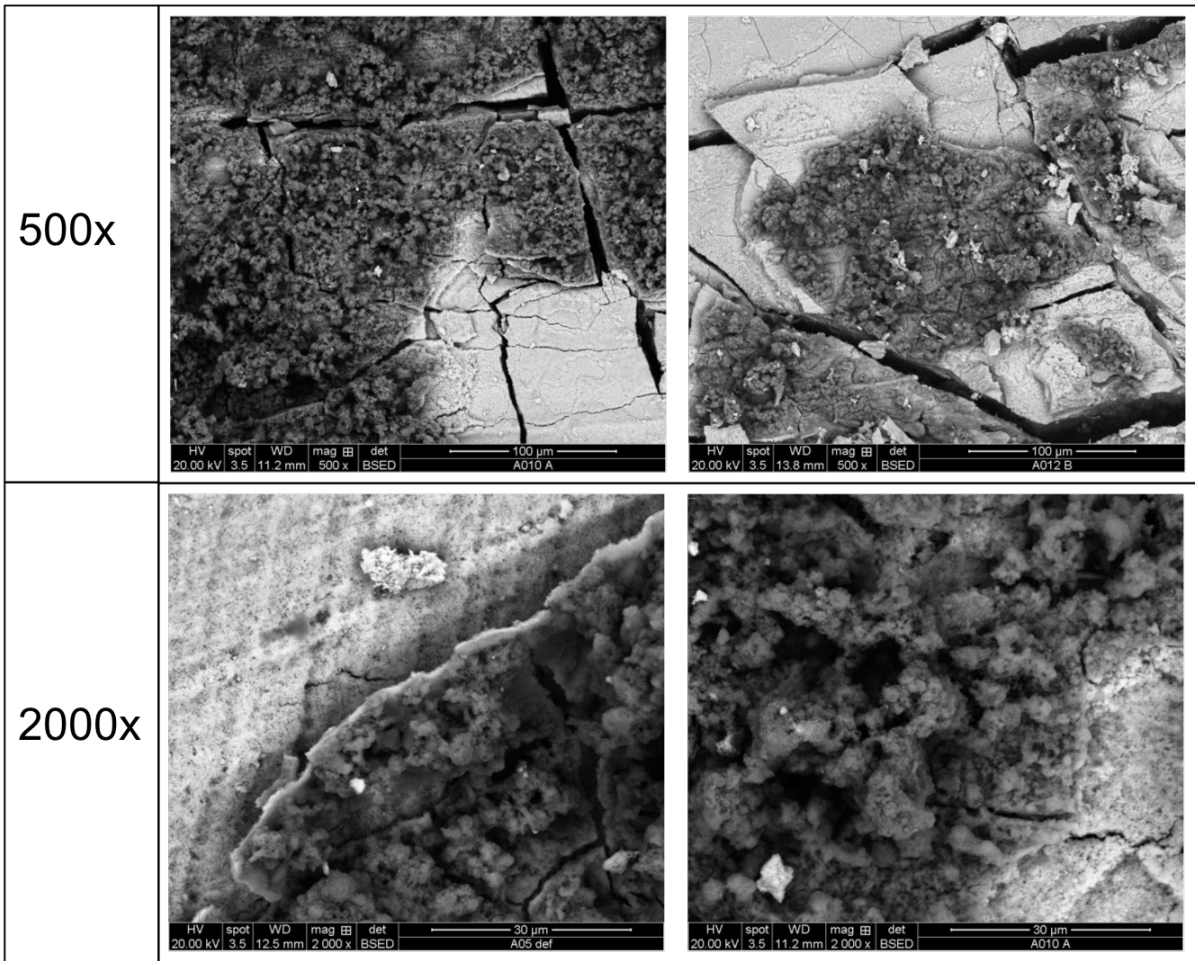

Figure 6. 4. Clusters of material above lead pipe surface are indicative of microbial biofilm. Material here appears to be sat on top of another layer, possibly a film of phosphate mineralisation which could be a vital factor influencing bacterial colonisation.

Figure 6.5 reveals the presence of some form of minerals embedded within the biofilm material, evidenced by the rectangular shape and contrasting smooth texture of crystal-like structures (Gilkes, Suddhiprakarn, & Armitage, 1980). X-ray diffraction (XRD) could be used in future studies for the identification of mineral phases present within biological samples. Microscopy at surface level can only provide a certain amount of detail about the specimen under investigation and so the coupling of this with energy dispersive x-ray analysis (EDX) will enable a more in-depth evaluation.

Comparisons through EDX analysis revealed clear differences in the elemental composition of the contrasting surfaces under SEM. In samples with grey inner pipe layers the surface was composed primarily of ~61% Pb and ~22%-O, as expected, with low levels of C too. Red/brown pipe layers displayed similar elemental profiles with the exception that Pb levels reduced to ~48-51% and O increased slightly to

~25-28%. These distinctions were most likely due to the presence of the PbO mineral litharge which was responsible for the red/brown colouring of the pipe surface in samples collected from a specific hot spot. Areas of the pipe colonised by what is assumed to be microbial matter display increases in the level of O within those sections, in addition to a heightened detection of P, Ca and Fe coupled with a reduction in the levels of Pb (Figure 6.6, 6.7 & 6.8). Results generated here indicate the presence of insoluble lead phosphorous complexes which have formed on the surface of the lead pipes through orthophosphate dosing of drinking water. These minerals could potentially play a part, or even enhance, the formation of biofilms here.

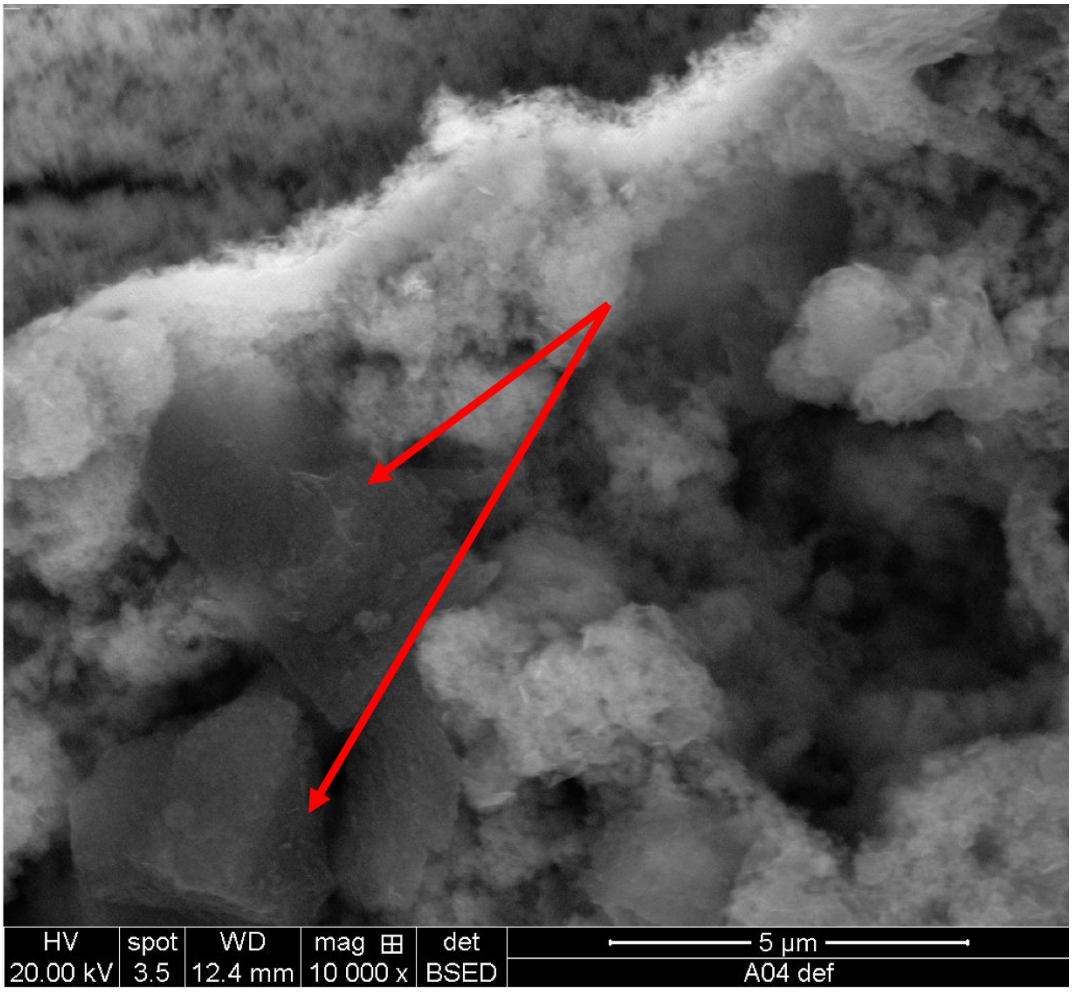

Figure 6. 5. Red arrows indicate potential mineralisation embedded within the suspected biofilm material.

A number of studies within the literature describe the link between the colonisation of bacterial communities and surface mineralisation (Edwards, Bach, & McCollom, 2005) (Rogers, Bennett, & Choi, 2005) (Jones & Bennett, 2017). Microorganisms are able to colonise material surfaces depending on nutrient availability within the vicinity, with carbon detected throughout the pipe surface potentially contributing to microbial survival in these environments. Cai *et al* demonstrated that the presence of the mineral kaolinite within soil samples encouraged microbial growth of *Escherichia coli* OH17:H7. This study also observed greater biomass production, albeit slower bacterial growth, whilst *E. coli* was exposed to goethite, an iron oxide mineral (Cai et al., 2018). Ghosh *et al* demonstrated successful adhesion of microbial biofilm onto insoluble phosphate granules, in addition to the further production of EPS matrix on the surface of these particles, as observed through SEM (Ghosh, Barman, & Mandal, 2019). Minerals and rocks provide niches for metabolically similar bacteria under harsh environmental conditions and could be considered independent ecosystems for microbes at the mineral-aqueous interface (Jones & Bennett, 2017).

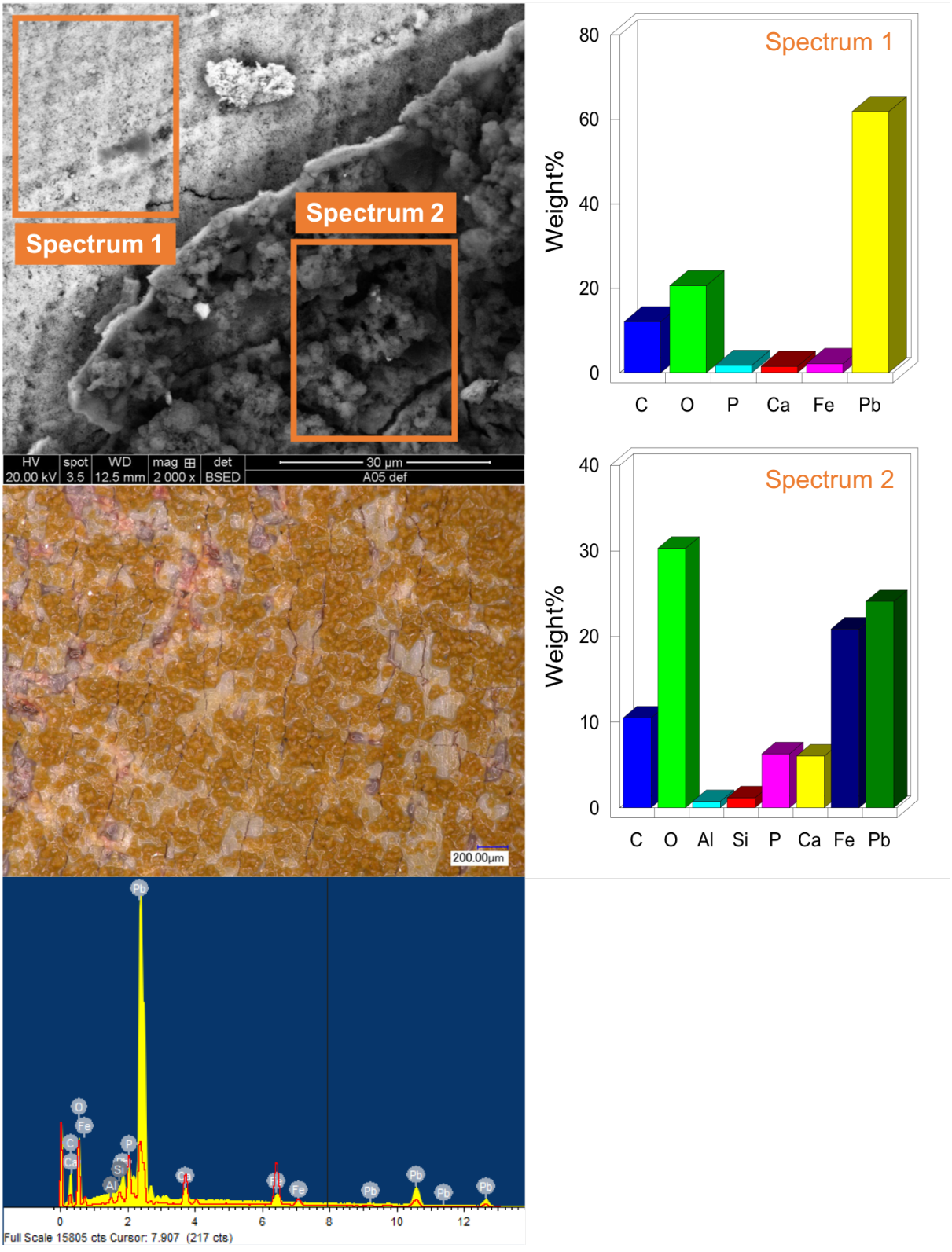

Figure 6. 6. EDX analysis of lead pipe surface indicating different elemental profiles in the two layers. The sample here displays a higher content of yellow suspected biofilm.

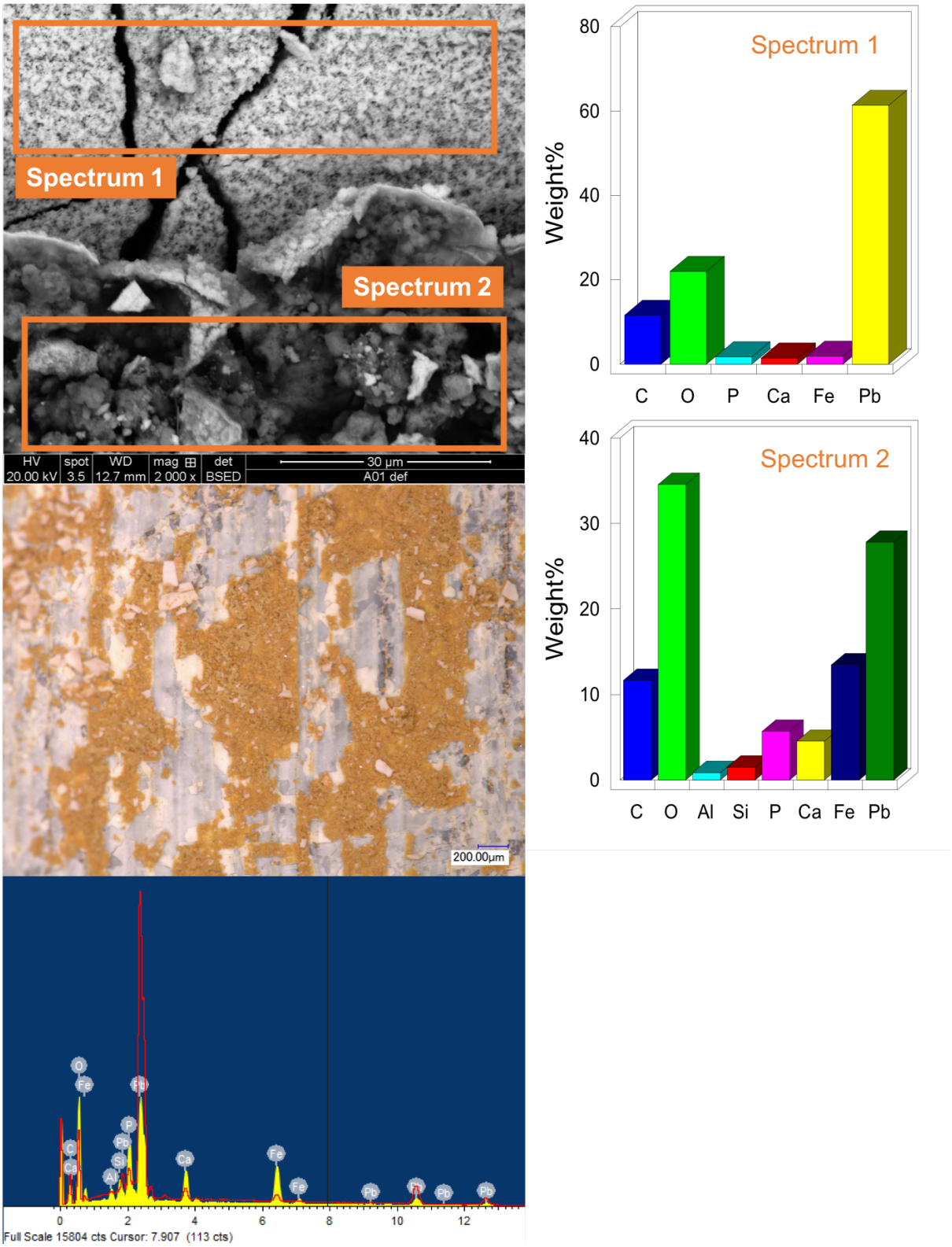

Figure 6. 7. Elemental profiling of lead pipe surfaces. This sample demonstrates a higher level of shedding of the lead layer underneath or possibly the phosphate mineralisation.

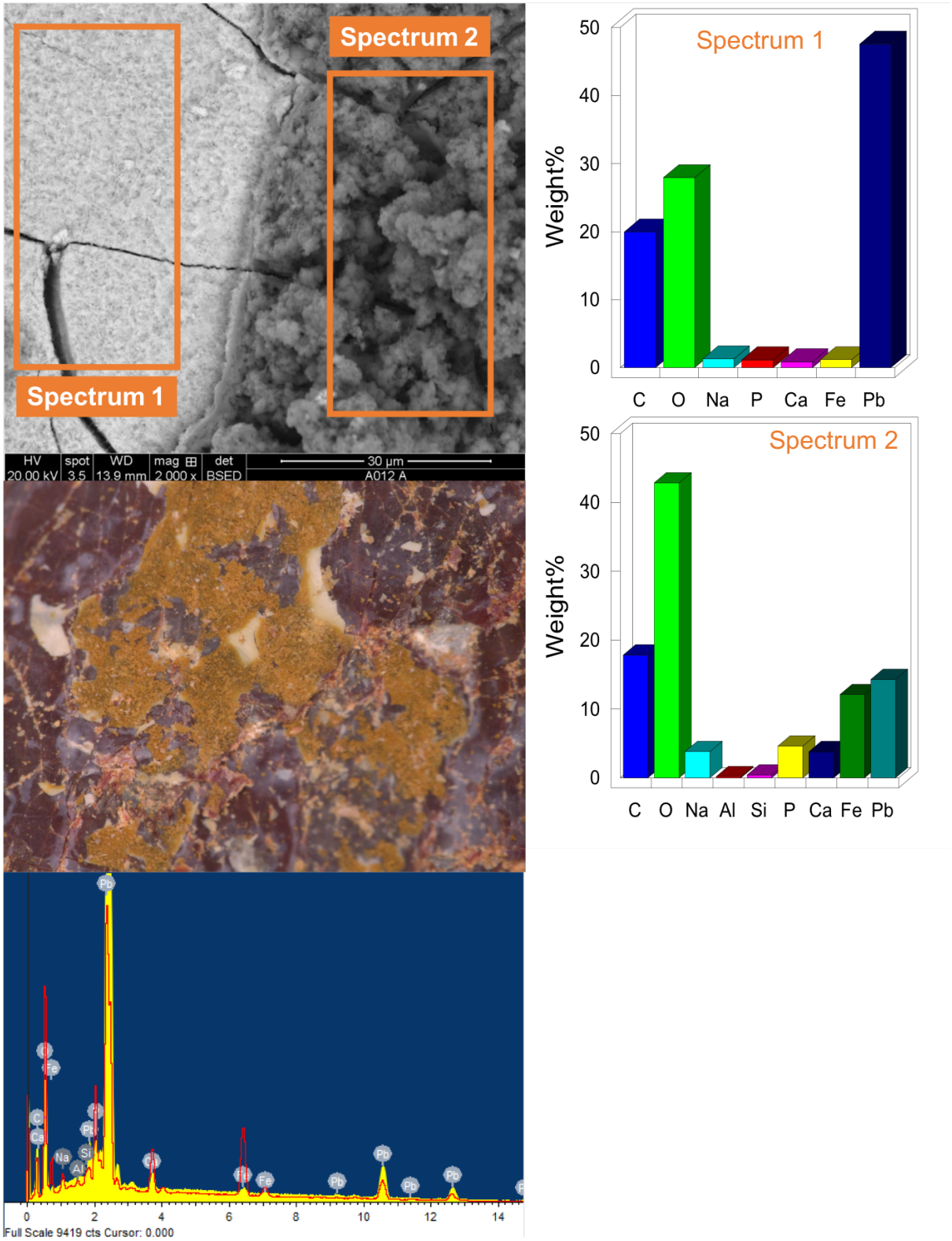

Figure 6. 8. EDX analysis of lead pipe layers. The sample here appears redder in colour, suggesting presence of a red lead oxide mineral.

EDX analysis provides a deeper understanding of the elements that play a major role in the surface composition of materials and subsequently how microorganisms may interact with them. Whilst the literature describe that biofilms could potentially form onto phosphate minerals developed on the pipe surface, SEM & EDX analysis gives no indication of the microbial components present, and consequently cannot alone confirm the presence of a biofilm at all. The next step was to apply biological stains to dye EPS potentially on the surface of lead pipes and then use confocal laser scanning microscopy (CLSM) to visualise them.

6.2.1.3 Confocal Laser Scanning Microscopy

The inverted set-up of the confocal microscope coupled with the irregular shape of lead pipe samples made visualisation through CLSM quite challenging. Sections of pipe were placed on glass sides facing downwards which allowed limited visible surface area under the microscope depending on the depth samples were cut (Figure 6.9).

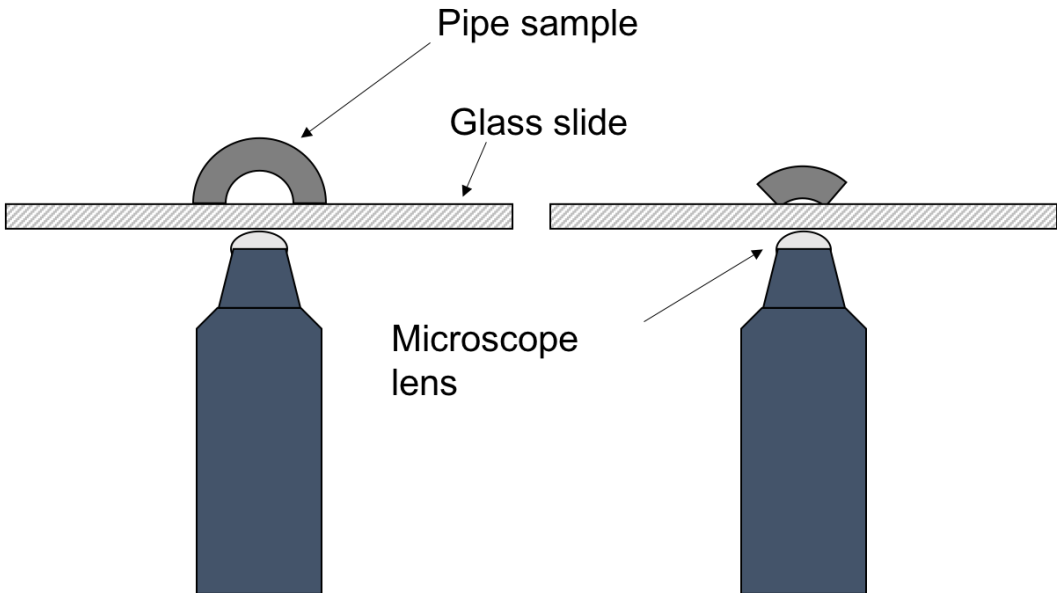

Figure 6. 9. Schematic diagram to show how visualisation of lead pipes by an inverted CLSM can differ depending on the size and shape of cut samples. The close distance of the surface of the pipe to the glass slide enhances visualisation of stained material.

CLSM revealed the presence of a range of EPS components on the lead pipe surface which were not present on a control sample where the surface had been washed of any suspected biofilm material. Lipids, proteins, sugars and eDNA (extracellular DNA) & cells were all detected, suggesting the microbes were growing in association with the lead pipe or mineralisation on the surface. Images shown in Figure 6.10 were taken from a sample where the main contact point was along the pipe edge where it interacted with the glass slide (Figure 6.11). A high protein content (Figure 6.10C) is observed within the biofilm which is consistent with formation upon surfaces due the important role proteins play in adhesion and attachment of cells (Fong & Yildiz, 2015). The conditioning films that prime surfaces ready for the colonisation of microbes is also largely composed of proteins (Dang & Lovell, 2015). The high level of eDNA present (Figure 6.10E) produces a negative charge which could be leading to the binding of Fe^{2+}/Fe^{3+} and Ca^{2+} ions to the EPS matrix, which is possibly why they were detected within phosphorous complexes – this in turn could promote aggregation further. Additionally, the structural integrity and surface adhesion ability of biofilms can also be reinforced by the presence of Ca^{2+} ions as described previously (Cruz, Cobine, & De La Fuente, 2012).

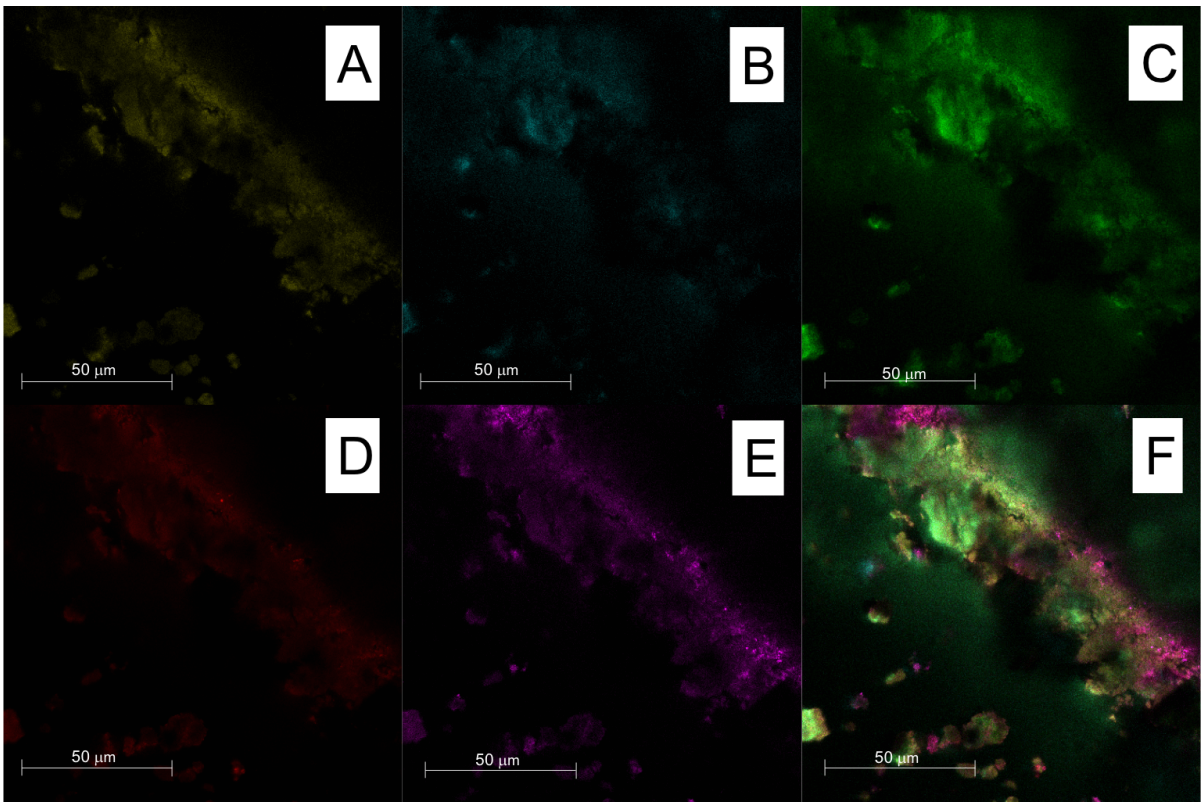

Figure 6. 10. CLSM investigation into lead pipe samples. Lipids [A], β-1,4 & β-1,3 polysaccharides [B], proteins [C], α-mannopyranosyl and α-glucopyranosyl sugars [D] and eDNA & cells [E] were all detected. [F] represents the channels merged together.

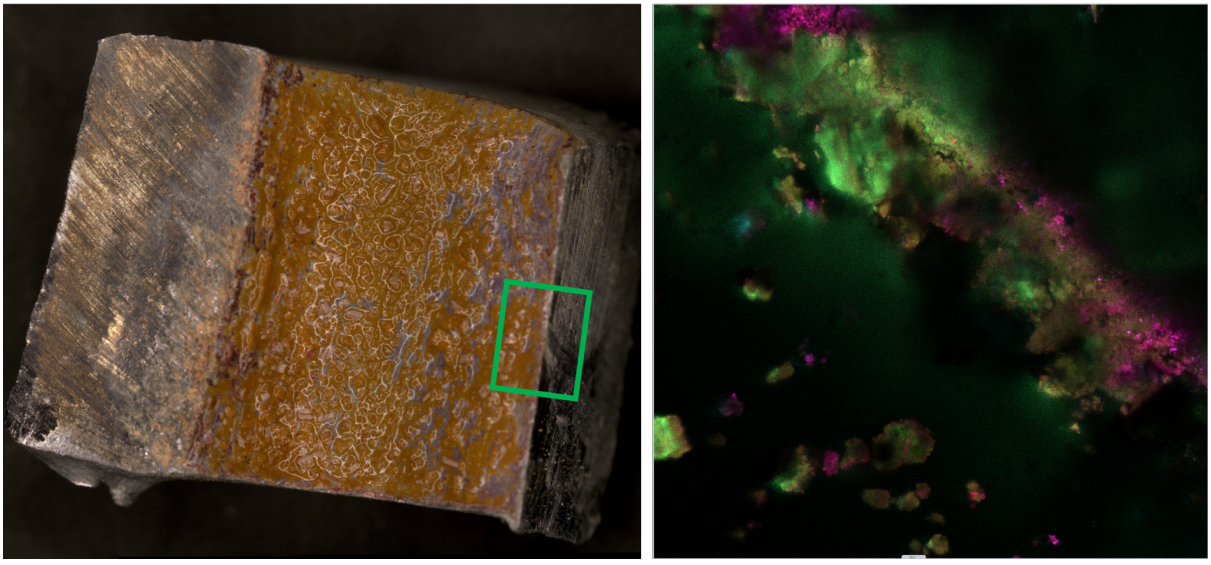

Figure 6. 11. Optical microscopy (left) indicates the location at which CLSM image (right) was most likely taken.

Figure 6.12 could support the claim that microbial biofilm forms on surface bound minerals as the distribution of EPS components appears consistent with the presence of multiple bioaggregates rather than a large clump of biological material. Some colocalization of polysaccharides and proteins was observed (Figure 6.7 B & C) which could be expected as they both play essential roles in the adhesion of biofilms as mentioned previously, with exopolysaccharides also providing in addition to acting as "molecular glue" (Limoli, Jones, & Wozniak, 2015). Sugars, eDNA & cells and lipids were all also detected through CLSM, further substantiating the claim that microbial biofilm was able to colonise the lead pipe surface or mineral aggregates.

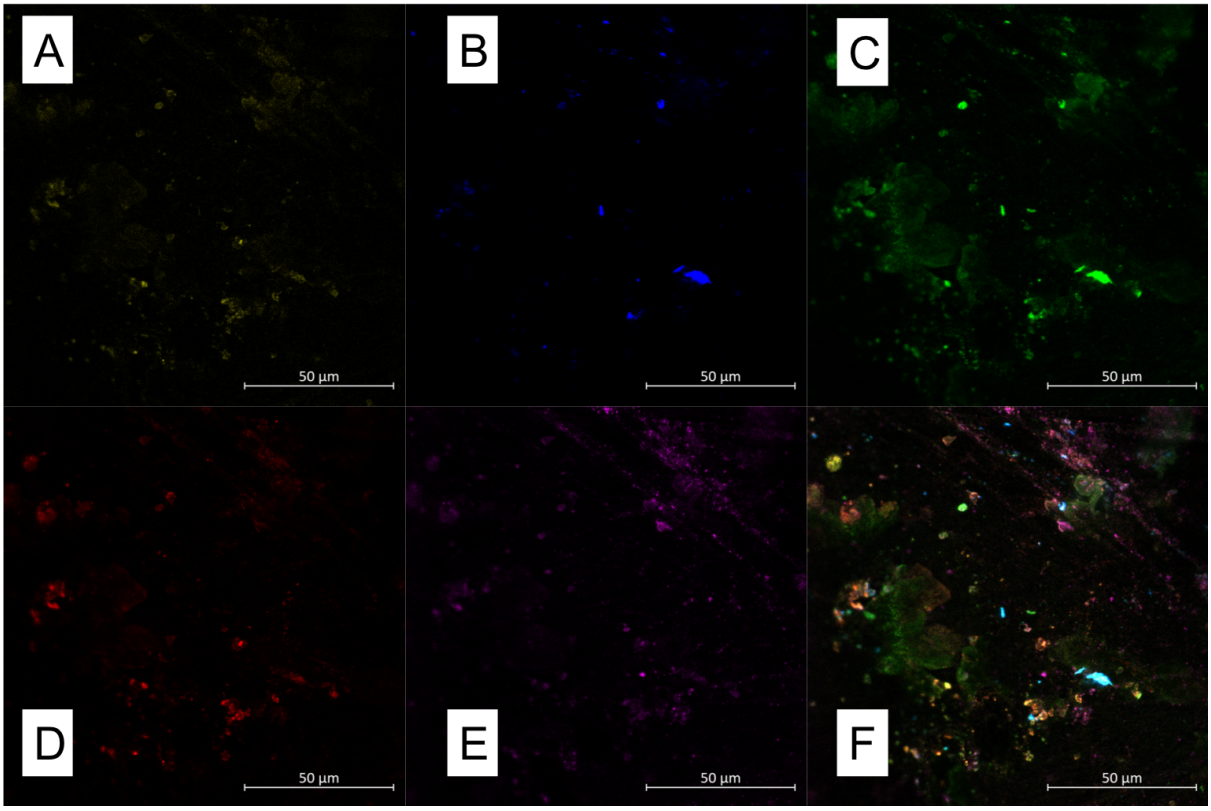

Figure 6. 12. CLSM imagery of lead pipe sample. All EPS components previously described were detected within this sample, with [F] again showing a combined image of all channels.

6.2.2 Cross-sectional Analysis

6.2.2.1 Elemental mapping

The study of a cross-sectional area of the pipe allowed the elemental profile of individual layers to be observed and analysed, the layers of which are displayed clearly in Figure 6.13. Elemental mapping of this sample is presented in Figure 6.14. As expected the base layer of the pipe was composed primarily of Pb (Figure 6.15A), and an increase in the level of measurable O within the adjacent layer (Figure 6.15B) consistent with the presence of PbO material. Figure 6.15C indicates that the thin deposit that sits atop the PbO layer contains no Pb at all but contains a high c content in addition to O. The reliability of the measurements of elements with a low atomic number is uncertain through EDX, but this data could suggest organic carbon potentially on the PbO surface may present itself as a carbon source for bacteria. However, the film containing carbon is too thin to accurately measure this, and elemental mapping also insinuates the carbon may be being detected as part of the resin. The aggregate assumed to be lead phosphate/ microbial biofilm was revealed to encompass a variety of components within its elemental profile (Figure 6.15D). Pb and O were found in the highest abundance, with P and Fe also detected therefore supporting data in 6.2.1.2. Data presented here suggests the addition of phosphates to control lead release into drinking water systems could encourage the formation of multicomponent aggregates on the pipe surfaces that later enhance colonisation of microbial biofilms.

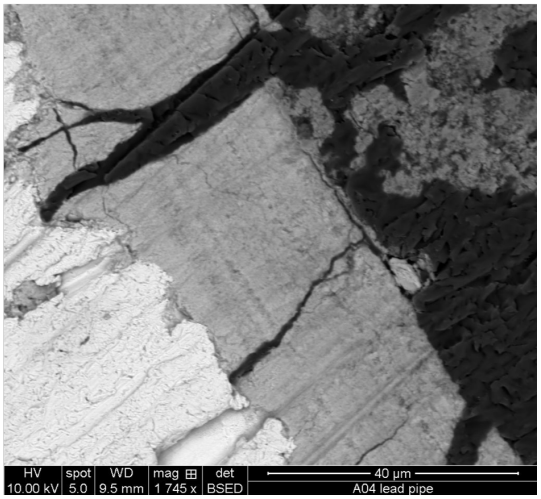

Figure 6. 13. SEM image of a cross-sectional area of a lead pipe. Here the layers are clearly depicted due to their different texture and brightness.

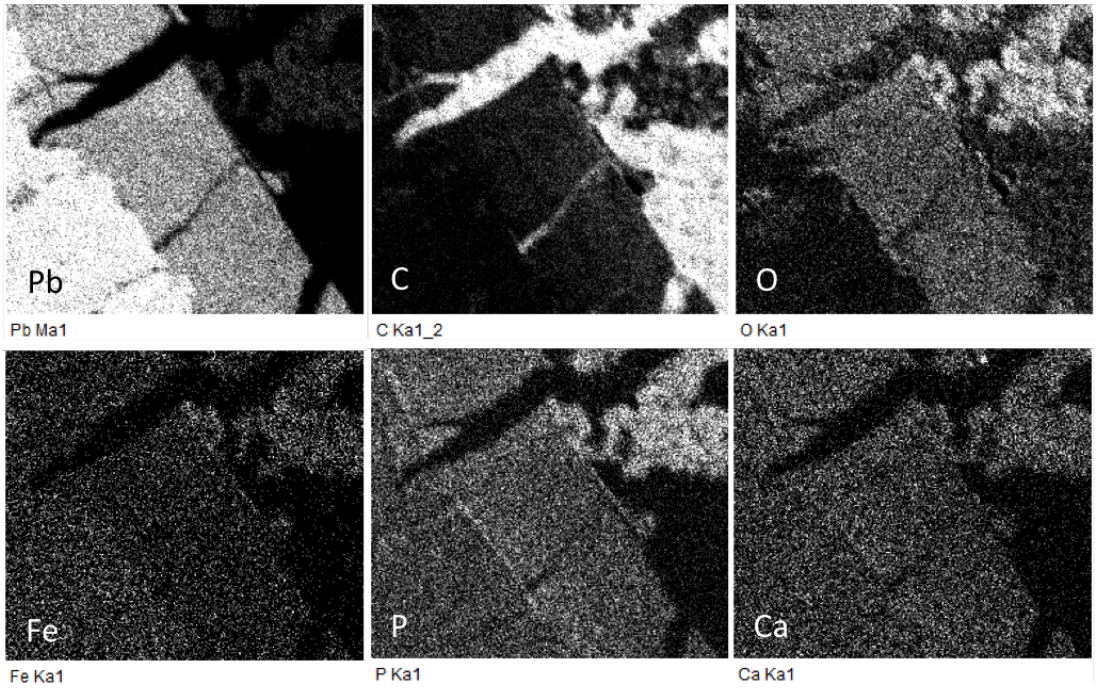

Figure 6. 14. Analysis using a mapping function to visually detect which areas contain an abundance of certain elements within a sample. High level of Pb and O were found on the pipe itself, as expected, with P, O and Fe detected in aggregates.

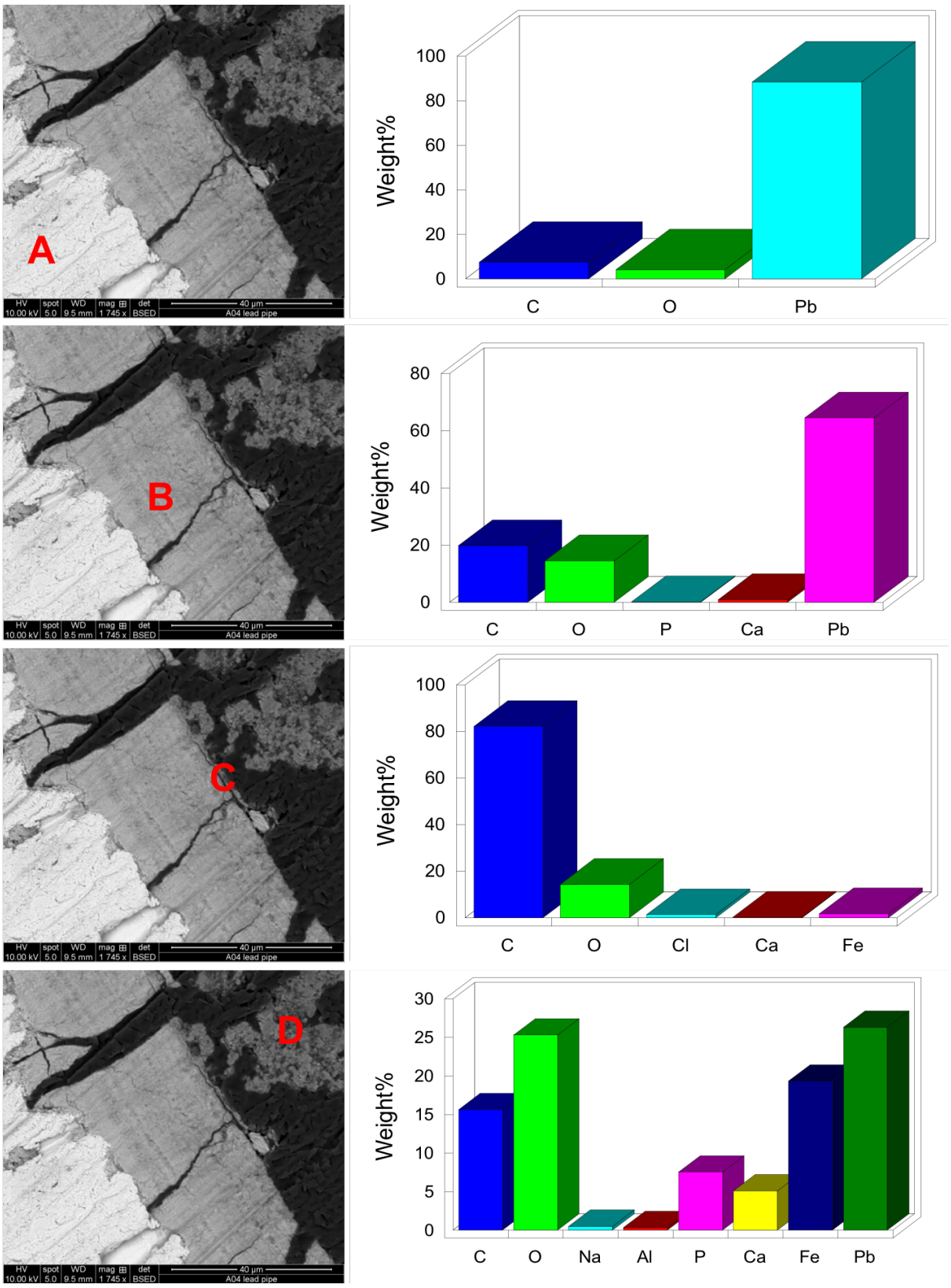

Figure 6. 15. Qualitative elemental analysis of the four distinct layers of the lead pipe sample presented in Figure 6.14. The presence of Fe, Ca and P within aggregate material indicates multicomponent lead phosphate complexes are likely playing a role in the colonisation of biofilm material.

SEM-EDX provides a combination of elemental and morphological information about the sample of interest and has the potential to detect microbial life at single cell level (Khan, Oh, & Kim, 2020). In this instance, it's likely biofilm material that may be present is closely associated or attached to a number of insoluble complexes which complicates the process of bacterial identification.

6.2.4 DNA Extraction

Surface-associated microbial communities may be examined through the extraction of nucleic acids from aggregate material within the pipe. During the extraction process it became apparent that there were features of the sample which were affecting the purity of DNA. It was concluded that the presence of humic acids (HA) were most likely contaminating samples, leading to the elution of a liquid that was opaque & brown in colour instead of clear & transparent. To combat this issue, samples were treated with acetic acid prior to DNA extraction in order to separate large HA into smaller sizes (von Wandruszka, 2000).

Extraction protocols yielded small amounts of DNA, a result which was expected considering the level of interference from HA within samples. Methods for microbial community analysis require a minimum concentration of DNA to proceed so samples were subjected to PCR techniques for amplification and subsequently nested once. Visualization of electrophoresis gel shown in Figure 6.16 reveals the presence of DNA bands from 4 out of the 5 samples run, the final concentrations of which are presented in Table 6.1.

PCR amplicon	Concentration (ng/ μL)
Positive control	120.4
LP1	41.4
LP2	N/ A
LP3	35.0
Negative control	26.4

Table 6. 1. Concentrations of PCR amplicons sent for sequencing.

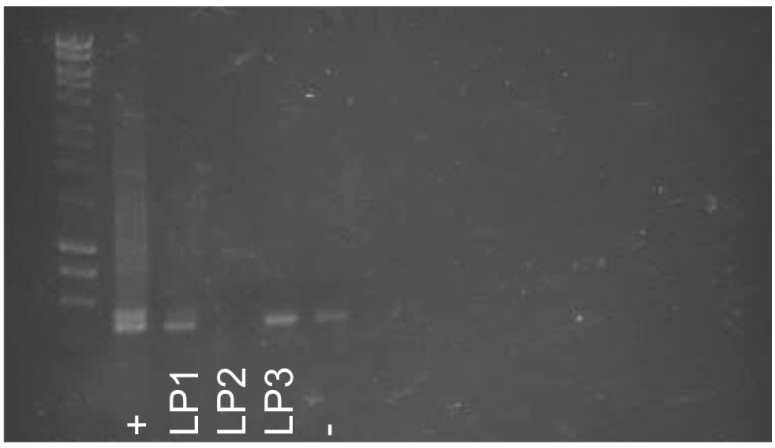

Figure 6. 16. Gel electrophoresis image of PCR amplicons. Bands indicate the presence of DNA.

Samples with measurable DNA content were sent for profiling however they did not pass the company's quality control measures therefore microbial community analysis was not generated. Nonetheless, data here shows that DNA of a bacterial biofilm formed on or within complex surfaces can be extracted and amplified in order to identify microbial communities associated with environmental surfaces. Exposing the taxonomic composition of a particular community could provide a deeper understanding of the interactions and processes that may occur at the microbe-surface/ microbe-mineral-surface interface (Jo, Oh, & Park, 2020).

6.3 Conclusion

The conclusion within this chapter is twofold:

A) Data generated here suggest the morphological changes to the inner surface of lead piping provide a platform for microbial colonisation. The addition of phosphates immobilises lead stripped off the pipes resulting in mineralisation of complexes on the surface, but it's possible biofilms could form on the surface of these minerals rather than at the expense of them. Exploration into the microbial community is required to further substantiate these claims, however CLSM imaging provides suitable evidence to demonstrate colonisation of microbial biofilm which can be coupled with the elemental profiling of surface bound aggregates.

B) By utilizing materials already exposed to suspected biofilm material the techniques for visualisation of colonised complex surfaces could be practiced and tailored for use later in this project. Optical and electron microscopy enables a whole host of uniquely shaped surfaces to be analysed with ease due to the upright setting of the microscopes, although CLSM proves slightly more difficult as the outcome relies on an interaction between the specimen and slide material. As a result of this, a different approach was then taken to better analyse biofilm samples in the next stage of the project. Adjustments made to the DNA extraction protocol within this chapter allowed different methods to be tried and tested, which in turn established the most appropriate technique to use for biofilm present on surfaces.

Chapter 7.0 Transport of Nickel under ILW-GDF conditions

7.1 Rationale

Radioactive nickel present within the structural elements of containers that house nuclear fuel subsequently becomes part of the ILW inventory during the decommissioning of nuclear reactors (Carboneau & Adams, 1995). The complexation of Ni and α-ISA has been previously described in the literature at hyperalkaline pH (Warwick et al., 2003), a process which could lead to the increased mobility of radioactive Ni within the ILW-GDF near-field and potentially out to the surrounding geosphere. This chapter focusses on the impact of biofilm forming bacteria and their associated flocs on the transport of ISA complexed Ni under far-field conditions of an ILW repository. This research employed sand columns operating at alkaline pH, exposed to both a microbial community, ISA and Ni. Within this chapter of work stable ^{60}Ni is employed as an analogue for radioactive ^{63}Ni.

7.2 Results & Discussion

7.2.1 Abiotic transport of nickel under ILW-GDF conditions

7.2.1.1 Single batch experiment for K_d determination

K_d values, or Partition coefficients, indicate the level of adsorption contaminants in solution have for a particular adsorbent ie. sand once equilibrium has been reached. K_d values for the adsorption of Ni on Ottawa sand are shown in Figure 7.1. At K_d values $\approx$ 0 it's assumed that the contaminant moves at the same rate as the surrounding water, suggesting no adsorption to a solid surface (Krupka, Kaplan, Whelan, Serne, & Mattigod, 1999). Batch adsorption results indicate that as the concentration of Ni in solution increases, the percentage of metal removal (% MR) increases (Table 7.1) until a concentration is reached where saturation of sand occurs. Above 0.125 mg/L Ni in solution a decrease in % MR is observed, signifying that binding sites on the surface of the sand become exhausted. At very low concentrations of Ni the probability of metal ions interacting with the sand is minimal hence complete removal of the Ni is not detected. The decrease in K_d at the highest concentration measured is consistent with expectations as the level of Ni adsorption should reduce as more sites on the sand surface are occupied. In addition, a low

sand to solid ratio (1g sand: 30mL solution) was tested in this experiment, which generally allows for measurable levels of the contaminant to be left in solution post equilibrium (Adey, 2005). The K_d values presented in Figure 7.1 were within the range of values (48-340 mL/ g) calculated by Rhoads *et al* for the batch adsorption of Ni to a sand, clay and silt mixture known as Hanford sediment (Rhoads et al., 1994).

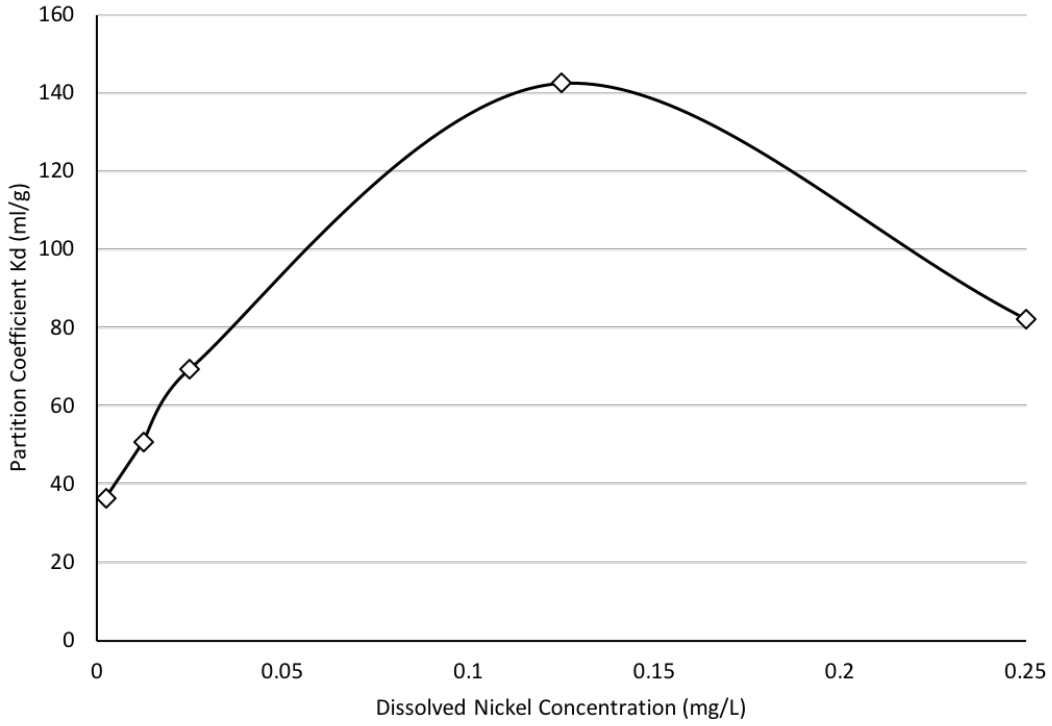

Figure 7. 1. Kd model to represent the adsorption of Ni ions to Ottawa sand as a function of initial concentration (mg/ L).

Dissolved concentration of Ni (mg/ L)	Metal removal (%)
0.0025	54.9
0.0125	62.8
0.025	69.8
0.125	82.6
0.25	73.3

Table 7. 1. Percentage of Ni removal in solution at varying concentrations post equilibrium

7.2.1.2 Abiotic sorption experiments

Breakthrough and exhaustion curves demonstrate the sorption of Ni through an abiotic sand column under ILW-GDF conditions by using Li as a conservative tracer. ICP-MS analysis indicated that the breakthrough time of Li (Ce/Co = 0.05) was calculated to be 4.17 hours, with exhaustion (Ce/Co = 0.95) of Li through the column occurring at approximately 5.98 hours (Figure 7.2). Under the same conditions, Ni was not detected in effluent fractions therefore indicating complete sorption of Ni to the sand column at pH 9.5 over an 18-hour flow through experiment (Figure 7.3).

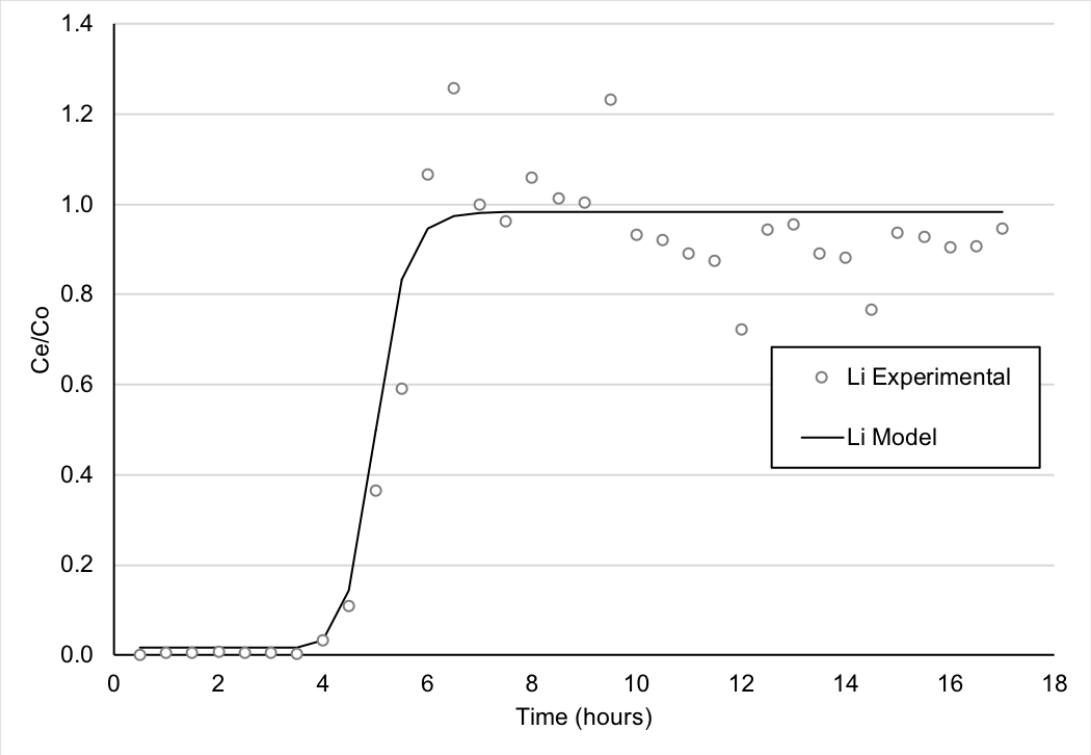

Figure 7. 2. Transport of Li (empty grey circles) through a pH 9.5 sand column under anaerobic & abiotic conditions. Li is mobile through the column as no sorption processes take place.

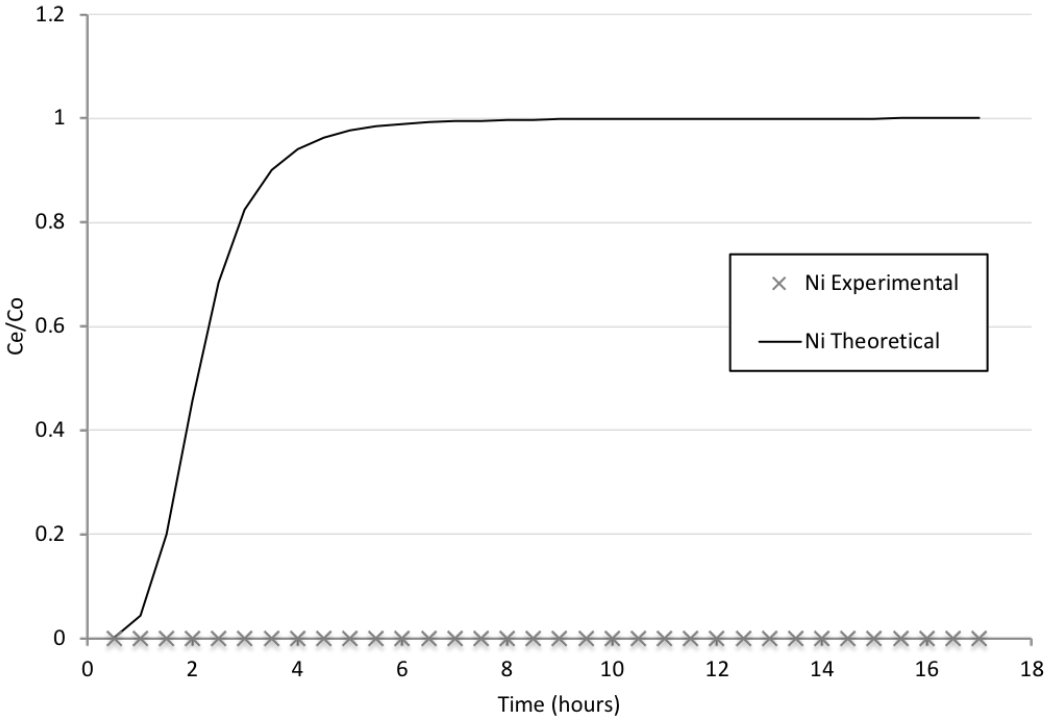

Figure 7. 3. Adsorption of Ni (grey crosses) through the same pH 9.5 sand column as Figure 7.2 under abiotic & anaerobic conditions. Ni is immobilised through the sand column due to sorption processes that take place.

Hydrolysed cellulose tissue (CDP) was utilized as a source of ISA to investigate the effect of complexants within an ILW repository on the mobility of adsorbed Ni. The composition of CDP stock is shown in Table 7.2.

Component	Mg/L in 1% CDP solution	Units
Na^+	22.44 ± 7.6	mg/ L
K^+	0.34 ± 0.15	
Ca^{2+}	6.32 ± 4.15	
Mg^{2+}	0.47 ± 0.50	
α-ISA	0.27 ± 0.077	mM
β-ISA	0.24 ± 0.078	

Table 7. 2. Cation and organic carbon composition of a 1% CDP solution.

Influent media spiked with CDP was passed through the Ni saturated column resulting in the detection of ISA (both α and β forms) and Ni in effluent fractions, indicating the formation of soluble complexes through the system and the ability of ISA to overcome the sorption of the Ni to the column. Breakthrough curves similar to

the conservative tracer were observed, with the presence of ISA identified at 3.09 hrs followed by the release of Ni at 3.65 hrs. Complete exhaustion of the components through the column system was established at 11.33 hrs (Ni) and 14.71 hrs (ISA) (Figure 7.4).

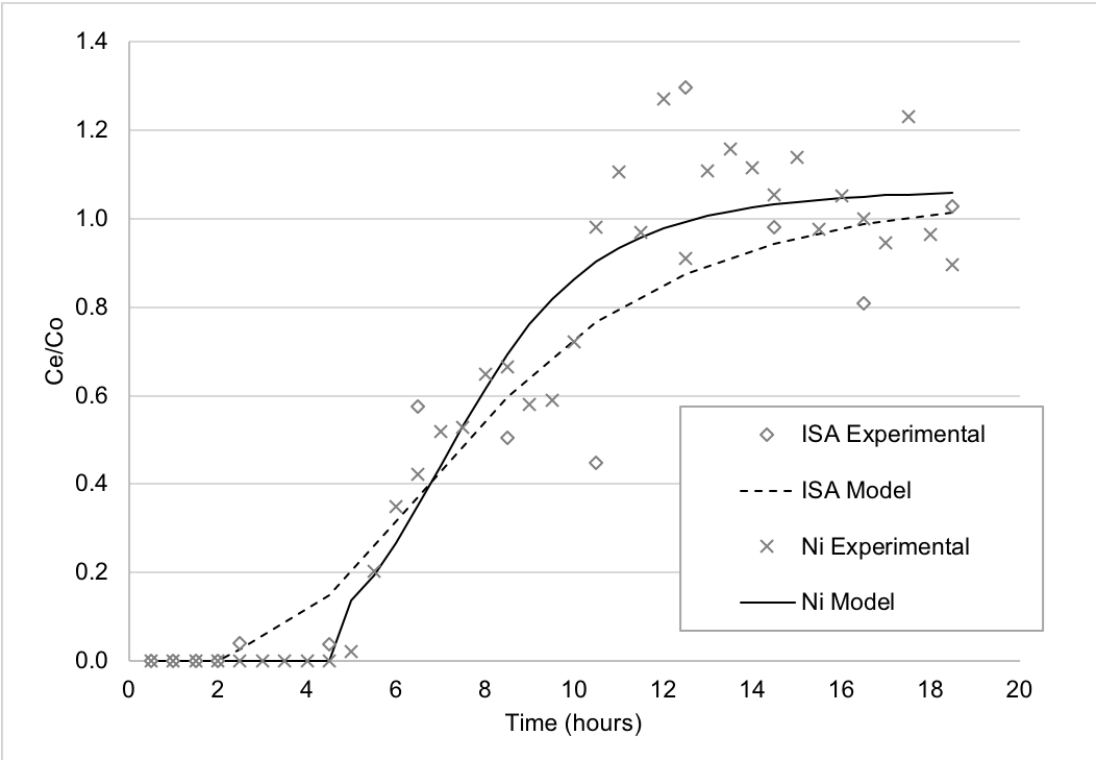

Figure 7. 4. The complexation of Ni + ISA under abiotic & anaerobic conditions. Ni (grey crosses) is stripped off the sand surface by the presence of ISA (empty grey diamonds) as they form soluble complexes at pH 9.5.

Influent media spiked with Ni and ISA resulted in the detection of both Ni and complexant in effluent fractions, indicating that complexation of the two had occurred in the liquid phase prior to entering the column (Figure 7.5). Breakthrough curves could not be calculated here as a result of Ni + ISA being introduced into the same column after the previous experiment.

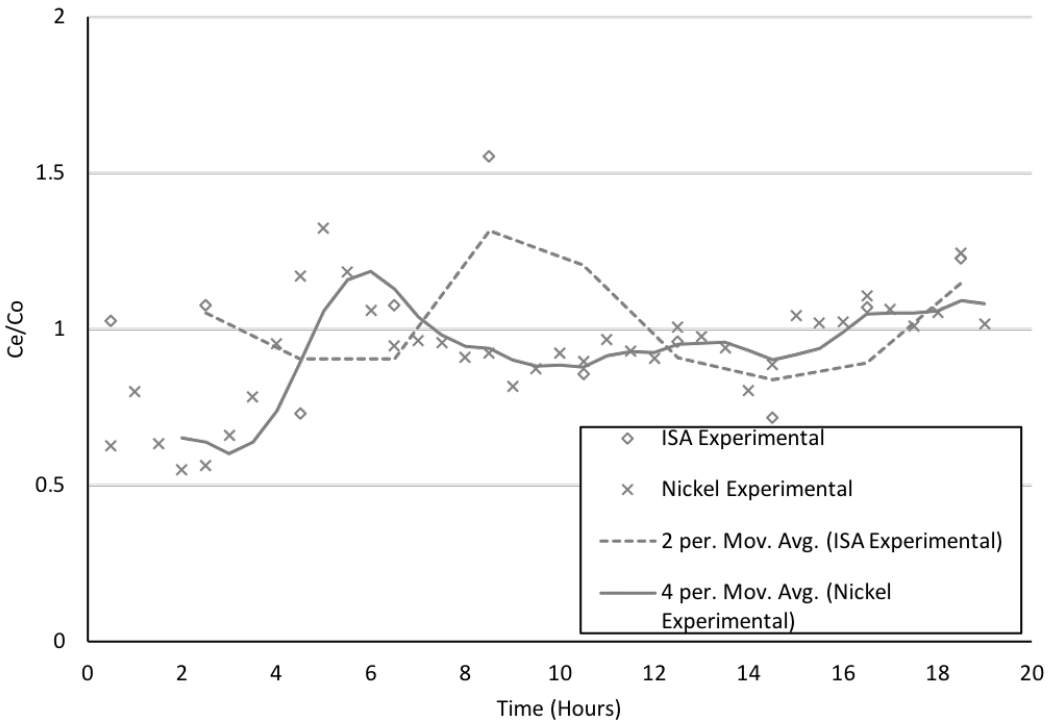

Figure 7. 5. Transport of the Ni-ISA complex at pH 9.5 through the sand column under abiotic & anaerobic conditions. Ni (grey crosses) and ISA (empty grey diamonds) form complexes during the liquid phase therefore no breakthrough is observed here.

7.2.2 Transport of nickel in biotic systems

7.2.2.1 Microbiome taxonomic profiling of floc-reactor

DNA from the bulk liquid of a previous established hyperalkaline floc-based biofilm reactor capable of ISA degradation was extracted and the 16s rRNA gene sequenced. Taxonomic composition of the microbial community at phylum level is presented in Figure 7.6, with the majority of sequences allocated to members of Firmicutes (48.1%), Bacteroidetes (33.2%) and Proteobacteria (18.5%).

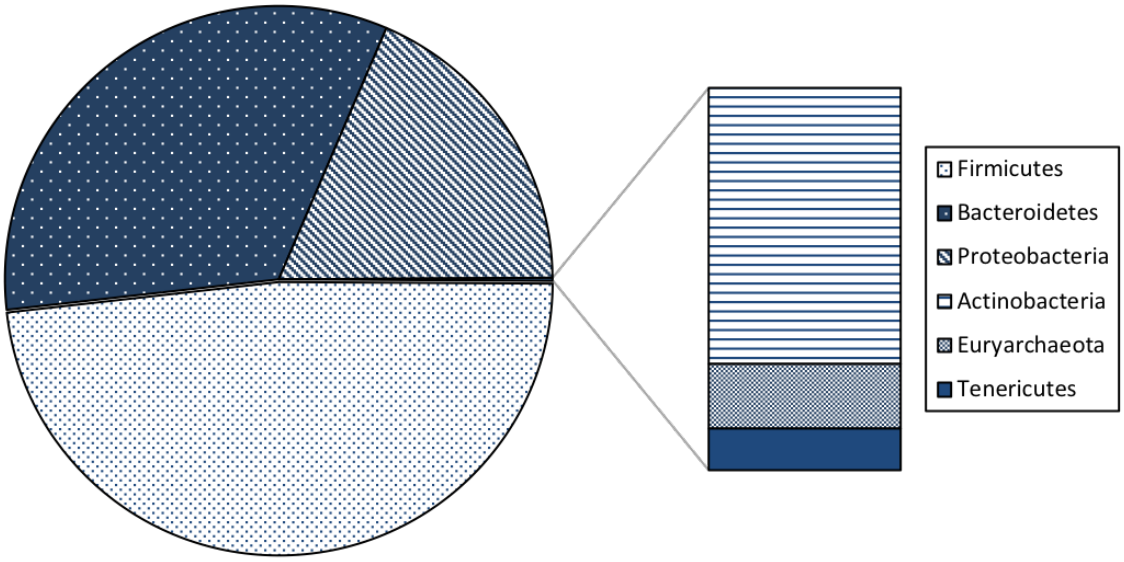

Figure 7. 6. Phylum-level taxonomic composition of pH 11.0 floc reactor. Microbial community analysis revealed Firmicutes to be the dominating phyla, followed by Bacteroidetes and Proteobacteria.

At class level members of Bacilli within the Firmicutes phylum accounted for almost half of (47.4%) of total sequences (Figure 7.7). Cytophagia dominated the Bacteroidetes representing 33.2% of sequences and the Alphaproteobacteria class prevailed within Proteobacteria making up 17.6% of total reads. *Alkalihalobacillus* formed a large portion of the Firmicutes population. This genus is comprised of predominately alkaliphilic/ halophilic species both facultative anaerobes and aerobes isolated from diverse surroundings including marine and soil environments (Patel & Gupta, 2019). Charles *et al* described a microcosm composed primarily of families within the Firmicutes phylum capable of ISA degradation at high pH (Charles et al., 2015a). In addition to reports of bacillus species able to survive under highly alkaline conditions, some alkaliphilic bacillus are also capable of EPS production (Perry et al., 2005). *Fontibacter* was the major genus representative of the class Cytophagia, members of which have been isolated from a circumneutral microbial fuel cell (pH 7.2) (Yang, Shungui, Wang, Yuan, & Zhuang, 2012) and an alkaline hot spring (pH 8.0) (Kämpfer et al., 2010). *Loktanella* genus prevailed within Alphaproteobacteria

and contains species previously isolated from microbial mats in the lakes of Antarctica (Van Trappen, Mergaert, & Swings, 2004).

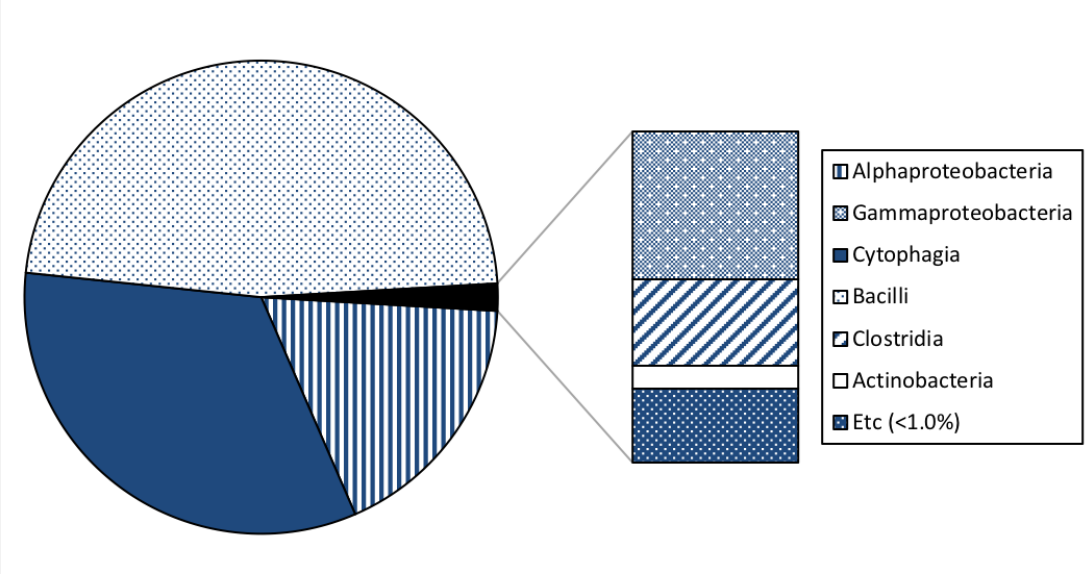

Figure 7. 7. Class-level community analysis of floc reactor operating at pH 11.0. Taxonomic comoposition revealed enrichment was predominantly comprised of members of the Bacilli, Alphaproteobacteria and Cytophagia classes.

The archaeal component only represented 0.03% of the total population, with 3 sequences belonging to the Methanobacterium genus and the remaining 1 sequence belonging to the Methanosarcina genus (Figure 7.8).

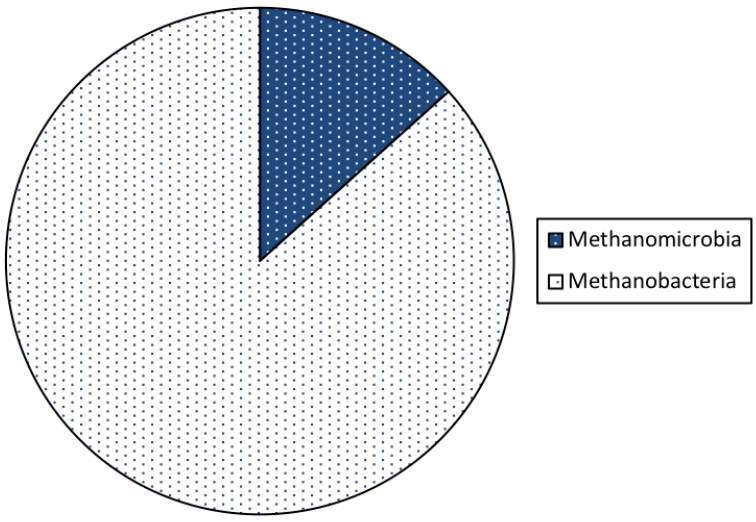

Figure 7. 8. Archael presence within pH 11.0 floc reactor. Here, Methanobacteria dominated with 1 sequence from Methanomicrobia also detected.

CLSM imaging revealed that microbial flocs present within the reactor system were primarily composed of lipids, protein, and extracellular DNA (eDNA), three of the main structural components of biofilm EPS. Also detected within the flocs were β-1,4 and β-1,3 polysaccharides, in addition to smaller quantities of α-mannopyranosyl and α-glucopyranosyl sugars. CLSM images exhibited large areas of concentrated protein, with regions of lipids closely associated with the presence of eDNA and cells (Figure 7.9). EPS proteins play various roles in the formation and propagation of microbial biofilms including enhancing cell to surface attachment in addition to stabilisation and development of the biofilm architecture (Fong & Yildiz, 2015).

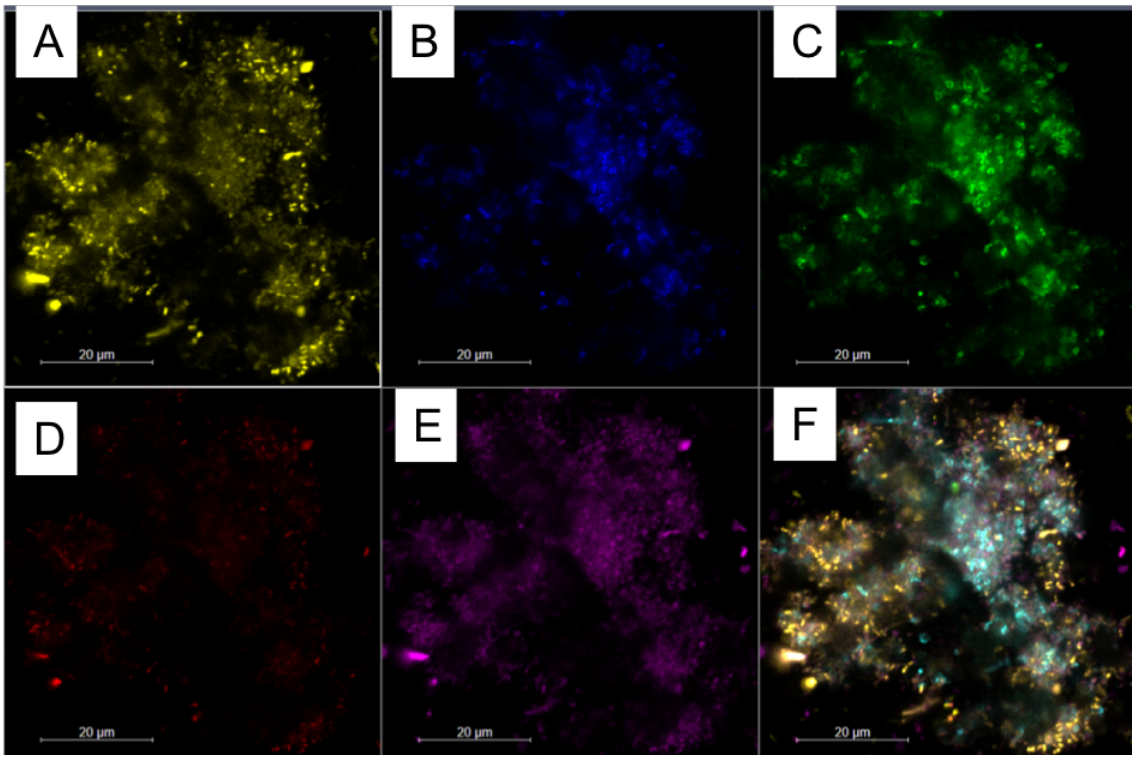

Figure 7. 9. CLSM investgation of microbial flocs within pH 11.0 microcosm. The EPS aggregate was composed of [A] lipids, [B] β-1,4 and β-1,3 polysaccharides, [C] proteins, [D] α-mannopyranosyl and α-glucopyranosyl sugars and [E] eDNA and cells. [F] is a combined image of all components.

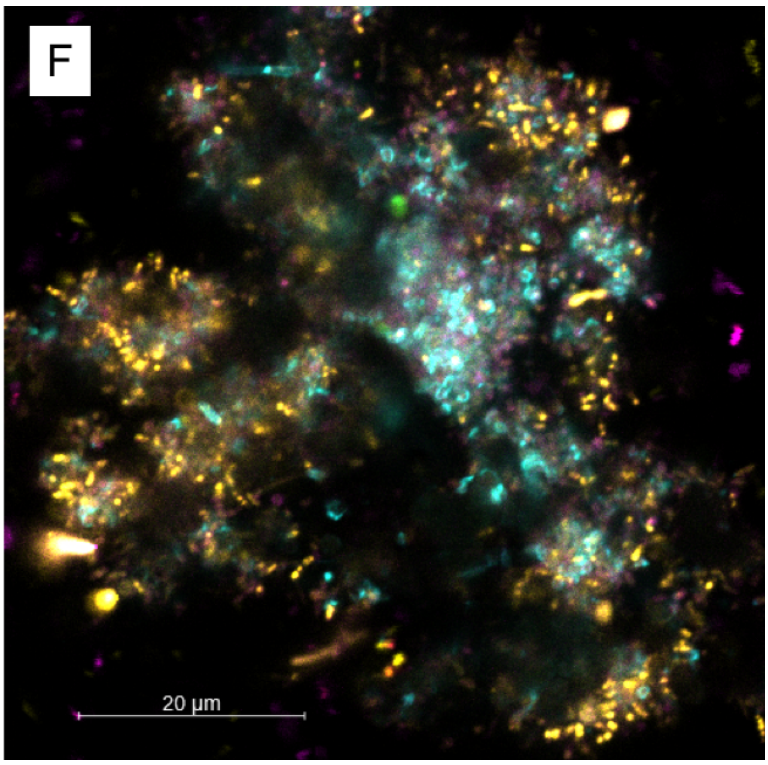

[F] Enlarged image of combined image.

7.2.2.2 Biotic sorption experiments

To investigate the effect of microbial biofilms on sorption reactions within the flow-cell system, influent media inoculated with floc reactor fluid was passed through the column to seed the sand surface with biofilm material. The same experimental procedure as previously described (for abiotic sorption) was setup with both Ni and ISA in the influent media and run for an 18-hour passage. Analytical analysis of effluent fractions demonstrated a ~60% reduction in total ISA across the column, however removal of Ni from solution was not observed (Figure 7.10). Degradation of ISA at pH 9.5 is supported by the generation of acetic acid as a direct result of fermentation processes (Figure 7.11), with small concentrations of other volatile fatty acids (VFAs) also detected in some of the fractions (Table 7.3). A complete removal of acetic acid seen at 15.5hr & 18hr was most likely due to methanogenesis. HPAEC data suggests that microorganisms present within the column do not favour the consumption of α-ISA over β-ISA (or vice versa), which negates the hypothesis that Ni could still be strongly complexed to one diastereomer while the other is easily degraded.

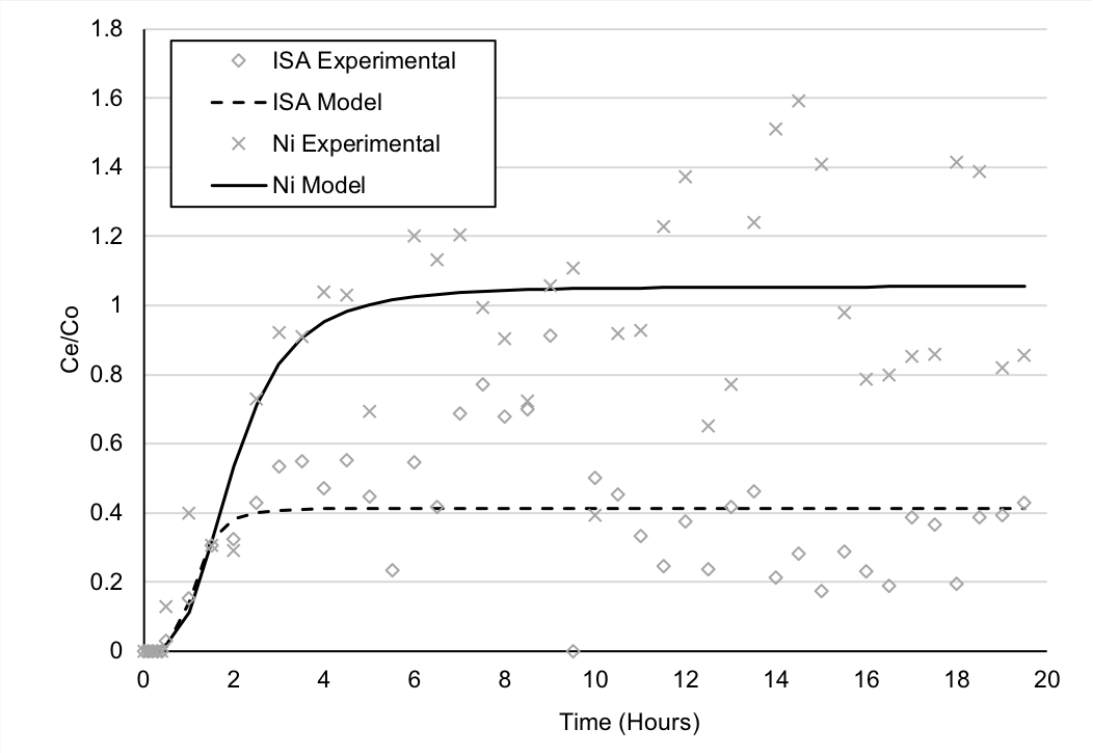

Figure 7. 10. ISA degradation by sand column biofilm at pH 9.5. Level of Ni (grey crosses) indicates no reduction at this point depsite 60% of complexed ISA (empty grey diamonds) being degraded within the system.

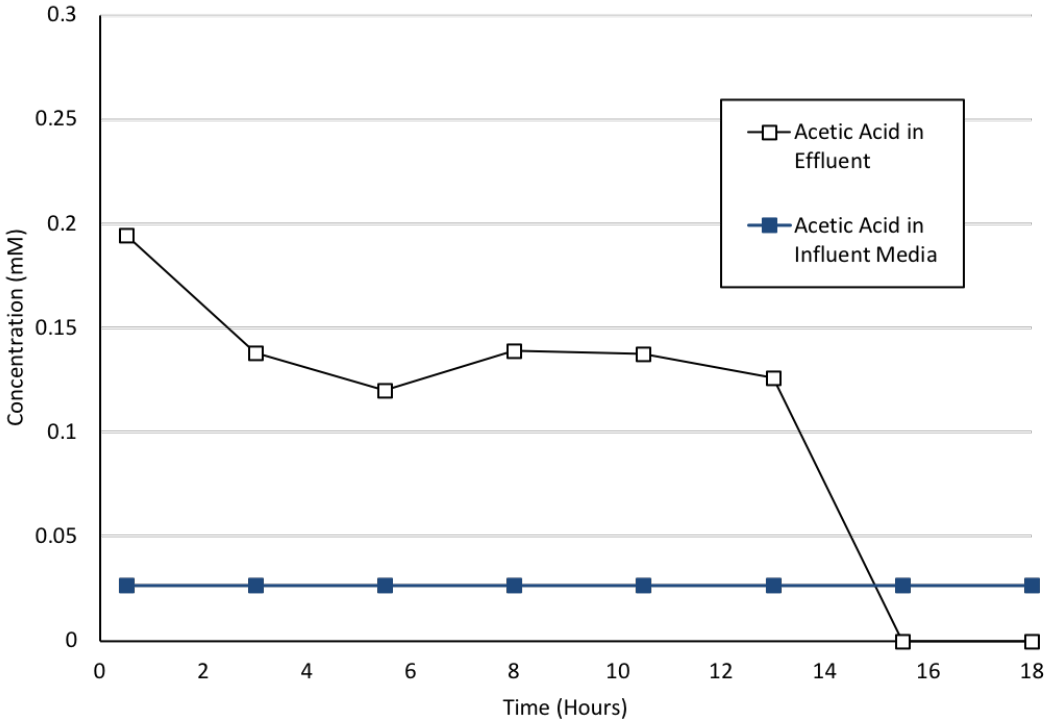

Figure 7. 11. Acetic acid levels within influent media (blue squares) and measured in effluent samples (empty black squares). Generation of acetic acid through the sand column indicates degradation of ISA seen in Figure. 7.10 is due to microbial processes occuring rather than sorption events.

	Concentration (mM)			
Time (hours)	Acetic Acid	Isobutyric	Isovaleric	Valeric
0.5	0.195	0.049	-	-
3	0.138	0.000	0.039	-
5.5	0.120	0.038	0.044	-
8	0.139	-	0.043	-
10.5	0.137	-	0.062	0.053
13	0.126	-	-	0.043
15.5	-	-	-	-
18	-	-	-	-

Table 7. 3. Concentration of acetic acid and other detected VFAs associated with Fig. 7.11.

Figures 7.4 & 7.5 demonstrate the successful complexation between Ni and ISA within the sand column therefore the observation of ISA degradation without any consequence for Ni suggests that there are possibly other influences present that are ensuring the transport of Ni. One theory that was explored what the possible biosorption of Ni ions to flocculate material detaching off the biofilm (Figure 7.12) which resulted in enhanced migration of Ni through and out of the column (Seneviratne, Vithanage, Madawala, & Seneviratne, 2015). The presence of both positive and negatively charged functional groups on the surface of the EPS matrix could allow for the binding of positively charged metal ions, with EPS having particularly high affinity for divalent cations (ie. Ni^{2+}) (Decho & Gutierrez, 2017). Influent media contaminated with Ni and ISA was passed through the column under the same experimental conditions previously described, with the exception that effluent samples were filtered through 0.45μM membrane filters upon collection to remove any bacterial aggregates from solution.

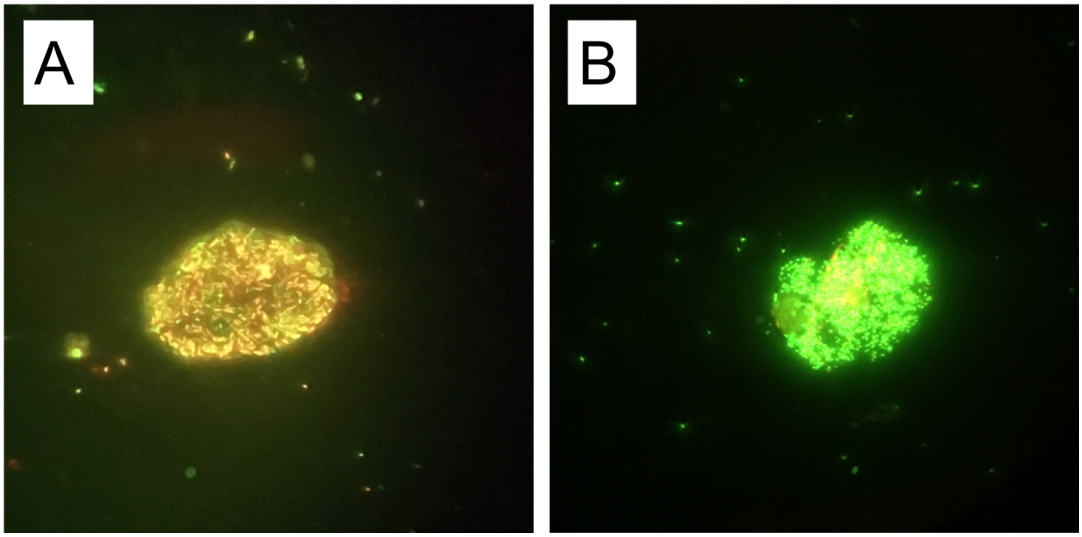

Figure 7. 12. Live/dead imagery of microbial flocs leaving sand column biofilm at pH 9.5 (images at x1000 magnification). Live (green) and dead (red) cells are both detected, with the reduction of live cells in [A] possibly due to lack of adhesion surfaces as it exits the sand column.

ICP-MS analysis indicated that over the course of an 18-hour experiment Ni levels in effluent solution decreased from ~50% to ~20% of the influent, a contrast from the previous experiment in which removal of Ni from solution was not observed at all (Figure 7.13). Furthermore, the concentration of ISA reduced by 80% on average across the column, with HPAEC-PAD analysis demonstrating the degradation of both α and β, and the production of acetic acid in liquid samples supporting the degradation of both forms of ISA (Figure 7.14). This data suggests that the presence of microbial biofilm could successfully limit the transport of Ni through an anaerobic and alkaline system by degrading the complexed ISA. Fermentation of ISA seen here is marginally greater than the previous experiment however the level of Ni removal is considerably higher, therefore it's possible that the shedding of microbial material from the biofilm could be linked to heightened Ni migration even under ISA degrading conditions (Figure 7.10).

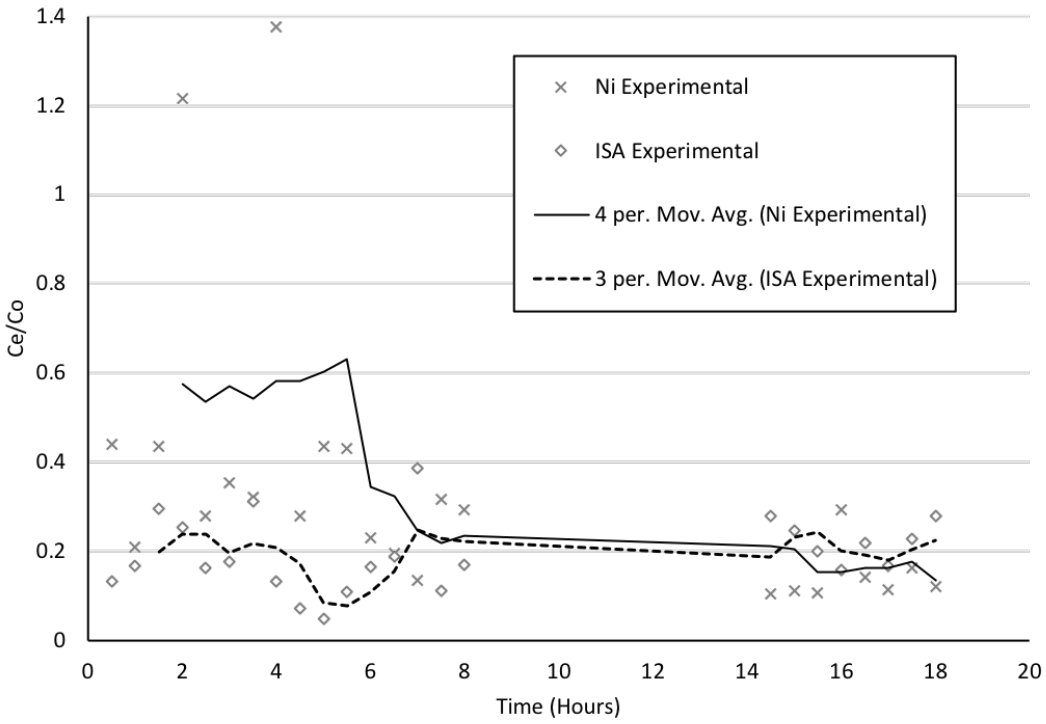

Figure 7. 13. ISA degradation & reduction measurable Ni in effluent samples. Ni (grey crosses) is immobilised (to around 60-20% of influent level) as it transports through the biotic and anaerobic sand column. ISA (empty grey diamonds) is degraded (to around 20% of influent) through the same system.

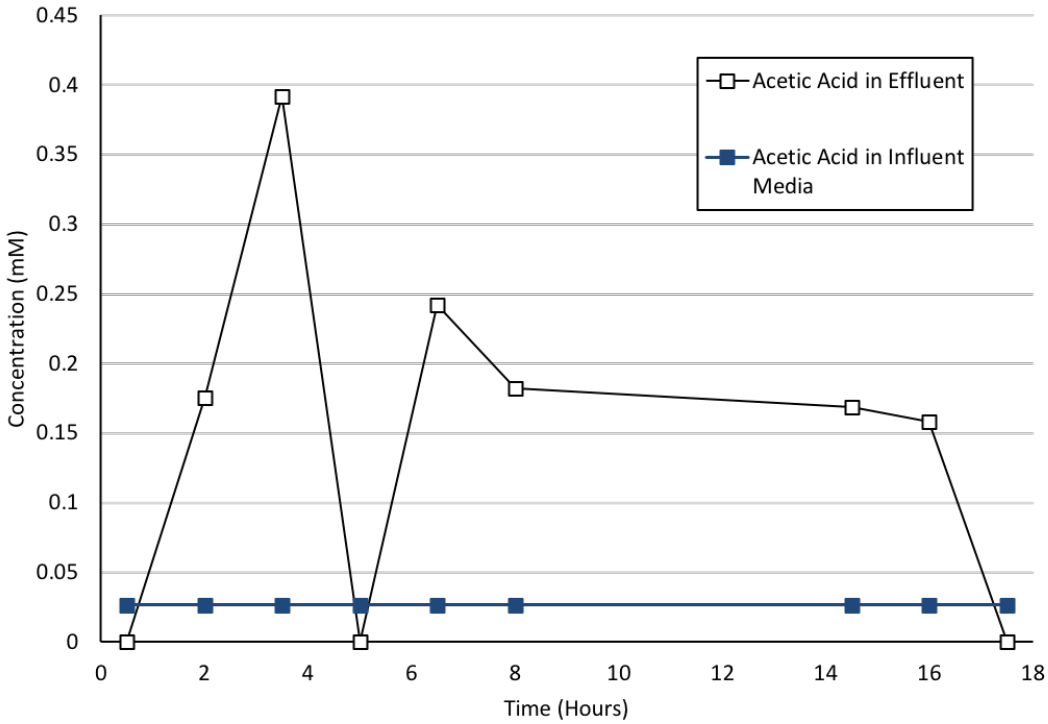

Figure 7. 14. Generation of acetic acid through the biofilm sand column. Data associated with Figure. 7.13 and indicates microbial proccesses are taking place within the system.

It can be theorised that the reduction in Ni over the course of the experimentation was caused by the filtering of flocculate material that potentially had Ni attached to the surface, thereby reducing the level of Ni in solution. To investigate this further microscopy methods were employed to study the filter membranes. An investigation using SEM imaging revealed clusters of material indicative of microbial biofilm on experimental filter membrane surfaces (Figure 7.15). Elemental analysis determined that the EPS material here was predominantly composed of carbon, oxygen and calcium but exhibited no trace of Ni within the matrix. Areas of brightness that portray the presence of heavier elements displayed higher levels of calcium (Ca) in comparison to darker areas, with an increase in oxygen also found in Ca rich spots (Figure 7.16). These regions of Ca dense clusters were also found on other filter samples. This could signify the formation of calcium carbonate precipitates or calcite embedded within or on top of EPS matter, most likely as a result of Ca that's present within CDP reacting with CO_2 produced during fermentation processes (Figure 7.17).

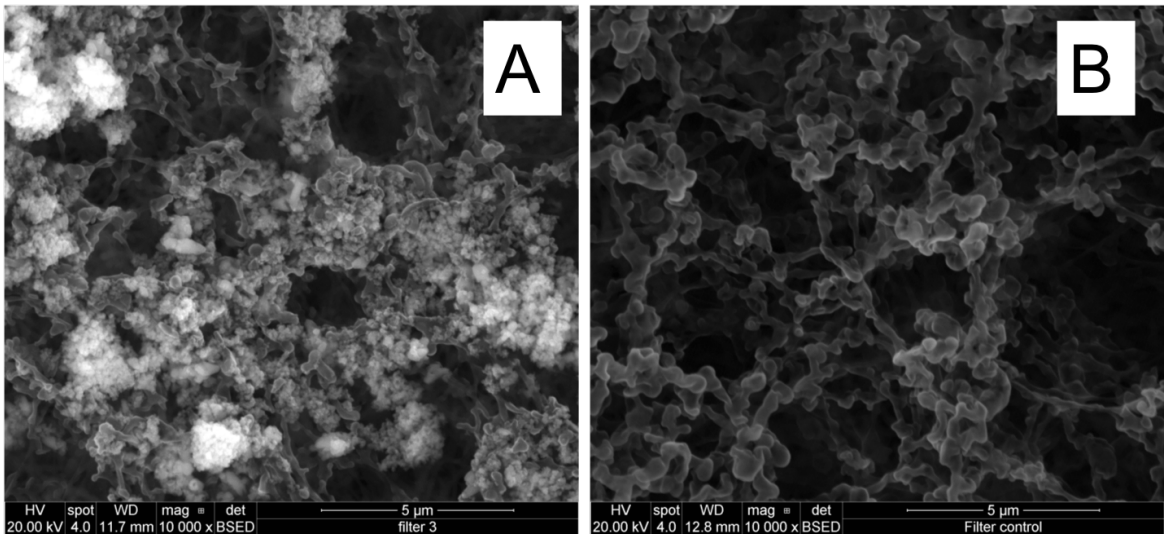

Figure 7. 15. SEM imagery of 0.45µM filter membranes. [A] Material indicative of microbial biofilm embedded within the filter in addition to clusters of heavier elements vs [B] Control membrane not exposed to column effluent samples.

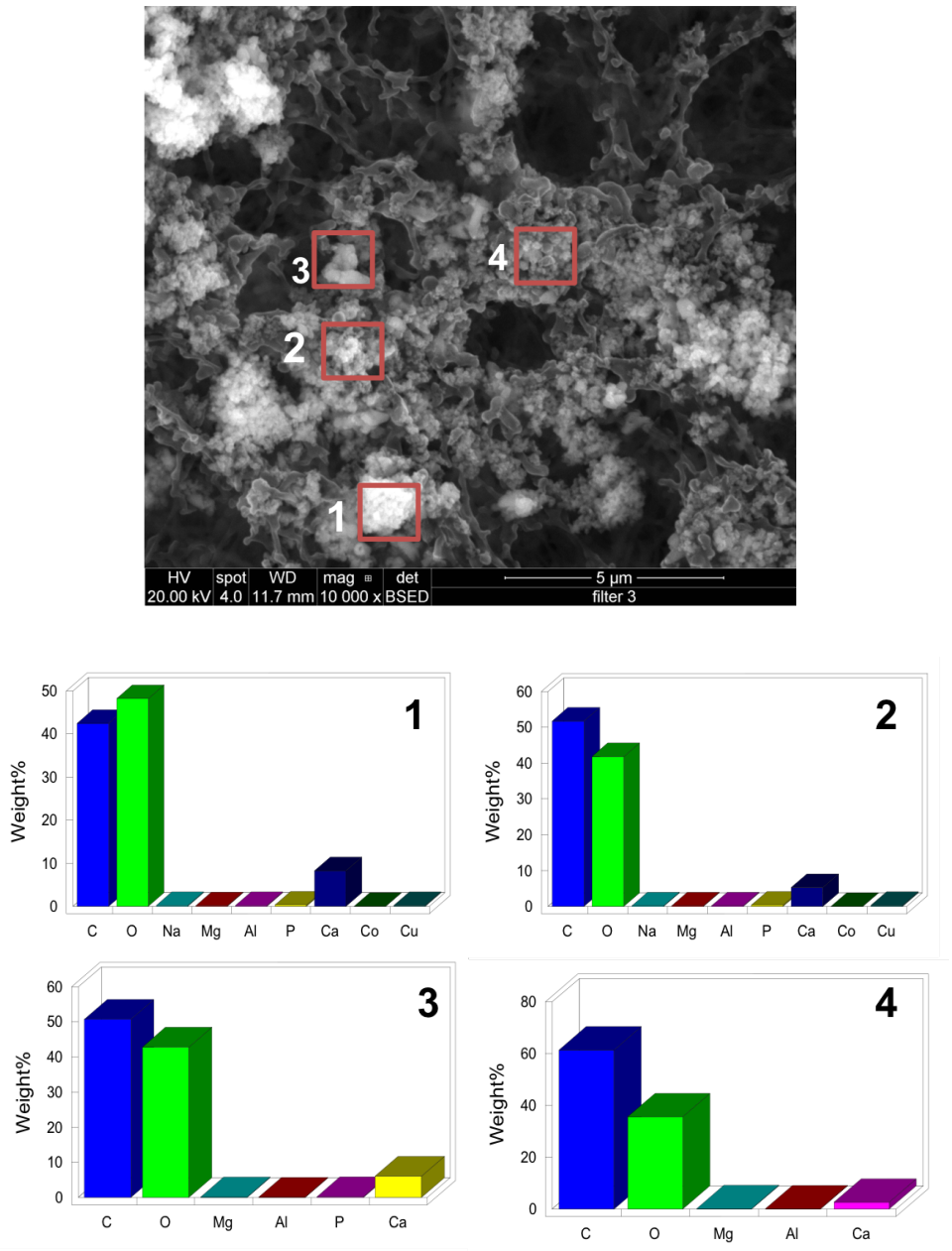

Figure 7. 16. EDX analysis of biofilm material embedded in filter membranes. High level of C within biofilm material. Ca rich spots also linked to increased levels of O, indicative of calcium carbonate formation.

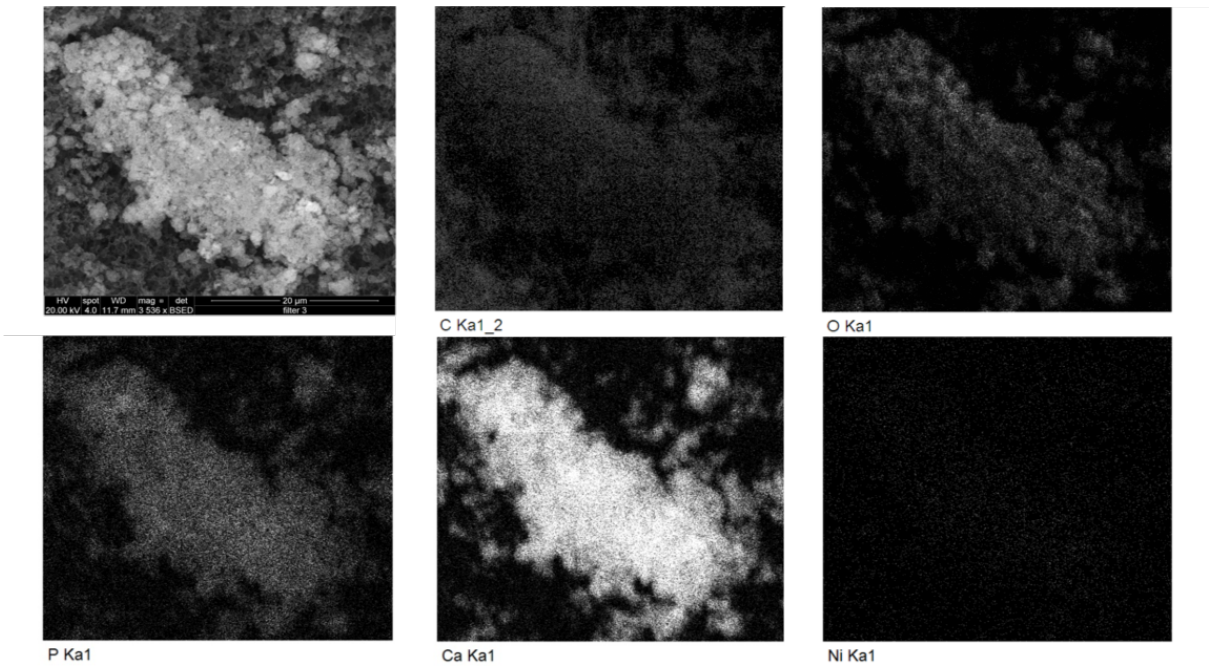

Figure 7. 17. Elemental mapping of large clusters of material found on filter membranes. High levels of Ca and O also present, with some P.

Further investigation found that a particular clump of material possessed traces of surface Ni. Elemental mapping (Figure 7.18) and quantitative EDX analysis (Figure 7.19) revealed that the aggregate was largely composed of iron and oxygen. Fe(II) hydroxides may form when Fe(II) salts in solution react with hydroxide ions, the precipitates of which are highly insoluble. Aggregates may form under continuous precipitation that could be capable of transporting dissolved Ni through adsorption processes. The size of the particle indicates it's too large to be a nanoparticle yet too small to be a singular microbial floc, therefore aggregate seems more applicable here. There was very little to no evidence of flocculate material found on the majority of experimental filter papers analysed by SEM/EDX microscopy, which implies that not enough material is detaching from microbial biofilm within the column to enhance Ni migration in this way. Data here suggests that under anaerobic and alkaline conditions of the column the formation of iron oxides, potentially with other minerals present in solution, could lead to the colloidal, rather than microbial, migration of Ni.

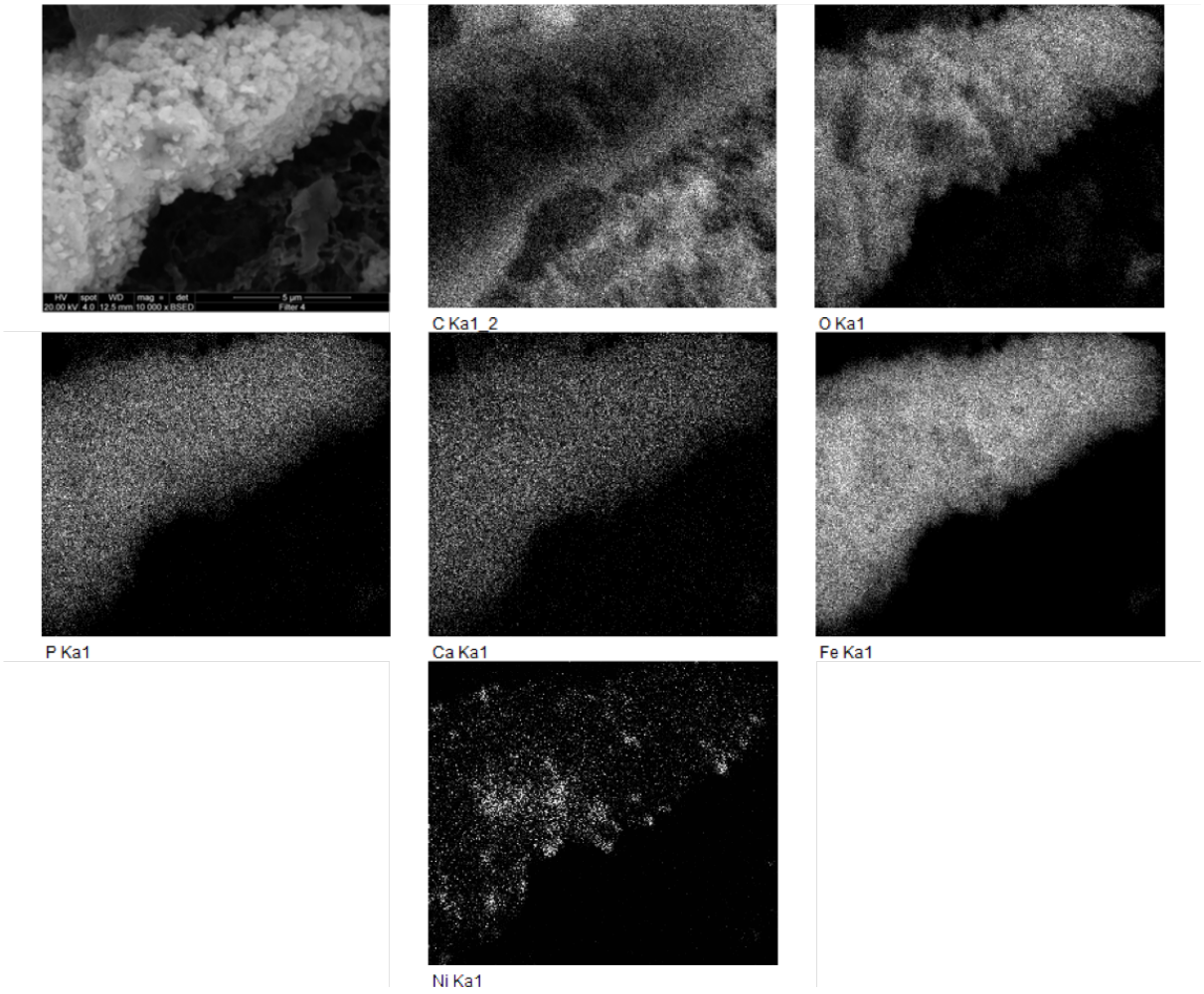

Figure 7. 18. Elemental mapping of aggregate of interest on filter membrane using EDX detector. Ni detected on the surface potentially indicating microbial transport through the sand column.

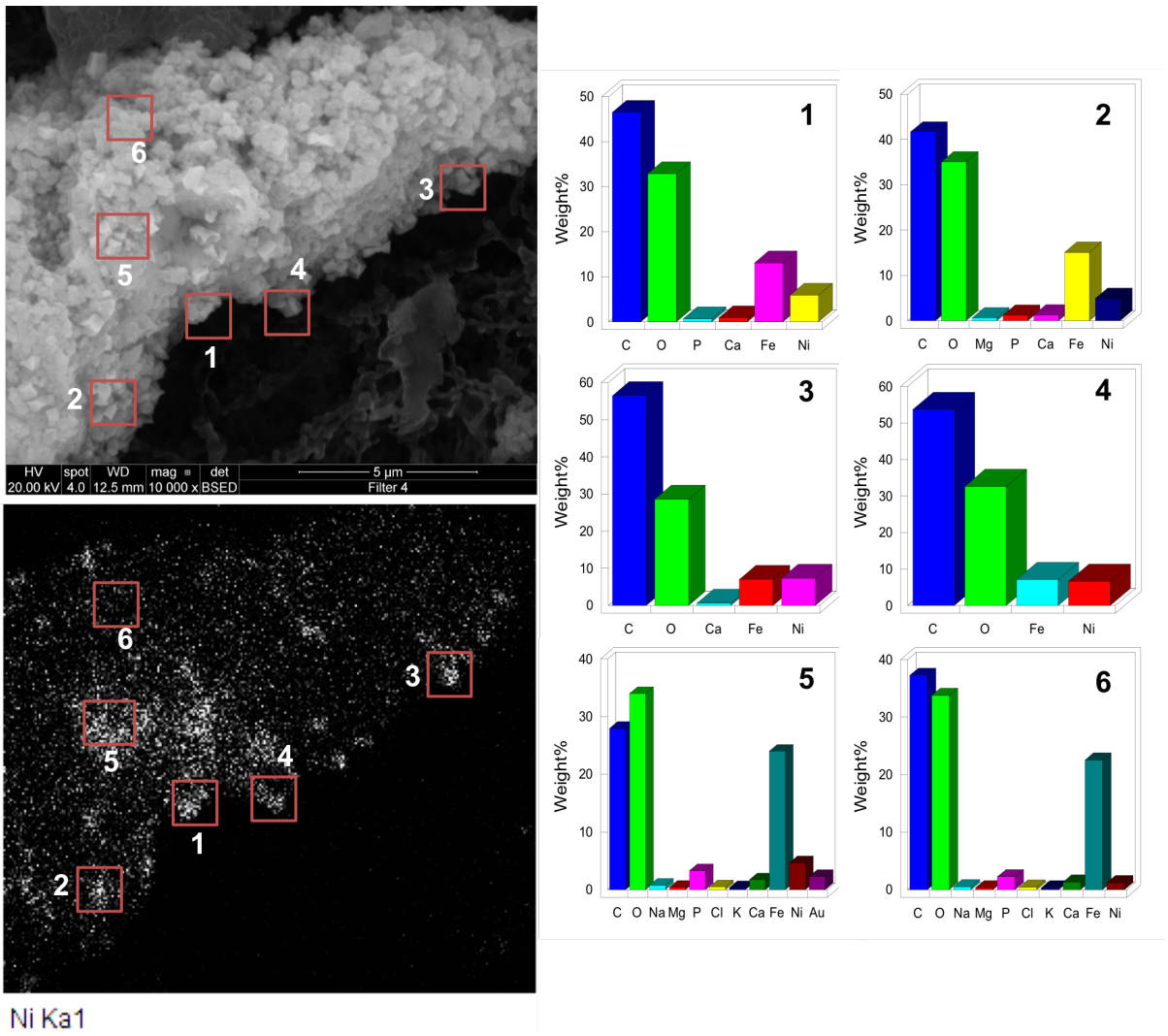

Figure 7. 19. Elemental profiles of Ni rich areas on the particle surface. High level of Fe and O, in addition to P, more likely this could be colloidal rather than microbial.

To determine whether the fate of Ni is due to sorption to flocculate or colloidal material or ISA degradation, another flow-through experiment was set up using the same conditions previously described. Briefly, influent media at pH 9.5 spiked with Ni and ISA was passed through the sand column over an 18-hour time period, with an additional end step that involved filtering half the volume of all samples while leaving the other half unfiltered. ICP-MS, HPAEC-PAD and GC-FID analysis of effluent fractions revealed no discernible differences between the profiles of unfiltered vs filtered samples indicating filtration of samples had no effect on the level of Ni remaining in solution, and therefore only unfiltered results are presented here for consistency with this dataset. Consequently, the data implies that the high level of Ni displayed in the effluent of previous experiments was not likely to be as a result of

colloidal/ flocculate transport. The subsequent data whereby ISA degradation is linked to immobilisation of Ni is a much more authentic representation of the behaviour of Ni under the far-field conditions of this investigation.

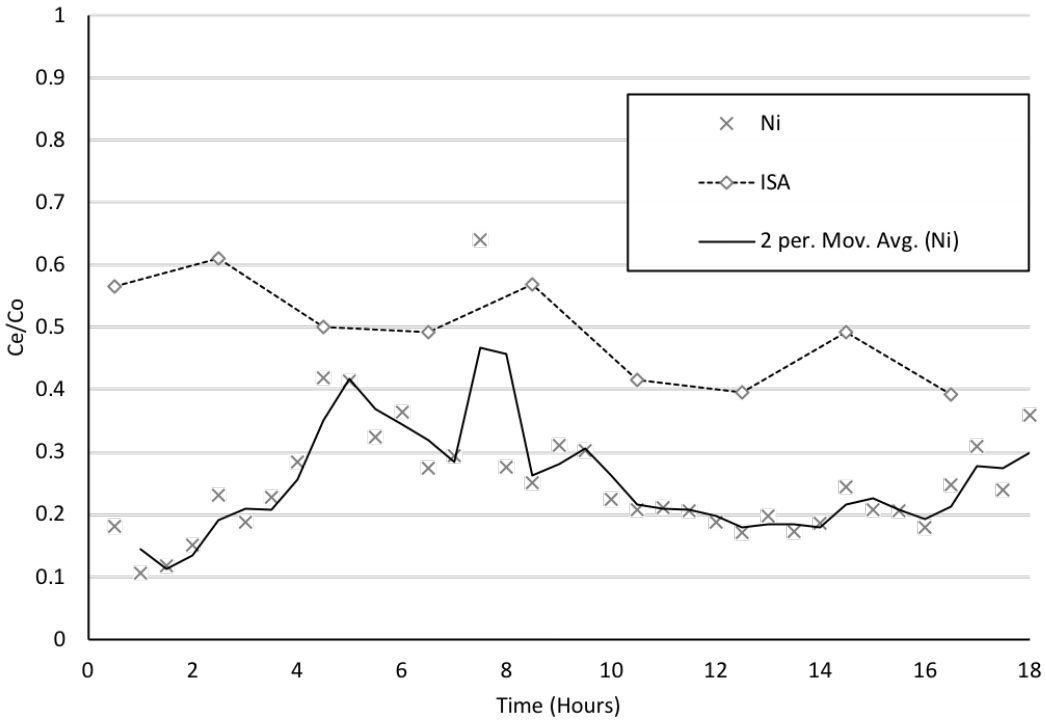

Figure 7. 20. Immobilisation of Ni (grey crosses) and degradation of ISA (empty grey diamonds) through a biotic & anaerobic sand column at pH 9.5. Under far-field conditions of thiis investigation ISA is degraded by biofilm forming microorganisms leading to the reduced transport of complexed Ni trough the system as it adsorbs back to the sand surface.

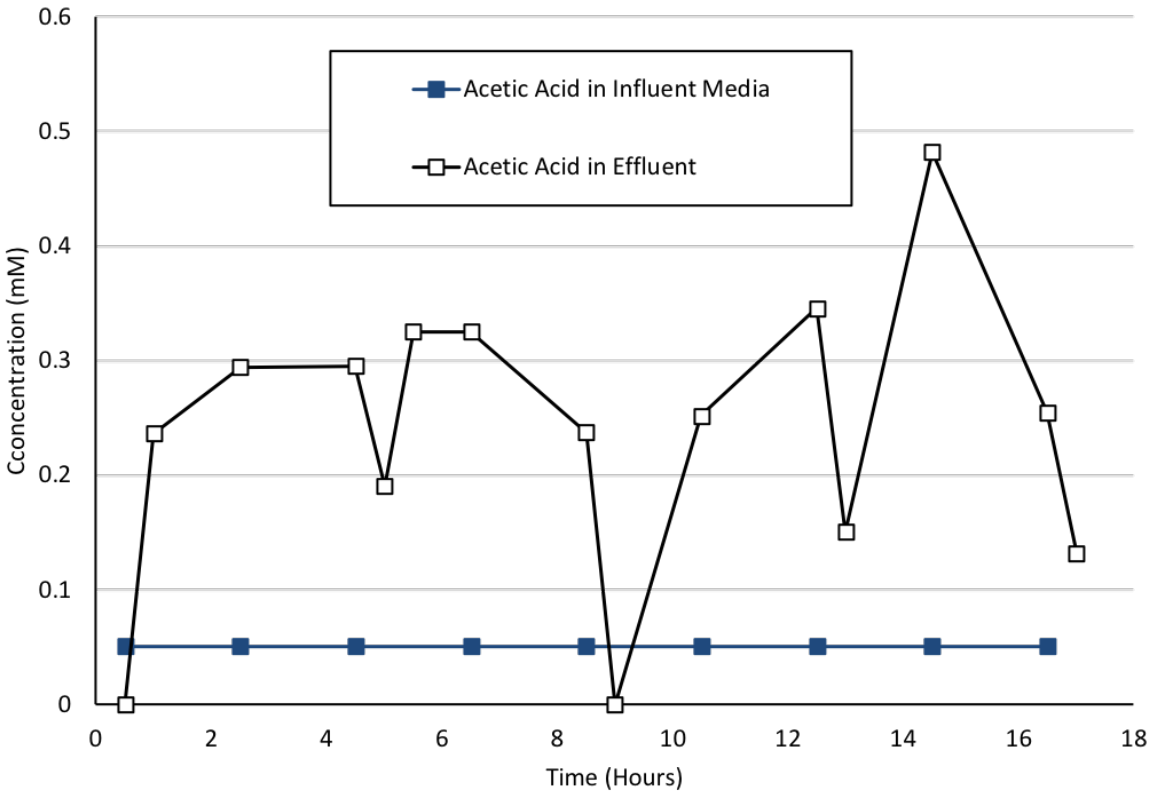

Figure 7. 21. Generation of acetic acid within effluent samples (empty black squares) and the level of acetic acid within influent media (blue squares). VFA indicates fermentation processes are taking place within the column.

An average ~75% of influent Ni had been removed across the length of the column (Figure 7.20), with total ISA levels reducing from ~60% of influent level to ~40% at the end of the 18-hours. Both α and β forms of the complexant were removed with similar degradation profiles (data not shown). While this data demonstrates again that complete removal of ISA is not observed fermentation processes are certainly taking place due to the presence of volatile fatty acids (acetic acid) in solution, indicating that ISA removal is microbially mediated rather than due to sorption events (Figure 7.21). A reduction in the level of ISA is consistent with a decrease in soluble Ni, thereby an assumption can be made that the ISA being degraded was in complexation with Ni.

Figure 7.20 successfully demonstrates that under the anaerobic and alkaline conditions of the far-field investigated within this chapter of work, the mobility of complexed Ni can be hindered under the influence of biofilm-forming microorganisms

which degrade the organic complexant and reduce the flow of Ni through the geosphere, allowing its adsorption back to sand material present in the subsurface.

7.2.2.3 $Ni(ISA)_2$ complexation

Data from Ni sorption experiments shown within this chapter indicate that a level of ISA degradation can occur that influences the transport of a $Ni(ISA)_2$ complex but that full degradation of ISA and complete immobilisation of Ni is not observed. An investigation by Rout *et al* demonstrated that under alkaline conditions (pH 9.0) *Macellibacteroides fermentans* Strain HH-ZS, an obligate anaerobe, successfully fermented ISA. In this study ISA is consistently removed over the course of the experiment but never reaches zero, with the concentration flattening out over the last 5 days at ~1mM ISA (Rout, Salah, Charles, & Humphreys, 2017). Similarly, Rout determined that under anoxic and slightly higher pH conditions (pH 9.7 - 9.8) that a novel strain *Exiguobacterium* sp Strain HUD was capable of degrading ISA over the first 14 days of experimentation from ~3.9 mmol L^{-1} to 2.1 mmol L^{-1}. Rate of degradation then reduced considerably and from day 45 – day 60 of the study ISA remained constant at 1.9 mmol L^{-1} (Rout, 2015). These data indicate that when $Ca(ISA)_2$ complex is utilized as a carbon source it is not completely degradable and is never fully removed from the system that ISA exists within. As a divalent cation it's entirely possible that the $Ni(ISA)_2$ complex depicted within this chapter of work is behaving in the same way which is why complete removal of Ni is not observed.

Complexation reactors were set up in both pure culture (*Exiguobacterium*) and mixed culture (floc reactor 7.2.2.1) in order to investigate how readily α-ISA is degraded when it is complexed to Ni. In pure culture degradation occurred over the first 4 days from 3.23 mM to 2.94 mM, after which concentration began to rise again before settling around 3.20 mM at day 10 (Figure 7.22). The pH of test reactors remained relatively unchanged which is most likely due to not enough fermentation occurring to produce sufficient acetic acid, however VFAs were not measured here. CO_2 was detected in both test and control reactors, indicating that perhaps there was some contamination here.

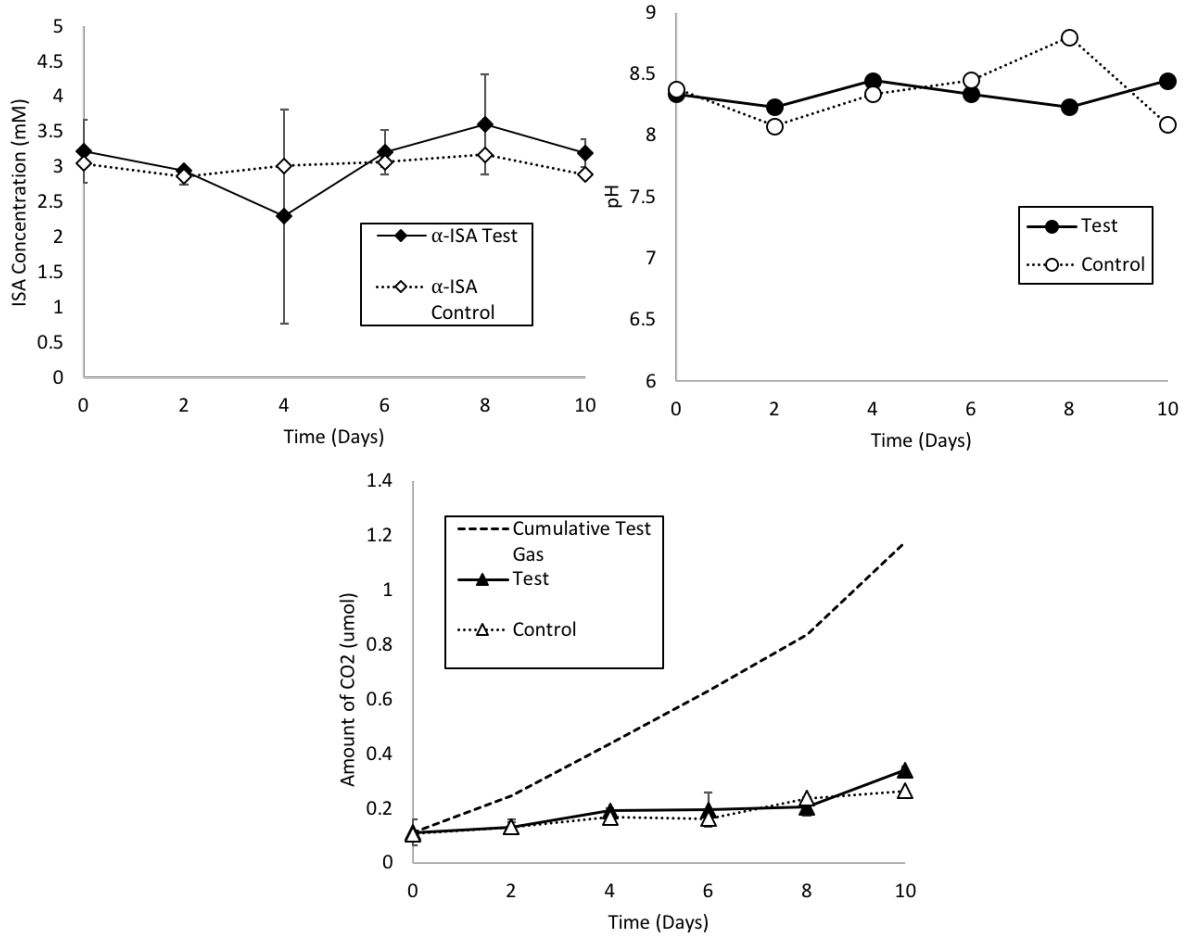

Figure 7. 22. α-isosaccharinic acid profile, pH and CO_2 levels within test and controls reactions studying the degradation of $Ni(ISA)_2$ complex by *Exiguobacterium.* α-ISA is not readily degraded under the conditions of the experiment over a 10-day period, pH is unchanged and CO_2 is detected in both test and control reactions.

In mixed culture reactors ISA removal was observed over the first 8 days from 4.95 mM to 3.63 mM, after which ISA appeared to remain constant and measuring 3.65 mM on day 14 of the experiment (Figure 7.23). The pH of test reactors appeared to drop after day 6, potentially due to acetic acid production. However, a drop in pH was also noted in control reactors although not as much. CO_2 was measured in test reactors over the 14 days but none was detected in control reactors which suggests that CO_2 was produced as a result of fermentation processes. Results here further suggest that when α-ISA is complexed to divalent Ni it's possible that the organic complexant is unable to undergo complete degradation.

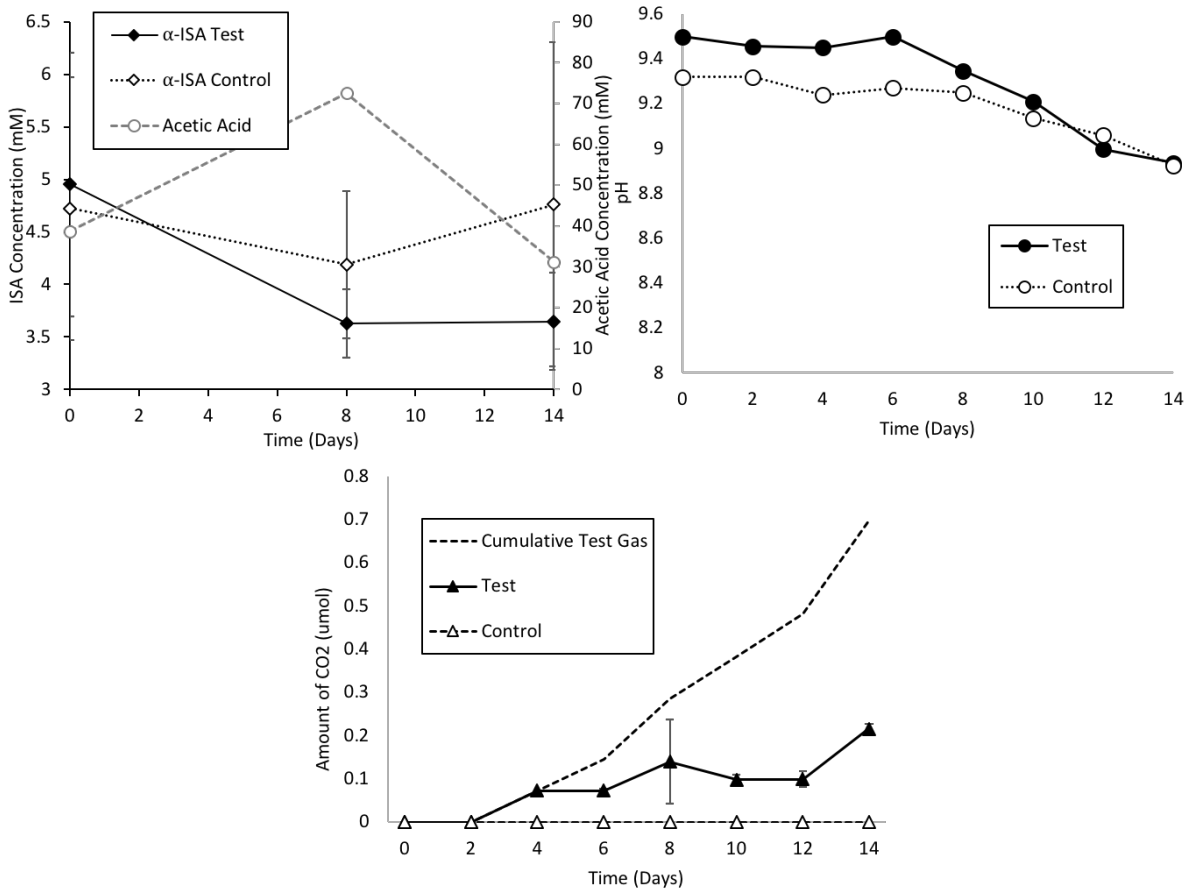

Figure 7. 23. α-isosaccharinic acid profile, pH and CO_2 levels within test and controls reactions studying the degradation of $Ni(ISA)_2$ complex in mixed culture. α-ISA is degraded over the first 8 days of the experiment after which concentration remains stable until day 14, a slight decrease in pH is detected most likely due to the production of acetic acid although this decrease is also measured in control reactors, and CO_2 production is observed in test reactions but not in controls which is indicative of fermentation processes taking place.

The effects of Ni toxicity on ISA degradation have been reported by Kuippers *et al* who showed that ISA removal was observed in systems with 0.1mM Ni but not 1mM Ni, a concentration which induces Ni toxicity to the microorganisms therefore preventing biodegradation of ISA. It's important to note that this investigation was carried out at circumneutral pH whereas conditions within the far-field are still expected to be in the alkaline range. However, the concentration of Ni described in this chapter of work falls below the "non-toxic" 0.1mM studied by Kuippers *et al,* and far below the expected level of Ni within a GDF post-evolution, therefore the toxicity of Ni on biodegradation was not investigated here (Kuippers et al., 2018).

7.2.3 Sand biofilm characterisation

Following completion of abiotic & biotic sorption experiments the sand column was dismantled and the material extracted in order to investigate the properties of the microbial biofilm and sand within. The length of the column was separated into three equal sections (influent, middle and effluent) which were analysed as individual groups in order to explore any characteristic changes of the sand or biofilm depending on position within the column. Sand material was portioned out and processed according to the analysis to be performed.

7.2.3.1 Microbiome Taxonomic Profiling

As the sand biofilm was not highly developed in terms of bulk biomass, multiple samples were taken from each section of the column and pooled during DNA extraction. Results here are based on DNA samples that were amplified through PCR and subsequently nested in order to reach the concentration required for metagenome analysis. In this study the microbial community only was investigated.

Taxonomic composition at phylum level revealed variation through the sectioning of the sand column (Figure 7.24). At the influent Actinobacteria and Proteobacteria dominated with 70.37% and 18.55% respectively. Towards the middle section of the column the abundance of Actinobacteria decreases to 46.05% and Firmicutes become more prominent with 36.26% of reads. At the effluent section Proteobacteria and Firmicutes become the dominating phyla with 39.79% and 32.49% abundance respectively.

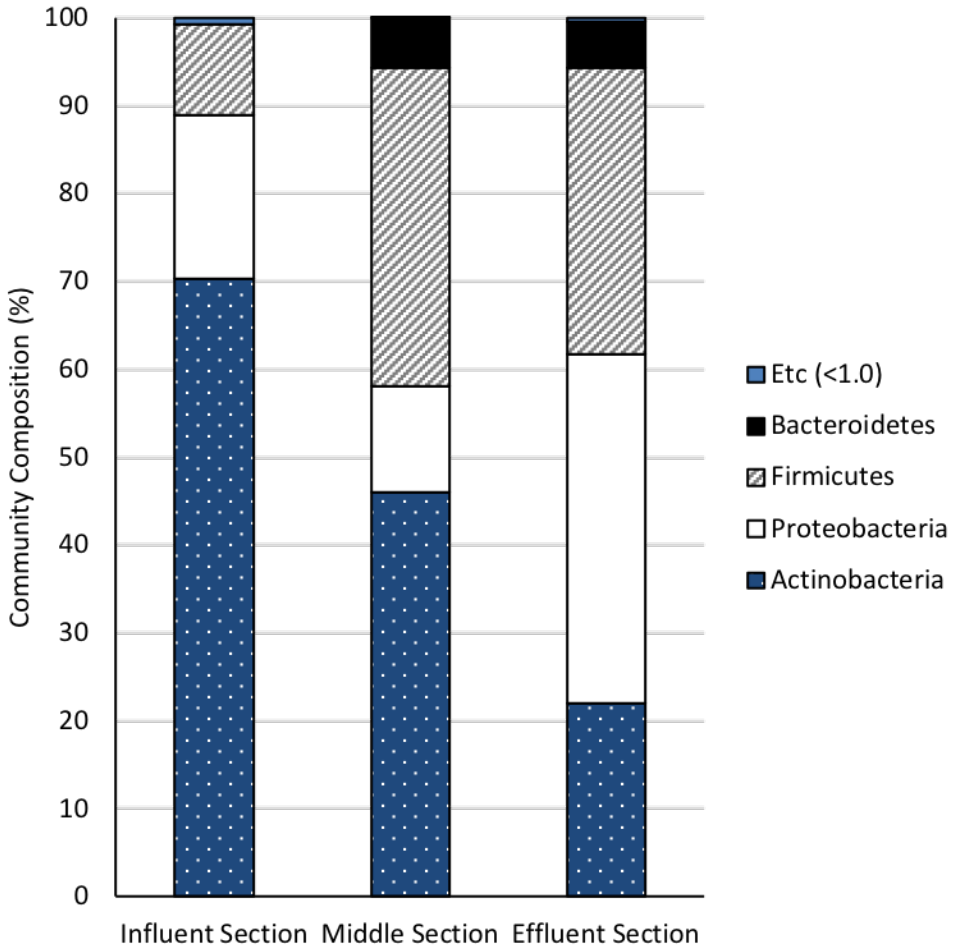

Figure 7. 24. Phylum-level composition of all three sections of the column. Actinobacteria dominates at the influent but reads reduce through the system, members of Proteobacteria are mainly present within the effluent section and members of the Firmicutes are predominantly situated within the middle and effluent sections.

At class level, Actinobacteria exhibits a decrease in reads from the influent (70.29%) to the middle section (46.05%) and a further reduction at the effluent (21.80%) (Figure 7.25). Actinobacteria play an important part in the degradation of organic matter including polysaccharides, organic acids, and cellulose. The existence of Actinobacteria in various extreme locations has been reported such as in alkaline dessert soil and sandy loam soil (Ranjani Anandan, 2016). Clostridia class are vital for the production of organic acids through fermentation processes (E. A. Johnson, 2009) and the composition of these within the column increased from 7.26% abundance at the influent to 32.5% in the mid-section then decreased to 19.6% of total reads at the effluent. These data potentially suggest that the majority of ISA degradation could occur through the middle of the column. At the column influent

Alphaproteobacteria made up 18.47% of the population which reduced to 11.71% around the middle and then gained prominence to represent 38.46% of sequences at the effluent section. Alphaproteobacteria are known to survive within nutrient-poor environments due to their oligotrophic character, a trait that is essential for thriving in subsurface conditions. Actinobacteria, Alphaproteobacteria and Clostridia classes were all main groups present within the original flocculate inoculum, suggesting these were integral to the formation and propagation of a microbial biofilm within the column. While Bacilli was the predominant class within the original inoculum it's abundance significantly reduces in the column but increases marginally from 0.0112% (influent), to 0.0975% (middle) and finally 0.3026% (effluent).

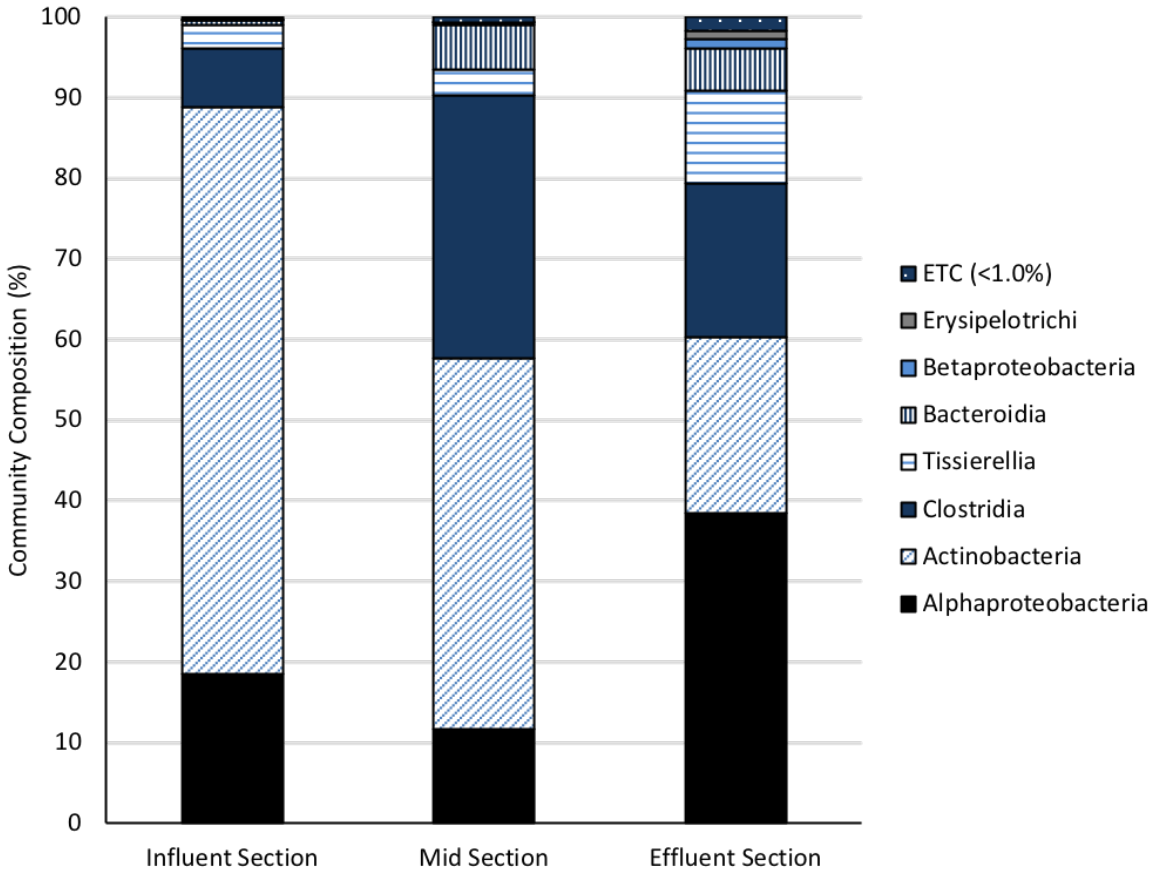

Figure 7. 25. Class-level distribution of sand column biofilm. Microbial community analysis reveals Actinobacteria dominates at class level within the influent but reads reduce through the column, with members of Alphaproteobacteria becoming more prominent through the system and in the effluent, with Clostridia class low level within the influent but dominating reads through the middle of the column.

At Genus level *Mycobacterium* was the major presence within the Actinobacteria population through all sections of the column, with 66.49% abundance at the influent decreasing to 44.77% around the middle and showing a further decrease to 20.09% at the effluent (Figure 7.26). Nontuberculous mycobacteria (NTM) are able to thrive in low carbon areas and are found in natural soils and waters, in addition to engineered water systems. Biofilm formation and surface adherence are two prominent features of the NTM due to the hydrophobic outer membrane they possess (Falkinham, 2009). Alphaproteobacteria was dominated by genera within the *Brucellaceae* family which gained popularity through the column with 3.81% at the influent, increasing to 4.36% in the middle and further still to 18.17% in the effluent region. While the genus *Brucella* generally prevails it is species belonging to the other less dominant genera including *Daeguia, Mycoplana and Paenochrobactrum* that are environmental isolates from soils, waters and sludges (Kämpfer, Wohlgemuth, & Scholz, 2014). *Thermohalobacter* prevailed within the Clostridia, making up 2.48% of sequences at the influent, 24.65% within the middle of the column and 10.24% around the effluent. Taxonomic profiling showed this genus is unclassified beyond the rank of family, suggesting this was the most closely related genus within the Clostridiaceae family (of which other genera include Alkalliphilus and Anaeromicrobium). At the influent *Tissierella* of the Tissierellia class of Firmicutes made up just 0.42% of the community, 1.22% in the middle of the column and a more substantial 7.5% around the effluent. *Tissierella* are strict anaerobes capable of surviving at pH > 9.0 and are able to utilise Fe(III) as a TEA under anoxic conditions (Fuller et al., 2014). A complete loss of the archaeal component present within the inoculum was observed here. The microbial community of the column is only described down to the Genus level in this chapter of work as sequences reads were too short to appoint specific species level identification.

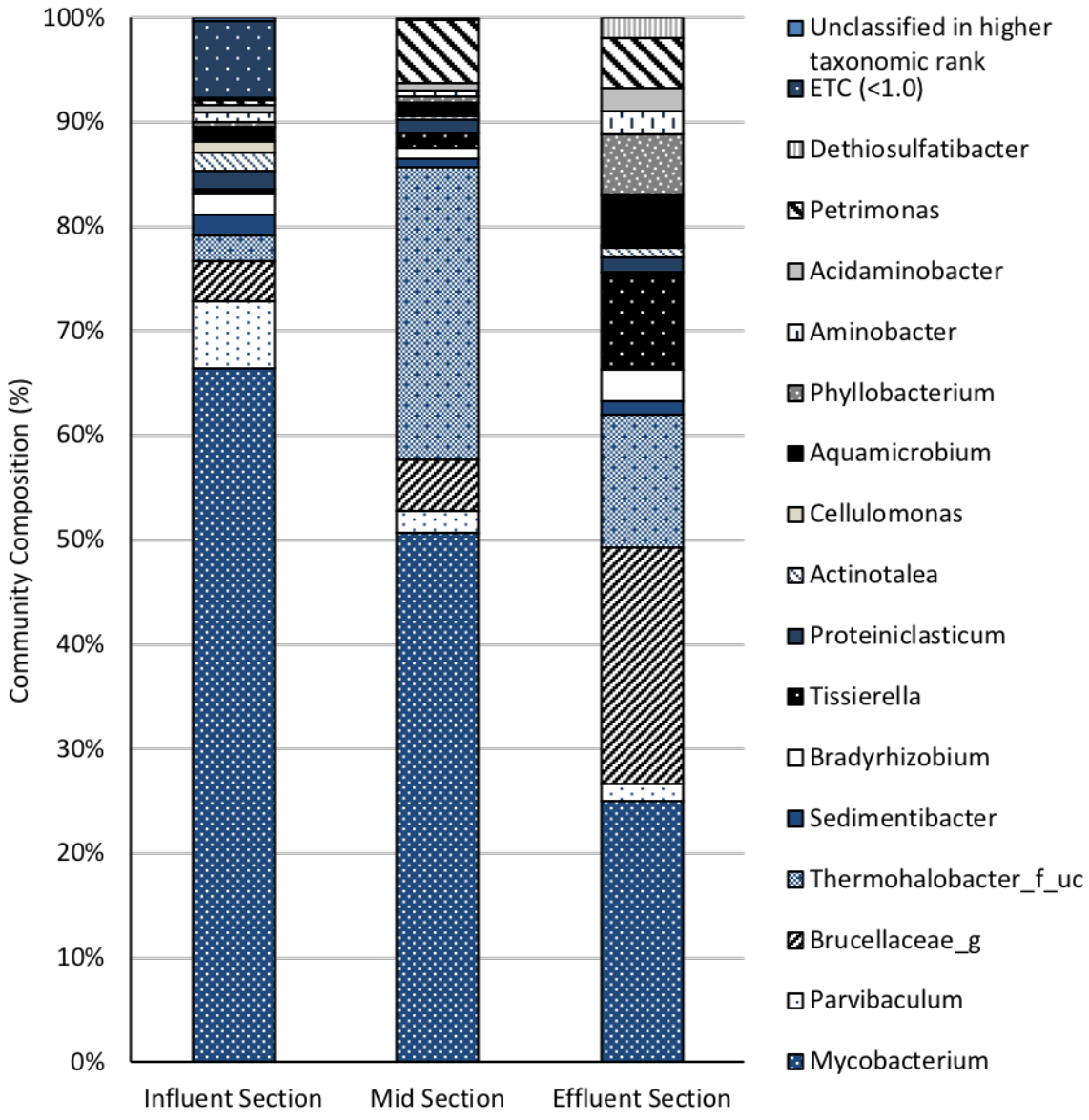

Figure 7. 26. Representation of the sand biofilm column at Genus level.

Microbial diversity through the column can be attributed to changes in the level of carbon that is available for bacteria to consume through the degradation of isosaccharinic acid. In addition, the production of acetic acid through fermentation processes could cause a reduction in pH, resulting in further changes to the microbial community. A pH fluctuation could lead to altering the ability of the community to degrade ISA as well as change the composition of biofilm EPS. The microbial population present within the effluent section was revealed to be the most diverse with a Shannon index of 3.69 in comparison to 2.71 in the mid-section and 1.93 at the influent. Rarefaction curve indicated sample size in terms of OTUs were

sufficient to demonstrate diversity of microbial communities present within all three sections. In addition, all three curves representing relatively average species diversity, with the effluent section exhibiting the least steep rank abundance curve therefore the most diverse community (Figure 7.27).

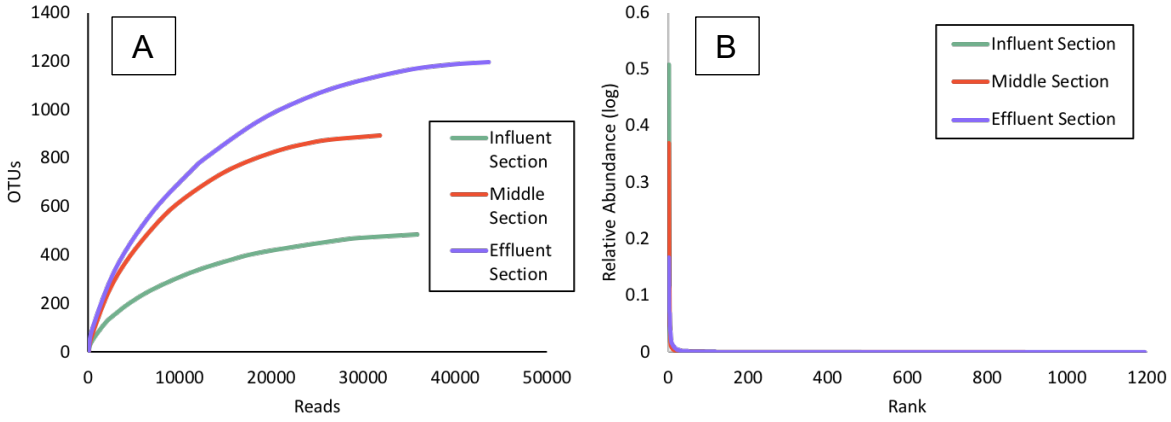

Figure 7. 27. [A] Rarefaction and [B] Rank Abundance curves of sand column biofilm. [A] Rarefaction curves indicate sample saturation was reached in terms of OTUs and [B] rank abundance curves reflect the species diversity of all three sections.

7.2.3.2 Microscopy

Scanning electron microscopy (SEM) imaging exposed major changes in the amount of microbial biofilm fixed upon the surface of the sand at different points of the column. Analysis of sand obtained from the influent area revealed the highest level of biofilm propagation and growth of all the three sections. The quantity of visible biomass considerably reduced towards the middle of the column and around the effluent area, with little to no biofilm material detected on the sand surfaces here (Figure 7.28). Even post-fixation biofilm morphology can be affected under SEM as a result of the EPS components collapsing during the drying process (Priester et al., 2007). Energy-dispersive x-ray spectroscopy (EDX) confirmed the presence of microbial biofilm on the surface of sand taken from the influent region. EDX analysis revealed differences in the elemental composition of clustered biomass showing an increase in organic components compared to areas of no biological material (predominately silicon and oxygen) (Figure 7.29). EDX also confirmed trace-level minerals within the EPS matrix however Ni was not detected within the biological matter nor on the sand surface.

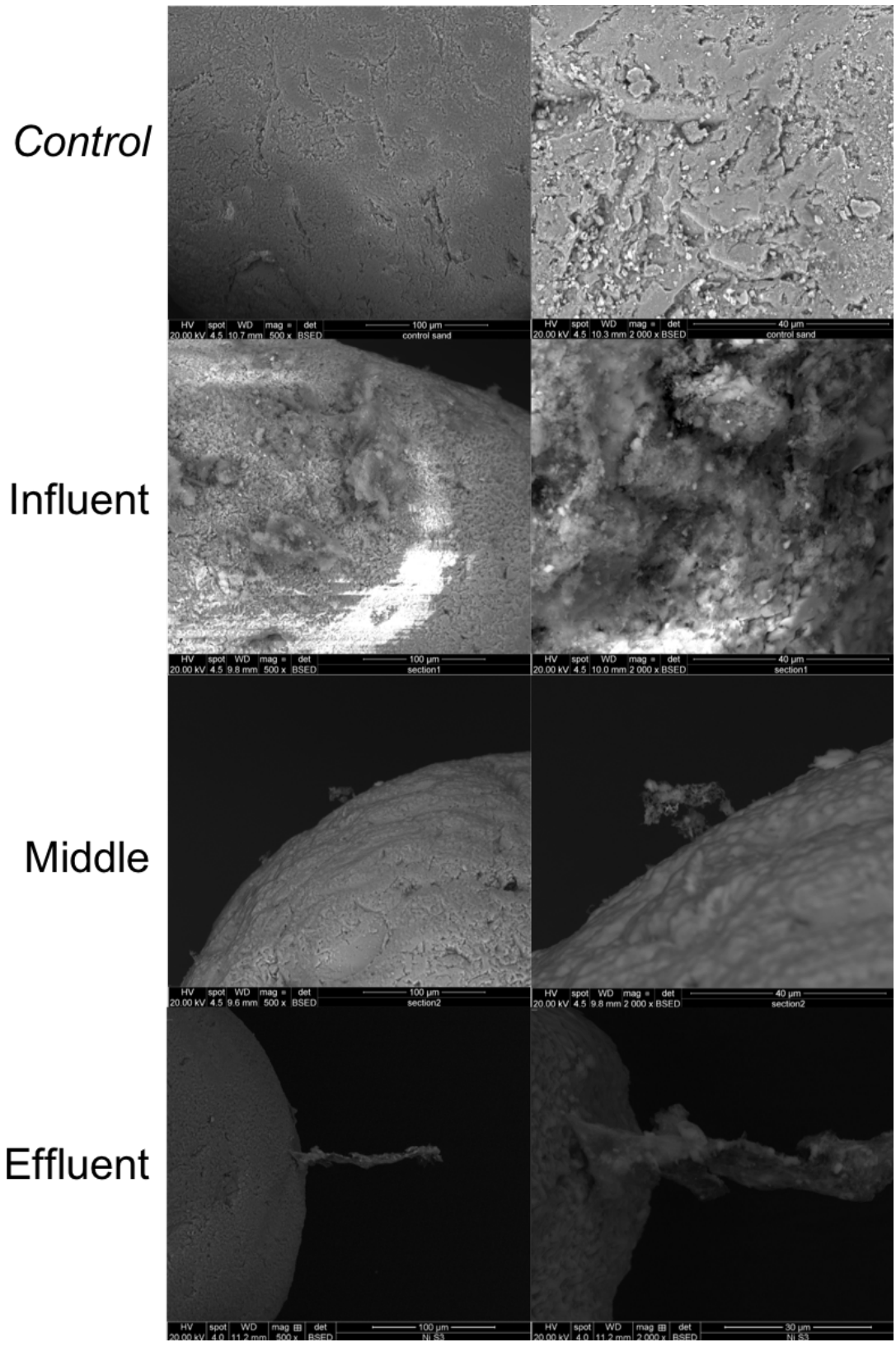

Figure 7. 28. SEM imagery of sand particles within the biofilm column. Samples extracted from the influent section exhibited the highest levels of microbial biofilm coverage on the surface of the particles, with middle and effluent samples still showing signs of colonisation but at a lower level. As the sand column was not continuously fed with microbes the biofilm itself was not extensive therefore parts of the biofilm were prone to detaching during sample extraction.

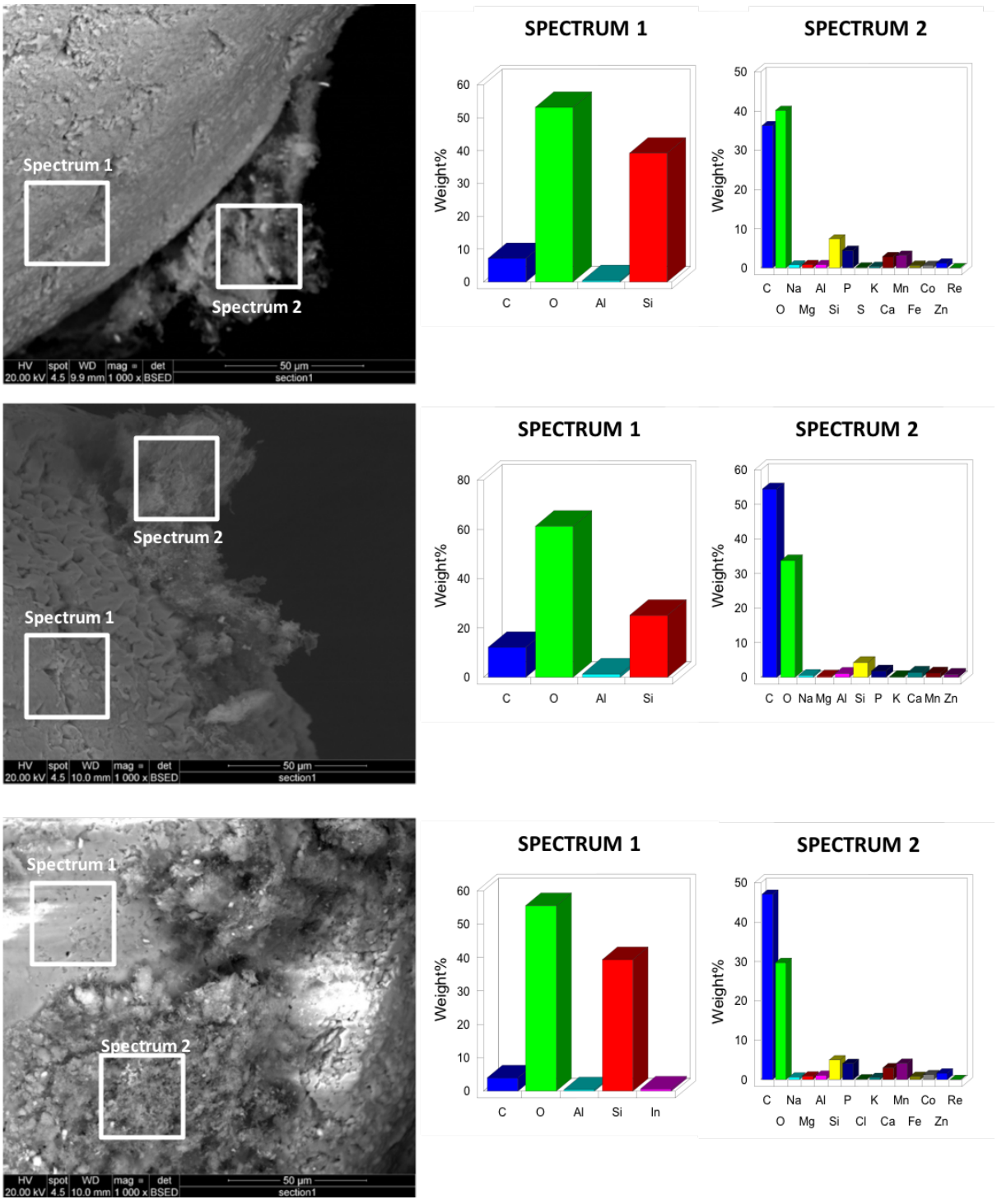

Figure 7. 29. Elemental profiles of microbial biofilm on sand samples extracted from column influent. EDX demonstrates contrast between SiO_2 sand surface and areas of colonisation rich in C, O and low levels of other components present within influent media.

These results can also suggest that that the reduction in soluble Ni seen in previous experiments is not due to immobilization due to sorption to the sand or biofilm material.

Confocal laser scanning microscopy (CLSM) imaging of the sand biofilm demonstrated changes in the individual elements and overall composition of EPS through the column. Organic material was detected in all three sections of the column, with differences in the level of EPS components most likely due to change in microbial community composition (Figure 7.30). Images of samples taken from the influent section were indicative of biofilm forming upon the surface of the sand supported by the high protein content seen here. Matrix proteins are involved in architecture stability and structure of biofilm and are therefore integral in their adhesion to surfaces (Fong & Yildiz, 2015). Microbial floc formation was also detected in this section (Figure 7.31). Reduced colonization of the sand surface was observed in samples taken from the middle of the column, with clusters of microbial flocs separated from the main biofilm distinguished instead (Figure 7.32). A decrease in the protein content of the biofilm is observed here, which explains why flocculates appear free-flowing rather than adhered to the sand. Further along the column around the effluent region EPS material appears less compacted together and more spread out (Figure 7.33). Although pH is not high enough to induce alkaline lysis, the dispersion of components within the EPS matrix could lead to priming of the surface of the sand which may instigate biofilm formation once again (Dunne, 2002). Results here suggest that EPS components are present on the surface of the sand but due to reduced protein content bulk biofilm material doesn't form as seen in SEM imaging. Cannibalism is a technique employed by the *Bacillus subtilis* strain of Bacilli in order to delay sporulation (López, Vlamakis, Losick, & Kolter, 2009) which could potentially explain why biofilm propagation is so low around the effluent of the column. Cells can produce cannibal toxins in response to environments of limited nutrients thereby eating away at their own cells as a survival technique. Although only a small percentage of the Bacilli were detected within the sand biofilm, the inoculum which initially seeded the sand column contained a considerably higher amount.

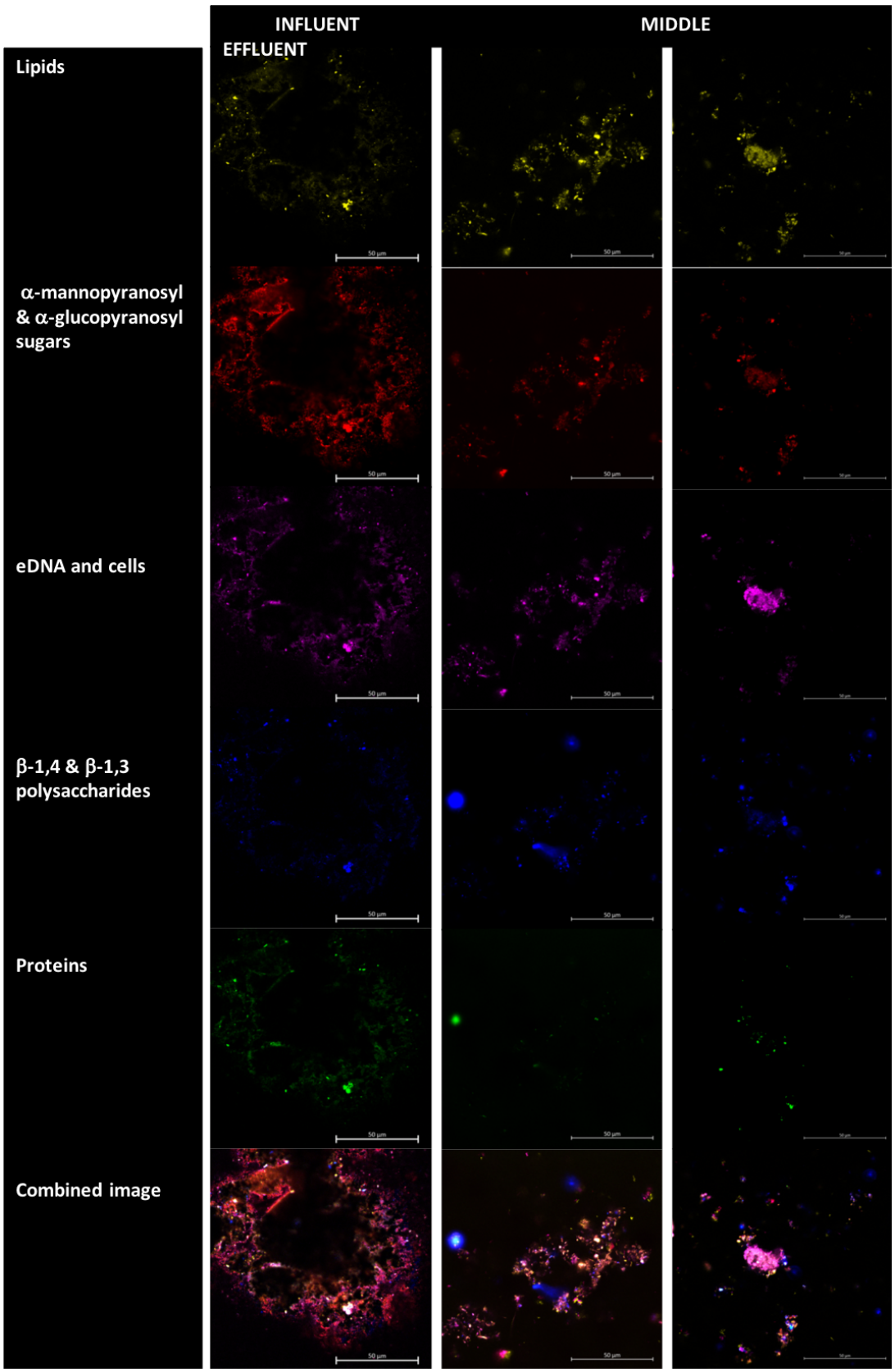

Figure 7. 30. CLSM imagery of individual components and combined image of samples extracted from all three sections of the column. At the influent biofilm appears more compact, with material from effluent sections more dispersed. Less protein appears in middle sections which could explain lack of microbial adhesion in SEM analysis.

It is likely that microorganisms entered the column and immediately secreted EPS components (proteins, eDNA, sugars, lipids and polysaccharides) to form a matrix upon attachment to the sand. As media pushed through the system flocculate material was pulled off the sand in small clusters which became free-flowing towards the middle section. Microbial flocs within the effluent could have disintegrated or broken into smaller pieces under the bottle neck pressure as media exits the column, fragmenting the EPS components. A decrease in biofilm forming mycobacterium seen through the system (Figure 7.26) could explain the loss of bulk biofilm material seen in SEM images due to a reduction in secreted EPS. In addition, large clumps of biomass were not expected to cover the surface of the sand in this system as the biofilm was not highly developed nor was it a continuously fed with inoculum. Furthermore, it was predicated that majority of the biofilm would be established and propagate in the vicinity of the column inlet as this is where microorganisms would first be introduced into the system to develop on the sand surface. A study by Ma *et al* reported that biofilm integrity can be compromised by the presence of minerals and metal oxides, with goethite in particular causing physical damage to bacterial cells by perforating cell walls. Here they investigated *Bacillus subtilis* biofilms, suggesting that biofilms formed from other soil bacteria or members of the Firmicutes phylum within the column system could be physically damaged by minerals or iron oxides (Ma et al., 2017).

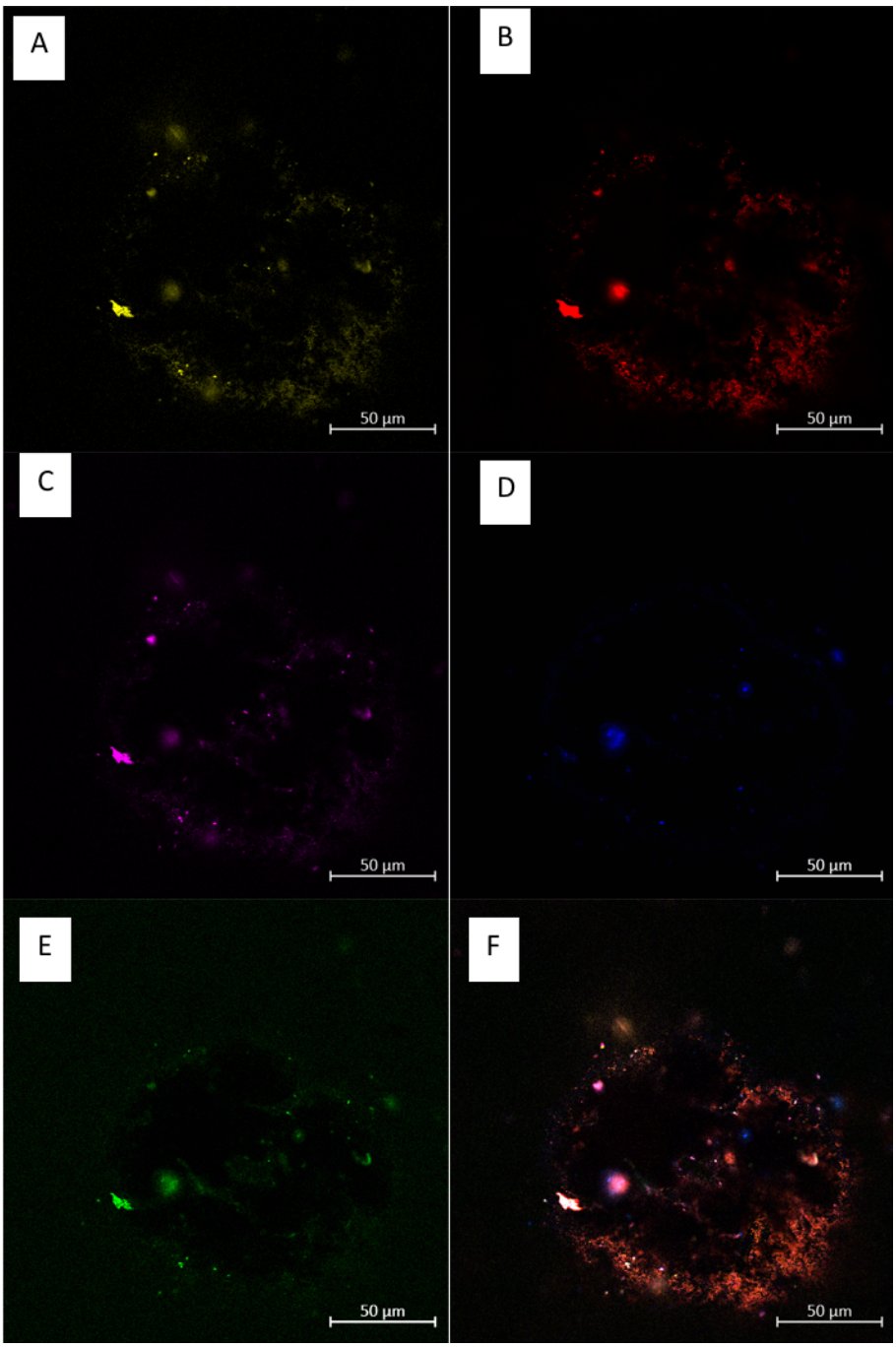

Figure 7. 31. CLSM investigation of sand biofilm extracted from the influent section of column. [A lipids, [B] β-1,4 and β-1,3 polysaccharides, [C] proteins, [D] α-mannopyranosyl and α-glucopyranosyl sugars and [E] eDNA and cells. [F] is a combined image of all components.

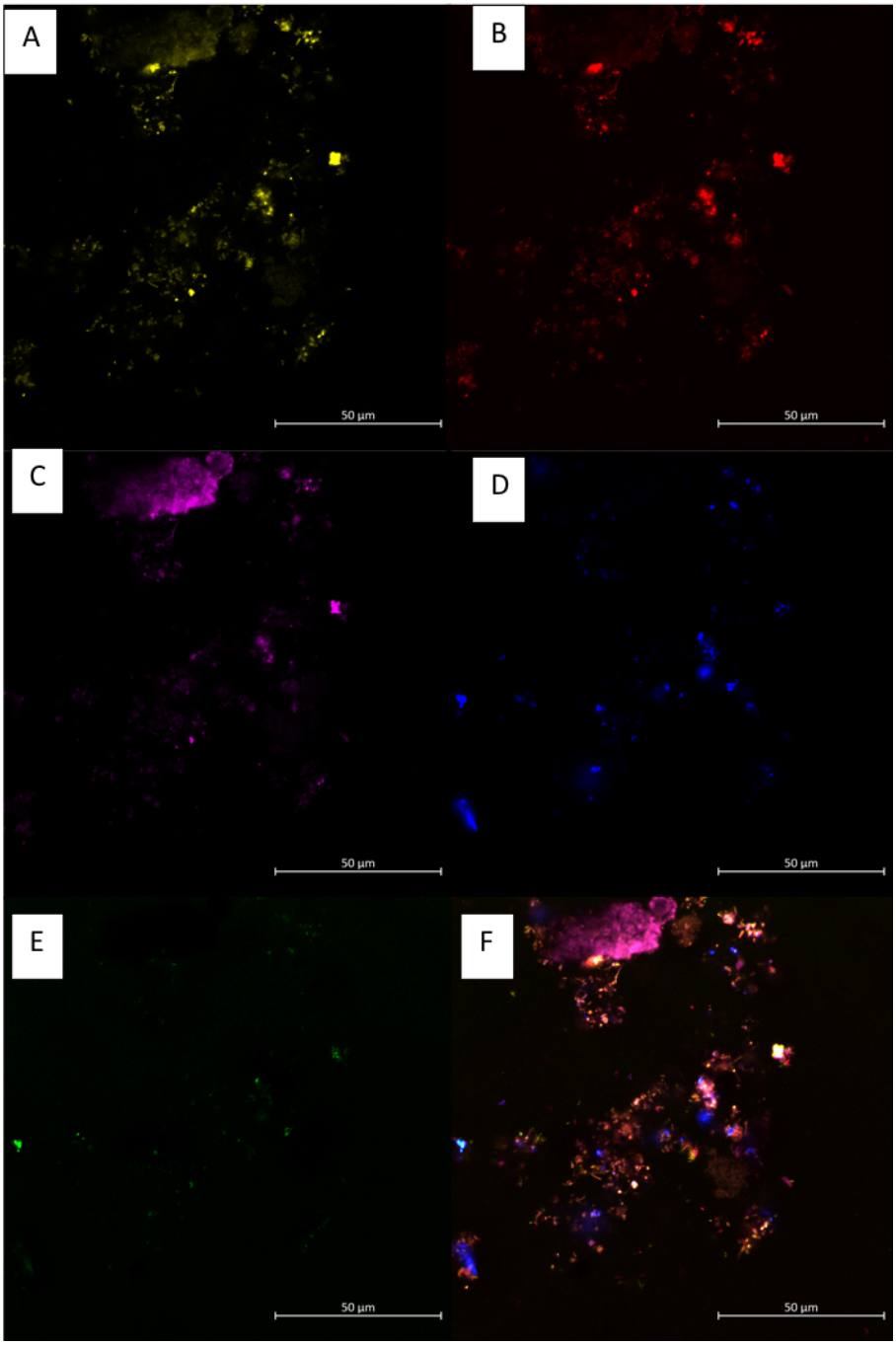

Figure 7. 32. CLSM investigation of sand biofilm extracted from the middle section of column. [A] lipids, [B] β-1,4 and β-1,3 polysaccharides, [C] proteins, [D] α-mannopyranosyl and α-glucopyranosyl sugars and [E] eDNA and cells. [F] is a combined image of all components.

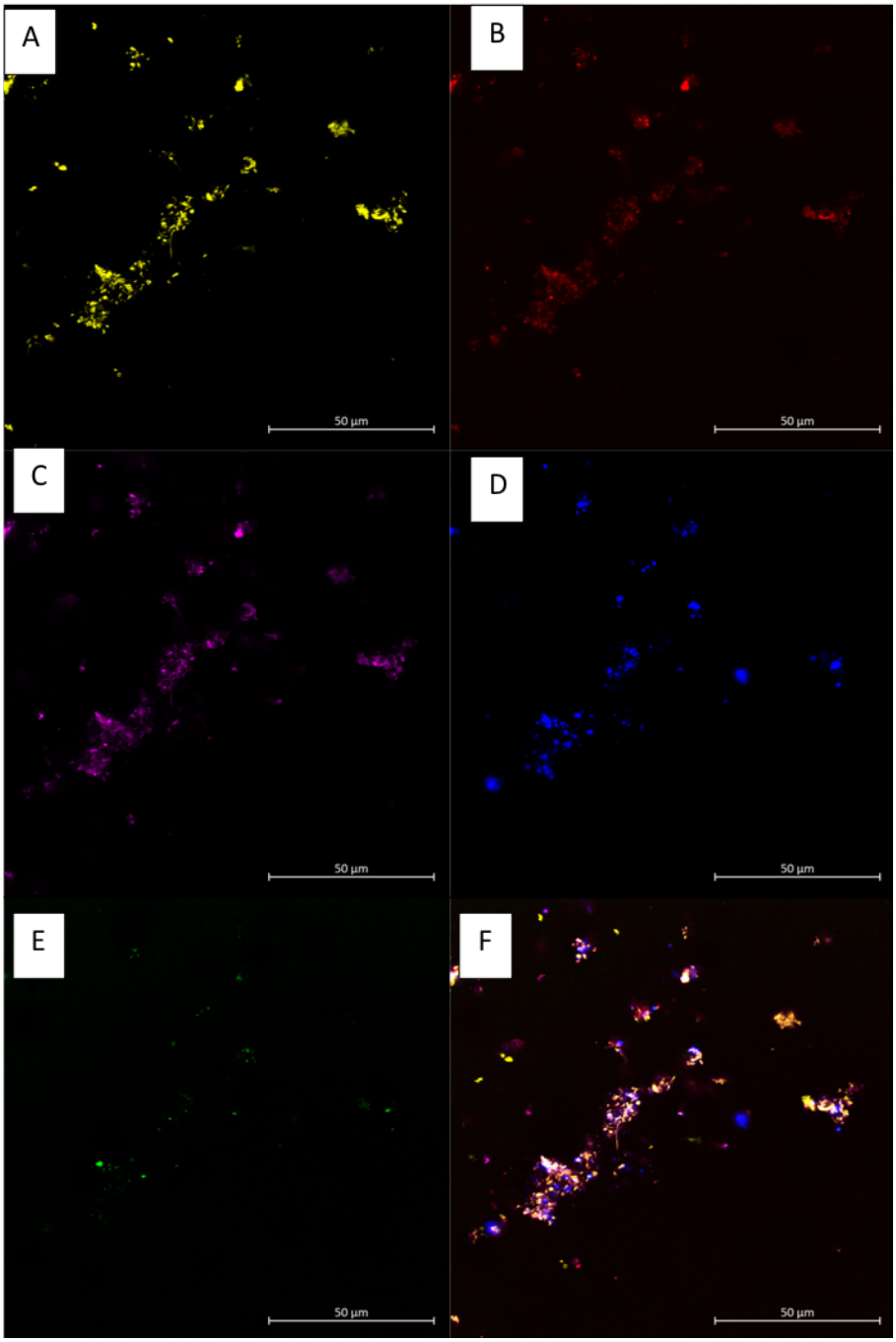

Figure 7. 33. CLSM investigation of sand biofilm extracted from the effluent section of column. **[**A] lipids, [B] β-1,4 and β-1,3 polysaccharides, [C] proteins, [D] α-mannopyranosyl and α-glucopyranosyl sugars and [E] eDNA and cells. [F] is a combined image of all components.

7.2.3.3 X-ray diffraction

X-ray diffraction analysis revealed some differences in mineral phases and their intensities between the three sections of the sand column. A diffraction profile of sand only against quartz (SiO_2) is shown in Figure 7.34 which signifies peaks within

the control sand that match phases of quartz. A number of other peaks were found within diffraction patterns of sand samples taken from the column, implying that minerals not associated with quartz were forming within the flow-cell system (Figure 7.35). Sand diffraction patterns were tested against XRD profiles of known minerals that could have possibly accumulated within the flow-through system. These diffraction patterns would need to be a complete match to the sand sample patterns in order to confirm the presence of a particular mineral, however the potential match of singular unknown peaks could indicate specific phases of these minerals upon the surface of the sand. It is therefore not possible from these results to accurately determine the existence of any particular mineral/s within the column, but the presence of certain phases of hematite, calcite, goethite and gypsum minerals is possible.

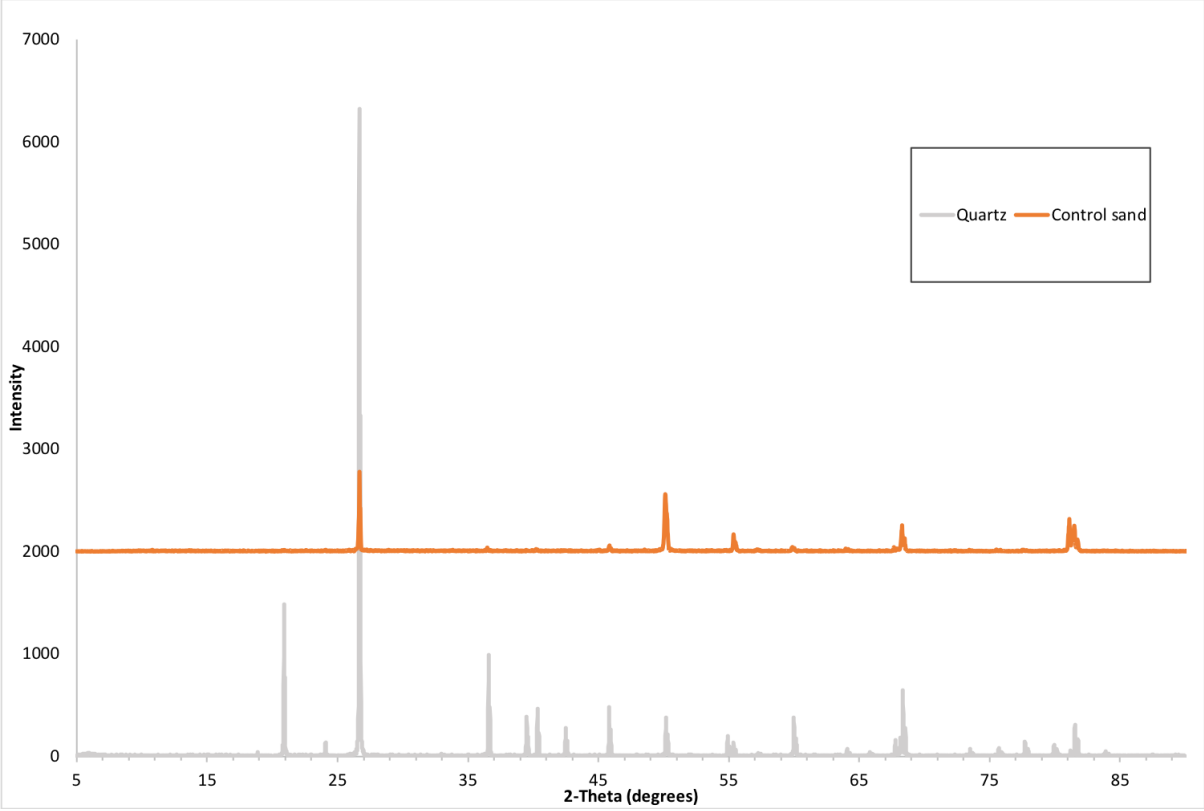

Figure 7. 34. XRD analysis of control Ottawa sand vs a known quartz profile. Signals generated from control sand are identified as being quartz peaks.

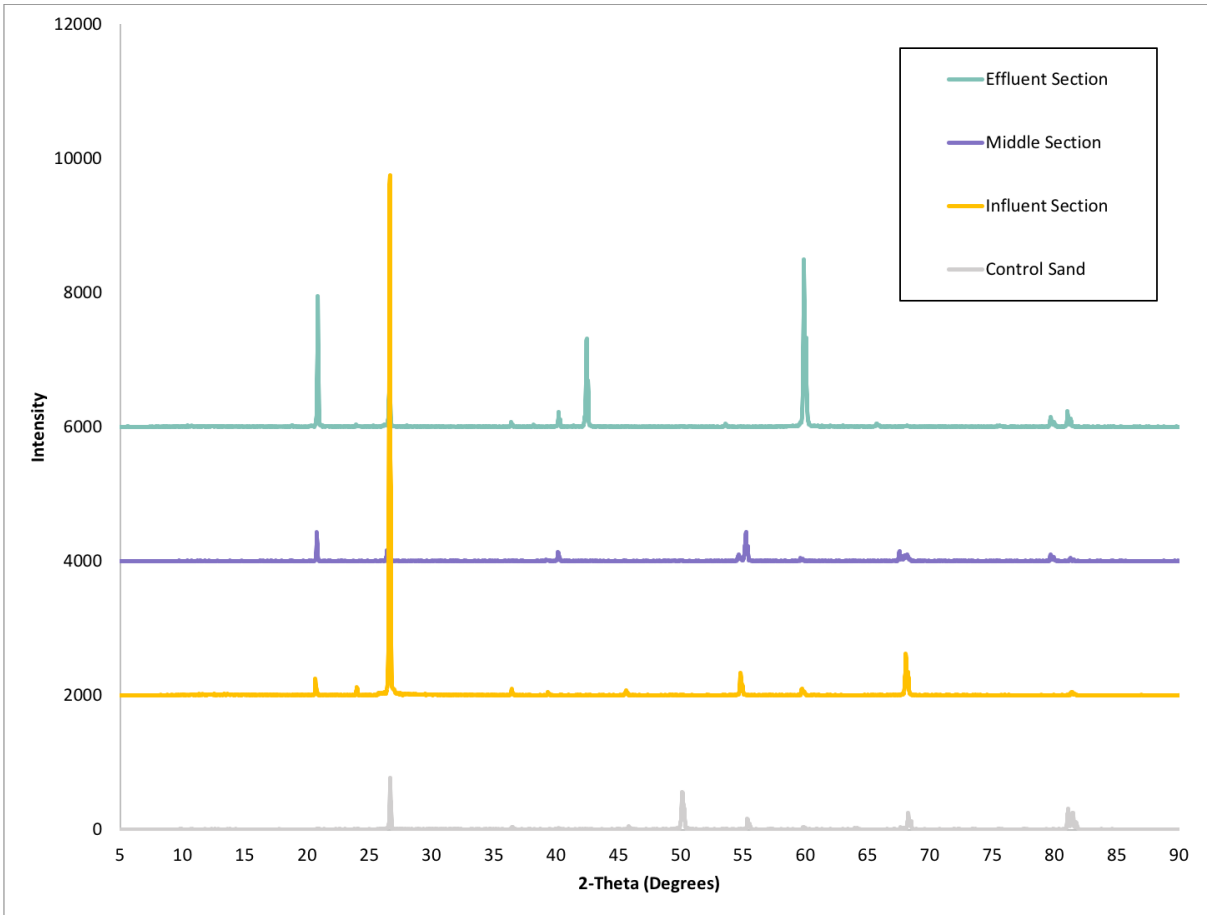

Figure 7. 35. XRD analysis of sand samples extracted from all three sections of the column vs control Ottawa sand. Column samples exhibit peaks not detected within the control and could suggest the presence of minerals upon the sand surface that could influence the integrity of the microbial biofilm.

7.3 Conclusion

Data presented in this chapter demonstrates the sorption of Ni to sand under conditions representative of the far-field environment of an ILW repository. In the presence of cellulose degradation products (CDP) generated through alkaline hydrolysis of cellulosic material Ni adsorbed to sand is pulled off forming a soluble $Ni(ISA)_2$ complex that is able to freely transport through an anaerobic and alkaline system. Under biotic conditions ISA is initially degraded however Ni transport is not influenced, indicating the possibility that ISA was complexed to other divalent components within the media or CDP such as Ca^{2+} or Mg^{2+} as it transports through the system. An investigation into biosorption of Ni to microbial flocs revealed potential precipitation or mineralisation of Ni upon the surface of an aggregate/

colloid which could lead to its enhanced mobility, but since it was not microbial there was no further evidence to support the biosorption theory. The data also suggested that minerals in solution could become embedded within the sand biofilm, as shown by EDX analysis of detached flocculate material, which could potentially hamper biofilm integrity. However, no evidence was found to suggest that Ni was being transported nor hindered in this way. Figure 7.20 shows that under conditions that allow Ni and ISA to become complexed (as demonstrated previously in Figure 7.4 & 7.5) biofilm-forming microorganisms present within the system can break this complexation by degrading complexant ISA. In doing so, the Ni is released and subsequently retained within the column. Ni is therefore successfully immobilised to an extent within the system, however full degradation and complete removal of Ni from solution does not occur. Data described within this chapter is optimistic and indicates the potential of microbial biofilm communities to have a positive impact on the safety aspect of radioactive waste disposal and the consequences of transport to the far-field. By limiting the mobility of both components, this ensures that Ni cannot flow as freely through the subsurface and potentially out to the biosphere. In addition, CDPs which may escape the wasteform can be degraded under conditions analogous to the GDF far-field and are therefore less likely to further complex with radioactive elements.

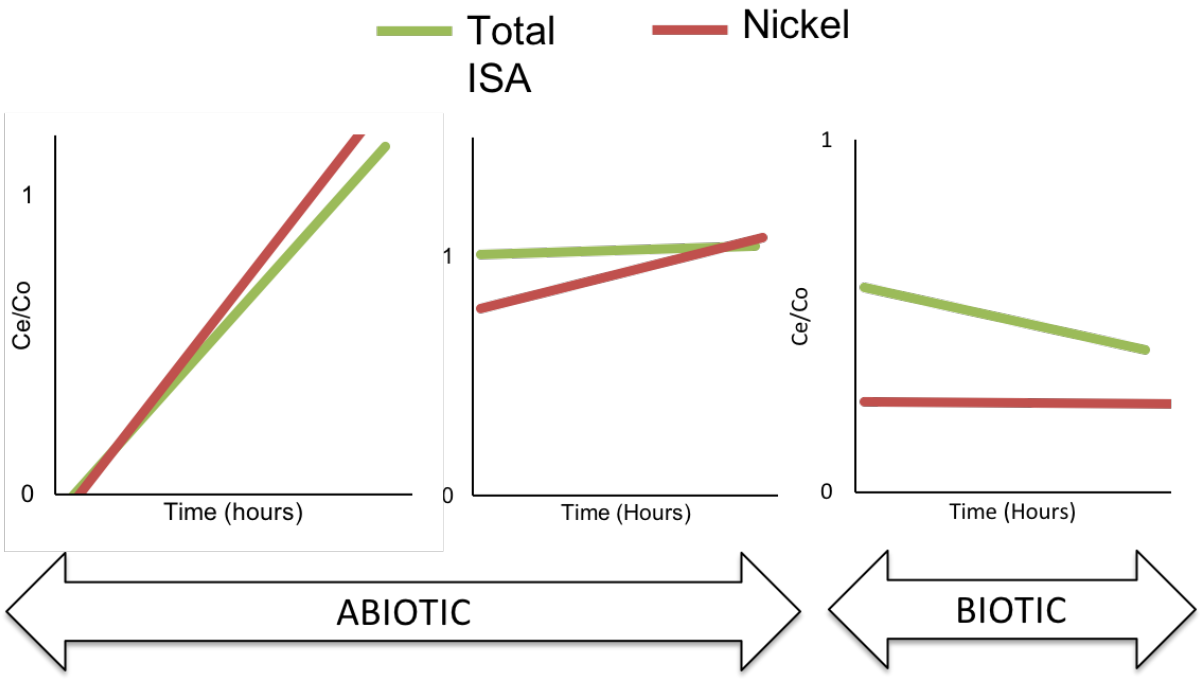

7.4 Key Findings

- ISA generated through the alkaline hydrolysis of cellulose are capable of mobilising Ni adsorbed within a sand column under abiotic anaerobic conditions
- The $Ni(ISA)_2$ complex will also form in the liquid phase and remain complexed as it transports through and out a pH 9.5 sand column
- A biofilm forming microbial community introduced within the column is able to ferment the ISA complexed to Ni, limiting the mobility of the two through the system
- Microcosm studies potentially suggest that the $Ni(ISA)_2$ complex is unable to undergo complete degradation
- Work presented here demonstrates that microbial biofilm capable of colonisation of geological surfaces under the far-field conditions of a GDF utilised in this study are able to degrade α and β ISA leading to the reduced transport of complexed Ni(II)

Chapter 8.0 Transport of Europium, Thorium and Uranium under ILW-GDF conditions

8.1 Rationale

The flow-cell system developed in Chapter 7.0 was next utilized as a model to investigate the transport of europium and actinides thorium & uranium under flow-conditions of a GDF far-field in the presence of CDPs. Radionuclide transport in subsurface environments is directed by the adsorption/ desorption interactions that occur at the solid/liquid interface. Under the relevant near-field conditions of a GDF Th is expected to exist as a range of mixed Th(IV) complexes depending on the chemistry of the surrounding water, with uranium occurring within the chemically disturbed zone of the GDF as both tetravalent U(IV) and hexavalent U(VI) forms (N.D.A, 2016a). After a period of time (a few decades to a hundred thousand years, depending on host rock permeability) (N.D.A, 2016e) re-saturation of groundwater will result in permeation of the cement encapsulating radioactive waste inducing a hyperalkaline environment through the dissolution of $Ca(OH)_2$. NRVB backfill material selected to encapsulate ILW is known to be an efficient sorbent for the removal of Eu(III) from solution, with Telchadder *et al* demonstrating that in the presence of the crushed cement all but 1.5% of all Eu is taking up by the material after just one day (Telchadder, Smith, & Bryan, 2012). Wieland *et al* reported that under near-field repository conditions the uptake of Eu(III) to Portland cement was slightly influenced in the presence of ISA. Felipe-Sotelo *et al* reported a high level of Th uptake onto NRVB backfill material in the absence of complexant ISA whilst under near-field conditions. However, in the presence of CDPs the retention of Th(IV) to NRVB decreased, an observation also described by Wieland *et al* who demonstrated a reduced uptake of Th(IV) onto hardened cement paste at pH 13.3 in the presence of α-ISA (Felipe-Sotelo, Hinchliff, Evans, Warwick, & Read, 2012) (Wieland et al., 2002). Uranium is understood to be relatively mobile in its U(VI) state, a trait which is different to other actinides. If disposed of in this way Uranium could readily transport out of the wasteform of GDF and into the surrounding host rock as the level of groundwater saturation in the near-field would not be sufficient enough to induce reducing conditions (N.D.A, 2015a). Under circumneutral pH U(VI) is mobile or semi-mobile, but some reports indicate subsurface migration of the radionuclide is enhanced when conditions are mildly alkaline (Qafoku et al., 2005). This chapter will investigate the potential outcomes of processes expected to take

place within the far-field of a GDF in the event that Eu(III), Th(IV) or U(VI) transports out of the chemically disturbed zone to the surrounding geosphere.

8.2 Results & Discussion

8.2.1 Europium (preliminary)

8.2.1.1 Abiotic transport

Whilst the majority of the literature focuses on the sorption and transport of Eu^{3+}, Eu^{2+} was utilized in this section of work as a chemical homologue of divalent Ni^{2+} in the previous chapter and therefore results described here are used as preliminary data only.

Employing the same sand column set-up and experimental conditions previously described in Chapter 7.0, a flow-through system was established to investigate the transport of Eu under a GDF far-field environment. ICP-MS analysis revealed that under alkaline, anaerobic and abiotic conditions Eu successfully binds to sand particles, hindering its mobility through the column (Figure 8.1). This observation was supported by the release of Li through the same system with a breakthrough and exhaustion of 4.1 hrs and 5.2 hrs, respectively (Figure 8.2). Eu and Ni have so far behaved in the same manner under identical conditions, a finding perhaps not so unexpected due to their divalent cation nature.

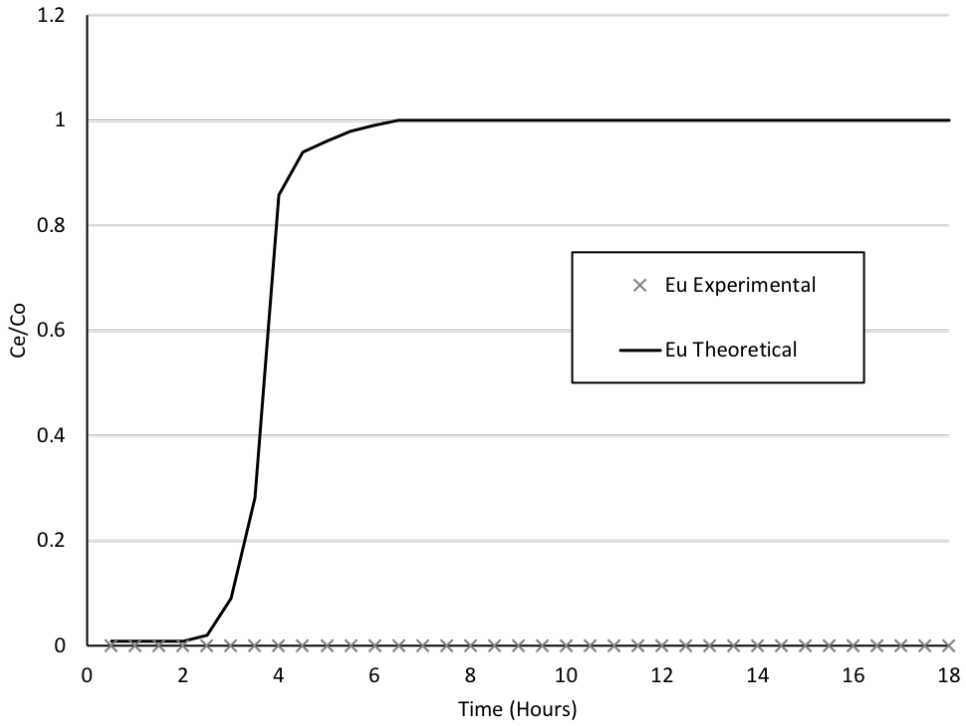

Figure 8. 1. Adsorption of Eu(II) (grey crosses) through a pH 9.5 sand column under anaerobic conditions. Europium is immobilised through adsorption to sand through this system.

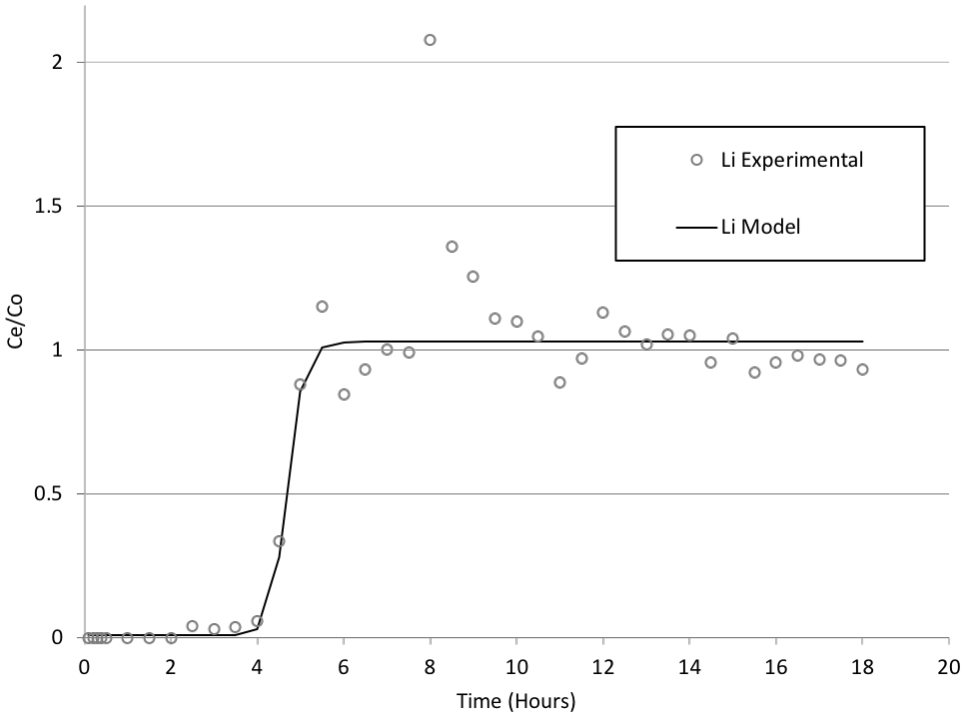

Figure 8. 2. Transport of Li (empty grey circles) through the same pH 9.5 sand column under anaerobic conditions. Li as a conservative tracer does not undergo adsorption to the sand and flows straight through the system.

Contrastingly, when a solution containing 1% CDP was applied to the sand system trace-level elemental analysis did not detect Eu in any of the effluent fractions from the column. Neither the complexation of α- nor β-ISA with the element had seemingly occurred within the flow-through system as indicated by the release of both forms of complexant in the effluent, with a total ISA breakthrough of 5.7 hrs (Figure 8.3).

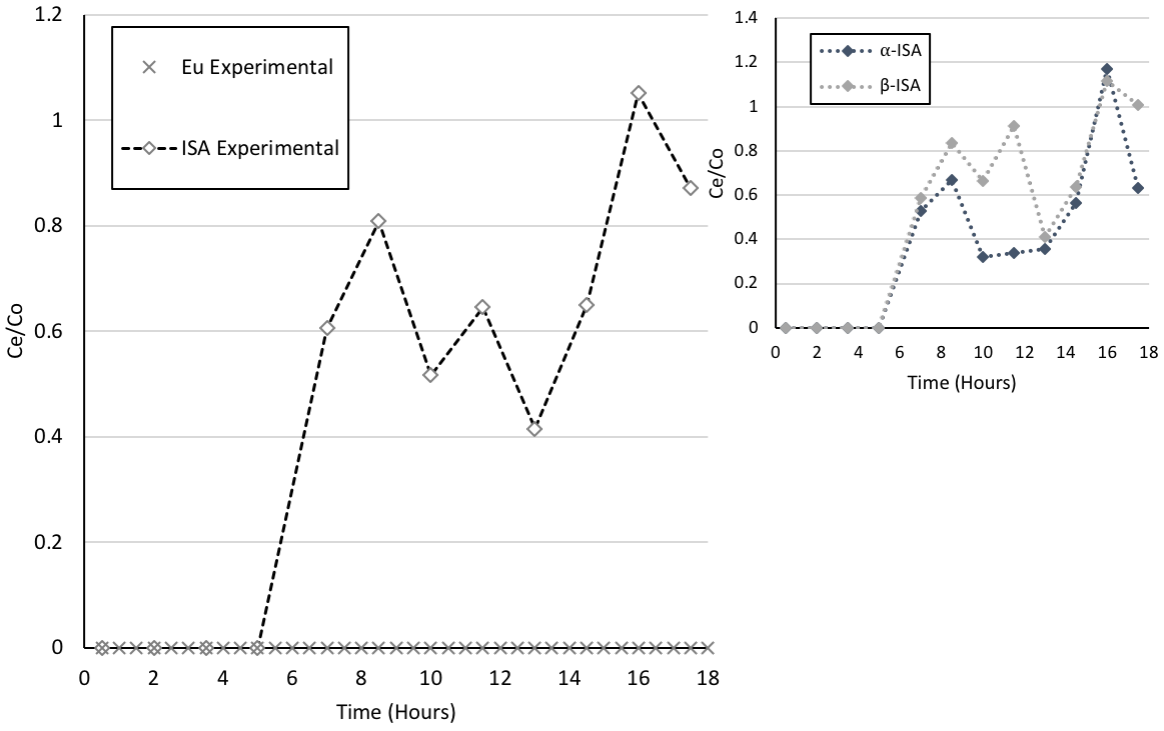

Figure 8. 3. The transport of ISA from a 1% CDP solution through the Eu(II) saturated sand column. Eu (grey crosses) was not stripped of the sand in this system but both forms of ISA, alpha (blue diamonds) and beta (grey diamonds), were detected in effluent fractions.

Data from this experiment suggests that under the far-field conditions of this system Eu immobilised through adsorption processes within the geosphere will not be liberated from the surface of sand in the presence of CDPs.

Studies within the literature focus on the complexation of ISA and Eu^{3+}, not Eu^{2+}, therefore the following statements are based on Eu^{3+} complexation. Van Loon & Glaus described the formation of Eu:ISA complexes as being 1:1 irrespective of the complexant derived from a pure form of ISA or mixed CDPs. Furthermore whereas

the presence of Ca can alter the formation of these complexes in relation to Th, there appeared to be no differences for the Eu complex (Loon & Glaus, 1998). The dominating 1:1 Eu:ISA complexes are well documented in the literature at pH 12.0 and 13.3 (Loon & Glaus, 1998) (Tits, Wieland, & Bradbury, 2005). It was briefly suggested by Vercammen that these complexes could form 2:1 at a lower pH of 10.7 although this was dismissed due to the unlikeness of polynuclear complexes forming at such low Eu concentrations (K. Vercammen, 2000).

In order to investigate whether the complexation of Eu + CDP prior to injection into the column would affect the mobility of Eu through the sand system both substances were added to influent media. HPAEC results demonstrate that ISA still transports straight through the column, as expected, however Eu is not complexed as evidenced by the absence of the metal in effluent samples ICP-MS analysis (Figure 8.4). There was also no indication of precipitation within the feed mix indicating Eu was still in solution. Results presented here suggest that Eu transport is not influenced by the presence of the organic complexant ISA at these concentrations under conditions expected within the far-field as the sorption to sand is strong enough to immobilise it. Loon & Glaus reported that within the near-field environment only concentrations > 10^{-2} M (ISA) could reduce the sorption of divalent metals (eg. Ni^{2+} and therefore Eu^{2+}) from cement (Loon & Glaus, 1998). Furthermore, the concentration of ISA will dilute and decrease as CDP exits the wasteform and disperse through the geosphere, therefore, assuming Eu has a high affinity for sand, it's unlikely that ISA could break that sorption with the extremely low concentrations expected.

Results generated from the current data set did not imply that the presence of ISA would have an adverse effect on the mobility of Eu within an ILW-GDF far-field therefore this section of the study was terminated here to focus on other radionuclides and the potential advantages of biofilm forming microorganisms.

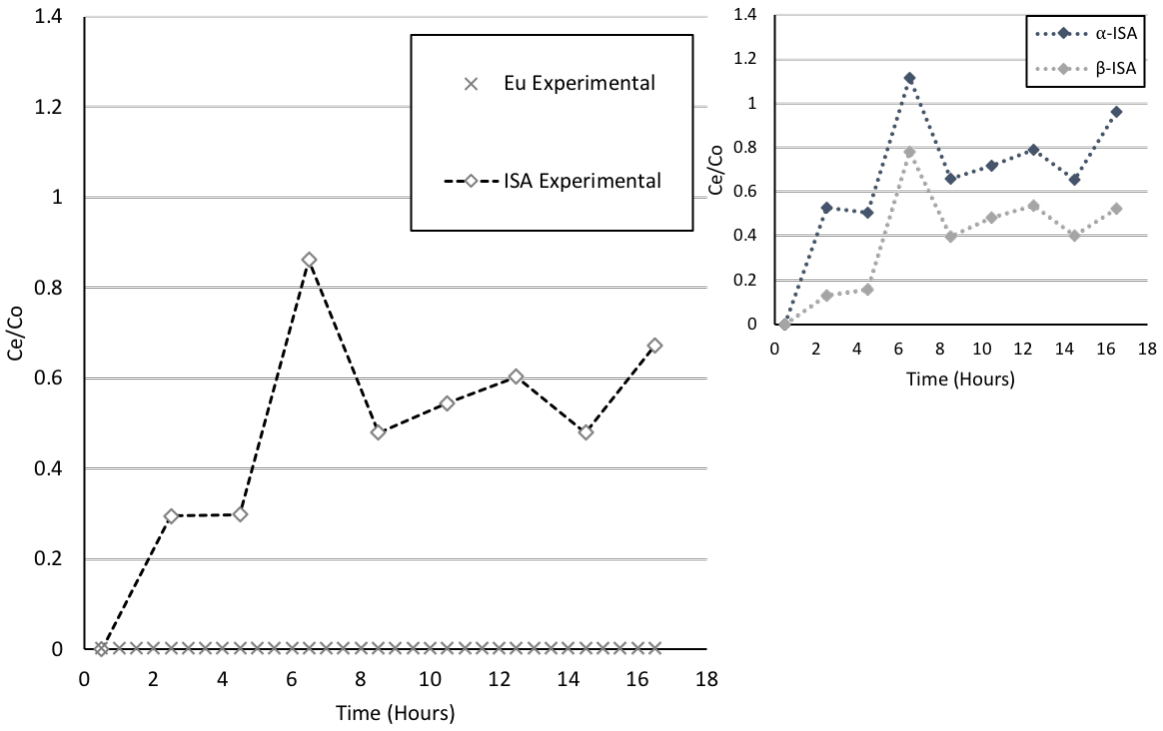

Figure 8. 4. The transport of ISA from an Eu+CDP solution through a pH 9.5 sand column. Eu (grey crosses) was not released from the system but both ISA forms (blue diamonds and grey diamonds) were detected in the effluent.

8.2.2 Thorium

8.2.2.1 Abiotic transport

Under abiotic ILW-GDF conditions at pH 9.5 Th ions adsorbed to sand over a 9- hour flow experiment, with very little to no detection in the effluent (an average of ~0.006 mg/L per fraction, implying 99.8% of total Th is attached) (Figure 8.5). This observation is supported by the breakthrough of Li as a conservative tracer through the same column. ICP-MS analysis revealed the breakthrough time of Li to be 2.4 hr with an exhaustion of 4.6 hrs (Figure 8.6).

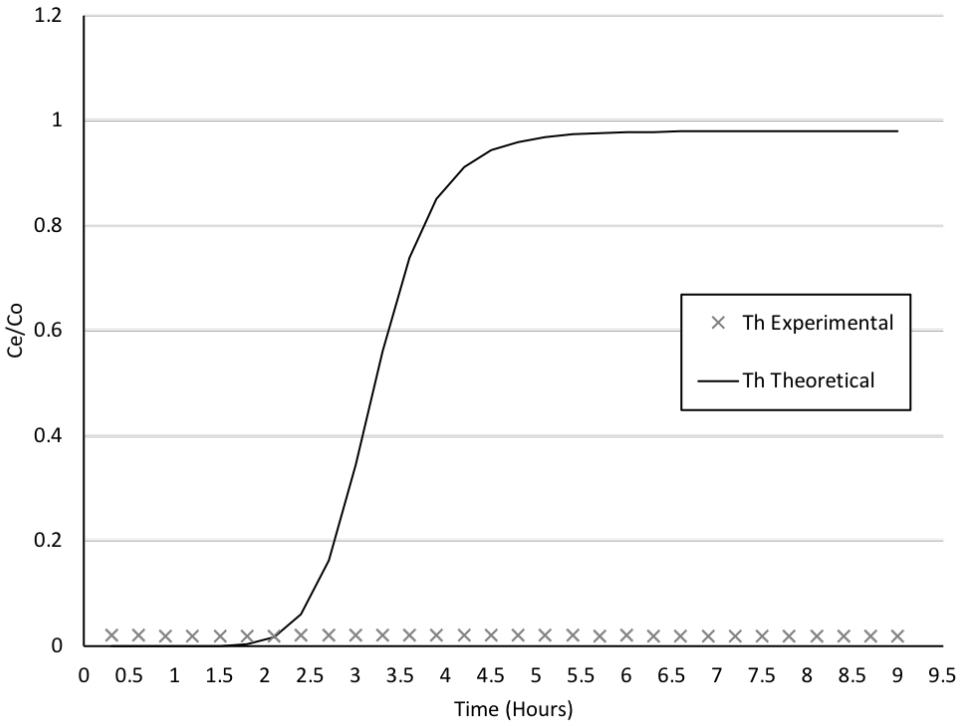

Figure 8. 5. Adsorption of Th(IV) (grey crosses) through a pH 9.5 sand column under anaerobic conditions.

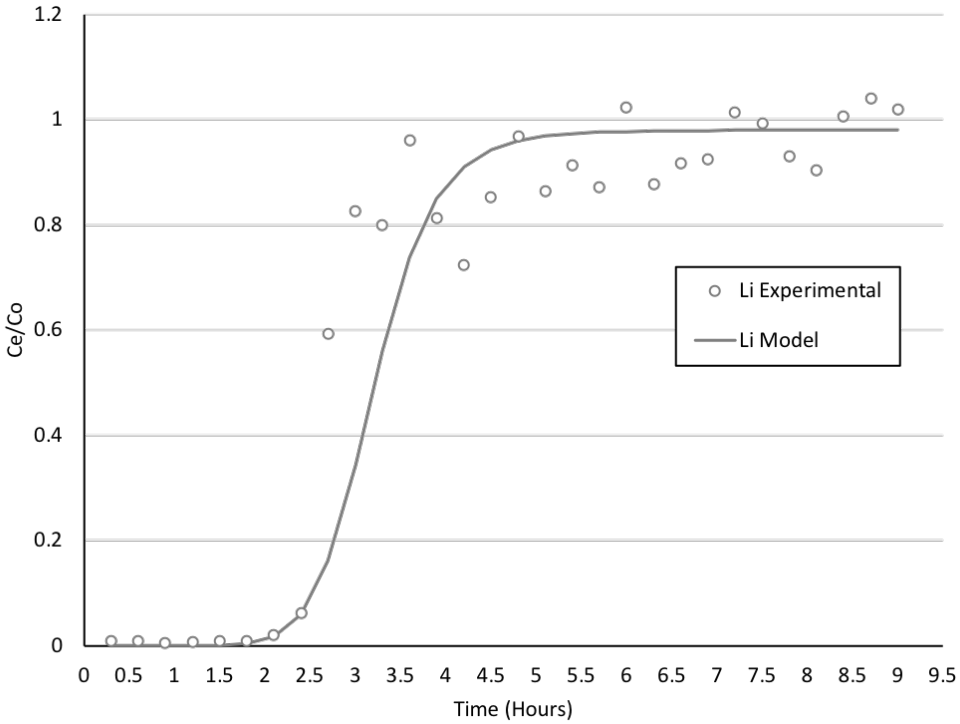

Figure 8. 6. Transport of Li (empty grey circles) through the same pH 9.5 sand column under anaerobic conditions.

ICP-MS data acquisition revealed that the level of Th within influent media was measuring at approximately 0.31 mg/L instead of 0.62 mg/L, indicating that half the Th in solution had possibly adsorbed to the borosilicate glass walls or the polypropylene plastic tubes. Influent media containing Th was subsequently left 24 hrs until it was assumed equilibration had been reached before running through sand columns.

ISA is reported to exhibit high affinity for the complexation of metals, a process which is successfully described in chapter 7.0 through the formation of water-soluble complexes that stripped Ni from the sand surface. Following the addition of a 1% CDP in media solution into the flow-cell system a radionuclide breakthrough was not observed, with 97.2% of Th still adsorbed to sand (~0.008 mg/L (average) released into effluent fractions) (Figure 8.7) These results indicate that the presence of α-ISA nor β-ISA could extensively disrupt the attachment of Th to the sand within this system. It's important to note that the potential for radioactive elements to become mobile would occur within the near-field due to the higher concentration level of CDPs available to interact with, in addition to being in a more alkaline and carbonate-rich environment. Therefore under the assumption that Th-ISA, either in

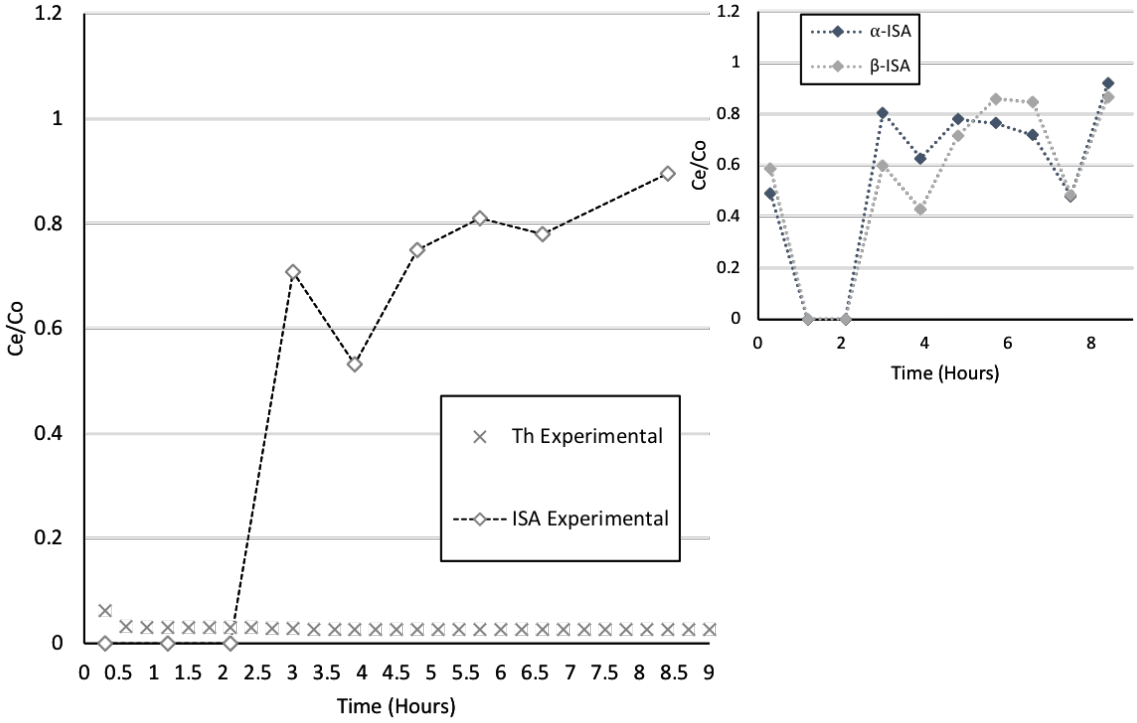

Figure 8. 7. The transport of ISA from a 1% CDP solution through the Th(IV) saturated sand column. Th (grey crosses) was not stripped of the sand in this system but both forms of ISA, alpha (blue diamonds) and beta (grey diamonds), were detected in effluent fractions.

the form Th:ISA:Ca (1:2:*k*) or Th:ISA (1:1) (X. Gaona, Montoya, Colàs, Grivé, & Duro, 2008) (K. Vercammen et al., 2001), migrates out of the wasteform to the far-field then the sorption of this complex to sand material must be explored.

A Th + CDP in media mixture was prepared as previously described and left to equilibrate for 24 hrs prior to pumping through the sand column. ICP-MS analysis of effluent fractions indicated that, despite allowing complexation to occur initially in the liquid phase, the release of a high concentration of Th from the system was not observed (Figure 8.8). Here, only ~0.002 mg/L of Th per fraction was detected, indicating that 99% Th passed through the column underwent adsorption processes to the sand. HPAEC detected the release of ISA (both α and β forms) in the effluent with a breakthrough of 1.9 hrs (similar to the previous experiment) suggesting that the two components are not complexed with one another upon entering or exiting the column. In the presence of Ca (within CDP) under the conditions described here the formation of Th:ISA:Ca would be even less likely to occur due to the high demand of ISA these complexes require (1:2:*k*). This may explain why the release of Th in the presence of Ca reduces in comparison to previous experiments where Th is introduced on its own. Th ions, with a 4+ charge, have a higher coulombic attraction compared to Ni ions with a 2+ charge. In the previous chapter Ni is readily stripped off the surface of sand in the presence of ISA, leading to the formation of soluble complexes through the system, a contrasting observation to what is demonstrated here by Th. With a 4+ charge Th could potentially bind to sand much more strongly and also require a considerably higher concentration of organic complex to be liberated. It's not anticipated that potential formation of $Th(OH)_4$ precipitates could have resulted in the absence of Th from the effluent as the solubility of this compound increases in the presence of carbonate species (Warwick, Evans, & Heath, 2012). In consideration of the safety aspect of an ILW-GDF and the potential for radioactive elements to transport out of the geosphere these results demonstrate that even in the presence of α- and β-ISA Th will not mobilise under the "far-field" conditions investigated in this study.

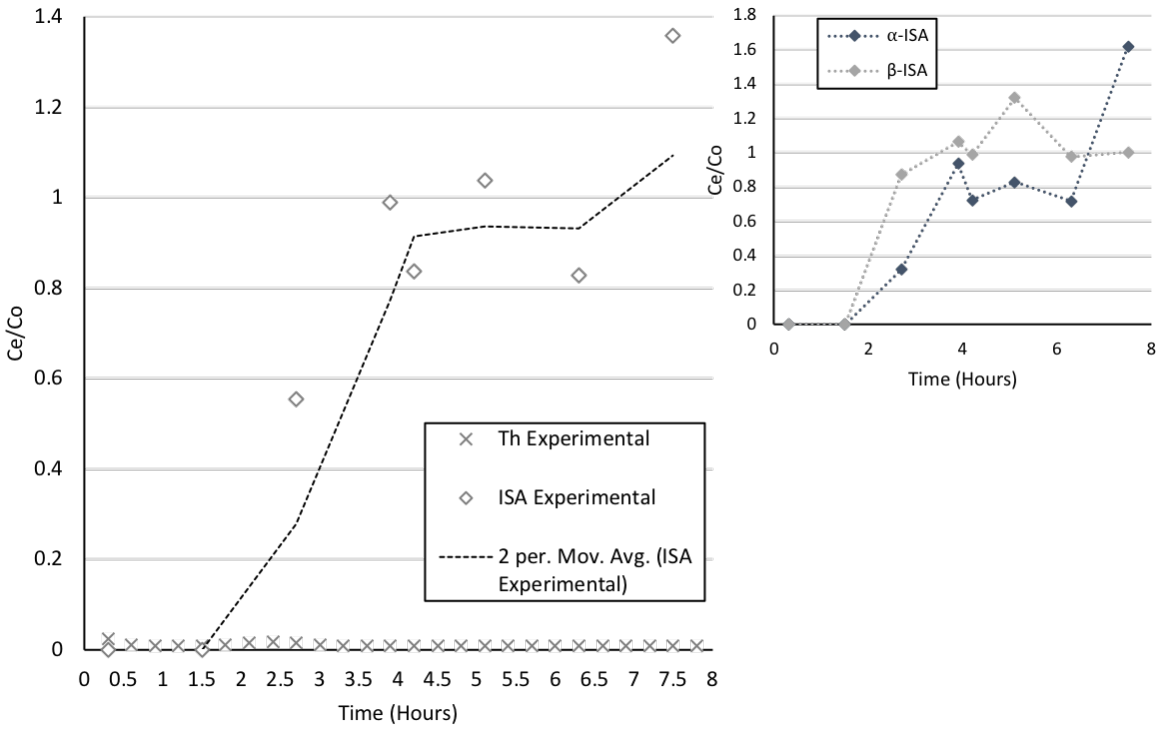

Figure 8. 8. The transport of ISA from an Th+CDP solution through a pH 9.5 sand column. Th (grey crosses) was not released from the system but both ISA forms (blue diamonds and grey diamonds) were detected in the effluent.

Results generated here demonstrate that the majority (>97%) of Th potentially mobilised within the chemically disturbed zone of an ILW-GDF will absorb to materials analogous to those within the "far-field" environment. In addition, there is no evidence within this chapter to suggest that Th mobility will be enhanced in the presence of organic complexants under the conditions investigated in this study.

8.2.3 Uranium

8.2.3.1 Abiotic transport

Data acquired through trace-level ICP-MS analysis revealed that at pH 9.5 hexavalent U(VI) does not adsorb to the surface of Ottawa sand under anaerobic and abiotic conditions. Figure 8.9 illustrates the mobility of U(VI) through the flow-cell system with a breakthrough time of 2.1 hrs and 3 hrs for exhaustion through the column, a contrasting observation to the sorption profiles of Ni and Th under the same environmental conditions. Here Li was not employed as a conservative tracer as U(VI) did not exhibit signs of adsorption. Despite U(VI) already being free-flowing

within the system a U + CDP solution was next injected into the column to study if the presence of complexants affects U(VI) adsorption in any way. ICP-MS analysis reveals that U(VI) is still mobile under the current conditions (Figure 8.10). U(VI) has a breakthrough time of 0.21 hrs here whereas ISA breakthrough does not occur until 1.4 hrs which suggests that the two are not in complexation prior to entering the system. Exhaustion of U(VI) through the column occurred at 0.74 hrs. This data suggests that U(VI) transport is independent of the presence of CDP under conditions analogous to that of an ILW-GDF far-field. However, potential complexation was not investigated further since it was clear that there were no sorption events taking place to hinder the transport of U(VI) in this setting.

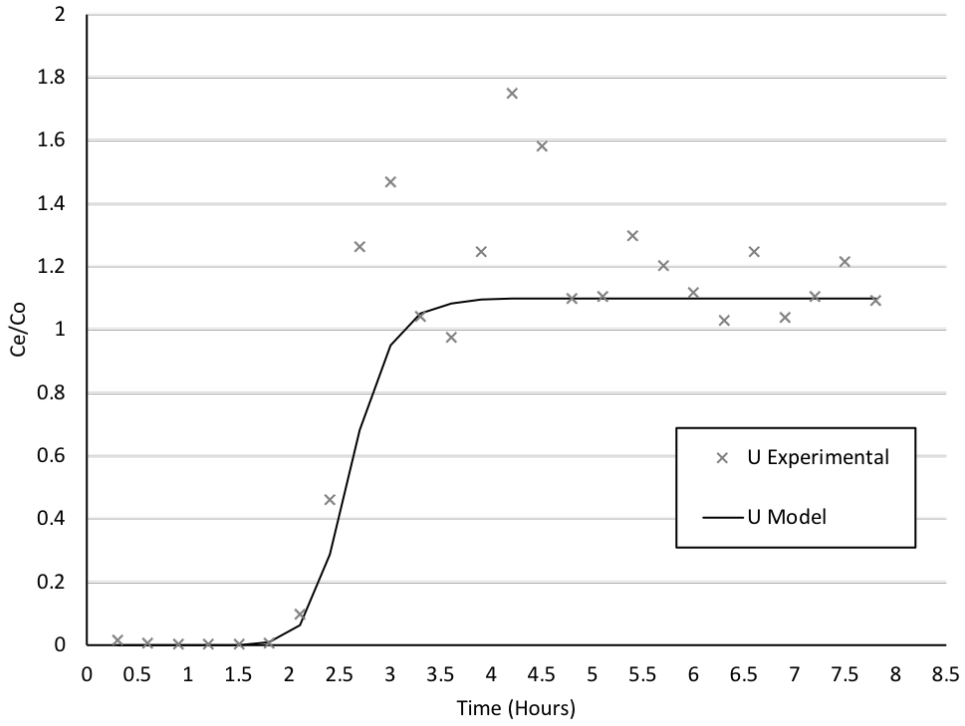

Figure 8. 9. The transport of U(VI) (grey crosses) through a pH 9.5 sand column under anaerobic conditions. U(VI) is mobile through the same system which previously limited the mobility of Ni/ Eu/ Th.

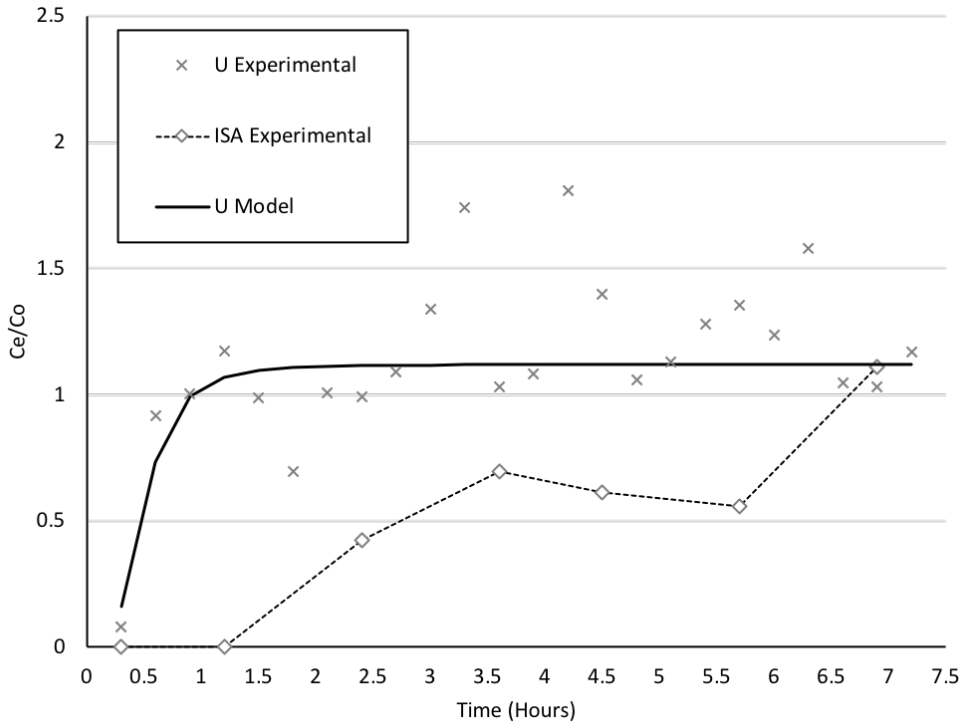

Figure 8. 10. The transport of U(VI) (grey crosses) and ISA (empty grey diamonds) from a U+CDP solution through a pH 9.5 sand column. U(VI) appeared to be mobile as it transported straight through the column with ISA released shortly after indicating the two were not complexed through the column.

8.2.3.2 Biotic transport

If U(VI) from the wasteform is released into the far-field/ geosphere uranium concentrations may be controlled under the highly reducing conditions expected within the deep subsurface as a result of buffering reactions taking place and the close proximity of microorganisms in the environment (N.D.A, 2015a). Uranium with a charge of 4+ is considered less soluble than its 6+ counterpart and therefore would more likely be immobilised through the groundwater in a far-field environment. In order to induce bioreduction, the sand column was exposed to an inoculum extracted from a highly reducing floc reactor operating at high pH, as previously described. The microbial community was revealed to predominantly comprise members of the Firmicutes (48.6%) and Proteobacteria (40.2%) phyla (Figure 8.11). At class level Bacilli and Clostridia dominated the Firmicutes making up 33.1% and 15.0% of sequences, respectively. Alphaproteobacteria prevailed within Proteobacteria and overall with 38.6% of total reads within the community (Figure 8.12).

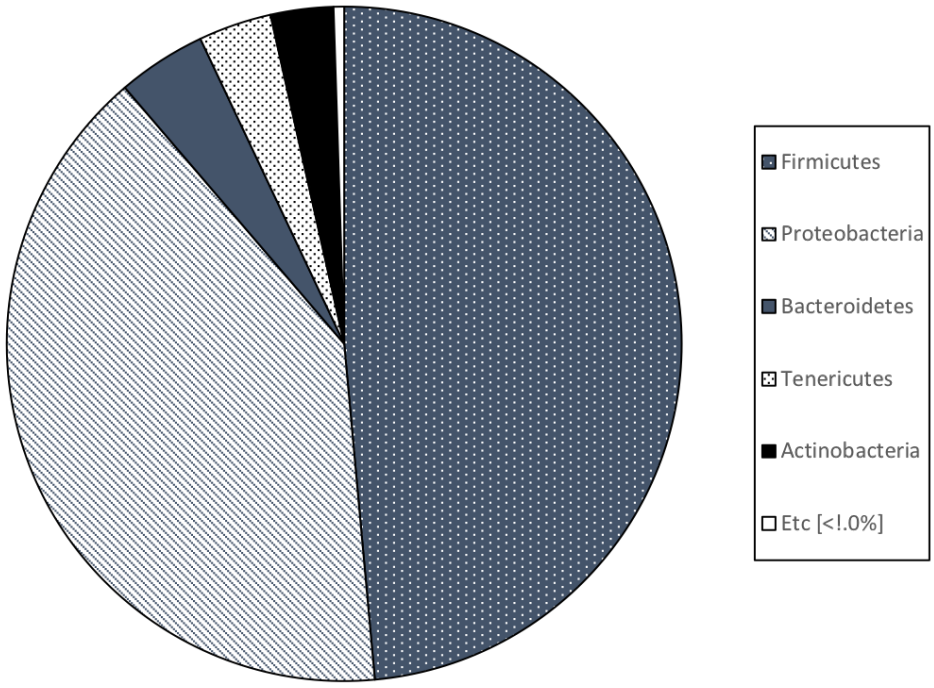

Figure 8. 11. Taxonomic composition of microbial floc reactor community at Phylum level. Microbial community analysis revealed Firmicutes dominated the population followed closely by Proteobacteria and then Bacteroidetes, Tenericutes and Actinobacteria in a smaller capacity.

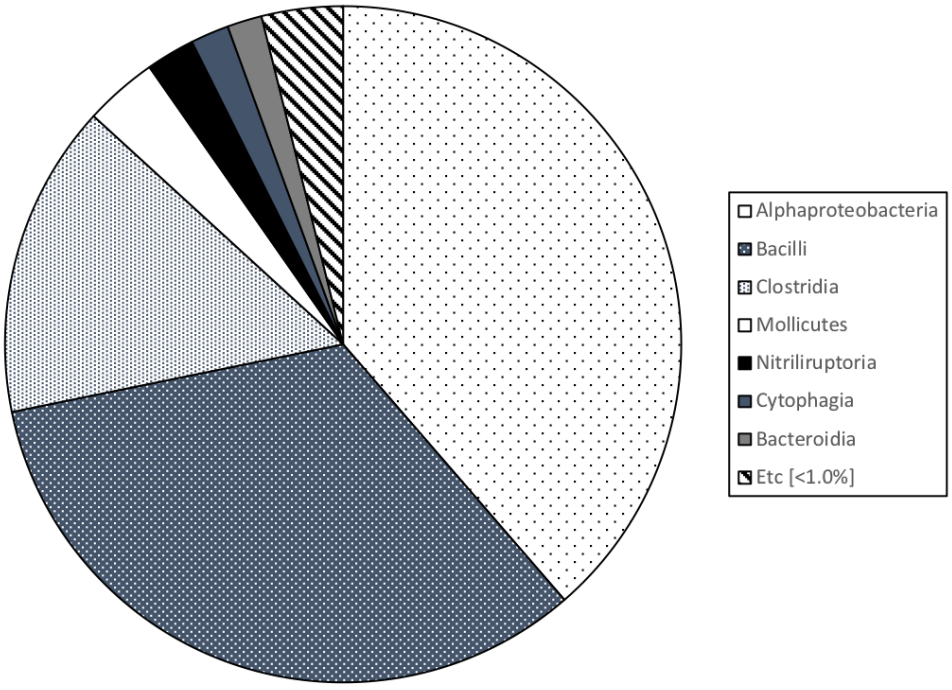

Figure 8. 12. Taxonomic composition of microbial floc reactor community at Class level. Sequences were primarily identified as being from Alphaproteobacteria, followed by Bacilli and Clostridia.

Due to time constraints U(VI), CDP (utilized as a source of carbon) and microbes were introduced into the column in the same influent media. ICP-MS analysis revealed that the concentration of uranium detected in effluent liquid samples decreased considerably over the period of the flow experiment. The level of measured soluble uranium fell from ~60% of the influent to ~10% between 0.5 – 2.5 hrs, reducing further still to ~2% of the influent, before increasing slightly at the end of the study to ~36% of influent concentration (Figure 8.13). Trace level determination of U(VI) (only) in effluent samples through UV-VIS spectroscopy is also displayed in Figure 8.13. The concentration of the soluble form of uranium reduces from ~65 % of the influent level U(VI) at 1.5 hrs to ~6% during the course of the experiment with a slight increase to ~16% at the end, supporting the ICP-MS data. This data indicates that uranium in the effluent is in the U(VI) form and that the retained uranium may be U(IV). Microorganisms are able to degrade ISA as a carbon source under the conditions of this system (as previously described), which could enable U(VI) to act as a terminal electron acceptor (TEA) during bio-reduction. Here, uranium only in its soluble form is measured through ICP-MS, suggesting that insoluble tetravalent U(IV) is immobilised through the flow cell system and not released into the effluent, resulting in a mix of valence states through the sand column.

Influent concentration of uranium in biotic media was found to be 0.6 mg/L (instead of 0.7 mg/L in abiotic experiments), possibly due to reduction already starting to take place at time of sampling. Here, it's not surprising that the majority of U(VI) within the influent had undergone reduction due to the initial concentration being very low, therefore a high reducing power was not required. Gao & Francis reported that at the higher concentrations within their study (0.6 mM) U(VI) was reduced but not completely, whereas at the lower concentrations (0.1 mM) the majority of U(VI) had been converted to U(IV) (Gao & Francis, 2008).

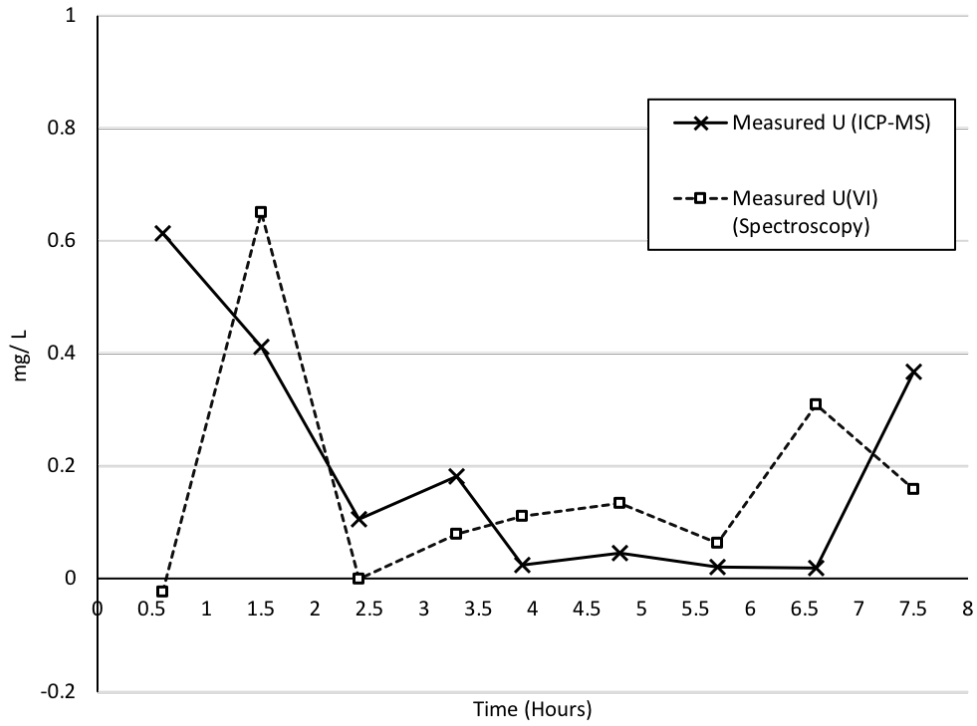

Figure 8. 13. Fate of U(VI) under biotic conditions. Soluble uranium measured by ICP-MS (black crosses) decreases over the period of the experiment due to reduction to insoluble U(VI). U(VI) only (empty black squares) measured by UV-VIS spectroscopy supports ICP-MS data.

A number of successful uranium reducers have been identified in the literature, those of which possess the ability to utilize uranium solely as an electron acceptor during respiration. While the majority of these reducers lie within the phyla of Firmicutes and Proteobacteria, both of which dominate the microbial consortia introduced within this study, none of the reducing species are identified as being present here. The reduction of U(VI) has previously been linked to bacteria within the phylum Clostridia under fermentative conditions. Gao & Francis investigated the reduction of U(VI) by various members of the Clostridia over a range of pH values (1.3 – 6.5). Results indicated that U(VI) reduction was successful, with varying levels of reduction, not only across all species tested but all pH levels too. In this study *Clostridium* sp. (ATCC 53464) showed a high resilience to extreme conditions, having been isolated from an acidic site, which could signify the potential of members of the Clostridia from alkaline environments to be able to reduce U(VI) in this way (Gao & Francis, 2008). Spear *et al* demonstrated the reduction of U(VI) to U(IV) by a mixed culture of sulphate-reducing bacteria (SRB), not just in pure culture (*Desulfovibrio desulfuricans*), at a range of concentrations (Spear, Figueroa, & Honeyman, 1999).

This evidence suggests that in mixed culture a number of species could play a part in the reduction of uranium under anaerobic conditions. Biosorption is a process which involves physical interaction between radionuclides and microorganisms and may also play a part in the removal of U(VI) from solution as observed here. A study by Liu *et al* demonstrated the success biosorption of U(VI) by *Bacillus amyloliquefaciens* a member of the *Bacillaceae* family, in just under 3 hours (Liu et al., 2019). The family *Bacillaceae* accounts for 33.1% of the microbial community introduced into the sand column, therefore it's possible there's potential for other biosorbents to act in a similar way to reduce the level of soluble uranium in aqueous solutions.

8.3 Conclusion

This chapter demonstrates the employment of a flow-through column developed in the earlier stages of the project to stimulate conditions analogous to that of an ILW-GDF far-field. By doing so, the behaviour of radionuclides in this environment within the vicinity of organic complexants and biofilm forming microorganisms can be observed on a laboratory scale. In systems containing Eu(II) and Th(IV) the presence of ISA appeared to have no effect on the sorption processes taking place between the sand material and these elements at pH 9.5. The literature reports reduced adsorption of Th(IV) in the presence of CDP but under hyperalkaline conditions and to cement backfill material (Tits et al., 2005) (Wieland et al., 2002). Under the conditions of the far-field where pH is far less alkaline due to an influx of groundwater and the geosphere is composed of host rock, clay, sand particles etc the sorption processes taking place here are likely to be quite different. Furthermore, within the chemically disturbed zone of an ILW-GDF the concentration of ISA in cement pore water is expected to be between $\sim 10^{-5} – 10^{4}$ M, which even before dilution and dispersion is much lower than the concentrations used within this chapter of work (Loon & Glaus, 1998). In regards to ILW disposal these results are optimistic for the retention and immobilisation of Eu(II) and Th(IV) within the far-field of an GDF. Results described within the later portion of the chapter indicate that under far-field conditions not all radionuclide will behave the same, demonstrated by the non-existent sorption processes taking place between U(VI) and sand material. The presence or absence of CDP is consequently made irrelevant in this scenario

and other methods for the immobilisation of U(VI) were explored. By introducing biofilm forming bacteria of the phyla Firmicutes and Proteobacteria a highly reducing atmosphere was generated within the influent media and sand column. In doing so a number of microbial processes were able to take place, resulting in the successful reduction of U(VI) to insoluble U(IV).

8.4 Key Findings

- Eu(II) and Th(IV) bind to sand under anaerobic and alkaline (pH 9.5) conditions
- In the presence of α and β forms of ISA Eu(II) nor Th(IV) is released into the pore water and is therefore immobilised within the system
- U(VI) does not adsorb to sand under the same conditions and the presence of ISA has no effect on its mobility
- Microorganisms can reduce the transport of U(VI) through a flow-cell system under the relevant conditions by conversion to insoluble U(IV)

Chapter 9.0

Concluding Remarks & Future Work

9.1 Concluding Remarks

The UK's current proposal for the long-term disposal of radioactive wastes involves disposal within cementitious facilities placed deep below the ground's surface known a geological disposal facility (GDF). Radioactive contaminants are expected to be contained within the wasteform through employment of a multi-component system comprising both engineered and natural barriers. Steel waste containers will be encased by a cement backfill material engineered to restrict the mobility of radionuclides through sorption or precipitation processes expected to take place.

Under the anaerobic and alkaline conditions of a GDF cellulosic content within the intermediate level waste inventory can undergo chemical hydrolysis leading to the generation of a collection of substances known as cellulose degradation products (CDPs), the main constituents of which are α- and β- isosaccharinic acids (ISA). The formation of soluble ISA-radionuclide complexes subsequently poses a serious threat to the safety and performance of long-term GDFs. The construction of a GDF will most likely introduce a number of microorganisms and nutrients to the near-field from the subsurface, however only those able to tolerate the harsh conditions will be capable of survival, such as alkaliphiles and anaerobes.

As the distance from the near-field or chemically disturbed zone of GDF increases, alkalinity of the surrounding pore water should reduce as cement hydration products are diluted and dispersed ($\sim$ pH 9.5). This environment known as the "far-field" would be home to a variety of pre-existing anaerobic and mildly alkaliphilic species surviving within cracks within the host rock/ geosphere. These micro-niches provide the ideal setting for the colonisation of microbial biofilms due to their ability to grow on a multitude of surfaces incorporating diverse microbial populations.

The data outlined within this thesis could help to predict the transport of radionuclides in the presence of organic complexants and biofilm-forming microorganisms in the far-field environment of an ILW-GDF.

Results Chapter 1

Initial investigations into the formation of suspect microbial biofilm on surface of lead pipes in Chapter 6.0 presented an opportunity to study the techniques required for the analysis of surface bound biofilms. While the microscopy/ analytical techniques themselves are well known, the use of them to examine complex and irregular surfaces can sometimes prove to be troublesome.

Optical microscopy was used for the visualisation of contrasting layers of the lead pipe inner lining, confirming the presence of not only lead metal but a form of mineralisation, in addition to what appeared to be organic deposits situated on top. In the case of sand biofilms this technique was not chosen during analysis as a mature biofilm was not expected to be produced in this case. Under scanning electron microscopy microbial biofilm appears clustered and irregular, distinct to the surface on which it is bound, therefore acts as a great tool for its identification (although visualisation alone could not prove microbial colonisation). At high magnification minerals can also be detected as shown in Figure 6.5, the presence of which can potentially be both an advantage and disadvantage in the structural integrity of microbial biofilms. Although the identification of minerals was not investigated further in this chapter it's possible that their presence affects the formation of sand biofilms therefore XRD was selected for use later in the project for the analysis of mineral phases.

Combining SEM with EDX analysis enabled suspected biofilm material to be examined further by generating an elemental profile of the contrasting surfaces. Here it was determined that a combination of surface bound lead complexes could play a part in the adhesion of biofilms. The techniques used up to this point allowed visualisation of the suspected biofilm material but not confirmation that biological constituents were present. Fluorescent staining coupled with confocal laser scanning microscopy of the lead pipe surfaces enabled individual EPS components to be studied at high magnification which allows the adhesion mechanisms of biofilms to surfaces to be studied in more detail. Although a profile of the microbial community could not be generated in this instance, most likely due to the presence of humics contaminating DNA, various techniques were pursued and trialled for the extraction of biofilm grown on surfaces.

Results Chapter 2

The preliminary investigations within (Chapter 7.0) sought to determine how nickel would behave in an abiotic environment under conditions analogous to that of an ILW-GDF far-field where sand is representative of a host-rock substrate. Flow-through experimentation revealed that nickel adsorbs to sand under alkaline (pH 9.5) and anaerobic conditions but in the presence of CDPs nickel is stripped off the surface as it forms soluble complexes with ISA. The data generated coincides with the release of the organic complexant, suggesting that ISA is able to enhance the migration of nickel previously retained through sorption processes.

Under biotic conditions 40-60% of influent ISA is degraded with <50% of influent nickel retained within the column. The production of acetic acids supports the claim that ISA is removed due to microbial rather than sorption processes. An investigation into flocculate material shedding off the main body of biofilm did not indicate that nickel biosorption, precipitation nor mineralisation had occurred. No discernible differences were displayed following the filtration of samples compared to their unfiltered profiles therefore suggesting flocculate transport does not lead to enhanced migration of complexed nickel under conditions investigated within this work.

Results here suggest that while ISA degradation does occur, complete fermentation is not observed, which questions whether the $Ni(ISA)_2$ complex can be fully degraded once formed. Microcosm experiments support this claim to some extent, revealing that in mixed culture α-ISA is fermented initially before concentration stabilised but in pure culture no degradation is observed.

Microbial community analysis revealed that members of Actinobacteria dominated the influent section of the column, with those within the Firmicutes phyla increasing in abundance through the middle and effluent, and Proteobacteria gaining reads within the effluent section. At class level Alphaproteobacteria gained abundance through the column to dominate at the effluent, members of Actinobacteria accounted for the majority of sequences at the influent but largely decreased through the system and those within the class Clostridia increased in abundance through the middle and effluent sections of the column. These results could suggest that under

harsh external stresses such as pH and anoxic conditions biofilm communities are able to adapt and change within the same system, potentially as a survival technique.

Sand samples extracted from the influent section exhibited higher levels of biofilm formation, most likely due to the influx of microorganisms entering the column and initially adhering to the sand surface. Confocal laser scanning microscopy revealed the presence of major EPS components within all three sections, the most abundant of which were found within the influent. EPS matrices showed similar compositions throughout the column although reduced association of these components was observed in the middle and effluent sections, potentially breaking apart as they passed through the sand column.

Data presented within this chapter demonstrates how under the anaerobic and alkaline subsurface conditions of an ILW-GDF far-field complexant ISA is removed by biofilm-forming microorganisms formed on geological substrates, leading to the reduced transport of nickel within the environment. Furthermore, this data indicates the potential for ISA degrading microbial communities to form biofilms on surfaces representative of those likely to exist within the far-field.

Results Chapter 3

Using the flow-cell system developed in Chapter 7.0 the transport of Europium, Thorium and Uranium were investigated under the same environmental conditions. Eu(II) adsorbs to the sand material as it passes through the abiotic system however the addition of CDPs does not result in its release from the column indicating that soluble Eu-ISA complexes may not form at pH 9.5. The data also reveals that when Eu(II) is combined with ISA prior to entering the column, Eu(II) is still not detected within the effluent suggesting Eu-ISA also don't form in the liquid phase as it's able to adsorb to the sand within the column. The detection of both α- and β-ISA within the effluent suggests that Eu-ISA complexation may not occur within the far-field conditions investigated within this study and that sand is a suitable substrate to trap migrating Eu(II).

At pH 9.5 Th(IV) undergoes adsorption to the sand material (99.8%), limiting it's mobility through the abiotic and anaerobic system. Similar to Eu(II), Th(IV) transport

is not majorly influenced by the presence of ISA, with ICP-MS analysis demonstrating 97.2% of the radionuclide is retained within the column. When Th(IV) and CDP were applied to the system in combination 99% of Th(IV) undergoes sorption processes to the sand. Th:ISA:Ca complexes require more ISA than Th:ISA to form, therefore in the presence of calcium (within CDP) complexation is less likely to occur. These results indicate that Th(IV) potentially released from ILW is not expected to migrate within the far-field environment simulated in this investigation, regardless of whether ISA is present.

The behaviour of hexavalent uranium within the flow-cell system was unlike what had been observed in the previous investigations of this thesis. ICP-MS analysis revealed U(VI) does not bind to sand under the far-field conditions investigated here, instead implying that it will freely migrate through the abiotic system. Evidently, no sorption processes were taking place between U(VI) and the sand therefore ISA as a mechanism of transport was not investigated further. Because of this, fermentation processes expected to occur would most likely have no impact on the migration of U(VI). Exposing the sand column to biofilm-forming microbes to induce microbial reduction resulted a decrease of soluble uranium measured within the effluent samples, data which was supported by the measuring of U(VI) only through UV-VIS spectroscopy. By utilising ISA as a carbon source during bioreduction microorganisms could further facilitate the removal of the complexing agent from the far-field environment. Taxonomic composition of the microbial community responsible revealed that members of Firmicutes and Proteobacteria dominated at phylum level, with the majority of sequences belonging to the classes of Alphaproteobacteria, Bacilli and Clostridia.

9.2 Key Points

- The transport of Ni(II), Eu(II) and Th(IV) is restricted through sorption processes within abiotic systems analogous to an ILW-GDF far-field
- In the presence of α and β ISA Ni(II) is mobilised through the formation of soluble complexes

- Eu(II) and Th(IV) do not show any indication of increased migration in the presence of CDPs and are therefore unlikely to reach the biosphere under conditions investigated here
- Microbes capable of the anaerobic and alkaline degradation of ISA can form biofilm on the surface of the sand, utilizing CDPs as a source of carbon to aid in survival
- Fermentation leads to the removal of complexant ISA and subsequently the retention of Ni(II) within the column, limiting it's migration
- U(VI) movement is not hindered through adsorption to sand and therefore does not rely on ISA as a mechanism of transport
- Biofilm-forming microorganisms stimulate reducing conditions leading to reduction of U(VI) to insoluble U(IV) within the flow-cell system
- Techniques studied for the analysis of biofilms grown on complex surfaces were utilised to characterise microbial biofilm capable of survival within the sand column under the conditions investigated

The data presented within this thesis addresses the aims outlined in Chapter 4.0 which involved developing a system in order to study and analyse the following on a laboratory scale:

- Transport of natural analogues and radionuclides within an abiotic system representative of an ILW-GDF far-field utilising sand as a geological substrate
- The modified behaviour of these substances in the presence of ISA as a complexing agent
- Formation of biofilm under the relevant conditions, including its physical and microbial composition
- The biological processes expected to occur that may affect the migration and long-term fate of complexed radionuclides within the geosphere

9.3 Future Work

Using the flow-cell set-up and techniques described here, this modelling system can be employed for the investigation into the transport of various other radionuclides and their natural analogues, the sorption capacities of different host rock material

and the presence of a range of complexing agents to aid in the safety assessments carried out for the long-term disposal of radioactive wastes.

References

Abdel Aal, G., Atekwana, E., & Atekwana, E. (2010). Effect of bioclogging in porous media on complex conductivity signatures. *Journal of Geophysical Research, 115*. doi:10.1029/2009JG001159

Abdullah, A., Yahaya, N., Noor, N., & Rasol, R. (2014). Microbial Corrosion of API 5L X-70 Carbon Steel by ATCC 7757 and Consortium of Sulfate-Reducing Bacteria. *Journal of Chemistry, 2014*, 1-7. doi:10.1155/2014/130345

Acinas, S. G., Sarma-Rupavtarm, R., Klepac-Ceraj, V., & Polz, M. F. (2005). PCR-Induced Sequence Artifacts and Bias: Insights from Comparison of Two 16S rRNA Clone Libraries Constructed from the Same Sample. *Applied and Environmental Microbiology, 71*(12), 8966. doi:10.1128/AEM.71.12.8966-8969.2005

Adey, J. (2005). *Development of the partition coefficient (Kd) test method for use in environmental risk assessments*. (Science Report SC020039/4). Rio House, Waterside Drive, Aztec West, Almondsbury, Bristol, BS32 4UD: Environment Agency

An, Y. H., Dickinson, R. B., & J, D. R. (2000). Mechanisms of Bacterial Adhesion and Pathogenesis of Implant and Tissue Infections. In Y. H. An & R. J. Friedman (Eds.), *Handbook of Bacterial Adhesion: Principles, Methods and Applications* (pp. 1-27). Totowa: Humana Press.

Anderson, C., Jakobsson, A.-M., & Pedersen, K. (2007). Influence of in situ Biofilm Coverage on the Radionuclide Adsorption Capacity of Subsurface Granite. *Environmental science & technology, 41*(3), 830-836. doi:10.1021/es0608702

Ansell, M. P., & Mwaikambo, L. Y. (2009). 2 - The structure of cotton and other plant fibres. In S. J. Eichhorn, J. W. S. Hearle, M. Jaffe, & T. Kikutani (Eds.), *Handbook of Textile Fibre Structure* (Vol. 2, pp. 62-94): Woodhead Publishing.

Antony, C. P., Kumaresan, D., Hunger, S., Drake, H. L., Murrell, J. C., & Shouche, Y. S. (2013). Microbiology of Lonar Lake and other soda lakes. *The ISME Journal, 7*(3), 468-476. doi:10.1038/ismej.2012.137

Avolio, M. L., Carroll, I. T., Collins, S. L., Houseman, G. R., Hallett, L. M., Isbell, F., . . . Wilcox, K. R. (2019). A comprehensive approach to analyzing community dynamics using rank abundance curves. *Ecosphere, 10*(10), e02881. doi:https://doi.org/10.1002/ecs2.2881

Banaszak, J. E., Rittmann, B. E., & Reed, D. T. (1999). Subsurface interactions of actinide species and microorganisms: Implications for the bioremediation of actinide-organic mixtures. *Journal of Radioanalytical and Nuclear Chemistry, 241*(2), 385-435. doi:10.1007/BF02347481

Banzhaf, S., & Hebig, K. (2016). Use of column experiments to investigate the fate of organic micropollutants - A review. *Hydrology and Earth System Sciences, 20*, 3719-3737. doi:10.5194/hess-20-3719-2016

Bassil, N. M., Bryan, N., & Lloyd, J. R. (2015). Microbial degradation of isosaccharinic acid at high pH. *The ISME Journal, 9*(2), 310-320. doi:10.1038/ismej.2014.125

Baum, M. M., Kainović, A., O'Keeffe, T., Pandita, R., McDonald, K., Wu, S., & Webster, P. (2009). Characterization of structures in biofilms formed by a Pseudomonas fluorescens isolated from soil. *BMC microbiology, 9*, 103-103. doi:10.1186/1471-2180-9-103

Beadle, I., Humphreys, P. N., Pettit, C., & Small, J. (2000). Integrating Microbiology into the Drigg Post-Closure Radiological Safety Assessment. *MRS Proceedings, 663*, 665. doi:10.1557/PROC-663-665

Bertran, E., Leavitt, W. D., Pellerin, A., Zane, G. M., Wall, J. D., Halevy, I., . . . Johnston, D. T. (2018). Deconstructing the Dissimilatory Sulfate Reduction Pathway: Isotope Fractionation of a Mutant Unable of Growth on Sulfate. *Frontiers in Microbiology, 9*, 3110-3110. doi:10.3389/fmicb.2018.03110

Bethke, C. M., Sanford, R. A., Kirk, M. F., Jin, Q., & Flynn, T. M. (2011). The thermodynamic ladder in geomicrobiology. *American Journal of Science, 311*(3), 183-210.

Boland, T., Latour, R. A., & Stutzenberger, F. J. (2000). Molecular Basis of Bacterial Adhesion. In Y. H. An & R. J. Friedman (Eds.), *Handbook of Bacterial Adhesion*. Totowa, NJ: Humana Press.

Bugg, T. D. H., Ahmad, M., Hardiman, E. M., & Rahmanpour, R. (2011). Pathways for degradation of lignin in bacteria and fungi. *Natural Product Reports, 28*(12), 1883-1896. doi:10.1039/C1NP00042J

Burke, I. T., Mortimer, R. J. G., Palaniyandi, S., Whittleston, R. A., Lockwood, C. L., Ashley, D. J., & Stewart, D. I. (2012). Biogeochemical Reduction Processes in a Hyper-Alkaline Leachate Affected Soil Profile. *Geomicrobiology Journal, 29*(9), 769-779. doi:10.1080/01490451.2011.619638

Cai, P., Liu, X., Ji, D., Yang, S., Walker, S. L., Wu, Y., . . . Huang, Q. (2018). Impact of soil clay minerals on growth, biofilm formation, and virulence gene expression of Escherichia coli O157:H7. *Environ Pollut, 243*(Pt B), 953-960. doi:10.1016/j.envpol.2018.09.032

Carboneau, M. L., & Adams, J. P. (1995). *National Low-Level Waste Management Program Radionuclide Report Series. Volume 10: Nickel-63*. Idaho Falls, Idaho: Idaho National Engineering Laboratory

Carpentier, B., & Cerf, O. (1993). Biofilms and their consequences, with particular reference to hygiene in the food industry. *Journal of Applied Bacteriology, 75*(6), 499-511. doi:10.1111/j.1365-2672.1993.tb01587.x

Cervantes, C., Campos-García, J., Devars, S., Gutiérrez-Corona, F., Loza-Tavera, H., Torres-Guzmán, J. C., & Moreno-Sánchez, R. (2001). Interactions of chromium with microorganisms and plants. *FEMS Microbiology Reviews, 25*(3), 335-347. doi:10.1111/j.1574-6976.2001.tb00581.x

Charles, C. J., Rout, S. P., Garratt, E. J., Patel, K., Laws, A. P., & Humphreys, P. N. (2015a). The enrichment of an alkaliphilic biofilm consortia capable of the anaerobic degradation of isosaccharinic acid from cellulosic materials incubated within an anthropogenic, hyperalkaline environment. *FEMS Microbiology Ecology, 91*(8). doi:10.1093/femsec/fiv085

Charles, C. J., Rout, S. P., Garratt, E. J., Patel, K., Laws, A. P., & Humphreys, P. N. (2015b). The enrichment of an alkaliphilic biofilm consortia capable of the anaerobic degradation of isosaccharinic acid from cellulosic materials incubated within an anthropogenic, hyperalkaline environment. *FEMS Microbiology Ecology, 91*(8), fiv085-fiv085. doi:10.1093/femsec/fiv085

Charles, C. J., Rout, S. P., Laws, A. P., Jackson, B. R., Boxall, S. A., & Humphreys, P. N. (2017). The Impact of Biofilms upon Surfaces Relevant to an Intermediate Level Radioactive Waste Geological Disposal Facility under Simulated Near-Field Conditions. *Geosciences, 7*, 57. doi:10.3390/geosciences7030057

Charles, C. J., Rout, S. P., Patel, K. A., Akbar, S., Laws, A. P., Jackson, B. R., . . . Humphreys, P. N. (2017). Floc Formation Reduces the pH Stress Experienced by Microorganisms Living in Alkaline Environments. *Applied and Environmental Microbiology, 83*(6), e02985-02916. doi:10.1128/AEM.02985-16

Chen, M. Y., Lee, D. J., Tay, J. H., & Show, K. Y. (2007). Staining of extracellular polymeric substances and cells in bioaggregates. *Appl Microbiol Biotechnol, 75*(2), 467-474. doi:10.1007/s00253-006-0816-5

Chun, J., Lee, J. H., Jung, Y., Kim, M., Kim, S., Kim, B. K., & Lim, Y. W. (2007). EzTaxon: a web-based tool for the identification of prokaryotes based on 16S ribosomal RNA gene sequences. *Int J Syst Evol Microbiol, 57*(Pt 10), 2259-2261. doi:10.1099/ijs.0.64915-0

Coombs, P., Wagner, D., Bateman, K., Harrison, H., Milodowski, A. E., Noy, D., & West, J. M. (2010). The role of biofilms in subsurface transport processes. *Quarterly Journal of Engineering Geology and Hydrogeology, 43*(2), 131. doi:10.1144/1470-9236/08-029

Costerton, J. W., Lewandowski, Z., Caldwell, D. E., Korber, D. R., & Lappin-Scott, H. M. (1995). MICROBIAL BIOFILMS. *Annual Review of Microbiology, 49*(1), 711-745. doi:10.1146/annurev.mi.49.100195.003431

Cruz, L. F., Cobine, P. A., & De La Fuente, L. (2012). Calcium increases Xylella fastidiosa surface attachment, biofilm formation, and twitching motility. *Appl Environ Microbiol, 78*(5), 1321-1331. doi:10.1128/aem.06501-11

Daae, F. L., Økland, I., Dahle, H., Jørgensen, S. L., Thorseth, I. H., & Pedersen, R. B. (2013). Microbial life associated with low-temperature alteration of ultramafic rocks in the Leka ophiolite complex. *Geobiology, 11*(4), 318-339. doi:10.1111/gbi.12035

Dang, H., & Lovell, C. R. (2015). Microbial Surface Colonization and Biofilm Development in Marine Environments. *Microbiology and molecular biology reviews : MMBR, 80*(1), 91-138. doi:10.1128/MMBR.00037-15

Dario, M., Molera, M., & Allard, B. (2006). Sorption of europium on TiO2 and cement at high Ph in the presence of organic ligands. *Journal of Radioanalytical and Nuclear Chemistry, 270*(3), 495-505. doi:10.1007/s10967-006-0455-4

Das, S., Kedari, C., & Tripathi, S. (2010). Spectrophotometric determination of trace amount of uranium (VI) in different aqueous and organic streams of nuclear fuel processing using 2-(5-bromo-2-pyridylazo-5-diethylaminophenol). *Journal of Radioanalytical and Nuclear Chemistry, 285*. doi:10.1007/s10967-010-0647-9

Davey, M., & O'Toole, G. (2001). Microbial Biofilms: from Ecology to Molecular Genetics. *Microbiology and molecular biology reviews : MMBR, 64*, 847-867. doi:10.1128/MMBR.64.4.847-867.2000

Davis, C. A., Atekwana, E., Atekwana, E., Slater, L. D., Rossbach, S., & Mormile, M. R. (2006). Microbial growth and biofilm formation in geologic media is detected with complex conductivity measurements. *Geophysical Research Letters, 33*(18). doi:https://doi.org/10.1029/2006GL027312

De Muynck, W., Debrouwer, D., De Belie, N., & Verstraete, W. (2008). Bacterial carbonate precipitation improves the durability of cementitious materials. *Cement and Concrete Research, 38*(7), 1005-1014. doi:https://doi.org/10.1016/j.cemconres.2008.03.005

Decho, A. W., & Gutierrez, T. (2017). Microbial Extracellular Polymeric Substances (EPSs) in Ocean Systems. *Frontiers in Microbiology, 8*(922). doi:10.3389/fmicb.2017.00922

Deng, Y., Wang, L., Chen, Y., & Long, Y. (2020). Optimization of staining with SYTO 9/propidium iodide: interplay, kinetics and impact on Brevibacillus brevis. *BioTechniques, 69*(2), 88-98. doi:10.2144/btn-2020-0036

Donlan, R. M. (2002). Biofilms: microbial life on surfaces. *Emerg Infect Dis, 8*(9), 881-890. doi:10.3201/eid0809.020063

Dunne, W. J. (2002). Bacterial Adhesion: Seen Any Good Biofilms Lately? *Clinical Microbiology Reviews, 15*(2), 155-166.

Edgar, R. C., Haas, B. J., Clemente, J. C., Quince, C., & Knight, R. (2011). UCHIME improves sensitivity and speed of chimera detection. *Bioinformatics, 27*(16), 2194-2200. doi:10.1093/bioinformatics/btr381

Edwards, K. J., Bach, W., & McCollom, T. M. (2005). Geomicrobiology in oceanography: microbe-mineral interactions at and below the seafloor. *Trends Microbiol, 13*(9), 449-456. doi:10.1016/j.tim.2005.07.005

El Abed, S., Saad, I., Latrache, H., & Hamadi, F. (2012). Scanning Electron Microscopy (SEM) and Environmental SEM: Suitable Tools for Study of Adhesion Stage and Biofilm Formation. In.

Falkinham, J. O., 3rd. (2009). Surrounded by mycobacteria: nontuberculous mycobacteria in the human environment. *J Appl Microbiol, 107*(2), 356-367. doi:10.1111/j.1365-2672.2009.04161.x

Fashola, M. O., Ngole-Jeme, V. M., & Babalola, O. O. (2016). Heavy Metal Pollution from Gold Mines: Environmental Effects and Bacterial Strategies for Resistance. *International Journal of Environmental Research and Public Health, 13*(11). doi:10.3390/ijerph13111047

Felipe-Sotelo, M., Hinchliff, J., Evans, N., Warwick, P., & Read, D. (2012). Sorption of radionuclides to a cementitious backfill material under near-field conditions. *Mineralogical Magazine, 76*(8), 3401-3410. doi:10.1180/minmag.2012.076.8.53

Fish, K. E., Osborn, A. M., & Boxall, J. (2016). Characterising and understanding the impact of microbial biofilms and the extracellular polymeric substance (EPS) matrix in drinking water distribution systems. *Environmental Science: Water Research & Technology, 2*(4), 614-630. doi:10.1039/C6EW00039H

Flemming, H.-C., Neu, T. R., & Wozniak, D. J. (2007). The EPS Matrix: The “House of Biofilm Cells”. *Journal of Bacteriology, 189*(22), 7945. doi:10.1128/JB.00858-07

Flemming, H.-C., & Wingender, J. (2010). The Biofilm Matrix. *Nature reviews. Microbiology, 8*, 623-633. doi:10.1038/nrmicro2415

Fones, E. M., Colman, D. R., Kraus, E. A., Nothaft, D. B., Poudel, S., Rempfert, K. R., . . . Boyd, E. S. (2019). Physiological adaptations to serpentinization in the Samail Ophiolite, Oman. *The ISME Journal, 13*(7), 1750-1762. doi:10.1038/s41396-019-0391-2

Fong, J. N. C., & Yildiz, F. H. (2015). Biofilm Matrix Proteins. *Microbiology spectrum, 3*(2), 10.1128/microbiolspec.MB-0004-2014. doi:10.1128/microbiolspec.MB-0004-2014

Foti, M., Sorokin, D. Y., Lomans, B., Mussman, M., Zacharova, E. E., Pimenov, N. V., . . . Muyzer, G. (2007). Diversity, Activity, and Abundance of Sulfate-Reducing Bacteria in Saline and Hypersaline Soda Lakes. *Applied and Environmental Microbiology, 73*(7), 2093. doi:10.1128/AEM.02622-06

Fuller, S. J., McMillan, D. G. G., Renz, M. B., Schmidt, M., Burke, I. T., & Stewart, D. I. (2014). Extracellular electron transport-mediated Fe(III) reduction by a community of alkaliphilic bacteria that use flavins as electron shuttles. *Applied and Environmental Microbiology, 80*(1), 128-137. doi:10.1128/AEM.02282-13

Ganesh, R., Robinson, K. G., Reed, G. D., & Sayler, G. S. (1997). Reduction of hexavalent uranium from organic complexes by sulfate- and iron-reducing bacteria. *Applied and Environmental Microbiology, 63*(11), 4385-4391. doi:10.1128/AEM.63.11.4385-4391.1997

Gao, W., & Francis, A. J. (2008). Reduction of Uranium(VI) to Uranium(IV) by Clostridia. *Applied and Environmental Microbiology, 74*(14), 4580. doi:10.1128/AEM.00239-08

Gaona, X., Kulik, D. A., Mace, N., & Wieland, E. (2012). Aqueous–solid solution thermodynamic model of U(VI) uptake in C–S–H phases. *Applied Geochemistry, 27*, 81-95.

Gaona, X., Montoya, V., Colàs, E., Grivé, M., & Duro, L. (2008). Review of the complexation of tetravalent actinides by ISA and gluconate under alkaline to hyperalkaline conditions. *Journal of Contaminant Hydrology, 102*(3), 217-227. doi:https://doi.org/10.1016/j.jconhyd.2008.09.017

Ghosh, R., Barman, S., & Mandal, N. C. (2019). Phosphate deficiency induced biofilm formation of Burkholderia on insoluble phosphate granules plays a pivotal role for maximum release of soluble phosphate. *Scientific reports, 9*(1), 5477. doi:10.1038/s41598-019-41726-9

Gilkes, R., Suddhiprakarn, A., & Armitage, T. M. (1980). Scanning Electron Microscope Morphology of Deeply Weathered Granite. *Clays and Clay Minerals, 28*, 29-34. doi:10.1346/CCMN.1980.0280104

Glaring, M. A., Vester, J. K., Lylloff, J. E., Abu Al-Soud, W., Sørensen, S. J., & Stougaard, P. (2015). Microbial Diversity in a Permanently Cold and Alkaline Environment in Greenland. *PLOS ONE, 10*(4), e0124863. doi:10.1371/journal.pone.0124863

Grant, W., & Sorokin, D. (2011). Distribution and Diversity of Soda Lake Alkaliphiles. In (Vol. 1, pp. 27-54).

Griffiths, R. I., Whiteley, A. S., O'Donnell, A. G., & Bailey, M. J. (2000). Rapid method for coextraction of DNA and RNA from natural environments for analysis of ribosomal DNA- and rRNA-based microbial community composition. *Appl Environ Microbiol, 66*(12), 5488-5491. doi:10.1128/aem.66.12.5488-5491.2000

Hallberg, K. B. (2010). New perspectives in acid mine drainage microbiology. *Hydrometallurgy, 104*(3), 448-453. doi:https://doi.org/10.1016/j.hydromet.2009.12.013

Hand, V. L., Lloyd, J. R., Vaughan, D. J., Wilkins, M. J., & Boult, S. (2008). Experimental Studies of the Influence of Grain Size, Oxygen Availability and Organic Carbon Availability on Bioclogging in Porous Media. *Environmental science & technology, 42*(5), 1485-1491. doi:10.1021/es072022s

Heggendorn, F. L., Fraga, A. G. M., Ferreira, D. d. C., Gonçalves, L. S., Lione, V. d. O. F., & Lutterbach, M. T. S. (2018). Sulfate-Reducing Bacteria: Biofilm Formation and Corrosive Activity in Endodontic Files. *International Journal of Dentistry, 2018*, 1-12. doi:10.1155/2018/8303450

Hemme, C. L., Deng, Y., Gentry, T. J., Fields, M. W., Wu, L., Barua, S., . . . Zhou, J. (2010). Metagenomic insights into evolution of a heavy metal-contaminated groundwater microbial community. *The ISME Journal, 4*(5), 660-672. doi:10.1038/ismej.2009.154

Herrmann, M., Vaudaux, P. E., Pittet, D., Auckenthaler, R., Lew, P. D., Perdreau, F. S., . . . Waldvogel, F. A. (1988). Fibronectin, Fibrinogen, and Laminin Act as Mediators of Adherence of Clinical Staphylococcal Isolates to Foreign Material. *The Journal of Infectious Diseases, 158*(4), 693-701. doi:10.1093/infdis/158.4.693

Hiroki, M. (1992). Effects of heavy metal contamination on soil microbial population. *Soil Science and Plant Nutrition, 38*(1), 141-147. doi:10.1080/00380768.1992.10416961

Ho, D., Jensen, P., Gutierrez-Zamora, M.-L., Beckmann, S., Manefield, M., & Batstone, D. (2016). High-rate, High Temperature Acetotrophic Methanogenesis Governed by a Three Population Consortium in Anaerobic Bioreactors. *PLOS ONE, 11*(8), e0159760. doi:10.1371/journal.pone.0159760

Horikoshi, K. (1999). Alkaliphiles: some applications of their products for biotechnology. *Microbiology and molecular biology reviews : MMBR, 63*(4), 735-750. Retrieved from https://pubmed.ncbi.nlm.nih.gov/10585964

Huang, Y., Niu, B., Gao, Y., Fu, L., & Li, W. (2010). CD-HIT Suite: a web server for clustering and comparing biological sequences. *Bioinformatics, 26*(5), 680-682. doi:10.1093/bioinformatics/btq003

Humphreys, P. N., Laws, A., & Dawson, J. (2010). *A Review of Cellulose Degradation and the Fate of Degradation Products Under Repository Conditions*. (SERCO/TAS/002274/001 Issue 2). Harwell, Didcot, Oxfordshire, UK: Nuclear Decommissioning Authority (Radioactive Waste Management Directorate)

Humphreys, P. N., West, J. M., & Metcalfe, R. (2010). *Microbial effects on repository performance*. Harwell, Didcot, Oxfordshire, UK: Quintessa contractors report prepared for the Nuclear Decommissioning Authority (Radioactive Waste Management Directorate)

Hurt, R. A., Jr., Robeson, M. S., II, Shakya, M., Moberly, J. G., Vishnivetskaya, T. A., Gu, B., & Elias, D. A. (2014). Improved Yield of High Molecular Weight DNA Coincides with Increased Microbial Diversity Access from Iron Oxide Cemented Sub-Surface Clay Environments. *PLOS ONE, 9*(7), e102826. doi:10.1371/journal.pone.0102826

Hutzler, N. J., Crittenden, J. C., Gierke, J. S., & Johnson, A. S. (1986). Transport of Organic Compounds With Saturated Groundwater Flow: Experimental Results. *Water Resources Research, 22*(3), 285-295. doi:https://doi.org/10.1029/WR022i003p00285

Igiri, B. E., Okoduwa, S. I. R., Idoko, G. O., Akabuogu, E. P., Adeyi, A. O., & Ejiogu, I. K. (2018). Toxicity and Bioremediation of Heavy Metals Contaminated Ecosystem from Tannery Wastewater: A Review. *Journal of Toxicology, 2018*, 2568038. doi:10.1155/2018/2568038

Jarvis, P., Quy, K., Macadam, J., Edwards, M., & Smith, M. (2018). Intake of lead (Pb) from tap water of homes with leaded and low lead plumbing systems. *Science of The Total Environment, 644*, 1346-1356. doi:https://doi.org/10.1016/j.scitotenv.2018.07.064

Jo, J., Oh, J., & Park, C. (2020). Microbial community analysis using high-throughput sequencing technology: a beginner's guide for microbiologists. *Journal of Microbiology, 58*(3), 176-192. doi:10.1007/s12275-020-9525-5

Johnson, E. A. (2009). Clostridia. In M. Schaechter (Ed.), *Encyclopedia of Microbiology (Third Edition)* (pp. 87-93). Oxford: Academic Press.

Johnson, M., Zaretskaya, I., Raytselis, Y., Merezhuk, Y., McGinnis, S., & Madden, T. L. (2008). NCBI BLAST: a better web interface. *Nucleic acids research, 36*(Web Server issue), W5-9. doi:10.1093/nar/gkn201

Jones, A. A., & Bennett, P. C. (2017). Mineral Ecology: Surface Specific Colonization and Geochemical Drivers of Biofilm Accumulation, Composition, and Phylogeny. *Frontiers in Microbiology, 8*(491). doi:10.3389/fmicb.2017.00491

Joye, S. B., Connell, T. L., Miller, L. G., Oremland, R. S., & Jellison, R. S. (1999). Oxidation of ammonia and methane in an alkaline, saline lake. *Limnology and Oceanography, 44*(1), 178-188. doi:10.4319/lo.1999.44.1.0178

Kämpfer, P., Wohlgemuth, S., & Scholz, H. (2014). The Family Brucellaceae. In D. E. F. Rosenberg E., Lory S., Stackebrandt E., Thompson F. (Ed.), *The Prokaryotes* (pp. 155-178). Berlin, Heidelberg: Springer.

Kämpfer, P., Young, C.-C., Chen, W.-M., Rekha, P. D., Fallschissel, K., Lodders, N., . . . Arun, A. B. (2010). Fontibacter flavus gen. nov., sp. nov., a member of the family 'Cyclobacteriaceae', isolated from a hot spring. *International journal of systematic and evolutionary microbiology, 60*(9), 2066-2070. doi:https://doi.org/10.1099/ijs.0.017210-0

Kanekar, P. P., Nilegaonkar, S. S., Sarnaik, S. S., & Kelkar, A. S. (2002). Optimization of protease activity of alkaliphilic bacteria isolated from an alkaline lake in India. *Bioresource technology, 85*(1), 87-93. doi:10.1016/s0960-8524(02)00018-4

Kelley, J. I., Turng, B., Williams, H. N., & Baer, M. L. (1997). Effects of temperature, salinity, and substrate on the colonization of surfaces in situ by aquatic bdellovibrios. *Appl Environ Microbiol, 63*(1), 84-90. doi:10.1128/aem.63.1.84-90.1997

Keylock, C. J. (2005). Simpson diversity and the Shannon–Wiener index as special cases of a generalized entropy. *Oikos, 109*(1), 203-207. doi:https://doi.org/10.1111/j.0030-1299.2005.13735.x

Khan, M. S. I., Oh, S.-W., & Kim, Y.-J. (2020). Power of Scanning Electron Microscopy and Energy Dispersive X-Ray Analysis in Rapid Microbial Detection and Identification at the Single Cell Level. *Scientific reports, 10*(1), 2368. doi:10.1038/s41598-020-59448-8

Knill, C., & Kennedy, J. (2003). Degradation of Cellulose under Alkaline Conditions. *Carbohydrate Polymers, 51*, 281-300. doi:10.1016/S0144-8617(02)00183-2

Kostakioti, M., Hadjifrangiskou, M., & Hultgren, S. J. (2013). Bacterial biofilms: development, dispersal, and therapeutic strategies in the dawn of the postantibiotic era. *Cold Spring Harbor perspectives in medicine, 3*(4), a010306-a010306. doi:10.1101/cshperspect.a010306

Krulwich, T. A., Federbush, J. G., & Guffanti, A. A. (1985). Presence of a nonmetabolizable solute that is translocated with Na+ enhances Na+-dependent pH homeostasis in an alkalophilic Bacillus. *J Biol Chem, 260*(7), 4055-4058.

Krupka, K. M., Kaplan, D. I., Whelan, G., Serne, R. J., & Mattigod, S. V. (1999). *Understanding variation in partition coefficients, Kd, values*. (EPA 402-R-99-004A).

Kuippers, G., Boothman, C., Bagshaw, H., Ward, M., Beard, R., Bryan, N., & Lloyd, J. R. (2018). The biogeochemical fate of nickel during microbial ISA degradation; implications for nuclear waste disposal. *Scientific reports, 8*(1), 8753. doi:10.1038/s41598-018-26963-8

Kulp, T. R., Hoeft, S. E., Miller, L. G., Saltikov, C., Murphy, J. N., Han, S., . . . Oremland, R. S. (2006). Dissimilatory Arsenate and Sulfate Reduction in Sediments of Two Hypersaline, Arsenic-Rich Soda Lakes: Mono and Searles Lakes, California. *Applied and Environmental Microbiology, 72*(10), 6514. doi:10.1128/AEM.01066-06

Kyeremeh, I. A., Charles, C. J., Rout, S. P., Laws, A. P., & Humphreys, P. N. (2016). Microbial Community Evolution Is Significantly Impacted by the Use of Calcium Isosaccharinic Acid as an Analogue for the Products of Alkaline Cellulose Degradation. *PLOS ONE, 11*(11), e0165832. doi:10.1371/journal.pone.0165832

Lear, G., Dickie, I., Banks, J., Boyer, S., Buckley, H., Buckley, T., . . . Holdaway, R. (2017). Methods for the extraction, storage, amplification and sequencing of DNA from environmental samples. *New Zealand Journal of Ecology*. doi:10.20417/nzjecol.42.9

Li, Y.-H., & Tian, X. (2012). Quorum sensing and bacterial social interactions in biofilms. *Sensors (Basel, Switzerland), 12*(3), 2519-2538. doi:10.3390/s120302519

Limoli, D. H., Jones, C. J., & Wozniak, D. J. (2015). Bacterial Extracellular Polysaccharides in Biofilm Formation and Function. *Microbiology spectrum, 3*(3). doi:10.1128/microbiolspec.MB-0011-2014

Liu, L., Liu, J., Liu, X., Dai, C., Zhang, Z., Song, W., & Chu, Y. (2019). Kinetic and equilibrium of U(VI) biosorption onto the resistant bacterium Bacillus amyloliquefaciens. *Journal of Environmental Radioactivity, 203*, 117-124. doi:https://doi.org/10.1016/j.jenvrad.2019.03.008

Lloyd, J. R. (2003). Microbial reduction of metals and radionuclides. *FEMS Microbiology Reviews, 27*(2-3), 411-425. doi:10.1016/s0168-6445(03)00044-5

Loon, L. R. V., & Glaus, M. A. (1998). Experimental and Theoretical Studies on Alkaline Degradation of Cellulose and it's Impact on the Sorption of Radionuclides. *Paul Sherrer Institut Villigen, Switzerland*.

López, D., Vlamakis, H., Losick, R., & Kolter, R. (2009). Cannibalism enhances biofilm development in Bacillus subtilis. *Molecular microbiology, 74*(3), 609-618. doi:10.1111/j.1365-2958.2009.06882.x

Lovley, D. R. (1993). DISSIMILATORY METAL REDUCTION. *Annual Review of Microbiology, 47*(1), 263-290. doi:10.1146/annurev.mi.47.100193.001403

Lovley, D. R., & Phillips, E. J. (1994). Reduction of Chromate by Desulfovibrio vulgaris and Its c(3) Cytochrome. *Applied and Environmental Microbiology, 60*(2), 726-728. doi:10.1128/AEM.60.2.726-728.1994

Luo, H., Sun, Z., Arndt, W., Shi, J., Friedman, R., & Tang, J. (2009). Gene Order Phylogeny and the Evolution of. *PLOS ONE, 4*, e6069. doi:10.1371/journal.pone.0006069

Ma, W., Peng, D., Walker, S. L., Cao, B., Gao, C.-H., Huang, Q., & Cai, P. (2017). Bacillus subtilis biofilm development in the presence of soil clay minerals and iron oxides. *NPJ biofilms and microbiomes, 3*, 4-4. doi:10.1038/s41522-017-0013-6

Machmudah, S., Wahyudiono, Kanda, H., & Goto, M. (2017). Chapter 3 - Hydrolysis of Biopolymers in Near-Critical and Subcritical Water. In H. Dominguez González & M. J. González Muñoz (Eds.), *Water Extraction of Bioactive Compounds* (pp. 69-107): Elsevier.

Macomber, L., & Hausinger, R. P. (2011). Mechanisms of nickel toxicity in microorganisms. *Metallomics : integrated biometal science, 3*(11), 1153-1162. doi:10.1039/c1mt00063b

Madhaiyan, M., Poonguzhali, S., & Sa, T. (2007). Metal tolerating methylotrophic bacteria reduces nickel and cadmium toxicity and promotes plant growth of tomato (Lycopersicon esculentum L.). *Chemosphere, 69*(2), 220-228. doi:https://doi.org/10.1016/j.chemosphere.2007.04.017

Marietou, A. (2016). Nitrate reduction in sulfate-reducing bacteria. *FEMS Microbiology Letters, 363*(15). doi:10.1093/femsle/fnw155

Masella, A. P., Bartram, A. K., Truszkowski, J. M., Brown, D. G., & Neufeld, J. D. (2012). PANDAseq: paired-end assembler for illumina sequences. *BMC Bioinformatics, 13*(1), 31. doi:10.1186/1471-2105-13-31

Mayes, W., Jarvis, A., Burke, I., Bublitz, M., Feigl, V., Klebercz, O., & Gruiz, K. (2011). Dispersal and Attenuation of Trace Contaminants Downstream of the Ajka Bauxite Residue (Red Mud) Depository Failure, Hungary. *Environmental science & technology, 45*, 5147-5155. doi:10.1021/es200850y

Mazurek, M. (2017). 9 - Far-field process analysis and radionuclide transport modeling for saturated media. In M. J. Apted & J. Ahn (Eds.), *Geological Repository Systems for Safe Disposal of Spent Nuclear Fuels and Radioactive Waste (Second Edition)* (pp. 229-266): Woodhead Publishing.

McKinley, I. G., & Grogan, H. A. (1991). Consideration of microbiology in modelling the near field of a L/ILW repository. *Cellular and Molecular Life Sciences, 46*(6).

Meier, J., Piva, A., & Fortin, D. (2012). Enrichment of sulfate-reducing bacteria and resulting mineral formation in media mimicking pore water metal ion concentrations and pH conditions of acidic pit lakes. *FEMS Microbiol Ecol, 79*(1), 69-84. doi:10.1111/j.1574-6941.2011.01199.x

Milanese, A., Mende, D. R., Paoli, L., Salazar, G., Ruscheweyh, H.-J., Cuenca, M., . . . Sunagawa, S. (2019). Microbial abundance, activity and population genomic profiling with mOTUs2. *Nature Communications, 10*(1), 1014. doi:10.1038/s41467-019-08844-4

Milodowski, A., Shaw, R., & Stewart, D. (2015). *The Harpur Hill Site: its geology, evolutionary history and a catalogue of materials present*.

Moeseneder, M. M., Arrieta, J. M., & Herndl, G. J. (2005). A comparison of DNA- and RNA-based clone libraries from the same marine bacterioplankton community. *FEMS Microbiol Ecol, 51*(3), 341-352. doi:10.1016/j.femsec.2004.09.012

Monballiu, A., Cardon, N., Tri Nguyen, M., Cornelly, C., Meesschaert, B., & Chiang, Y. W. (2015). Tolerance of Chemoorganotrophic Bioleaching Microorganisms to Heavy Metal and Alkaline Stresses. *Bioinorganic chemistry and applications, 2015*, 861874-861874. doi:10.1155/2015/861874

Müller, V. (2008). Bacterial Fermentation. In.

Muyzer, G., & Stams, A. J. M. (2008). The ecology and biotechnology of sulphate-reducing bacteria. *Nature Reviews Microbiology, 6*(6), 441-454. doi:10.1038/nrmicro1892

N.D.A. (2010a). *Geological Disposal: An introduction to the generic Disposal System Safety Case*. Harwell, Didcot, Oxfordshire, UK: Nuclear Decommissioning Authority (Radioactive Waste Management Directorate)

N.D.A. (2010b). *Geological Disposal: Generic Disposal System Safety Case data report*. (Report no. NDA/RWMD/044). Harwell, Didcot, Oxfordshire, UK: Nuclear Decommissioning Authority (Radioactive Waste Management Directorate)

N.D.A. (2010c). *Geological Disposal: Near-field evolution status report*. (Report no. NDA/RWMD/033). Harwell, Didcot, Oxfordshire, UK: Nuclear Decommissioning Authority (Radioactive Waste Management Directorate)

N.D.A. (2015a). *Geological Disposal: Investigating the Implications of Managing Depleted, Natural and Low Enriched Uranium through Geological Disposal: Progress Report*. (NDA/RWM/123). Harwell, Didcot, Oxfordshire, UK: Nuclear Decommissioning Authority (Radioactive Waste Management Directorate)

N.D.A. (2015b). *Understanding Activities that Produce Radioactive Wastes in the UK.* Harwell, Didcot, Oxfordshire, UK: Nuclear Decommissioning Authority (Radioactive Waste Management Directorate)

N.D.A. (2016a). *Geological Disposal: Behaviour of Radionuclides and Non-radiological Species in Groundwater Status Report*. (Report no. DSSC/456/01). Harwell, Didcot, Oxfordshire, UK: Nuclear Decommissioning Authority (Radioactive Waste Management Directorate)

N.D.A. (2016b). *Geological Disposal: Gas Status Report*. (Report no. DSSC/455/01). Harwell, Didcot, Oxfordshire, UK: Nuclear Decommissioning Authority (Radioactive Waste Management Directorate)

N.D.A. (2016c). *Geological Disposal: Generic Disposal Facility Design*. (Report no. DSSC/412/01). Harwell, Didcot, Oxfordshire, UK: Nuclear Decommissioning Authority (Radioactive Waste Management Directorate)

N.D.A. (2016d). *Geological Disposal: Generic Disposal System Specification Part B: Technical Specification*. (Report no. DSSC/402/01). Harwell, Didcot, Oxfordshire, UK: Nuclear Decommissioning Authority (Radioactive Waste Management Directorate)

N.D.A. (2016e). *Geological Disposal: Geosphere Status Report*. (Report no. DSSC/453/01). Harwell, Didcot, Oxfordshire, UK: Nuclear Decommissioning Authority (Radioactive Waste Management Directorate)

N.D.A. (2017). *Radioactive Wastes in the UK: A Summary of the 2016 Inventory*. Harwell, Didcot, Oxfordshire, UK: Nuclear Decommissioning Authority (Radioactive Waste Management Directorate)

N.D.A. (2019a). *2019 UK Radioactive Waste Inventory*. Harwell, Didcot, Oxfordshire, UK: Nuclear Decommissioning Authority (Radioactive Waste Management Directorate)

N.D.A. (2019b). *Integrated Waste Management: Radioactive Waste Strategy*. Nuclear Decommissioning Authority (Radioactive Waste Management Directorate)

NNL. (2016). *The Behaviour of Lead in and Around a Geological Disposal Facility*. Harwell, Didcot, Oxfordshire: NNL/ RWM

Oliveira, A., & Pampulha, M. E. (2006). Effects of long-term heavy metal contamination on soil microbial characteristics. *Journal of Bioscience and Bioengineering, 102*(3), 157-161. doi:https://doi.org/10.1263/jbb.102.157

Omelina, E. S., Ivankin, A. V., Letiagina, A. E., & Pindyurin, A. V. (2019). Optimized PCR conditions minimizing the formation of chimeric DNA molecules from MPRA plasmid libraries. *BMC Genomics, 20*(7), 536. doi:10.1186/s12864-019-5847-2

Padan, E., Bibi, E., Ito, M., & Krulwich, T. A. (2005). Alkaline pH homeostasis in bacteria: new insights. *Biochimica et biophysica acta, 1717*(2), 67-88. doi:10.1016/j.bbamem.2005.09.010

Pan, X., Angelidaki, I., Alvarado-Morales, M., Liu, H., Liu, Y., Huang, X., & Zhu, G. (2016). Methane production from formate, acetate and H2/CO2; focusing on kinetics and microbial characterization. *Bioresource technology, 218*, 796-806. doi:10.1016/j.biortech.2016.07.032

Patel, S., & Gupta, R. (2019). A phylogenomic and comparative genomic framework for resolving the polyphyly of the genus Bacillus: Proposal for six new genera of Bacillus species, Peribacillus gen. nov., Cytobacillus gen. nov., Mesobacillus gen. nov., Neobacillus gen. nov., Metabacillus gen. nov. and Alkalihalobacillus gen. nov. *International journal of systematic and evolutionary microbiology, 70*. doi:10.1099/ijsem.0.003775

Paul, D., Kumbhare, S. V., Mhatre, S. S., Chowdhury, S. P., Shetty, S. A., Marathe, N. P., . . . Shouche, Y. S. (2016). Exploration of Microbial Diversity and Community Structure of Lonar Lake: The Only Hypersaline Meteorite Crater Lake within Basalt Rock. *Frontiers in Microbiology, 6*(1553). doi:10.3389/fmicb.2015.01553

Peck, H. D., Jr. (1961). Enzymatic basis for assimilatory and dissimilatory sulfate reduction. *Journal of Bacteriology, 82*(6), 933-939. doi:10.1128/JB.82.6.933-939.1961

Perry, Klepac-Ceraj, V., Zhang, X. V., McNamara, C. J., Polz, M. F., Martin, S. T., . . . Mitchell, R. (2005). Binding of Harvested Bacterial Exopolymers to the Surface of Calcite. *Environmental science & technology, 39*(22), 8770-8775. doi:10.1021/es0508368

Priester, J. H., Horst, A. M., Van De Werfhorst, L. C., Saleta, J. L., Mertes, L. A. K., & Holden, P. A. (2007). Enhanced visualization of microbial biofilms by staining and environmental scanning electron microscopy. *Journal of Microbiological Methods, 68*(3), 577-587. doi:https://doi.org/10.1016/j.mimet.2006.10.018

Puls, R. W., & Bohn, H. L. (1988). Sorption of Cadmium, Nickel, and Zinc by Kaolinite and Montmorillonite Suspensions. *Soil Science Society of America Journal, 52*(5), 1289-1292. doi:10.2136/sssaj1988.03615995005200050013x

Qafoku, N. P., Zachara, J. M., Liu, C., Gassman, P. L., Qafoku, O. S., & Smith, S. C. (2005). Kinetic Desorption and Sorption of U(VI) during Reactive Transport in a Contaminated Hanford Sediment. *Environmental science & technology, 39*(9), 3157-3165. doi:10.1021/es048462q

Quast, C., Pruesse, E., Yilmaz, P., Gerken, J., Schweer, T., Yarza, P., . . . Glöckner, F. O. (2013). The SILVA ribosomal RNA gene database project: improved data

processing and web-based tools. *Nucleic acids research, 41*(Database issue), D590-D596. doi:10.1093/nar/gks1219

Rajala, P., Carpén, L., Vepsäläinen, M., Raulio, M., Sohlberg, E., & Bomberg, M. (2015). Microbially induced corrosion of carbon steel in deep groundwater environment. *Frontiers in Microbiology, 6*(647). doi:10.3389/fmicb.2015.00647

Ranjani Anandan, D. D. a. G. P. M. (2016). An Introduction to Actinobacteria. In D. D. a. Y. Jiang (Ed.), *Actinobacteria - Basics and Biotechnological Applications*: IntechOpen.

Rappé, M. S., & Giovannoni, S. J. (2003). The uncultured microbial majority. *Annu Rev Microbiol, 57*, 369-394. doi:10.1146/annurev.micro.57.030502.090759

Rhoads, K., Bjornstad, B. N., Lewis, R. E., Teel, S. S., Cantrell, K. J., Serne, R. J., . . . Wurstner, S. K. (1994). *Estimation of the release and migration of nickel through soils and groundwater at the Hanford site 218-E-12B burial ground*. (PNL-9791 UC-603). Richland, Washington: Pacific Northwest Laboratory

Rizoulis, A., Milodowski, A. E., Morris, K., & Lloyd, J. R. (2016). Bacterial Diversity in the Hyperalkaline Allas Springs (Cyprus), a Natural Analogue for Cementitious Radioactive Waste Repository. *Geomicrobiology Journal, 33*(2), 73-84. doi:10.1080/01490451.2014.961107

Rizoulis, A., Steele, H. M., Morris, K., & Lloyd, J. R. (2012). The potential impact of anaerobic microbial metabolism during the geological disposal of intermediate-level waste. *Mineralogical Magazine, 76*(8), 3261-3270. doi:10.1180/minmag.2012.076.8.39

Rogers, J., Bennett, P., & Choi, W. J. (2005). *Enhanced weathering of silicates by subsurface microorganisms : a strategy to release limiting inorganic nutrients ?*

Rojas, P., Rodríguez, N., de la Fuente, V., Sánchez-Mata, D., Amils, R., & Sanz, J. L. (2018). Microbial diversity associated with the anaerobic sediments of a soda lake (Mono Lake, California, USA). *Can J Microbiol, 64*(6), 385-392. doi:10.1139/cjm-2017-0657

Rout, S. P. (2015). *Biodegradation of Anaerobic, Alkaline Cellulose Degradation Products.* (Doctoral thesis). University of Huddersfield,

Rout, S. P., Charles, C. J., Doulgeris, C., McCarthy, A. J., Rooks, D. J., Loughnane, J. P., . . . Humphreys, P. N. (2015). Anoxic Biodegradation of Isosaccharinic Acids at Alkaline pH by Natural Microbial Communities. *PLOS ONE, 10*(9), e0137682. doi:10.1371/journal.pone.0137682

Rout, S. P., Charles, C. J., Garratt, E. J., Laws, A. P., Gunn, J., & Humphreys, P. N. (2015). Evidence of the Generation of Isosaccharinic Acids and Their Subsequent

Degradation by Local Microbial Consortia within Hyper-Alkaline Contaminated Soils, with Relevance to Intermediate Level Radioactive Waste Disposal. *PLOS ONE, 10*(3), e0119164. doi:10.1371/journal.pone.0119164

Rout, S. P., Payne, L., Walker, S., Scott, T., Heard, P., Eccles, H., . . . Humphreys, P. N. (2018). The Impact of Alkaliphilic Biofilm Formation on the Release and Retention of Carbon Isotopes from Nuclear Reactor Graphite. *Scientific reports, 8*(1), 4455-4455. doi:10.1038/s41598-018-22833-5

Rout, S. P., Radford, J., Laws, A. P., Sweeney, F., Elmekawy, A., Gillie, L. J., & Humphreys, P. N. (2014). Biodegradation of the Alkaline Cellulose Degradation Products Generated during Radioactive Waste Disposal. *PLOS ONE, 9*(9), e107433. doi:10.1371/journal.pone.0107433

Rout, S. P., Salah, Z. B., Charles, C. J., & Humphreys, P. N. (2017). Whole-Genome Sequence of the Anaerobic Isosaccharinic Acid Degrading Isolate, Macellibacteroides fermentans Strain HH-ZS. *Genome Biology and Evolution, 9*(8), 2140-2144. doi:10.1093/gbe/evx151

Roychoudhury, A. (2010). Sulfate Respiration in Extreme Environments: A Kinetic Study. *Geomicrobiology Journal, January-February 2004*, 33-43. doi:10.1080/01490450490253446

Ruggiero, C., Boukhalfa, H., Forsythe, J., Lack, J., Hersman, L., & Neu, M. (2005). Actinide and metal toxicity to prospective bioremediation bacteria. *Environmental microbiology, 7*, 88-97. doi:10.1111/j.1462-2920.2004.00666.x

Saeki, K., Kunito, T., Oyaizu, H., & Matsumoto, S. (2002). Relationships between Bacterial Tolerance Levels and Forms of Copper and Zinc in Soils. *Journal of Environmental Quality, 31*(5), 1570-1575. doi:10.2134/jeq2002.1570

Schubotz, F., Hays, L. E., Meyer-Dombard, D. A. R., Gillespie, A., Shock, E. L., & Summons, R. E. (2015). Stable isotope labeling confirms mixotrophic nature of streamer biofilm communities at alkaline hot springs. *Frontiers in Microbiology, 6*(42). doi:10.3389/fmicb.2015.00042

Scimeca, M., Bischetti, S., Lamsira, H. K., Bonfiglio, R., & Bonanno, E. (2018). Energy Dispersive X-ray (EDX) microanalysis: A powerful tool in biomedical research and diagnosis. *European journal of histochemistry : EJH, 62*(1), 2841-2841. doi:10.4081/ejh.2018.2841

Seewald, J. S., Zolotov, M. Y., & McCollom, T. (2006). Experimental investigation of single carbon compounds under hydrothermal conditions. *Geochimica et Cosmochimica Acta, 70*(2), 446-460. doi:https://doi.org/10.1016/j.gca.2005.09.002

Seneviratne, M., Vithanage, M., Madawala, S., & Seneviratne, G. (2015). A Novel Microbial Biofilm for Bioremoval of Nickel from Aqueous Media. *Bioremediation Journal, 19*. doi:10.1080/10889868.2014.995374

Shand, P., Edmunds, W. M., Lawrence, A. R., Smedley, P. L., & Burke, S. (2007). *The natural (baseline) quality of groundwater in England and Wales.* (RR/07/06). Retrieved from

Shtangeeva, I. (2004). Thorium. In (Vol. 20).

Shukla, A., Saraf, M., & Parmar, P. (2017). Radiation, radionuclides and bacteria: An in-perspective review. *Journal of Environmental Radioactivity, 180*, 27-35. doi:10.1016/j.jenvrad.2017.09.013

Smith, S. L., Rizoulis, A., West, J. M., & Lloyd, J. R. (2016). The Microbial Ecology of a Hyper-Alkaline Spring, and Impacts of an Alkali-Tolerant Community During Sandstone Batch and Column Experiments Representative of a Geological Disposal Facility for Intermediate-Level Radioactive Waste. *Geomicrobiology Journal, 33*(6), 455-467. doi:10.1080/01490451.2015.1049677

Sonesson, A., Przybyszewska, K., Eriksson, S., Mörgelin, M., Kjellström, S., Davies, J., . . . Schmidtchen, A. (2017). Identification of bacterial biofilm and the Staphylococcus aureus derived protease, staphopain, on the skin surface of patients with atopic dermatitis. *Scientific reports, 7*(1), 8689. doi:10.1038/s41598-017-08046-2

Spear, J. R., Figueroa, L. A., & Honeyman, B. D. (1999). Modeling the Removal of Uranium U(VI) from Aqueous Solutions in the Presence of Sulfate Reducing Bacteria. *Environmental science & technology, 33*(15), 2667-2675. doi:10.1021/es981241y

Stam, M. C., Mason, P. R. D., Pallud, C., & Van Cappellen, P. (2010). Sulfate reducing activity and sulfur isotope fractionation by natural microbial communities in sediments of a hypersaline soda lake (Mono Lake, California). *Chemical Geology, 278*(1), 23-30. doi:https://doi.org/10.1016/j.chemgeo.2010.08.006

Stewart, P. S. (2002). Mechanisms of antibiotic resistance in bacterial biofilms. *International Journal of Medical Microbiology, 292*(2), 107-113. doi:https://doi.org/10.1078/1438-4221-00196

Stewart, P. S., & Franklin, M. J. (2008). Physiological heterogeneity in biofilms. *Nat Rev Microbiol, 6*(3), 199-210. doi:10.1038/nrmicro1838

Stillman, B. (2013). Deoxynucleoside triphosphate (dNTP) synthesis and destruction regulate the replication of both cell and virus genomes. *Proceedings of the National Academy of Sciences, 110*(35), 14120. doi:10.1073/pnas.1312901110

Strand, S. E., Dykes, J., & Chiang, V. (1984). Aerobic Microbial Degradation of Glucoisosaccharinic Acid. *Applied and Environmental Microbiology, 47*(2), 268. Retrieved from http://aem.asm.org/content/47/2/268.abstract

Surakasi, V. P., Wani, A. A., Shouche, Y. S., & Ranade, D. R. (2007). Phylogenetic Analysis of Methanogenic Enrichment Cultures Obtained from Lonar Lake in India: Isolation of Methanocalculus sp. and Methanoculleus sp. *Microbial Ecology, 54*(4), 697-704. doi:10.1007/s00248-007-9228-z

Takahashi, S., Tomita, J., Nishioka, K., Hisada, T., & Nishijima, M. (2014). Development of a Prokaryotic Universal Primer for Simultaneous Analysis of Bacteria and Archaea Using Next-Generation Sequencing. *PLOS ONE, 9*(8), e105592. doi:10.1371/journal.pone.0105592

Tebo, B. M., & Obraztsova, A. Y. (1998). Sulfate-reducing bacterium grows with Cr(VI), U(VI), Mn(IV), and Fe(III) as electron acceptors. *FEMS Microbiology Letters, 162*(1), 193-199. doi:10.1111/j.1574-6968.1998.tb12998.x

Telchadder, R., Smith, K., & Bryan, N. D. (2012). Europium interaction with a vault backfill at high pH. *Mineralogical Magazine, 76*(8), 3083-3093. doi:10.1017/minmag.2012.076.8.23

Tiago, I., Chung, A. P., & Veríssimo, A. (2004). Bacterial Diversity in a Nonsaline Alkaline Environment: Heterotrophic Aerobic Populations. *Applied and Environmental Microbiology, 70*(12), 7378. doi:10.1128/AEM.70.12.7378-7387.2004

Tits, J., Wieland, E., & Bradbury, M. H. (2005). The effect of isosaccharinic acid and gluconic acid on the retention of Eu(III), Am(III) and Th(IV) by calcite. *Applied Geochemistry, 20*(11), 2082-2096. doi:https://doi.org/10.1016/j.apgeochem.2005.07.004

Turpeinen, R., Kairesalo, T., & Häggblom, M. M. (2004). Microbial community structure and activity in arsenic-, chromium- and copper-contaminated soils. *FEMS Microbiology Ecology, 47*(1), 39-50. doi:10.1016/S0168-6496(03)00232-0

Urbieta, M. S., González-Toril, E., Bazán Á, A., Giaveno, M. A., & Donati, E. (2015). Comparison of the microbial communities of hot springs waters and the microbial biofilms in the acidic geothermal area of Copahue (Neuquén, Argentina). *Extremophiles, 19*(2), 437-450. doi:10.1007/s00792-015-0729-2

Van Trappen, S., Mergaert, J., & Swings, J. (2004). Loktanella salsilacus gen. nov., sp. nov., Loktanella fryxellensis sp. nov. and Loktanella vestfoldensis sp. nov., new members of the Rhodobacter group, isolated from microbial mats in Antarctic lakes. *Int J Syst Evol Microbiol, 54*(Pt 4), 1263-1269. doi:10.1099/ijs.0.03006-0

Vercammen, K. (2000). *Complexation of calcium, thorium and europium by αisosaccharinic acid under alkaline conditions.* (Doctor of Natural Sciences). ETH - Swiss Federal Institute of Technology Zurich,

Vercammen, K., Glaus, M., & Van Loon, L. (2001). Complexation of Th(IV) and Eu(III) by α-isosaccharinic acid under alkaline conditions. *Radiochimica Acta - RADIOCHIM ACTA, 89*. doi:10.1524/ract.2001.89.6.393

Vercammen, K., Glaus, M. A., & Loon, L. R. V. (1999). Rapid Communication: Evidence for the Existence of Complexes between Th(IV) and α-Isosaccharinic Acid under Alkaline Conditions. *Radiochimica Acta, 84*(4), 221. doi:https://doi.org/10.1524/ract.1999.84.4.221

Vercammen, K., Glaus, M. A., & Loon, L. R. V. (2001). Complexation of Th(IV) and Eu(III) by ±-isosaccharinic acid under alkaline conditions. *Radiochimica Acta, 89*, 393 - 402.

Verma, A., Sharma, R., Sharma, A., & Shrikot, P. (2014). *Production, purification and characterization of Taq DNA polymerase from indigenous isolate of Thermus aquaticus*.

von Wandruszka, R. (2000). Humic acids: Their detergent qualities and potential uses in pollution remediation. *Geochemical Transactions, 1*(1), 10. doi:10.1186/1467-4866-1-10

W., L. J., L., L. Y., T., D., E., L., F., I. J., & K., L. (1998). Is there a synergistic effect between mixed bacterial infection in biofilm formation on biliary stents? *Gastrointestinal Endoscopy, 48*, 250-257.

Warwick, P., Evans, N., Hall, T., & Vines, S. (2003). Complexation of Ni (II) by α-isosaccharinic acid and gluconic acid from pH 7 to pH 13. *Radiochimica Acta, 91*. doi:10.1524/ract.91.4.233.19971

Warwick, P., Evans, N., Hall, T., & Vines, S. (2004). Stability constants of uranium(IV)-alpha-isosaccharinic acid and gluconic acid complexes. *Radiochimica Acta, 92*. doi:10.1524/ract.92.12.897.55106

Warwick, P., Evans, N., & Heath, C. (2012). *Effect of Experimental Method On The Solubility Of Thorium In The Presence Of Cellulose Degradation Products*. (LBORO CMNDA2). N.D.A Waste Management Directorate: Loughborough University

Watnick, P. I., Fullner, K. J., & Kolter, R. (1999). A role for the mannose-sensitive hemagglutinin in biofilm formation by Vibrio cholerae El Tor. *J Bacteriol, 181*(11), 3606-3609. doi:10.1128/jb.181.11.3606-3609.1999

Wieland, E., Tits, J., Dobler, J., & Spieler, P. (2002). The effect of α-isosaccharinic acid on the stability of and Th(IV) uptake by hardened cement paste. *Radiochimica Acta, 90*, 683-688. doi:10.1524/ract.2002.90.9-11_2002.683

Williamson, A. J., Morris, K., Law, G. T. W., Rizoulis, A., Charnock, J. M., & Lloyd, J. R. (2014). Microbial Reduction of U(VI) under Alkaline Conditions: Implications for Radioactive Waste Geodisposal. *Environmental science & technology, 48*(22), 13549-13556. doi:10.1021/es5017125

Williamson, A. J., Morris, K., Shaw, S., Byrne, J. M., Boothman, C., & Lloyd, J. R. (2013). Microbial Reduction of Fe(III) under Alkaline Conditions Relevant to Geological Disposal. *Applied and Environmental Microbiology, 79*(11), 3320. doi:10.1128/AEM.03063-12

Willis, A. D. (2019). Rarefaction, Alpha Diversity, and Statistics. *Frontiers in Microbiology, 10*, 2407-2407. doi:10.3389/fmicb.2019.02407

Wingender, J., Neu, T. R., & Flemming, H.-C. (1999). *Microbial Extracellular Polymeric Substances. Characterization, Structure and Function.* Heidelberg: Springer.

Worakit, S., Boone, D. R., Mah, R. A., Abdel - Samie, Eldin, M.-., & El - Halwagi, M. M. (1986). Methanobacterium alcaliphilum sp. nov., an H2-Utilizing Methanogen That Grows at High pH Values. *International journal of systematic and evolutionary microbiology, 36*(3), 380-382. doi:https://doi.org/10.1099/00207713-36-3-380

Wormald, R. M., Rout, S. P., Mayes, W., Gomes, H., & Humphreys, P. N. (2020). Hydrogenotrophic Methanogenesis Under Alkaline Conditions. *Frontiers in Microbiology, 11*, 614227-614227. doi:10.3389/fmicb.2020.614227

Wuana, R. A., & Okieimen, F. E. (2011). Heavy Metals in Contaminated Soils: A Review of Sources, Chemistry, Risks and Best Available Strategies for Remediation. *International Scholarly Research Notices, 2011*. doi:https://doi.org/10.5402/2011/402647

Yang, G.-Q., Shungui, Z., Wang, Y., Yuan, Y., & Zhuang, L. (2012). Fontibacter ferrireducens sp. nov., an Fe(III)-reducing bacterium isolated from a microbial fuel cell. *International journal of systematic and evolutionary microbiology, 63*. doi:10.1099/ijs.0.040998-0

Yin, W., Wang, Y., Liu, L., & He, J. (2019). Biofilms: The Microbial "Protective Clothing" in Extreme Environments. *International journal of molecular sciences, 20*(14), 3423. doi:10.3390/ijms20143423

Yoon, S.-H., Ha, S.-M., Kwon, S., Lim, J., Kim, Y., Seo, H., & Chun, J. (2017). Introducing EzBioCloud: a taxonomically united database of 16S rRNA gene

sequences and whole-genome assemblies. *International journal of systematic and evolutionary microbiology, 67*(5), 1613-1617. doi:10.1099/ijsem.0.001755

Associated Data

Chapter 6.0

Element	App	Intensity	Weight%	Weight%	Atomic%
	Conc.	Corrn.		Sigma	
C K	25.68	0.6040	12.11	0.29	36.95
O K	46.26	0.6394	20.61	0.26	47.20
P K	9.81	1.5714	1.78	0.06	2.10
Ca K	4.77	0.8875	1.53	0.05	1.40
Fe K	7.32	0.9622	2.17	0.09	1.42
Pb M	202.95	0.9353	61.81	0.31	10.93
Totals			100.00		

Table S6. 1. Quantitative analysis associated with Figure 6.6 spectrum 1

Element	App	Intensity	Weight%	Weight%	Atomic%	
	Conc.	Corrn.		Sigma		
C K	10.92	0.4895	10.47	0.36	23.70	
O K	46.98	0.7285	30.30	0.33	51.47	
Al K	1.17	0.7456	0.74	0.05	0.74	
Si K	2.15	0.8638	1.17	0.05	1.13	
P K	17.84	1.3267	6.31	0.11	5.54	
Ca K	12.33	0.9596	6.04	0.09	4.09	
Fe K	39.86	0.8969	20.88	0.22	10.16	
Pb M	42.32	0.8252	24.09	0.31	3.16	
Totals			100.00			

Table S6. 2. Quantitative analysis associated with Figure 6.6 spectrum 2

Element	App	Intensity	Weight%	Weight%	Atomic%	
	Conc.	Corrn.		Sigma		

C K	25.11	0.6052	11.57	0.28	34.88	
O K	51.17	0.6482	22.01	0.26	49.83	
P K	9.91	1.5684	1.76	0.06	2.06	
Ca K	4.53	0.8873	1.42	0.05	1.28	
Fe K	6.55	0.9601	1.90	0.08	1.23	
Pb M	205.43	0.9340	61.33	0.31	10.72	
Totals			100.00			

Table S6. 3. Quantitative analysis associated with Figure 6.7 spectrum 1

Element	App	Intensity	Weight%	Weight%	Atomic%	
	Conc.	Corrn.		Sigma		
C K	17.89	0.5127	11.63	0.31	24.93	
O K	76.06	0.7345	34.53	0.29	55.57	
Al K	2.03	0.7785	0.87	0.04	0.83	
Si K	4.04	0.8919	1.51	0.05	1.39	
P K	23.11	1.3585	5.67	0.09	4.71	
Ca K	12.78	0.9403	4.53	0.07	2.91	
Fe K	35.93	0.8908	13.45	0.15	6.20	
Pb M	69.74	0.8360	27.81	0.27	3.46	
Totals			100.00			

Table S6. 4. Quantitative analysis associated with Figure 6.7 spectrum 2

Element	App	Intensity	Weight%	Weight%	Atomic%	
	Conc.	Corrn.		Sigma		
C K	27.26	0.2911	19.95	0.41	44.00	
O K	48.73	0.3714	27.95	0.32	46.28	
Na K	3.94	0.6454	1.30	0.06	1.50	
P K	7.76	1.4309	1.16	0.05	0.99	
Ca K	3.47	0.8351	0.89	0.04	0.59	
Fe K	4.99	0.8948	1.19	0.06	0.56	
Pb M	172.33	0.7719	47.57	0.35	6.08	
Totals			100.00			

Table S6. 5.Quantitative analysis associated with Figure 6.8 spectrum 1

Element	App	Intensity	Weight%	Weight%	Atomic%	
	Conc.	Corrn.		Sigma		
C K	15.76	0.2440	17.87	0.46	30.46	
O K	68.38	0.4414	42.86	0.38	54.84	
Na K	7.59	0.5474	3.84	0.09	3.41	
Al K	0.45	0.6677	0.19	0.03	0.14	
Si K	1.17	0.7936	0.41	0.03	0.30	
P K	20.64	1.2333	4.63	0.08	3.06	
Ca K	12.36	0.8976	3.81	0.06	1.95	
Fe K	36.61	0.8378	12.09	0.15	4.43	

Pb M	36.02	0.6968	14.31	0.23	1.41	
Totals			100.00			

Table S6. 6. Quantitative analysis associated with Figure 6.8 spectrum 2

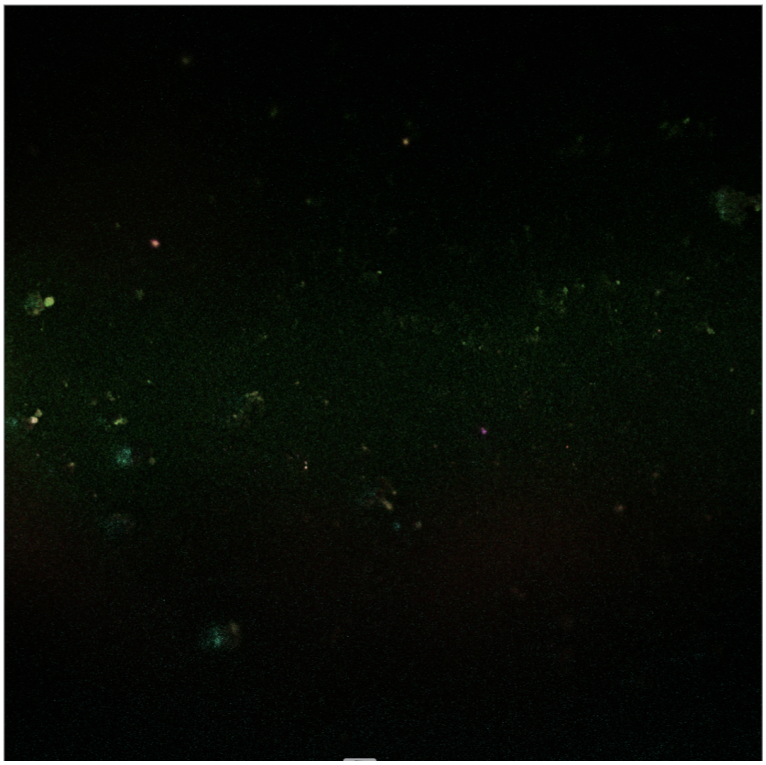

Figure S6. 1. Autofluorescence control for CLSM imagery

Chapter 7.0

Nickel mg/L

Initial average	Initial StDev	Final average	Final StDev	Vol (L)	Mass (Kg)	Kd	%MR
0.007799487	0.001784484	0.00352014	0.000688269	0.03	0.001	36.47024845	54.8670259
0.01562204	0.002968047	0.005805662	0.003305438	0.03	0.001	50.72485376	62.8367243
0.02866157	0.002939328	0.008655093	0.003823726	0.03	0.001	69.34579597	69.8024464
0.226874006	0.067675503	0.039442019	0.009127959	0.03	0.001	142.5626726	82.615012
0.362217153	0.032484533	0.096786575	0.017340964	0.03	0.001	82.27295237	73.2794058

Table S7. 1. Batch sorption data

Time (hrs)	60 Ni (ppm)	Time (hrs)	7 Li (ppm)
0.5	0	0.5	0.00088341
1	0	1	0.00100998
1.5	0	1.5	0.0013247
2	0	2	0.0010008
2.5	0	2.5	0.00074721
3	0	3	0.00064184
3.5	0	3.5	0.0057154
4	0	4	0.01841301
4.5	0	4.5	0.06218211
5	0	5	0.10064482
5.5	0	5.5	0.1814708
6	0	6	0.21368148
6.5	0	6.5	0.17007319
7	0	7	0.16380844
7.5	0	7.5	0.18010971
8	0	8	0.17216933
8.5	0	8.5	0.17074775
9	0	9	0.20960019
9.5	0	9.5	0.15863509
10	0	10	0.15675125
10.5	0	10.5	0.15129132
11	0	11	0.14877526
11.5	0	11.5	0.12287854
12	0	12	0.16045325
12.5	0	12.5	0.16253807
13	0	13	0.15142758
13.5	0	13.5	0.1498093
14	0	14	0.13042714
14.5	0	14.5	0.15929785
15	0	15	0.15780423
15.5	0	15.5	0.15367126
16	0	16	0.15431497
16.5	0	16.5	0.16104247
17	0	17	0.15595701
Influent	0.25	Influent	0.17

Table S7. 2. Data associated with Figures 7.2 & 7.3

Time (hrs)	60 Ni (ppm)	Time (hrs)	Alpha-ISA (mM)	Beta-ISA (mM)	Total ISA (mM)
0.5	0	0.5	0	0	0
1	0	1	0	0	0

1.5	0	1.5	0	0	0
2	0	2	0	0	0
2.5	0	2.5	0.005493038	0.005990227	0.011483265
3	0				
3.5	0				
4	0				
4.5	0	4.5	0.005140502	0.005605782	0.010746284
5	0.00548379				
5.5	0.0505106				
6	0.08709057				
6.5	0.10541842	6.5	0.079843629	0.087070479	0.166914108
7	0.12960821				
7.5	0.1320506				
8	0.16180809				
8.5	0.16626438	8.5	0.069982003	0.076316252	0.146298256
9	0.14489729				
9.5	0.14750506				
10	0.18042603				
10.5	0.2449618	10.5	0.062153727	0.067779419	0.129933147
11	0.27631304				
11.5	0.24237069				
12	0.31751101				
12.5	0.22743552	12.5	0.179791817	0.196065231	0.375857048
13	0.27718837				
13.5	0.28973327				
14	0.27860212				
14.5	0.26327694	14.5	0.13594618	0.148251014	0.284197194
15	0.28458775				
15.5	0.24432895				
16	0.26293313				
16.5	0.25009103	16.5	0.112075866	0.122220138	0.234296004
17	0.23661674				
17.5	0.30785227				
18	0.24134303				
18.5	0.22377307	18.5	0.142712683	0.155629971	0.298342654

Table S7. 3. Data associated with Figure 7.4

Time (hrs)	60 Ni (ppm)	Time (hrs)	Alpha-ISA (mM)	Beta-ISA (mM)	Total ISA (mM)
0.5	0.156676898	0.5	0.187925657	0.109925293	0.29785095
1	0.200077022				
1.5	0.158670764				

2	0.137856546				
2.5	0.14078364	2.5	0.168927146	0.143205005	0.312132151
3	0.165095188				
3.5	0.196196745				
4	0.238471589				
4.5	0.292468569	4.5	0.086651453	0.12563537	0.212286823
5	0.330485475				
5.5	0.29609462				
6	0.265077901				
6.5	0.236696379	6.5	0.1568577	0.155345964	0.312203665
7	0.241034338				
7.5	0.239371814				
8	0.227935506				
8.5	0.231230622	8.5	0.301890726	0.1484803	0.450371025
9	0.203919917				
9.5	0.218696927				
10	0.230923048				
10.5	0.224185102	10.5	0.170260003	0.078604531	0.248864534
11	0.24173887				
11.5	0.23231325				
12	0.226522588				
12.5	0.251770936	12.5	0.163708631	0.11479141	0.27850004
13	0.244116872				
13.5	0.235040284				
14	0.200733577				
14.5	0.222078735	14.5	0.143800561	0.063820448	0.20762101
15	0.260780188				
15.5	0.255036269				
16	0.255715161				
16.5	0.276504127	16.5	0.171802245	0.138700738	0.310502983
17	0.265809487				
17.5	0.252650848				
18	0.263164602				
18.5	0.31077619	18.5	0.218664601	0.136945854	0.355610456
Influent	0.25				

Table S7. 4. Data associated with Figure 7.5

Time (hrs)	60 Ni (ppm)	Time (hrs)	Alpha-ISA (mM)	Beta-ISA (mM)	Total ISA (mM)	Time	Acetic acid (mM)
0.5	0.03253491	0.5	0.00843607	0	0.008436069	0.5	0.194673391
1	0.09974482	1	0.04467939	0	0.044679386		
1.5	0.07613981	1.5	0.08849289	0	0.088492893		

2	0.07291933	2	0.09381915	0	0.093819152		
2.5	0.18200864	2.5	0.08639987	0.038399944	0.124799817		
3	0.23027283	3	0.07505532	0.07947034	0.154525662	3	0.137985527
3.5	0.22778253	3.5	0.09059987	0.06902847	0.159628337		
4	0.25991528	4	0.09631059	0.040746789	0.13705738		
4.5	0.25711432	4.5	0.10562397	0.054633086	0.160257051		
5	0.17365734	5	0.08750853	0.041851907	0.12936044		
5.5	0.3753709	5.5	0.02038497	0.04756493	0.0679499	5.5	0.119907017
6	0.30029577	6	0.09632507	0.062327987	0.158653057		
6.5	0.2830346	6.5	0.0513043	0.069411695	0.120715992		
7	0.30137483	7	0.10449398	0.095273924	0.199767905		
7.5	0.24858788	7.5	0.10919758	0.114657459	0.223855039		
8	0.22571145	8	0.11047121	0.086221435	0.196692648	8	0.139140433
8.5	0.18097198	8.5	0.11170736	0.090924598	0.202631961		
9	0.26397671	9	0.10653452	0.15832849	0.264863007		
9.5	0.27683412	9.5	0.12945396	0.015534475	0.144988435		
10	0.09804641	10	0.10947605	0.021895209	0.131371254		
10.5	0.22966667	10.5	0.06985629	0.026867803	0.096724091	10.5	0.137492669
11	0.23216548	11	0.04365469	0.027284182	0.070938873		
11.5	0.30710776	11.5	0.06507862	0.043385746	0.108464365		
12	0.34331231	12	0.05135439	0.017118131	0.068472525		
12.5	0.16263791	12.5	0.07060635	0.050433105	0.121039453		
13	0.19258141	13	0.05161597	0.082585554	0.134201525	13	0.126275552
13.5	0.30968483	13.5	0.01033421	0.051671058	0.062005269		
14	0.37746387	14	0.02337515	0.058437877	0.081813028		
14.5	0.39772019	14.5	0	0.05020431	0.05020431		
15	0.35237166	15	0.02385014	0.059625346	0.083475485		
15.5	0.24481398	15.5	0.04001304	0.026675361	0.066688404	15.5	0
16	0.1966501	16	0.02741162	0.027411624	0.054823248		
16.5	0.1999956	16.5	0.04216178	0.070269639	0.112431422		
17	0.21294009	17	0.06614178	0.039685066	0.105826844		
17.5	0.21493848	17.5	0.01416702	0.042501051	0.056668069		
18	0.35380832	18	0.056053	0.056053003	0.112106005	18	0
Influent	0.25						

Table S7. 5. Data associated with Figure 7.10 & 7.11

Time (hrs)	60 Ni (ppm)	Alpha ISA (mM)	Beta ISA (mM)	Time (hrs)	Acetic acid (mM)
0.5	0.11015176	0.039160988	0.023519303	0.5	0
1	0.05201949	0.036428618	0.042525427		
1.5	0.10901674	0.084305324	0.054683564		
2	0.30384426	0.06171702	0.057225984	2	0.17584826
2.5	0.0695356	0.03678762	0.039743671		
3	0.0885146	0.048980525	0.033911729		

3.5	0.08028732	0.095703373	0.05062395	3.5	0.391570969
4	0.34429163	0.031692591	0.030884899		
4.5	0.06986397	0.019732553	0.01409303		
5	0.10878039	0.022650731	0	5	0
5.5	0.10745047	0.033793376	0.018007426		
6	0.05775343	0.042943077	0.034795626		
6.5	0.04863591	0.047752567	0.040800811	6.5	0.242412199
7	0.03370967	0.100197988	0.081490713		
7.5	0.07885168	0.027244167	0.025298894		
8	0.07304783	0.043060771	0.036594342	8	0.181986366
14.5	0.02596717	0.066892043	0.064656309	14.5	0.168979206
15	0.02764398	0.062942121	0.053440175		
15.5	0.02685447	0.04904855	0.044807147		
16	0.07307842	0.04009842	0.033763783	16	0.158491434
16.5	0.03524047	0.052339959	0.049947752		
17	0.02856417	0.038405061	0.039681751		
17.5	0.04081203	0.058129919	0.049075081	17.5	0
18	0.03006383	0.073091178	0.05792465		
Influent	0.25				

Table S7. 6. Data associated with Figure 7.13 & 7.14

Time (hrs)	60 Ni (ppm)	Alpha ISA (mM)	Beta ISA (mM)	Acetic acid (mM)
0.5	0.045148736	0.094145725	0.092591203	0
1	0.026713585			0.236635327
1.5	0.029550214			
2	0.037911127			
2.5	0.057767418	0.098053358	0.103536605	0.294724379
3	0.046841478			
3.5	0.056796675			
4	0.07089802			
4.5	0.104827675	0.104213421	0.061154664	0.295589576
5	0.103640054			0.190694203
5.5	0.081243067			0.325645318
6	0.09108191			
6.5	0.068669662	0.109989826	0.052266706	0.325645318
7	0.073500378			
7.5	0.160183965			
8	0.068784746			
8.5	0.062728468	0.077223014	0.110509634	0.23762136
9	0.07769057			0
9.5	0.075436074			

10	0.055983911			
10.5	0.052029757	0.079850253	0.057263707	0.252131557
11	0.052806724			
11.5	0.051452528			
12	0.047030136			
12.5	0.042609563	0.071095422	0.059707139	0.346056241
13	0.049237972			0.150620909
13.5	0.043288388			
14	0.046497851			
14.5	0.061132736	0.05836918	0.103897141	0.482465417
15	0.052089013			
15.5	0.051588657			
16	0.044667723			
16.5	0.061858633	0.065019181	0.064708509	0.255175421
17	0.077320834			0.132326391
17.5	0.059896018			
18	0.089651563			
Influent	0.25			

Table S7. 7. Data associated with 7.20 & 7.21

		Test Alpha ISA (mM)		**Control Alpha ISA (mM)**	
EXIGUO (PURE CULTURE)	Day	Average	StDev	Average	StDev
	0	3.227935996	0.450619881	3.0482906	0.024676392
	2	2.941966169	0.011673047	2.864625818	0.113803342
	4	2.295252046	1.520059921	3.01581627	0.010891078
	6	3.21168542	0.312794575	3.067602215	0.071016983
	8	3.606170614	0.71585992	3.177042514	0.031093188
	10	3.201647506	0.195871742	2.889844506	0.022899459
	CO2	Test gas amount raw average	Control gas amount raw data	Test gas amount cumulative data	
	Day				
	0	0.11266319	0.106573288	0.11266319	
	2	0.13321661	0.13321661	0.245879801	
	4	0.191324427	0.168233548	0.437204227	
	6	0.195538909	0.164000376	0.632743137	
	8	0.204890899	0.237413264	0.837634036	
	10	0.341650762	0.264372614	1.179284798	
	pH	Test	Control		
	Day	Average	Average		
	0	8.34	8.38		
	2	8.235	8.08		

	4	8.45	8.34		
	6	8.595	8.453333333		
	8	8.745	8.803333333		
	10	8.15	8.09		

Table S7. 8. Data associated with Figure 7.22

		Test pH	Control pH			
FLOC REACTOR (MIXED CULTURE)	Day	Average	Average			
	0	9.5	9.32			
	2	9.456666667	9.32			
	4	9.45	9.24			
	6	9.5	9.27			
	8	9.346666667	9.25			
	10	9.21	9.135			
	12	8.996666667	9.06			
	14	8.936666667	8.925			
	Day	Test gas amount raw average	Control gas amount raw data	Test gas amount cumulative data		
	0	0	0	0		
	2	0	0	0		
	4	0.072571334	0	0.072571334		
	6	0.072538628	0	0.145109962		
	8	0.139846169	0	0.284956131		
	10	0.097614503	0	0.382570635		
	12	0.09896091	0	0.481531545		
	14	0.215479402	0	0.697010947		
		Test Alpha ISA (mM)		Control Alpha ISA (mM)		Test Acetic acid (mM)
	Day	Average	StDev	Average	StDev	
	0	4.950867815	1.251660838	4.72278627	1.25099696	38.695
	8	3.629365684	0.325383921	4.189401061	0.70012983	72.55
	14	3.64934495	0.4639601	4.762602665	1.54618338	31.185

Table S7. 9. Data associated with Figure 7.23

Taxon name	Count	Proportion (%)
Actinobacteria	25,211	70.3726
Proteobacteria	6,646	18.5513
Firmicutes	3,726	10.4006
Bacteroidetes	209	0.5834
Deinococcus-Thermus	21	0.0586
Acidobacteria	6	0.0167
Gemmatimonadetes	2	0.0056
Nitrospirae	2	0.0056
Fusobacteria	1	0.0028
Verrumicrobia	1	0.0028

Table S7. 10. Phylum taxonomic composition data associated with Figure 7.24 (Influent)

Taxon name	Count	Proportion(%)
Actinobacteria	14637	46.0486
Firmicutes	11527	36.2644

Proteobacteria	3831	12.0525
Bacteroidetes	1771	5.5716
Tenericutes	8	0.0252
Chloroflexi	5	0.0157
Deinococcus-Thermus	3	0.0094
Acidobacteria	2	0.0063
Planctomycetes	1	0.0031
Verrucomicrobia	1	0.0031

Table S7. 11. Phylum taxonomic composition data associated with Figure 7.24 (Middle)

Taxon name	Count	Proportion(%)
Proteobacteria	17355	39.7895
Firmicutes	14169	32.485
Actinobacteria	9590	21.9868
Bacteroidetes	2332	5.3465
Deinococcus-Thermus	117	0.2682
Chloroflexi	37	0.0848
Tenericutes	10	0.0229
Acidobacteria	3	0.0069
Armatimonadetes	1	0.0023
Nitrospirae	1	0.0023
Spirochaetes	1	0.0023
Verrucomicrobia	1	0.0023

Table S7. 12. Phylum taxonomic composition data associated with 7.24 (Effluent)

Taxon name	Count	Proportion(%)
Actinobacteria_c	25184	70.2973
Alphaproteobacteria	6618	18.4731
Clostridia	2603	7.2659
Tissierellia	1059	2.956
Bacteroidia	203	0.5666
Erysipelotrichi	35	0.0977
Betaproteobacteria	27	0.0754
Negativicutes	25	0.0698
Acidimicrobiia	22	0.0614
Deinococci	21	0.0586
Solibacteres	5	0.014
Bacilli	4	0.0112
Cytophagia	4	0.0112
Rubrobacteria	3	0.0084
Flavobacteria	2	0.0056
Thermoleophilia	2	0.0056
Gemmatimonadetes_c	2	0.0056
Nitrospira_c	2	0.0056

Gammaproteobacteria	1	0.0028
Spartobacteria	1	0.0028
Fusobacteria_c	1	0.0028
Vicinamibacter_c	1	0.0028

Table S7. 13. Class level composition data associated with 7.25 (Influent)

Taxon name	Count	Proportion(%)
Actinobacteria_c	14625	46.0108
Clostridia	10330	32.4986
Alphaproteobacteria	3723	11.7127
Bacteroidia	1762	5.5433
Tissierellia	1019	3.2058
Negativicutes	131	0.4121
Betaproteobacteria	98	0.3083
Bacilli	31	0.0975
Erysipelotrichi	16	0.0503
Acidimicrobiia	10	0.0315
Gammaproteobacteria	9	0.0283
Mollicutes	8	0.0252
Caldilineae	5	0.0157
Cytophagia	5	0.0157
Flavobacteria	4	0.0126
Deinococci	3	0.0094
Nitriliruptoria	2	0.0063
Deltaproteobacteria	1	0.0031
Planctomycetia	1	0.0031
Solibacteres	1	0.0031
Spartobacteria	1	0.0031
Vicinamibacter_c	1	0.0031

Table S7. 14. Class level composition associated with Figure 7.25 (Middle)

Taxon name	Count	Proportion(%)
Alphaproteobacteria	16774	38.4575
Actinobacteria_c	9510	21.8034
Clostridia	8317	19.0683
Tissierellia	5042	11.5597
Bacteroidia	2255	5.17
Betaproteobacteria	502	1.1509
Erysipelotrichi	463	1.0615
Negativicutes	211	0.4838
Bacilli	132	0.3026
Deinococci	117	0.2682
Gammaproteobacteria	79	0.1811
Cytophagia	70	0.1605

Acidimicrobiia	40	0.0917
Nitriliruptoria	35	0.0802
Anaerolineae	25	0.0573
Caldilineae	12	0.0275
Mollicutes	10	0.0229
Flavobacteria	6	0.0138
Firmicutes_uc	4	0.0092
Vicinamibacter_c	3	0.0069
Rubrobacteria	2	0.0046
Thermoleophilia	2	0.0046
Coriobacteriia	1	0.0023
Fimbriimonadia	1	0.0023
Spartobacteria	1	0.0023
Sphingobacteriia	1	0.0023
Spirochaetia	1	0.0023
Nitrospira_c	1	0.0023

Table S7. 15. Class level composition associated with Figure 7.25 (Effluent)

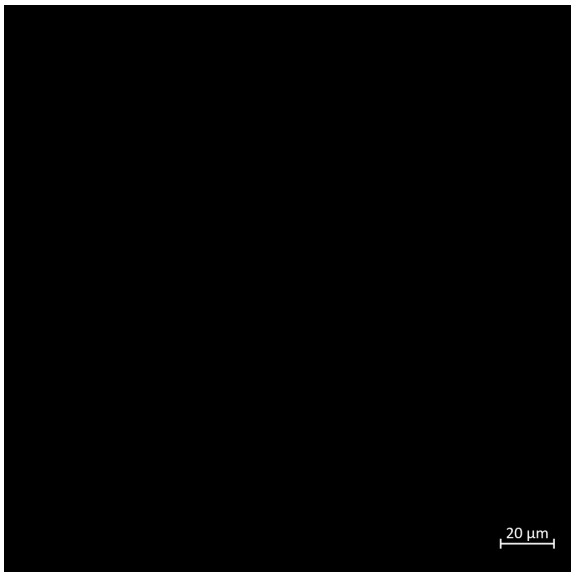

Figure S7. 1. Autofluorescence CLSM imagery 1 associated with Chapter 7.0

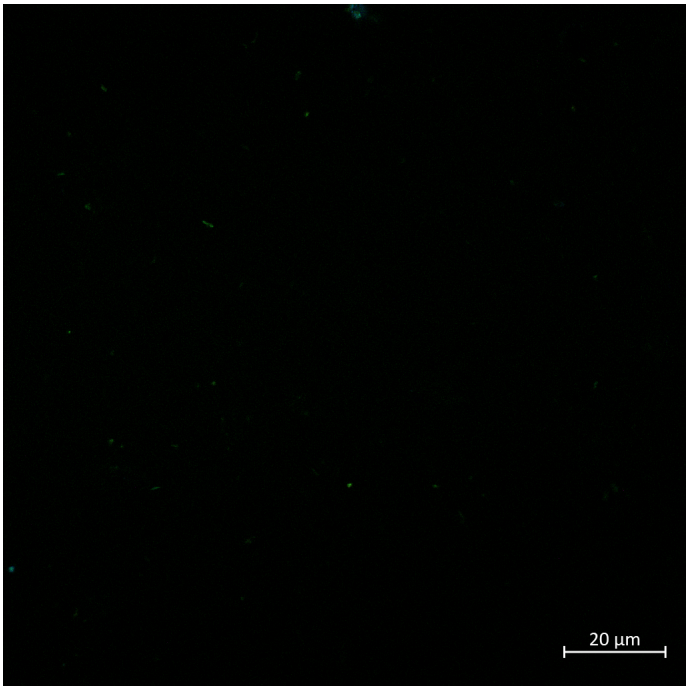

Chapter 8.0

Time (hrs)	151 Eu (ppm)	Time (Hrs)	7 Li (ppm)
0.5	0	0.5	0
1	0	1	0
1.5	0	1.5	0
2	0	2	0
2.5	0	2.5	0.00669086
3	0	3	0.00488217
3.5	0	3.5	0.00609643
4	0	4	0.01011433
4.5	0	4.5	0.05727025
5	0	5	0.14965602
5.5	0	5.5	0.19554909
6	0	6	0.14408147
6.5	0	6.5	0.15863966
7	0	7	0.17030067
7.5	0	7.5	0.16884309
8	0	8	0.35373313
8.5	0	8.5	0.23130342
9	0	9	0.2133784
9.5	0	9.5	0.18888174
10	0	10	0.18709776
10.5	0	10.5	0.17824563
11	0	11	0.15076657
11.5	0	11.5	0.16509341
12	0	12	0.19228337
12.5	0	12.5	0.18114899
13	0	13	0.17334051
13.5	0	13.5	0.1792742
14	0	14	0.17843446
14.5	0	14.5	0.16265531
15	0	15	0.17674834
15.5	0	15.5	0.15697077
16	0	16	0.16285839
16.5	0	16.5	0.1669535
17	0	17	0.16458133
17.5	0	17.5	0.16390035
18	0	18	0.1587703
Influent	0.7	Influent	0.17

Table S8. 1. Data associated with Figure 8.1 & 8.2

Time running	151 Eu (ppm)	Alpha ISA (mM)	Beta ISA (mM)	Total ISA

0.5	0.000214773	0	0	0
1	0			
1.5	0			
2	0	0	0	0
2.5	1.07374E-06			
3	0			
3.5	0	0	0	0
4	0			
4.5	0			
5	8.70662E-06	0	0	0
5.5	0			
6	0			
6.5	0			
7	7.39001E-05	0.14440011	0.128459838	0.272859947
7.5	0			
8	7.51285E-05			
8.5	0	0.181781855	0.182071779	0.363853634
9	3.17119E-05			
9.5	2.75813E-05			
10	1.46996E-05	0.087583706	0.145091842	0.232675548
10.5	1.1953E-05			
11	0			
11.5	9.45454E-06	0.09187474	0.198656659	0.290531399
12	0			
12.5	1.2881E-05			
13	1.54898E-05	0.097368191	0.089444434	0.186812625
13.5	1.71777E-05			
14	2.68053E-05			
14.5	0	0.15404283	0.138626114	0.292668944
15	0			
15.5	1.60959E-05			
16	2.25738E-05	0.318874919	0.243351912	0.562226831
16.5	0			
17	1.65062E-06			
17.5	0	0.172357623	0.22011616	0.392473783
18	1.67625E-05			

Table S8. 2. Data associated with Figure 8.3

Time (Hrs)	151 Eu (ppm)	Alpha ISA (mM)	Beta ISA (mM)	Total ISA (mM)
0.5	0.00246132	0	0	0
1	0.00175217			
1.5	0.00169559			

2	0.00169711			
2.5	0.00169099	0.105587845	0.027025113	0
3	0.00167068			
3.5	0.00168285			
4	0.00167287			
4.5	0.00168011	0.101388556	0.032975641	0
5	0.00168142			
5.5	0.00167476			
6	0.00167626			
6.5	0.00167451	0.223258091	0.164592707	0
7	0.00168444			
7.5	0.00168111			
8	0.00169585			
8.5	0.00168713	0.131760125	0.083851028	0
9	0.00168564			
9.5	0.00168431			
10	0.00167272			
10.5	0.00168195	0.143640339	0.101299249	0
11	0.00173329			
11.5	0.00167187			
12	0.00167094			
12.5	0.00167047	0.158547096	0.112860392	0
13	0.00187151			
13.5	0.00172186			
14	0.00168943			
14.5	0.00166864	0.131305225	0.084364724	0
15	0.00167588			
15.5	0.00190228			
16	0.00172682			
16.5	0.00167013	0.192345181	0.109996841	0
Influent	0.7			

Table S8. 3. Data associated with Figure 8.4

Time (hrs)	232 Th (ppm)	Time (hrs)	7 Li (ppm)
0.3	0.006325092	0.3	0.00150403
0.6	0.006148336	0.6	0.00157619
0.9	0.005936967	0.9	0.00104953
1.2	0.005870219	1.2	0.0013438
1.5	0.005850592	1.5	0.00149483
1.8	0.005897623	1.8	0.00149768
2.1	0.006027496	2.1	0.00352699

2.4	0.006299856	2.4	0.01055295
2.7	0.006596556	2.7	0.10066547
3	0.006625457	3	0.14058849
3.3	0.006514781	3.3	0.1358331
3.6	0.00618584	3.6	0.16322129
3.9	0.006355689	3.9	0.13802235
4.2	0.006483013	4.2	0.12297927
4.5	0.006578425	4.5	0.14489619
4.8	0.006410232	4.8	0.16451135
5.1	0.006466121	5.1	0.14700842
5.4	0.00638739	5.4	0.15513511
5.7	0.006093894	5.7	0.14818006
6	0.006219822	6	0.17394145
6.3	0.006073882	6.3	0.14913752
6.6	0.00594044	6.6	0.1559257
6.9	0.005894628	6.9	0.1572378
7.2	0.005929981	7.2	0.17224858
7.5	0.005904652	7.5	0.16865316
7.8	0.005893524	7.8	0.15799904
8.1	0.005853989	8.1	0.15366323
8.4	0.005965311	8.4	0.17108213
8.7	0.005843825	8.7	0.17675977
9	0.005942312	9	0.1732311
Influent	0.31		

Table S8. 4. Data associated with Figure 8.5 & 8.6

Time (hrs)	232 Th (ppm)	Time (hrs)	Alpha ISA (mM)	Beta ISA (mM)	Total ISA
0.3	0.010420592	0.3	0.166534368	0.181910509	0.34844488
0.6	0.010123507				
0.9	0.009529556				
1.2	0.00942774	1.2	0	0	0
1.5	0.009446709				
1.8	0.009210081				
2.1	0.009231724	2.1	0	0	0
2.4	0.00916946				
2.7	0.00900782				
3	0.008501725	3	0.27391667	0.185985026	0.4599017
3.3	0.008304178				
3.6	0.00827852				
3.9	0.008254289	3.9	0.213174597	0.132646035	0.34582063
4.2	0.008277594				

4.5	0.008267283				
4.8	0.008224669	4.8	0.265194701	0.221653126	0.48684783
5.1	0.008228118				
5.4	0.008196395				
5.7	0.008207433	5.7	0.259934984	0.266488824	0.52642381
6	0.008163761				
6.3	0.008246202				
6.6	0.008238582	6.6	0.24412117	0.262368387	0.50648956
6.9	0.008200898				
7.2	0.008210948				
7.5	0.00819628	7.5	0.162887092	0.149995031	0.31288212
7.8	0.008222202				
8.1	0.008185704				
8.4	0.008176837	8.4	0.312565517	0.269047473	0.58161299
8.7	0.008173666				
9	0.008178228				

Table S8. 5. Data associated with Figure 8.7

Time (hrs)	232 Th (ppm)	Time (Hrs)	Alpha ISA (mM)	Beta ISA (mM)	Total ISA
0.3	0.007256423	0.3	0	0	0
0.6	0.003400312				
0.9	0.002784475				
1.2	0.002823616				
1.5	0.002840842	1.5	0	0	0
1.8	0.002952347				
2.1	0.004553225				
2.4	0.00534191				
2.7	0.004704373	2.7	0.085665231	0.171330462	0.25699569
3	0.003380379				
3.3	0.002697511				
3.6	0.002548163				
3.9	0.002498742	3.9	0.25085237	0.209043642	0.45989601
4.2	0.002508323	4.2	0.194333163	0.194333163	0.38866633
4.5	0.002341795				
4.8	0.002316772				
5.1	0.002428764	5.1	0.222487438	0.259568677	0.48205611
5.4	0.002271764				
5.7	0.002264543				
6	0.002235425				
6.3	0.002240573	6.3	0.192197634	0.192197634	0.38439527
6.6	0.002282354				

6.9	0.002184674				
7.2	0.002201018				
7.5	0.002221033	7.5	0.433962026	0.197255466	0.63121749
7.8	0.002252743				
Influent	0.31				

Table S8. 6. Data associated with Figure 8.8

Time (hrs)	238 U (ppm)
0.3	0.010440679
0.6	0.004772955
0.9	0.002317883
1.2	0.00190074
1.5	0.002078446
1.8	0.003952003
2.1	0.067381968
2.4	0.322854409
2.7	0.884404968
3	1.026862588
3.3	0.729798565
3.6	0.682998035
3.9	0.873774803
4.2	1.224407986
4.5	1.108349371
4.8	0.768582338
5.1	0.773470182
5.4	0.908912405
5.7	0.841113449
6	0.783478431
6.3	0.719949037
6.6	0.873582506
6.9	0.727540619
7.2	0.772622991
7.5	0.850905844
7.8	0.765699937
Influent	0.7

Table S8. 7. Data associated with Figure 8.9

Time (hrs)	238 U (ppm)	Time (hrs)	Alpha ISA (mM)	Beta ISA (mM)	Total ISA (mM)
0.3	0.05595908	0.3	0	0	0
0.6	0.6403781				
0.9	0.70304971				

1.2	0.81996895	1.2	0	0	0
1.5	0.69087639				
1.8	0.48810747				
2.1	0.70534182				
2.4	0.69528492	2.4	0.105224624	0.094148348	0.199372972
2.7	0.76294677				
3	0.93676498				
3.3	1.22017139				
3.6	0.72053274	3.6	0.177973691	0.149497901	0.327471592
3.9	0.75685615				
4.2	1.26720886				
4.5	0.97984685	4.5	0.168548389	0.120391706	0.288940095
4.8	0.74040615				
5.1	0.79111284				
5.4	0.89538264				
5.7	0.94895728	5.7	0.135013675	0.128584452	0.263598127
6	0.86544294				
6.3	1.10673749				
6.6	0.73390916				
6.9	0.72307799	6.9	0.275265976	0.247739378	0.523005354
7.2	0.8179911				
Influent	0.7				

Table S8. 8. Data associated with Figure 8.10

Time (hrs)	238 U (ppm)	U(VI) ppm
0.6	0.368352331	-0.014285714
1.5	0.246508624	0.39047619
2.4	0.063560845	1.23909E-17
3.3	0.109440396	0.047619048
3.9	0.015181061	0.066666667
4.8	0.027424435	0.080952381
5.7	0.012833629	0.038095238
6.6	0.011682601	0.185714286
7.5	0.220633164	0.095238095
Influent	0.6	0.6

Table S8. 9. Data associated with Figure 8.13

Taxon name	Count	Proportion(%)
Firmicutes	34119	48.5507
Proteobacteria	28240	40.185
Bacteroidetes	2991	4.2561

Tenericutes	2460	3.5005
Actinobacteria	2110	3.0025
Gemmatimonadetes	170	0.2419
Deinococcus-Thermus	134	0.1907
Planctomycetes	37	0.0527
Acidobacteria	14	0.0199

Table S8. 10. Taxonomic composition at phylum level. Data associated with Figure 8.11

Taxon name	Count	Proportion(%)
Alphaproteobacteria	27155	38.6411
Bacilli	23295	33.1483
Clostridia	10543	15.0025
Mollicutes	2460	3.5005
Nitriliruptoria	1637	2.3294
Cytophagia	1289	1.8342
Bacteroidia	1165	1.6578
Gammaproteobacteria	546	0.7769
Betaproteobacteria	533	0.7584
Sphingobacteriia	365	0.5194
Actinobacteria_c	339	0.4824
Tissierellia	225	0.3202
Flavobacteria	172	0.2448
Longimicrobia	170	0.2419
Deinococci	134	0.1907
Acidimicrobiia	128	0.1821
Erysipelotrichi	37	0.0527
Planctomycetia	37	0.0527
Negativicutes	19	0.027
Solibacteres	11	0.0157
Rubrobacteria	6	0.0085
Epsilonproteobacteria	5	0.0071
Acidobacteriia	3	0.0043
Deltaproteobacteria	1	0.0014

Table S8. 11. Taxonomic composition at class level. Data associated with Figure 8.12